Technische Universität München
Department Chemie
WACKER-Lehrstuhl für Makromolekulare Chemie

Novel Functional Poly(2-oxazoline)s as Potential Carriers for Biomedical Applications

Robert Luxenhofer

Vollständiger Abdruck der von der Fakultät für Chemie der Technischen Universität München zur Erlangung des akademischen Grades eines

Doktors der Naturwissenschaften
(Dr. rer. nat.)

genehmigten Dissertation.

Vorsitzender:		Univ.-Prof. Dr. Kai-Olaf Hinrichsen
Prüfer der Dissertation:	1.	Priv.-Doz. Dr. Rainer Jordan
	2.	Univ.-Prof. Dr. Horst Kessler
	3.	Univ.-Prof. Dr. Andreas Türler

Die Dissertation wurde am 29.05.2007 bei der Technischen Universität München eingereicht und durch das Department Chemie am 26.06.2007 angenommen.

In Vivo Veritas!

Die vorliegende Arbeit wurde am WACKER-Lehrstuhl für Makromolekulare Chemie (zuvor Lehrstuhl für Makromolekulare Stoffe) im Department Chemie der Technischen Universität München in der Zeit von März 2004 bis Mai 2007 unter der Leitung von Herrn PD Dr. Rainer Jordan angefertigt.

Insbesondere möchte ich mich bei meinem Mentor und Betreuer PD Dr. Rainer ´Ray´ Jordan sehr herzlich bedanken, dass er mir die Möglichkeit gegeben hat, an diesem Projekt zu arbeiten. Ich glaube das war die interessanteste Doktorarbeit die ich hätte finden können, selbst wenn ich gesucht hätte. Ich war sehr froh über all die Freiheit die ich hatte, wobei man immer vorbeikommen konnte, wenn man ein Problem hatte. Außerdem bin ich dankbar für die Arbeits- und Konferenzaufenthalte in New York, Flic en Flac, Budapest, San Francisco etc., die ich genießen konnte und die große Geduld mit mir.

Prof. Dr.-Ing. Oskar Nuyken und Prof. Dr. Bernhard Rieger danke ich für die Aufnahme bzw. die Möglichkeit meines Verbleibs am Lehrstuhl. Bei Prof. Nuyken möchte ich mich auch für das entgegengebrachte Vertrauen und das Interesse an meiner Arbeit danken, sowie die Möglichkeit meine Arbeiten an verschiedenen Gelegenheiten zu präsentieren.
Frau Dr.-Ing. Heidi Samarian danke ich für die viele Hilfe hinter den Kulissen.

Den Leitern und Mitarbeitern der Gruppen unserer Kooperationspartner gilt ebenso mein großer Dank. Ohne diese Zusammenarbeit wäre nur ein Stumpf dieser Arbeit möglich gewesen. Prof. Dr. Horst Kessler, Prof. Dr. Hans-Jürgen Wester und PD Dr. Markus Essler danke ich für Ihr Interesse an der Entwicklung von polymeren Therapeutika. Ihren Mitarbeitern Dr. Lopéz-García, Florian Manzenrieder, Florian Opperer, Oliver Demmer, Andreas Frank, Janine Eckardt, Florian Gärtner und Dr. Thorsten Poethko danke ich für die Synthese der Peptide, Unterstützung bei der Analytik oder der Durchführung bzw. Unterstützung bei der Durchführung der Tierversuche.

Prof. Dr. R. J. Gillies, Prof. V. J. Hruby und Dr. L. Xu von der Universität von Arizona danke ich für die Durchführung der Affinitätsstudien der MTII Konjugate.

Dr. Steffen Jungermann, mein Laborkollege über einen großen Teil der Arbeit, gilt mein großer Dank für die angenehme Zeit. Ich denke Du warst ein Hauptgrund neben

dem Projekt, warum ich ein Makro wurde, sicher eine der besseren Entscheidungen meines Lebens. Ausserdem danke ich dir für die ganze Hilfe mit den Computern und für die MALDI Messungen, für die Zeit am Kaffeetisch, die Balkonbiers, die WoW Zeit und das ganze andere Zeug.

Ausserdem danke ich allen Mitgliedern der alten und neuen Makros. Insbesondere möchte ich dabei Dr. Benjamin Rossbach (gibt einem das Gefühl KEIN Workaholic sein), Dr. Martin Bortenschlager (immer hervorragend enspannt), Dr. Martin Mayershofer (immer ein Hilfe), Dr. Doris Kaufmann (einfach immer Spass), Marin Steenackers (das peinliche Gesicht :-D), Julia Müller (ich will an den SEE!) für das hervorragende und entspannte Arbeitsklima über die Jahre danken. Nicht weniger angenehm war die Arbeit in jüngerer Zeit mit den neueren Makros, dafür danke ich Timo Anselment, Andi Feigl, Caro Gantner, Udo Schmidt, Uli Will und allen anderen Makros.
Dr. Martin Mayershofer, Dr. Jens Krause, Dr. Tobias Zarka, Julia Müller und Martin Schneider danke ich für die GPC Messungen über die Jahre, Herrn Krause sowie Stephan Huber danke ich für die MALDI-TOF Messungen.

Desweiteren gilt mein Dank meinem 'medizinischen Beraterstab', Melanie Bosse, Margot Roth und Dr. Joanna Eger, auch wenn es hauptsächlich 'nur' darum ging meine Fragerei zu ertragen.

"Meinen" Diplomanden Christian Taubmann, Alexander Kurek und Timo Anselment danke ich für die gute und fruchtbare Zusammenarbeit.
Meinen Knechten Florian Brandhuber, Sabine Scholz, Manuela Bezen, Tobias Förster, Richard Knapp, Martin Schneider, Jens Emmerich, Alexander Bochen, Anja Friedrich und Max Ehrhardt, meinen Azubis Martin Schellerer und Floriane, von den vielen Praktikanten insbesondere Luisa Long, Christian Benda und Wenting Zhang und zuletzt meiner ersten Bachelorette Anita Schulz, danke ich vielmals für die Unterstützung bei meiner Arbeit. Ich hoffe und glaube, dass wir voneinander gelernt haben. Ich hoffe auch keine Knechte vergessen zu haben.

Für das Korrekturlesen von Teilen dieser Arbeit danke ich meinem Bruder Georg, Timo Anselment, Julia Müller, Florian Manzenrieder und Florian Opperer. Ein spezieller Dank geht an die Rettung in letzter Sekunde, Michael Bank.

Meinem Vater, meiner Familie

Contents

Abbreviations and Symbols

Abbreviations

abs.	absolute
ACN	acetonitrile
ACTH	adrenocorticotropic hormone
Ala	L-alanine; (S)-2-aminopropanoic acid, A
ANT	[Ac-4-NO_2-Phe-c(D-Cys-Tyr-D-Trp-Lys-Thr-Cys)-D-Tyr-NH_2]
AOAC	(2-aminooxy)acetic acid
Arg	L-arginine; (S)-2-amino-5-guanidinovalerianic acid, R
Asp	L-aspartic acid; (S)-2-aminosuccinic acid, D
ATR	attenuated total reflection/reflectance
ATRP	atom transfer radical polymerization
a.u.	arbitrary units
bl	block
BNCT	boron neutron capture therapy
Boc	*tert*-butyloxycarbonyl
Boc-AOAc	*N*-Boc(2-aminooxy)acetic acid
BocPip	*N*-*tert*-butyloxycarbonylpiperazine
bp.	boiling point
c	cyclo
CCMSH	[$Cys^{3,4,10}$,D-Phe^{7}]MSH_{3-13}
CP	cloud point
CROP	cationic ring-opening polymerization
d	day(s)

D	L-aspartic acid, Asp
$\dot{\text{D}}$	tBu protected Arg
DCM	dichloromethane
Dde	4,4-dimethyl-2,6-dioxocyclohexylideneethyl
DeMix	mixture of TFA/H_2O/TIBS (95/2.5/2.5; v/v/v) for removal of acid labile protection groups
DIPEA	diisopropylethylamine (Hünig base)
DMAc	*N*,*N*-dimethylacetamide
DMF	*N*,*N*-dimethylformamide
DNA	desoxyribonucleic acid
DOTA	1,4,7,10-tetraazacyclododecane-1,4,7,10-tetraacetic acid
DP	degree of polymerization
DPOx	2-[3-(1,3)-dioxolan-2-ylpropyl]-2-oxazoline
Dpr	2,3-diaminopropionic acid
DTPA	diethylenetriamine pentaacetic acid
DTT	1,4-dithio-DL-threitol (Clelands reagent)
E	L-Glu
EC_{50}	half-maximum effective concentration *in vivo*
ECM	extracellular matrix
EDCI ×HCl	*N*-Ethyl-*N*'-(3-dimethylaminopropyl)carbodiimide hydrochloride
ELP	elastin-like polymer
EOB	ethyl-4-(oxazol-2-yl)butanate
EPR	enhanced permeability and retention (effect)
equiv	equivalent
Et_2O	diethyl ether
EtOx	2-ethyl-2-oxazoline
f	D-Phe
F	L-Phe
FBOA	N-(4-fluorobenzylidene)oxime
g	graft
G	amino acid: glycine, Gly, G
G	dendrimers: number of generation of dendrimer, e.g. G3, 3^{rd} generation dendrimer
GC	gas chromatography

Glu	L-glutamic acid; (S)-2-aminopentanedioic acid, E
Gly	glycine; 2-aminoacetic acid, G
GPC	gel permeation chromatography
GPCR	G-protein coupled receptor
GSP	general synthetic procedure
H	L-histidine, His
HEG	hexaethylenglycole
HEPES	2-[4-(2-hydroxyethyl)piperazine]ethanesulfonic acid
His	L-histidine; (S)-2-amino-3-(3H-imidazol-4-yl)propanoic acid, H
HKR	hydrolytic kinetic resolution
hMCxR	human melanocortin receptor, subtype x (1 - 5)
HOBt	1-hydroxybenzotriazole
HPhOx	2-(4-hydroxyphenyl)-2-oxazoline
HPLC	high performance liquid chromatography
HPMA	*N*-(2-hydroxypropyl)methacrylamid
HSA	human serum albumin
hsstr_x	human somatostatin receptor, subtype x (1 - 5)
HUVEC	human umbilical vein endothelial cells
IC_{50}	half-maximum inhibitory concentration *in vitro*
iPOx	2-*iso*-propyl-2-oxazoline
IR	infrared spectroscopy
IUPAC	International Union of Pure and Applied Chemistry
i.v.	intravenously
LCST	lower critical solution temperature
LET	linear energy transfer
LDA	lithium diisopropylamide
MAG3	mercaptoacetyltriglycine
MALDI	matrix assisted laser desorption/ionization
MCT	mercury-cadmium-telluride
MeOH	methanol
MeOTf	methyltriflate (methyl trifluoromethylsulfonate)
MeOx	2-methyl-2-oxazoline
MOP	methyl-3-(oxazol-2-yl)propionate
MS	mass spectrometry

MSH	melanocyte stimulating hormone (subtypes α, β and γ)
MTII	melanotan II, Ac-Nle-c[Asp-His-DPhe-Arg-Trp-Lys]-NH_2
MWCO	molecular weight cut off
NAPamide	[Nle^4,Asp^5,D-Phe^7]-α-MSH_{4-11}
nBuLi	n-buthyllithium
NCL	native chemical ligation
NCS	neocarcinostatin
NIPAAm	N-isopropylacrylamide
NIR	near infra-red
Nle	L-norleucine; (S)-2-aminohexanoic acid
NMP	nitroxide mediated radical polymerization
NMR	nuclear magnetic resonance (spectroscopy)
NonOx	2-nonyl-2-oxazoline
OC	octreotide; D-Phe-c[Cys-Phe-D-Trp-Lys-Thr-Cys]-Thr(ol)
OctreoScan	[^{111}In]-$DTPA^0$-octreotide
OctreoTher	[^{90}Y]-$DOTA^0$-TOC
Pbf	2,2,4,6,7-pentamethyldihydrobenzofuran-5-sulfonyl-
PBS	phosphate buffered saline
PDT	photodynamic (laser) therapy
PDI	polydispersity index = $\frac{\overline{M}_w}{\overline{M}_n}$
PEG	poly(ethylen glycole)
PEI	poly(ethylen imine)
PET	positron emission tomograpy
PEtOx	poly(2-ethyl-2-oxazoline)
PhCl	chlorobenzene
Phe	L-phenylalanine; (S)-2-amino-3-phenylpropanoic acid, F
p.i.	post injection
Pid	piperdine
Pip	piperazine
PMeOx	poly(2-methyl-2-oxazoline)
POx	poly(2-oxazoline); unspecified substituent at 2-position
PRI	peptide receptor imaging
PRRT	peptide receptor (mediated) radionuclide therapy

^{P}PRRT	polymer supported peptide receptor radionuclide therapy
PyBop	benzotriazole-1-yl-oxy-tris-pyrrolidino-phosphinium hexafluorophosphate
PynOx	2-(pent-4-ynyl)-2-oxazoline
p-AcPh-DOTA	1,4,7,10-tetraazacyclododecane-4,7,10-*tert*-butylester-1-(4-acetyl-phenyl)-acetic acid methylester
p-SCN-Bn-DOTA	2-(4-isothiocyanatobenzyl)-1,4,7,10-tetraazacyclododecane-1,4,7,10-tetraacetic acid
R	L-arginine, Arg
$\dot{\text{R}}$	Pbf protected Arg
RAIT	radioimmunotherapy /-therapeutics
RCY	radiochemical yield
RES	reticuloendothelial system
c[RGDfK(N_3)]	cyclo[RGDfK(4-(3-azido-propylamino)-4-oxobutanoate)]
ROI	region of interest
RT	room temperature
SAR	structure activity relationship
SD	standard deviation
SMANCS	conjugate of neocarcinostatin (NCS) and poly(styrene-co-maleic acid)
SPECT	single-photon emission computed tomography
SPIO	super paramagnetic iron oxide
SPPS	solid phase peptide synthesis
SST	Somatostatin
t-Bu	*tert*-butyl
TATE	Tyr^3-octreotate; D-Phe-c[Cys-Tyr-D-Trp-Lys-Thr-Cys]-Thr
tBu	*tert*-butyl
TEA	triethylamine
TFA	trifluoroacetic acid
THF	tetrahydrofuran
TIBS	triisobutylsilane
TLC	thin layer chromatography

TMEDA	*N*,*N*,*N*',*N*'-tetramethylethylendiamine
TMS	trimethylsilyl
TOC	Tyr^3-octreotide; D-Phe-c[Cys-Tyr-D-Trp-Lys-Thr-Cys]-Thr(ol)
TOF	time-of-flight
TRITC	tetramethylrhodamine isothiocyanate (mixed isomers)
Trp	L-tryptophan, (S)-2-amino-3-(1H-indol-3-yl)- propionic acid, W
D-Tyr	D-tyrosine, (R)-2-amino-3-(4-hydroxyphenyl)propionic acid, y
y	D-Tyr

Symbols

Å	Ångström, 10^{-10} m
Bq	Becquerel; 1 decay per second [s^{-1}]
Ci	Curie; out-dated but common unit of radioactivity, activity of 1 g $^{226}Ra \mathrel{\hat{=}} 37$ GBq
cm	centimeter
°C	degree Celcius
eV	Electronvolt: $1.602\ 176\ 53 \times 10^{-19}$ J
δ	chemical shift = $\frac{\text{precessing frequence of nucleus}}{\text{operating frequency of the magnet}}$
%ID/g	percent injected dose per gram (tissue)
G	giga, 10^9
h	hour
m	milli, 10^{-3}
M	molar
M	mega, 10^6
$\overline{M}_n$	number average molar mass: $\frac{\sum_i^i n_i \times M_i}{\sum_i^i n_i}$
M_P	peak average molar mass
$\overline{M}_w$	weight average molar mass: $\frac{\sum_i^i n_i \times M_i^2}{\sum_i^i n_i \times M_i}$
min	minute
μ	micro, 10^{-6}
n	nano, 10^{-9}

X

N	normal
$\widetilde{\nu}$	wavenumber [cm^{-1}] (IR-spectroscopy)
ppm	parts per million
K	Kelvin
kDa	kilo Dalton (1000 g/mol)
k_p^{app}	apparent propagation rate constant
S_WD	$\frac{\text{m(swollen)-m(dry)}}{\text{m(dry)}}$
t	time
T	Temperature
t_r	retention time
v/v	volume ratio
w/w	weight ratio
%wt	weight %

Terms that are written in CAPITAL LETTERS are described and explained in the glossary. Journal title abbreviations in the bibliography are taken from the *Web of Science* (*Science Citation Index*) of the *Institute for Scientific Information*.

The abbrevitations of the polymers presented in this work constitutes as follows: In the case an initiator salt has been used, the abbreviation of the respective monomer stands at first place of the polymer. The monomers that constitute the polymer chain, each followed by the subscript average number of monomer units are put in brackets which are preceded with an P for poly. The abbreviated termination reagent. Accordingly **PynOxP(MeOx$_{25}$DPOx$_5$)Pid** denotes a copolymer of 25 units of 2-methyl-2-oxazoline (MeOx) and 5 units of 2-[3-(1,3)-dioxolan-2-ylpropyl]-2-oxazoline (DPOx) that was initiated by the initiator salt of 2-(pent-4-ynyl)-2-oxazoline (PynOx) and terminated with piperidine (Pid). The numbers denominating the amount of monomers in the polymer are calculated from $[M]_0/[I]_0$. The only block copolymer synthesized in this work, **P20**, is denoted accordingly. Side chain modified polymers carry preceding to the abbreviation of the attached group or peptide a term denoting nature of attachment in superscript (^{Oxim} for the oxime ligation, ^{Triaz} for click-chemistry, ^{NCL} for native ligation).

1 Introduction

´Targeted cancer therapy is the mantra now chanted by oncologists of all types´[1].

Cancer is one of the oldest and abundant diseases of mankind. It is said that the term cancer was coined by the most famous ancient physician *Hippokrates* II of Kos (ca. 460 BC - 370 BC, Figure 1.1). At the moment, about 12.5 % of all deaths worldwide[2] and 25 % of deaths in Germany[3] are caused by various types of cancer. Despite the common use of the term 'cancer' the meaning is vague, as it stands for about 100 different malign NEOPLASIA. They originate from different cell types, differ in growth rate and aggressiveness, need different methods of treatment and result in varying survival rates. The most abundant cancers worldwide are lung cancer and stomach cancer in men, and breast and cervical cancer in women[2]. These four tumor types can also stand as examples of different ways to acquire a cancer. Unhealthy nutrition (stomach) and habits such as smoking (lung) as well as unsafe sexual practices (cervical cancer caused by human papillomavirus) and genetical predisposition (breast) are the main reasons. However, one has to be aware that in most cases there might not be one single reason for development of the disease but rather a cascade of events that trigger the fatal mutation and proliferation of cells[4]. 35% of all cancer deaths worldwide can be attributed to nine habit dependent risk factors. The most damaging are smoking (21% of cancer deaths) and alcohol consumption (5% of cancer deaths), followed by obesity, physical inactivity, low fruit and vegetable

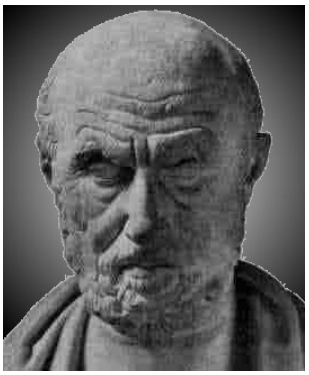

Figure 1.1: Hippokrates, often regarded as father of ´scientific´ medicine (vs. spiritualistic). He supposedly also coined the term cancer for neoplasia.

consumption, unsafe sex, urban air pollution, indoor smoke from household fuels, and contaminated injections in health care settings[5–7].

Just as the diseases are diverse (not only which cells mutated, but also how), individual treatment is recently thought to be crucial for success in various cancers[8]. This individual treatment involves identifying patient specific peculiarities and reacting upon them. Subsequent patient treatment can be specific in terms of the targeting strategy as well as the treatment strategy.

Traditional treatment of tumors involves surgical excision or systemic administration of cytotoxic substances which distribute all over the body and kill cells during mitosis (cell division). Many tumor cells are proliferating fast, thus dividing at a high rate. In this way tumors can be treated with cis-platinum, doxorubicin or other highly cytotoxic compounds. But this treatment results in a high whole body toxicity and leaves the patient with serious side effects, since not only tumor cells are attacked (e.g. loss of hair). Radiation is also widely used to destroy malignant cells. However, radiation does not discern between cells in general, which means that specific delivery is even more crucial in the case of radiation therapy. Both latter treatment strategies lack universal applicability, as various tumors are highly resistant against various chemotherapeutics or radiation.

There are a number of strategies to specifically target cancer cells. One concept is to apply polymers as carriers for moieties that serve as ´homing device´ towards the tumor. Along with the homing device, the polymer carries a pharmacological active component which eventually kills the cells. This concept goes back to Prof. *Helmut Ringsdorf* of Mainz University[9]. As homing devices, chemical structures can be used which bind specifically to tumor cells, the extracellular matrix surrounding the tumor or to blood vessels that grow into the tumor. Antibodies, small peptidic fragments or peptidomimetics can serve this purpose and all have advantages as well as disadvantages which will be discussed later. Also macromolecules themselves can exhibit a certain homing effect via the enhanced permeability and retention effect. This effect will also be explained in more detail in following chapters.

When this work was started, the aim was to develop a novel polymer carrier system for tumor-homing peptides as well as diagnostic and therapeutic radionuclides. However, poly(2-oxazoline)s might be much more versatile and could possibly be applied in a number of different biomedical applications as a highly defined, modular and biocompatible polymeric carrier system.

2 State of Knowledge

In this chapter, the underlying principles, ideas and concepts of this work are discussed. A focus is put on the biomedical background, even though the work presented is nearly purely chemical, and only in the final stages touches the biological realm. The background is discussed in more detail and to a wider scope than might seem necessary. This work is hopefully only the beginning of much more detailed and extensive work on poly(2-oxazoline)s for biomedical applications. Thus it is necessary to consider the factors that need to come together, and need to be kept in mind together for the development of polymer therapeutics for the peptide mediated radionuclide cancer therapy and other applications. These aspects include the biocompatibility and bioavailability of the polymer together with the factors that influence its pharmacokinetics and excretion pattern. Additionally, the target, which normally is, or is related to, diseased cells or tissues and its unique features and availability needs to be known and understood. Finally, after reaching the target, how can it be effectively modified or killed without creating to much havoc in the surrounding tissue or the whole organism itself? These issues and problems will be addressed in this chapter. Moreover, poly(2-oxazoline)s (POx) will be discussed as well as possible methods for effective polymer analog reactions. Finally hydrogels, another possible future biomedical application of poly(2-oxazoline)s will be mentioned.

2.1 Targeted Drug Delivery

2.1.1 Conventional and non-targeted cancer therapy

Nowadays, conventional cancer therapy mainly relies on three approaches, which are often applied in combination. Surgical excision of a primary, solid tumor, systemically administered chemotherapeutics[1] and radiation therapy[10]. Table 2.1 summarizes these therapies with some of their advantages and disadvantages. In the case of

Table 2.1: Conventional and non-targeted tumor treatment

Type of Therapy	Advantages	Disadvantages
Surgery	fast and cheap	complete removal often difficult limited applicability
Chemotherapy	broad spectrum of therapeutics and applicable tumors	often serious side effects (systemic administration)
Radiation therapy	limited side effects broad applicability	some resistant tumors, limitations for metastatic lesions

surgical removal of the tumor, it is often difficult for the surgeon to define the exact boundaries of the malignant tissue. A single remaining cancer cell can lead to relapse of the tumor, or even worse, to metastasis. The possibility for surgical excision may be also limited when the tumor tissue is within or very close to vital organs, as in the case of brain tumors.

Both remaining conventional treatment methods lack specificity. However, in modern external radiation therapies (teletherapy, *greek: tele = far/long*) the radiation beam can be adjusted so that the main effective volume of the radiation is located around the tumor. Internal radiation therapy (brachytherapy, *greek: brachy = close/short*) uses the local incorporation of radioactive materials into the tumor or its proximity.

Great efforts are undertaken in pharmaceutical research to reduce side effects and other inadequacies due to systemic administration and action of drugs such as chemotherapeutics. The optimal drug concentration (in terms of pharmacological efficiency towards the target) is often clinically/routinely not achievable, since the conventional

[1] The term ´chemotherapeutics´ in this work always refers to anti-neoplastic chemotherapeutics (cytostatics), not anti-microbials (antibiotics).

drugs distribute rapidly throughout the organism with no preference for diseased cells or tissue. Even if the mode of action of the drug has a certain degree of specificity (as seen in cytostatics), this is typically not exclusive. Chemotherapeutics interfere with cells only during mitosis. This happens either by interaction with the deoxyribonucleic acid (DNA) (e.g. alkylation, intercalation or cross-linking) to prevent replication, interference directly during mitosis (either with the microtubuli or the mitotic spindle, e.g. paclitaxel, colchicin) or important enzymes during DNA replication (e.g. topoisomerase inhibitors). Since most tumor cells replicate faster than most normal cells a certain specific toxicity is observed.
However, a number of normal cells are also rapidly dividing, including hair follicles, the intestinal epithelium and mucosae cells. This, and other cross-toxicities (e.g. cardiotoxicity of anthracyclins) leads on a regular basis to dose limitations. Recent clinical developments in administration schedules and dosage, strongly reduces side effects and increases the therapeutic effect. Although developments within conventional cancer treatment protocols is promising, it is commonly regarded as a necessity to develop more specific treatment of the various types of tumors.
Two main goals for the development of targeted drug delivery can be identified[11].

- Identification of biological targets in diseased cells which are selective for the target

- Improvement of the targeting selectivity of drugs towards specific organs, tissues or cells by means of drug formulation, administration or conjugation.

Available strategies for targeting are circumstantial targeting (aiming at general characteristics of the target cells), passive targeting and active molecular targeting. The latter two will be discussed in more detail in this chapter.

2.1.2 Targeting strategies

Although ongoing developments conventional therapeutic approaches for cancer treatment are promising, great efforts are undertaken to establish truly specific treatment of cancer. Two main approaches can be distinguished:

- **Targeting on the molecular level/ligand targeting:** Upon mutation to become cancer cells, specific features connected to these cells may form or alter. This certainly includes differences on the genetic level and the metabolism of the cells which is, in many cases, accompanied by alteration in the pattern and abundance of various cell membrane receptors.

- **Targeting on the macroscopic level:** The aforementioned changes on the molecular level result in distinct changes on the macroscopic level in solid tumors, often referred to as the tumor microenvironment. These changes include hypoxia (subnormal oxygen level), acidosis (low pH value) as well as disorganized blood vessels in tumor vicinity together with the lack of lymphatic drainage (vide infra, Chapter 2.1.2).

In addition, a further distinction of targeting strategies is important, where sometimes both modi may be used simultaneously:

- The targeting moiety itself is the therapeutic. This is currently the way most approved and commercial available compounds act (e.g. HERCEPTIN® (Trastuzumab), GLEEVEC® (Glivec, Imatinib), Iressa, Avastin)[8] with more compounds in clinical trials (e.g. cilengitide[12]) .

- The homing device serves as a carrier for a therapeutic agent, that can be a cytostatic or a radionuclide (e.g. MYLOTARG®, ZEVALIN®).

A great number of research groups are trying to utilize the various peculiarities of different types of cancer to find new, specific ways to treat cancer. *Allen*[13] recently reviewed ligand-targeted therapeutics while *Juillerat-Jeanneret* and *Schmitt*[11] discussed targeted therapy in general. They identify the aims and necessities for active drug targeting. After defining suitable targets the appropriate drug has to be attached by suitable chemistry via an adequate linker. Release of the drug (if necessary) needs to fit the delivery profile. Additionally, the complete conjugate must be stable against biotransformation and degradation during the transport to the target. In the following chapters some of these aspects will be discussed in some more detail which will lead eventually to the basis of this work; namely the use of small peptidic, tumor specific structures for tumor targeting.

Down to the basis, gene targeted therapy or targeted gene therapy

The changes cancer cells undergo to become malign typically include the deregulation of TRANSCRIPTION FACTORS, an important event for the uncontrolled proliferation of these cells[14]. Three main approaches of targeting of cancer cells on the genetic level can be identified:

- Cancer-specific introduction of gene fragments: Due to the specific delivery and/or specific expression of the gene a minimal toxicity for the organism is expected (targeted gene therapy). A therapeutic effect can be achieved in two ways.
  1) Boosting the immunogenicity of the tumor, leading to enhanced immune response of the organism against the cancer cells (introducing genes encoding e.g. cytokines)[15,16].
  2) Introducing a gene encoding an enzyme that eventually produces cytotoxic substances within the cell[17,18].

- Targeting Genes: Gene fragments, that bind to cancer specific genes are administered and are expected to bind only to the DNA of cancer cells (e.g. by triple helix formation, DNA triplexes). This alone can block transcription of the gene. In addition, radionuclides can cause damage of the DNA by e.g. double strand breaks (DSB), leading to cell death[1].

- Oncolytic Virotherapy: A virus with specificity for certain cancer cells is administered. The virus reproduces itself only in tumor cells and therefore, as typical for virus-infected cells, leads to their death.

Despite promising results of gene therapy in general, one major obstacle remains: The intact delivery of systemic administered DNA to the nuclei of cancer cells. Free DNA is very rapidly decomposed *in vivo*. To prevent this, a vector -biological or non-biological- has to be used to protect and transport the DNA. Among others, the major side effects include formation of gene-therapy derived tumors, strong immunoresponse and the stability of expression of transferred genes. Reviews on cancer specific gene therapy[14,19,20] and delivery systems[21–23] can be found in literature.

Excursion: Physiological aspects of soluble polymers in the blood stream. *Before we go into details about the blood vessels within tumor tissue, a short glance should be taken to the fate of solutes in the blood as they pass through the kidney.* RENAL *excretion is, together with the excretion via the* HEPATOBILLIARY *tract, the major way mammals can get rid of waste (other pathways include lung and skin). The processes in the liver generally involve metabolization of transported substances. In general, this is time-consuming and requires the involvement of and uptake into cells. This may lead to toxicity, if cytotoxic compounds, such as cytostatics or particle emitters are involved.*
The primary effect of the kidney, in contrast is only filtration. Here no uptake into cells is necessary. The filtration of the blood takes place in the MALPIGHIAN CORPUSCLE *(renal corpuscle) (Figure 2.1a)) of the kidney and can be separated into several steps, corresponding to the respective barriers. The Malpighian corpuscle consists of the*

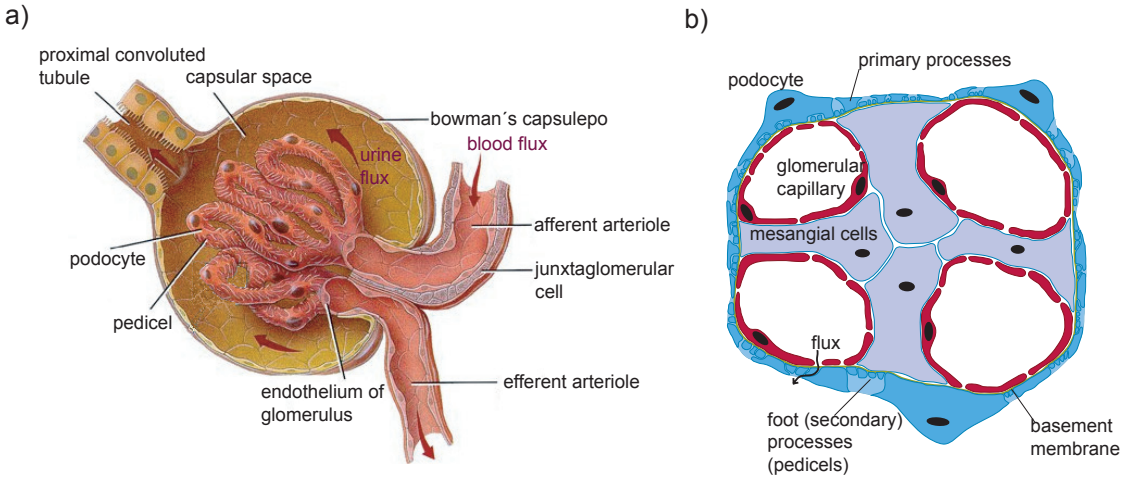

Figure 2.1: *a)Illustration of the Malpighian corpuscle (taken from[24], with modifications). b)Illustration of the glomerular filtration barrier[25].*

glomerulus and Bowman´s capsule surrounding it. The glomerular capillaries are leaky (fenestrated, vide infra, Figure 2.3) and are surrounded by the mesangial cells (important support for the capillaries) and the basement membrane. Behind this membrane (in terms of flux direction) the podocytes follow, finishing the filtration barrier as illustrated in Figure 2.1b). The blood is filtered into the capsule. The first step is filtration through the fenestrated capillaries. Here only big, cellular components of the blood or other particles (>50 - $100\,nm$, e.g. erythrocytes, lymphocytes) are restrained. Directly adjacent to the capillaries, the basement membrane (secreted by both capillaries and podocytes, thickness approx. $300\,nm$) is an effective barrier for large proteins and is believed to serve as a mechanical scaffold. As a last barrier, already on the urine side of the capsule, the podocytes are found[25, 26]. Podocytes are highly specialized cells which are mainly responsible for the restrainment of valuable

proteins in the blood stream. A vast number of extensions of first and second order (pedicels) are formed. Especially the interdigitation of the pedicels gives an effective filtration, while a high exchange area is maintained (Figure 2.2). Podocytes completely cover the outer surface of the glomerular capillaries, but between the pedicels small slits are left, through which the filtrate can pass. This slits are spanned by a thin diaphragm and are small enough to hold back proteins and polymers of a diameter of 4 - 8 nm. All these barriers are negatively charged (endothelium and podocytes on their

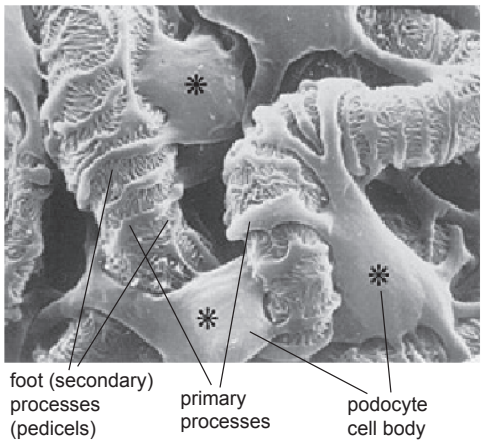

Figure 2.2: *Scanning electron micrograph of podocytes surrounding glomerular capillaries. The cell bodies (asterisks), primary and secondary processes (pedicels) can be seen (with kind approval of Prof. Witzgall, University of Regensburg)*[27].

surface, basement membrane as a structure), which leads to coulomb interaction with charged solutes. It is generally assumed that negatively charged macromolecules have a reduced filtration rate, due to coulomb repulsion[28, 29]. *However, various examples have shown that this is not necessarily the case. It has been reported that a negative charge on the macromolecules has no effect*[30], *whereas in other cases an enhanced filtration has been observed*[31–33]. *This contradicts a repulsive effect. In literature it is generally stated that polymers of a molar mass of 35 kDa and greater evade renal clearance. However, it is important to keep in mind that not the molar mass, but a combination of size, charge, shape and flexibility determines the renal filtration of macromolecules.*

After filtration, reabsorption into the blood can occur within the tubulus. Without going into detail, it has been reported that this event, again, is charge dependent and negatively charged compounds (proteins) are generally reabsorbed less then positively charged ones[34].

Size does matter - the EPR effect

In this chapter the mode of action of the majority of polymer therapeutics is described. It will focus on how the targeting of tumors is possible, while in subsequent chapters actual examples of polymer therapeutics, utilizing this mode of targeting will be discussed.

The *E*nhanced *P*ermeability and *R*etention (EPR) effect, described by *Matsumura* and *Maeda*[35] for the use of SMANCS, but also described earlier by other researchers[36–39], arises from two physiological peculiarities of tumor tissue. At the same time it can only come into effect due to the reduced filtration of macromolecules in the kidney.

The PHARMACOKINETICs and distribution of a drug is strongly dependent on the way it was administered. The compounds that are discussed in this work are to be applied intravenously (i.v.). This chapter will therefore deal with physiological aspects of polymeric compounds within the bloodstream.

Upon entering the bloodstream, solutes are distributed rapidly all over the body within 1 - 2 min, but how can they leave the bloodstream again? Small molecules can easily diffuse through the blood vessels into surrounding tissue (other than brain). This becomes increasingly restricted as the molar mass and thus, the hydrodynamic or Stokes radius increases. In order that the EPR effect can occur, the molecules must maintain a high blood pool concentration over a prolonged time. In the case of rodents, a minimum of 6 h is reported[40].

An early review of *Jain*[39] outlines the ways, how (macro-)molecules travel from the blood stream into the tumor tissue on the cellular level. The various types of blood vessels found in tumor tissue and their peculiarities and influences on tumor growth and tumor spreading are described. On the tumors perpetual quest for growth, it stimulates formation of blood vessels towards the tumor. The newly formed blood vessels are at times ill grown and do not have a tight endothelium and are leaky in consequence (*enhanced permeability*). Among others, the following types can be present (Figure 2.3):

- Non-fenestrated (continuous) capillaries: These are the common ´normal´ capillaries consisting of an intact ENDOTHELIUM which is surrounded by a BASEMENT MEMBRANE.

- Fenestrated capillaries: The endothelium shows circular openings (fenestrae) of ~ 400 - $800\,\text{Å}$ size. The basement membrane is intact. This type can be found in intestinal mucosa, glomerulus and other tissue as well as some tumor types.

- Discontinuous capillaries (sinusoids): Ill-defined vessels with large holes in both endothelium and basement membrane (might be absent altogether). Found in liver, spleen, bone marrow and various carcinomas.

- Postcapillary venules: Having weak interendothelial junctions, in tumor tissue even devoid of basement membrane. Highly permeable and sites of intravasation of cancer cells.

- Blood channels: Blood channels formed directly between tumor cells, connected to actual vessels.

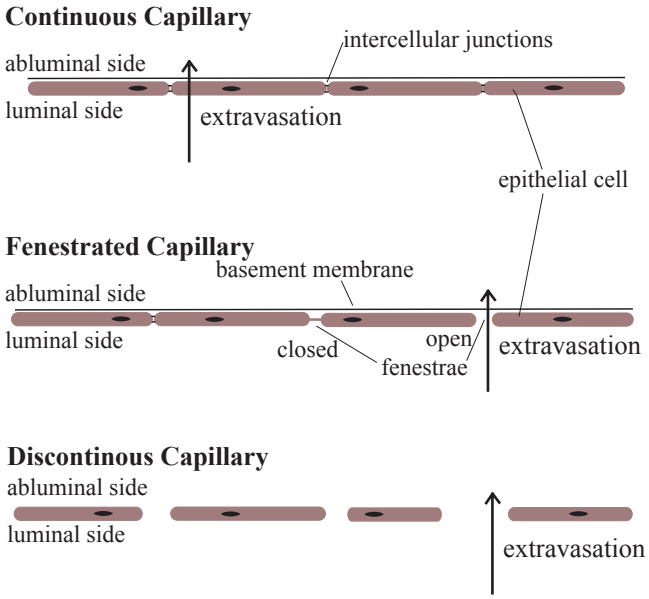

Figure 2.3: Illustration of some different types of capillary vessels. The permeability for solutes through the blood vessel increases from the continuous capillaries towards the discontinuous capillaries[39].

Jain addresses the problems to obtain comparable data for different tissues and different types of vessels. However, two trends are identified. The permeability of blood

vessels for solutes decreases with the molecular size and with increasing negative charge of the solute. While this approach is based on fluid dynamics studies and uses mathematical models for the interpretation, the approach of *Maeda* and co-workers is rather phenomenological.

In the early 1980s it was noted that in tumor bearing rats a raise in the systolic blood pressure (induced by angiotensin II infusion) significantly increased the blood flow within the tumor while leaving the blood flow in normal tissue and organs unaffected[40]. This is attributed to the ill-defined and ill-grown blood vessels found in tumors and absent regulation as it occurs in normal tissue (Figure 2.4). This increased blood flow leads to an increased concentrations of solutes in the tumor. However, only macromolecules are retained to a high degree in the tumor interstitium, while low molar mass compounds diffuse back into the blood stream as the blood pool concentration drops. One reason for prolonged retention of solutes in cancerous tissue is the lack of functioning lymphatic drainage, reducing the transport of interstitial fluid, and eventually dissolved macromolecules back to circulation (*enhanced retention*) in comparison to normal tissue (Figure 2.4). There is a variety of polymer-drug conjugates on the market or in clinical trials that utilize this effect. In literature recent reviews about the EPR effect and polymer therapeutics can be found[40–49]. While the EPR effect allows the targeting of the polymer-drug conjugate to the polymer, the bound drug remains inactive (PRODRUG concept). Neither does it diffuse throughout the body rendering deleterious side effects nor is it rapidly excreted. The size-threshold, from which the EPR effect can be observed varies from 30 to 45 kDa. Strictly speaking, it does not reflect the molar mass of the compounds, but rather the hydrodynamic radius at physiological pH.

The targeting effect with EPR is effective and has led to a number of approved cancer therapeutics. However, the targeting is rather slow. This may arise problems for the application in radionuclide therapy, since prolonged whole-body exposure of cytotoxic radionuclides could lead to serious side effects. Thus, a more rapid - *active* - targeting is needed. This can be achieved by specific 'homing' molecules that target structures which are only, or predominately present on, or in the vicinity of cancer cells.

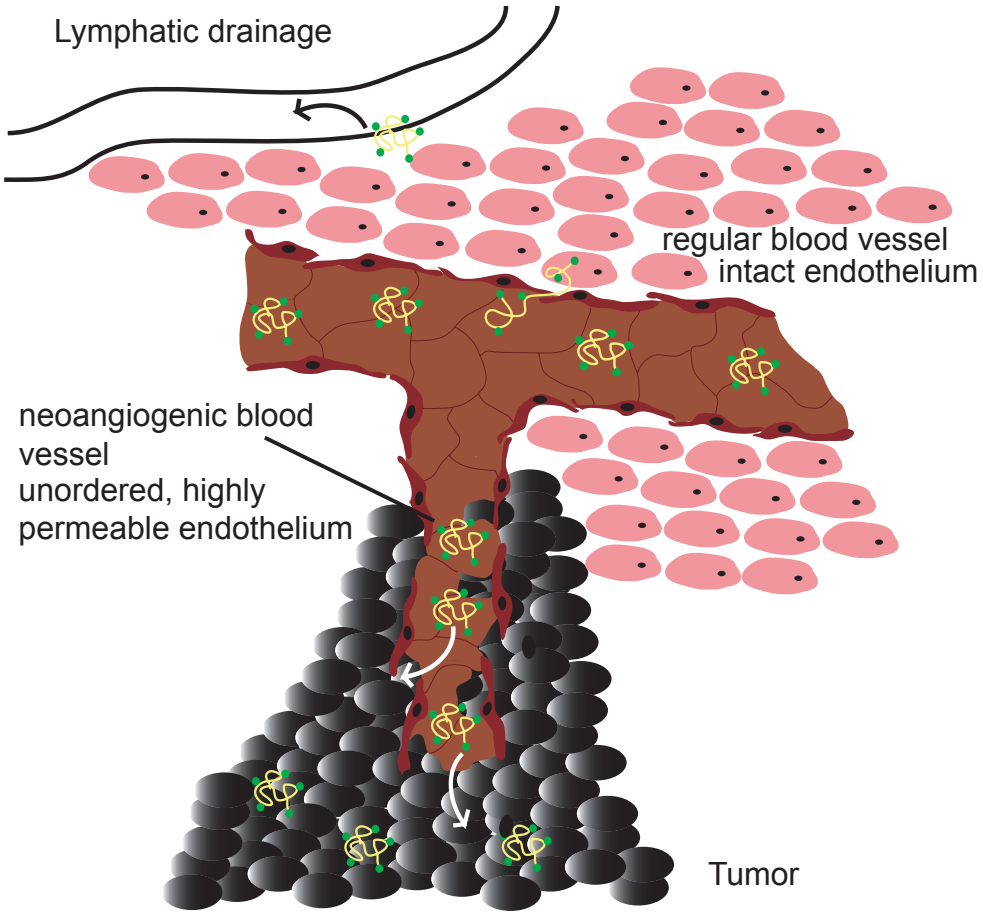

Figure 2.4: Illustration of the ENHANCED PERMEATION AND RETENTION EFFECT. Macromolecules are hindered to leave the bloodstream when the endothelium is intact. Tumor-associated blood vessels, however, are ill-grown and leaky so that large molecules can escape from circulation. Due to the absent lymphatic drainage in tumor tissue macromolecules can remain there for a prolonged period of time in comparison to normal tissue.

Ligand targeted therapeutics (LTT´s)

In this section the major targeting mode actively targeted drugs will be discussed, the binding of ligands to cancer specific receptors (or other cancer related structures). There are some basic considerations that are important to identify suitable targets, ligands, drugs and combinations thereof[13].

Target The targets are typically cell membrane receptors of cancer cells or tumor associated cells (mostly tumor vasculature) or, other types of ANTIGENs (expressed factors, like growth factors, enzymes and alike). The homogeneity and density of target expression is of considerable importance. The density should be high, especially in comparison to normal tissue. If the targets are not found uniformly distributed throughout the tumor, not all parts might be accessible for the treatment (depending on the applied method). Additionally, depending on the drug, it might be of interest if cell membrane receptor are internalized (ENDOCYTOSIS) or not. Cytotoxic drugs that are covalently bound to the homing motif, normally need to be released to become active. This typically happens by hydrolysis at lowered pH (e.g. in endosomes/lysosomes) or by enzymatic cleavage in lysosomes. This requires internalization of the ligand-receptor complex. In contrast, internalization is not necessary if radionuclides (other than auger-electron emitters) are applied and it might be even disadvantageous, as in the case of antibody-directed enzyme prodrug therapy, ADEPT[50].

Ligand The ligands used in LTT can be peptides, peptidomimetics, non-peptide receptor ligands (e.g. folic acid (vitamin B_9), (oligo-)saccharides), antibodies or antibody fragments or the recently developed APTAMERS[51,52]. A list of compounds used as LTTs can be found in a review by *Allen*[13]. Peptides and peptidomimetics are often relatively easy available and comparably stable, both on the shelf and *in vivo*. Molecular modeling can be applied for the design and improvement of structures. Cyclic structures and non-degradable motifs (e.g. non-natural amino acids) may lead to increased binding strength and stability and/or increased *in vivo* half-life. Typically limited or no immunogenicity must be expected. Antibodies generally show high AFFINITY or AVIDITY and specificity. Tissue specific antibodies (or fragments) or smaller peptides can be obtained by a relatively new

method, the PHAGE-DISPLAY TECHNOLOGY[53–55]. These can be, as mentioned above, therapeutic themselves (Herceptin) and/or serve as carriers for cytotoxic drugs or nuclides (Zevalin). Despite their high selectivity and activity, clinical approval is often hampered by immunogenicity, sometimes even if humanized or fully human antibodies are applied[2]. Additionally, high costs, difficult production and limited storage time can be problems related to antibody or antibody fragment based therapeutics.

Addressing the binding affinity or avidity of the ligands to their targets, it is worth mentioning that an improvement of binding strength is not always beneficial. If the target is universally present in the organism this may lead to an increased co-localization in other organs. There is also evidence that very high binding constants can sometimes lead to a 'binding-site barrier'. Administered ligands bind to the first encountered targets and do not diffuse deeper into a solid tumor. This can leave a major part of a tumor lesion unaffected, impairing an effective treatment of the cancer. However, in the case of well accessible targets like tumor vasculature, metastases or haematological malignancies, a high affinity or avidity is normally desirable.
When choosing the drug, again several aspects should be considered. Most importantly, the release of the drug[3] should match the pharmacokinetic profile of the ligand-drug conjugate. Depending on the homogeneity of the target tissue the drugs (homo- or heterogeneous solid tumor, metastases or haematological malignancies) can, should cause or avoid a BYSTANDER EFFECT.
A selection of LTTs is depicted in Figure 2.5. Radioimmunotherapeutics (RAIT, Figure 2.5d) are constructs of tissue selective antibodies or fragments thereof with therapeutic radionuclides (vide infra, Chapter 2.4). Immunotoxins are internalizing ligands which carry potent toxins like diphtheria toxin or ricin [4]. In contrast to the typical chemotherapeutics, these toxins are not restricted to mitosis in their action. However, despite some examples of approved compounds[5] and others in clinical trials, this type of therapeutic often produces problems like immunogenicity, whole body toxicity and displays limited effectiveness.

[2] see the dramatic failure of phase I trials of TNG1412[56]
[3] e.g. diffusion out of liposomes/micelles, half life of radionuclies or cleavage of hydrolyseable linkers
[4] while immunoconjugates carry cytostatics
[5] Ontak, denileukin diftitox, an interleukin-2-diphtheria toxin fusion protein and Mylotarg, a humanized anti-CD33 calicheamicin conjugate

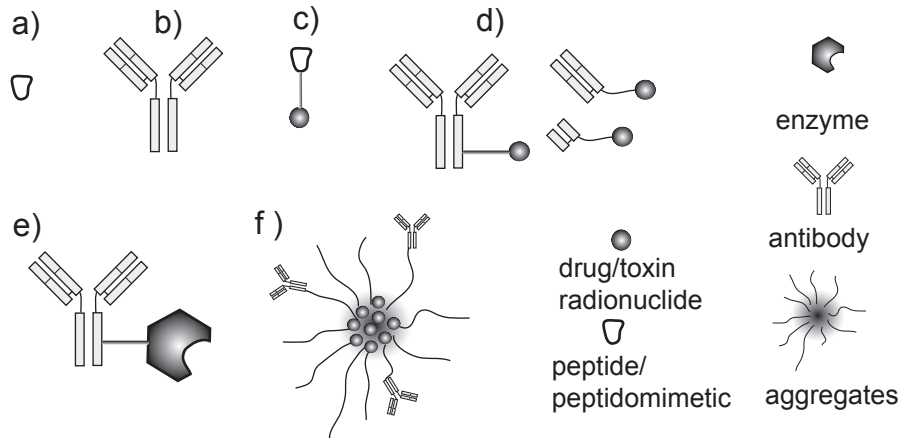

Figure 2.5: Examples of LTTs. Active small molecules a) antibodies b) or small drug conjugates. d) Radiolabeled antibodies or antibody fragments for RAIT. e) Antibody enzyme constructs for ADEPT and f) targeted aggregates carrying drugs.

Antibody-directed enzyme prodrug therapy (ADEPT) is a two step approach where an antibody (attached to an enzyme, Figure 2.5e) is the targeting device. After clearance of unbound antibody from the organism, a prodrug is administered, which is converted into a toxic compound by the enzyme.
Among other drawbacks, the risk of immunogenicity often drastically limits the applicability of these constructs.
A major mechanism leading to an immune response is recognition of short peptidic fragments of 8 -24 amino acids unknown to the body. This is impossible in the case of peptidomimetics which do not consist of amino acids[6]. Similarly, short peptides that can be used for targeting, often do not provoke an immune response. This can be partly contributed to the use of small cycles or non-natural amino acids preventing degradation by peptidases and therefore presentation to the immune system. In the following section, the use of some peptide receptors as targets, the respective ligands (peptides or peptidomimetics) and their use in peptide receptor (mediated) radionuclide therapy (PRRT) will be discussed in more detail.

[6]unless the formation of immunogenic haptens occurs

2.1.3 Summary

Despite important improvements in conventional cancer therapy, it is generally agreed that it is important to develop more cancer specific, targeted treatment methods. The aim is to interact specifically with cancer cells or cancer related tissue, e.g. the tumor vascularity. This interaction can take place on the genetic level (Chapter 2.1.2) or the macroscopic level, utilizing the defect vascularity of solid tumors (Chapter 2.1.2). Additionally, the targeting of specific structures, typically peptides or proteins on cell surfaces is under investigation. The targeting can be carried out by antibodies or their fragments, oligonucleotides (aptamers), peptides or peptidomimetics.
While the genetic approach still struggles with problems of the delivery of gene fragments *in vivo*, the EPR effect has proven its efficacy in a number of cases. However, its applicability is limited to solid tumors and the targeting needs time to come into effect. This normally will exclude radionuclide therapy, where rapid targeting is crucial. Targeting with antibodies can be fast and effective, however, severe restriction like immunogenicity often apply. Small molecules, like peptides or peptidomimetics often lack immunogenicity but sometimes also the antibodies' selectivity and affinity/avidity.

2.2 Peptide receptor mediated radionuclide therapy

In this chapter the peptide receptor mediated radionuclide therapy (PRRT) (and imaging/diagnosis (PRI)) will be discussed. Excursions into various peptide receptors, the actual targets, suitable nuclides and possibilities of their incorporation will be undertaken.
After current PRRT is discussed, some recent examples and the effect of multimerization of cell-recognizing motifs for enhanced avidity towards the target cells will be summarized.

2.2.1 Peptide receptors as targets

As discussed in the previous chapter, cell membrane associated proteins are an important group of targets for cancer specific homing devices, such as antibodies or peptides. Among these proteins, cell membrane receptors play a major role. They are important structures for communication of cells among each other (cell-cell recognition/interaction), within an organism (e.g. via hormone receptors or cell-matrix recognition) and even between organisms and their surroundings (via pheromones). Development of the phage display technology introduced a powerful technique to find and exploit such peptide binding targets in pathological tissue[57]. In the following sections some cell-membrane receptors relevant in this work, their targeting and applicability in PRRT will be discussed.

Integrins and RGD´s; a versatile ligand-receptor pair

In the early 1980s, the tripeptide sequence arginine-glycine-aspartic acid (RGD) was found to be responsible for the attachment of cells to FIBRONECTIN by *Pierschbacher* and *Ruoslahti*[58,59]. Other RGD recognition sites in ECM proteins and elsewhere where found soon[60–62].

The integrin receptor family (Figure 2.6 is of great importance in cell-cell and cell-matrix communication[63,64]). Integrins are heterodimeric transmembrane glycoproteins that consist of non-covalent bound α- and β-subunits, and the binding of the integrins to their ligands depends on divalent cations. To date, 18 α- and 8 β-subunits are known, forming 24 different distinct integrin heterodimers, some of which exist in various splicing[7] and glycosylation/activation variations. Furthermore, 6 α- and 1 β-subunits have been identified on the genetic level during the human genome project, but these remain to be unknown as actually expressed proteins[66]. As can be seen in Figure 2.6 half of the β-subunits form integrins with a number of different α-subunits with affinities to different ligands[65,67,68]. In contrast, most of α-chains

[7] especially of the cytosolic domain

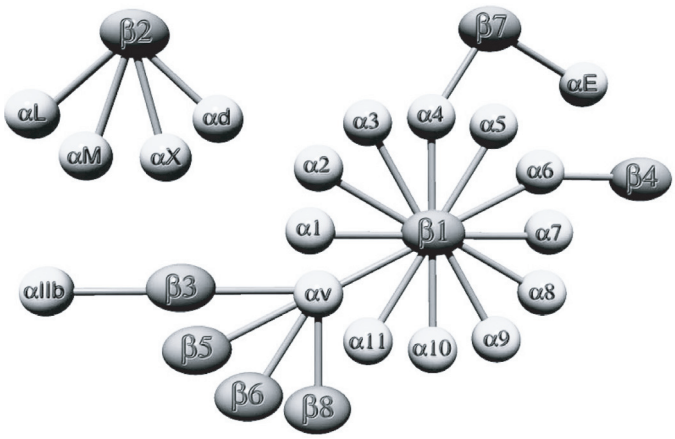

Figure 2.6: Classes of integrin receptors (taken from *Hynes*[65]).

dimerize exclusively with one β-chain. Several research groups reported that integrins are often concentrated in so-called LIPID RAFTS[69–72] and also control the distribution and internalization of these rafts. This, in turn, could modulate a number of other cellular signaling pathways, since they are affected by lipid rafts[73]. Interestingly, the effect of ligand binding can be different if the respective integrin is located in a lipid raft or on 'normal' plasma membrane surface as reported for $\alpha_6\beta_4$[71].

Integrins are the most important receptors for the attachment of the cells within the ECM (in particular the β_1 subfamily). Hereby, they 'integrate' the cytoskeleton via the actin stress fibers through focal adhesion complexes to the various peptides of the ECM, including fibronectin, collagen, laminin and others[65,67,68]. At the same time, the affinity of integrins is modulated by the mechanical force applied[74,75]. The integrins serve important purposes via *inside-out* and *outside-in* signaling and cell-cell recognition (particularly β_2 subfamily)[63,68]. Among others aspects, the integrin family is important for the regulation of embryogenesis, cell migration (e.g. T cells of the immune system[69]), cell cycle progression, apoptosis and gene expression. One can imagine the integrins as an integral part of a complex system of receptors to signal the cells if they are in the appropriate surrounding, thus crucial for any multicellular organism. This also explains the ubiquitous occurance of integrins in the animal kingdom. Correct cell location is important building up organs and tissues, but also for migratory cells this is an important aspect. Here T-cells of the immune system[69] and thrombocytes (platelets) can be mentioned. Both cell types need interaction with

integrins for functioning. Thrombocytes are activated by binding of their $\alpha_{IIb}\beta_3$ integrin to thrombin and/or collagen whereupon the platelets can bind to fibrinogen and other coagulation factors[68] which, eventually leads to vessel wall adhesion, platelet aggregation and thus, hemostasis.

In stationary cells, alteration or bypassing of integrin-associated processes uncontrolled cell growth and migration can occur, two important and characteristic features of cancer[70]. Their importance, especially for the physical attachment of the cell to its surroundings is reflected by the number of receptors that can be found on cells. *Akiyama* et al.[76] found an average of 130,000 fibronectin binding sites on baby hamster kidney cells, later identified as integrins. However, this number varies strongly, e.g. with receptor subtype, cell type, or during the cell cycle.

Interaction of integrins with their respective ligands are relatively weak. With dissociation constants (K_D) of 10^{-6} to 10^{-8} mol/L they have a much lower affinity than, e.g. hormone receptors with K_D values of 10^{-9} to 10^{-11} mol/L. However, interaction of hundreds or thousands of integrins with binding sites on the ECM dramatically increases the overall avidity[77] and is eventually sufficient to strongly bind cells to their surrounding[68]. The necessity of relatively low affinity can be explained in the context of migrating cells. The binding of integrins to e.g. lymphocytes and the blood stream at the site of an inflammation is not supposed to be permanent. Only transition of the lymphocytes through the endothelium into the inflamed tissue is intended and high affinity binding is disadvantageous in this case.

As already mentioned, integrins play a major role in cell proliferation, migration and thus, also in metastasis of cancer cells[78]. Hence, some subtypes are closely related with malignant diseases. However, no general trend can be observed for the different integrin subtypes in malignant tissue. While some subtypes are up-regulated, others are down-regulated. In some cases contradictory reports regarding the same subtype and the same cell type can be found. *Gilcrease* very recently reviewed this complex issue in a short but comprehensible way[64]. The integrin $\alpha_v\beta_3$ has been found to be overexpressed on vascular endothelium of blood vessels that grow into the tumor (neoangiogenic vessels) as well as on several cancer cells themselves. Therefore targeting of the integrin $\alpha_v\beta_3$ is targeting of the tumor.

Arg-Gly-Asp, an important ligand of integrins: As already stated above, the tripeptide sequence Arg-Gly-Asp (RGD) is recognized by a number of integrins including $\alpha_v\beta_3$[79,80], although not exclusively[81,82]. When used in cancer treatment, the peptide sequence itself can be active, showing antiangiogenic and antimetastatic effects[82–84] and, in addition or alternatively, can be used as homing device to carry cytotoxic drugs[85–87], therapeutic siRNA[88] , radioactivity[88–92] and boron (for boron neutron capture therapy, BNCT)[93] to the tumor or its vasculature (Figure 2.7). By now, all different types of carriers have been functionalized with the RGD motif: Liposomes[93], viruses[94], antibodies[95], nanoparticles[96,97], quantum dots[98] and polymers[99,100] have been coupled to RGD and some of the constructs have been evaluated in respect to their affinity/avidity to integrin and integrin positive cells. Confinement of the RGD sequence into a cycle alters its selectivity for the various integrin subtypes. Two structures proved to bind with high affinity and high selectivity to the $\alpha_v\beta_3$ subtype. Cyclo[RGDfX][104] (where X can be e.g. V or K) being monocyclic and RGD4C (A[CD[CRGDC]FC]G)[105] consisting of two cycles formed by disulfide formation. Cilengitide (c[RGDf-*N*(Me)-V], Figure 2.8a), where the cycle is constraint further by *N*-methylation of the valine residue, was developed by our cooperation partners in the group of Prof. *Kessler* and shows affinity in the subnanomolar range for $\alpha_v\beta_3$[106]. It is currently in phase II clinical trials for the treatment of various cancers[12]. The derivative containing a lysine residue (c(RGDfK)[107]) shows still high affinity and is an ideal candidate for chemical modification, like attachment of drugs[87] and pharmacokinetic modifiers like sugar moieties[108,109] (Figure 2.8b) via the ϵ-amino group of lysine. Galacto-RGD labeled with ^{18}F shows high metabolic stability *in vivo*, very favorable pharmacokinetics, good tumor uptake and is a good candidate to become an *in vivo* marker for the quantitative evaluation of $\alpha_v\beta_3$ expression levels[109–111]. c[RGDfE] was used to produce defined oligomeric structures (Figure 2.8c)[89] that were radiolabeled and evaluated *in vivo*[101]. RGD4C has been discovered by the phage display technique. Similar to c[RGDfX] it has been used to target drugs. Since it consists only of natural amino acids it can be introduced by recombinant means into peptides. However, the same reason accounts for a higher degradability by proteases and the reversible disulfide bridges allow linear as well as alternative mono- and bicyclic structures which have decreased binding affinity[112].

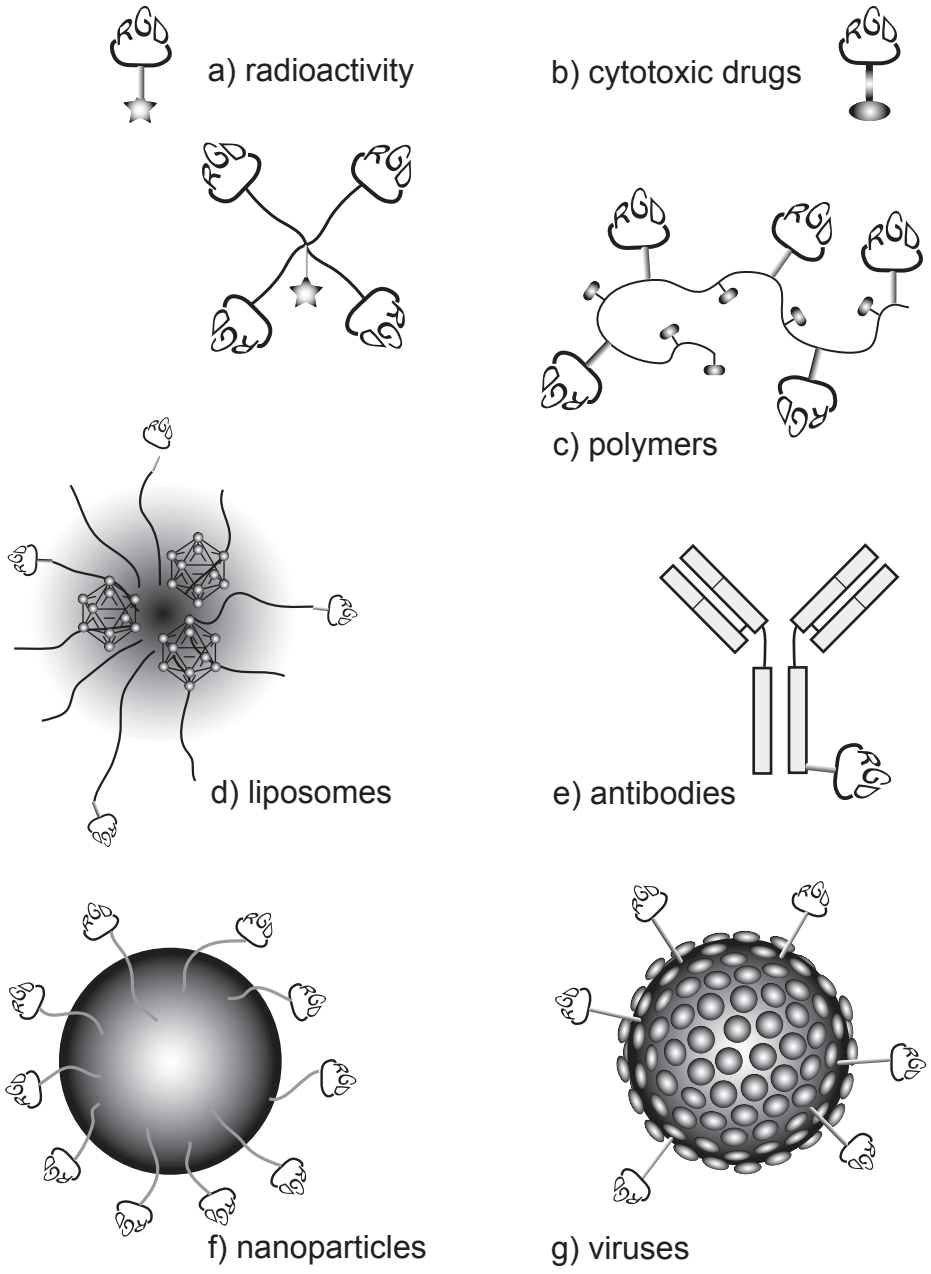

Figure 2.7: Schematic representation of various examples of RGD peptide conjugates for targeting cancer tissue or vasculature and delivery of bioactive substances: a) radionuclides[101] b) conjugates with cytostatics like doxorubicin or paclitaxel[86,87] c) polymers carrying drugs or nuclides simultaneously[42,100] d) liposomes or micelles carrying RGD peptides on their periphery and bioactive compounds (e.g. boron for BNCT[93] or doxorubicin[102]) in the interior e) antibodies[95] f) nanoparticles[96,103] g) virus shell proteins[94].

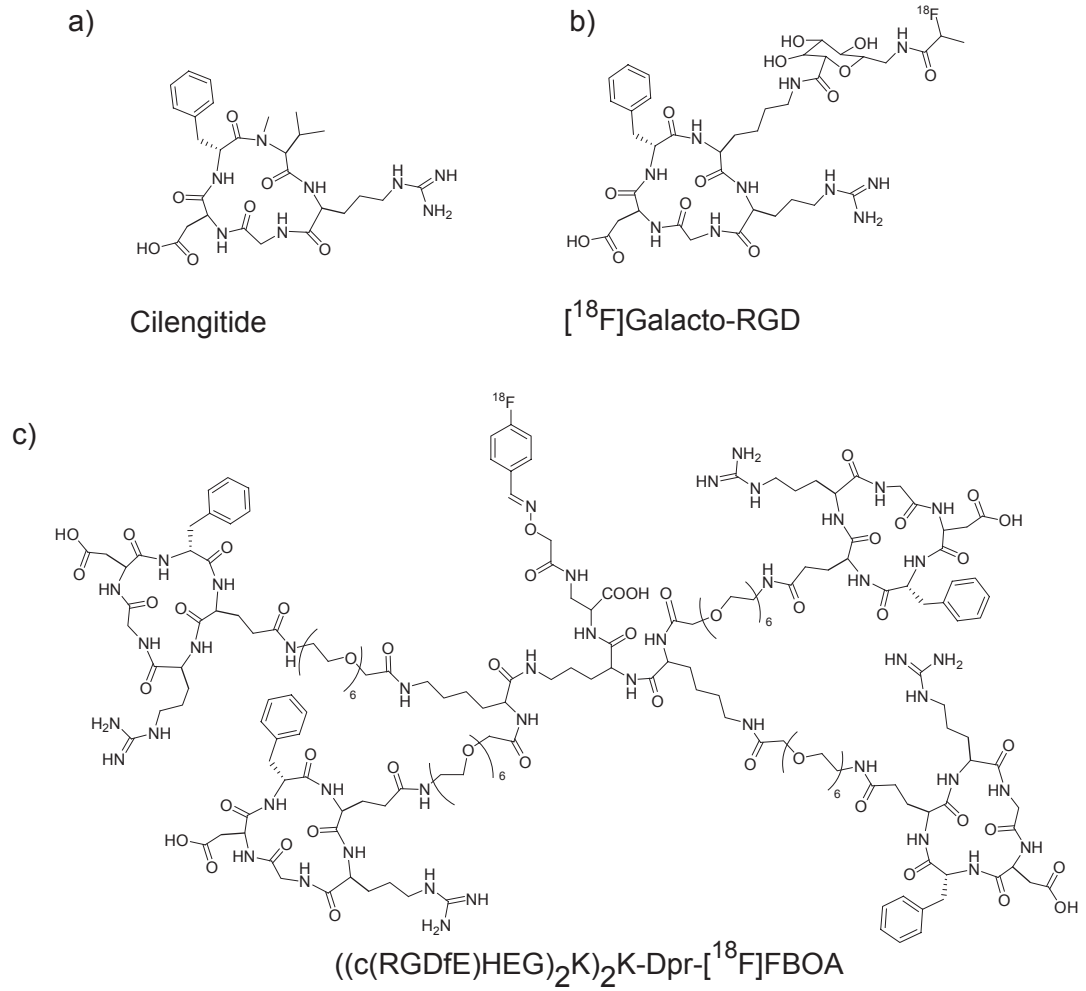

Figure 2.8: Structures of some cyclic RGD peptides developed for targeted cancer therapy.

Affinity of the RGD constructs towards the different receptors is an important feature to be assessed. However, the attachment/detachment of cells to/from a substrate, in which the integrins play an important role, is not necessarily reflected by the affinities of the substrate immobilized RGD peptides involved. Despite of a plethora of studies[113] that tried to shed light on this complex, considerable nescience remains about structure activity relationships (SAR). The same problem accounts for soluble RGDs and RGD oligo- and multimers. For example, *Hersel*[67] describes the decrease of IC_{50} values (concentration of half-maximum inhibition) for the binding of vitronectin of c(RGDfE)-derivatives in the order monomer > dimer > tetramer > oktamer (WM164 melanoma cells). However, the very same peptide, oligomerized via a different spacer showed the affinity order of monomer > tetramer > dimer, albeit in a different essay[114]. The authors suggest that steric hindrance in the case of the tetramer may diminish binding avidity[114]. The depth of the binding 'pocket' should play no major role in the case of $\alpha_v\beta_3$ since it has been shown to be only a couple of Ångströms deep[79, 80]. It is not clear if the different experimental setup or the different nature of the spacer (length, hydrophilicity, flexibility) or both is responsible. Even more puzzling is the fact that the ability of the RGD mono- and oligomers to detach cells from a vitronectin-substrate does not correspond with the affinity of the respective compounds to the receptors[67, 114]. The interaction of RGD multimers with their receptors is yet not fully understood. Contributions to the binding like the entropy term, which will be less favorable in the case of long flexible spacers do not help to ease understanding. In general, it must be also kept in mind that inhibition of cell attachment by RGD peptides strongly depends on the cells used in the setup.

Despite these hiatuses in the knowledge about the complex integrin-RGD interactions, the RGD motif is a very promising candidate to target tumors and their vasculature, alone, as carrier for drugs or in combination with other cell targeting peptide sequences[115]. Additionally, there are several other peptide/receptor pairs which are evaluated for their use in targeted therapy. One of the most intriguing is the somatostatin receptor and synthetic somatostatin analogues.

Somatostatin, its receptor and analogs

Somatostatin (SST) is a neuropeptide (hormone) which plays an important role in a wide range of functions of living organisms, ranging from all vertebrates to even primitive invertebrates[116]. It has regulatory function in proliferation in general and intervenes in processes of the gastrointestinal tract and in the pancreas. Furthermore, it inhibits activated cells of the immune system and acts as a stimulatory and inhibitory neurotransmitter in the central nervous system[117].
Somatostatin occurs predominantly in two biological active forms, SST14 and SST28. Both act on a family of receptors, the somatostatin receptors 1 - 5 ($hsstr_1$ - $hsstr_5$). These receptors consist of 7 α-helical transmembrane domains and are so-called G-PROTEIN coupled receptors (GPCR). GPCR are numerous and approximately 50 % of pharmaceuticals actually target this type of receptor[118]. As typical for GPCRs, $hsstr_x$ are of utmost importance for regulatory cellular processes, which is underlined by the very high degree of conservation of this receptor type across the species. Besides $hsstr_1$ all $hsstr_x$ can, but do not necessarily, internalize upon binding of a ligand[119–125]. In a number of cases it also has been observed that after receptor-agonist binding homo- and heterodimerization of $hsstr_x$ occurs, followed by internalization. This may be of special interest for the design of SST analog oligo- and multimers. The spacing of the binding sites in these dimers has been reported to range between 50 and 60 Å[126–128]. $Hsstr_x$ are found in the central nervous system and endocrine tissues. However, while $hsstr_x$ appear in the NEUROENDOCRINE system with a rather low density, they are overexpressed on a variety of human tumors[129–133]. Native SST is of little use as a therapeutic. It has a very short serum stability with a plasma half-life of only 1 min. Consequently, a number of somatostatin analogs (AGONISTS and ANTAGONISTS, peptides and peptidomimetics[134]) have been synthesized and evaluated in terms of their stability, binding capacity to the various $hsstr_x$, and feasibility for therapeutic and diagnostic use in various diseases[116,135–137]. The primary structure of some of these peptides and their affinities for the receptor subtypes are listed in Table 2.2. A number of these SST analogs are investigated for the delivery of diagnostic and therapeutic radionuclides to various tumors[140]. Further modification with sugar moieties results in changed *in vitro* and *in vivo* behavior of SST analogs similar as in the case of RGDs[139,141–143].

Table 2.2: The primary structure and affinities towards the hsstr-subtypes of the two natural SST and selected synthetic analogs[135, 137–139]. Amino acids in bold belong to the binding sequence.

Name	Structure	IC_{50} (nM)	
SST-28	Ser-Ala-Asn-Ser-Asn-Pro-Ala-Met-Ala-Pro-Arg	SST14	SST28
	Glu-Arg-Lys-Ala-Gly-Cys-Lys-Asn-Phe-**Phe**-**Trp**-**Lys**	sst_1 1.1	2.2
	SST-14: Cys-Ser-Thr-Phe-**Thr**	sst_2 1.3	4.1
		sst_3 1.6	6.1
		sst_4 0.53	1.1
		sst_5 0.9	0.07
SMS 201-995 octreotide (OC)	DPhe-Cys-**Phe**-**DTrp**-**Lys**-Thr(ol)-Cys-**Thr**	sst_1	>1000
		sst_2	2.1
		sst_3	4.4
		sst_4	>1000
		sst_5	5.6
BIM23014 lanreotide	DβNal-Cys-**Tyr**-**DTrp**-**Lys**-Thr-Cys-**Val**	sst_1	>1000
		sst_2	1.8
		sst_3	43
		sst_4	66
		sst_5	0.62
RC-160 vapreotide	DPhe-Cys-**Tyr**-**DTrp**-**Lys**-Trp-Cys-**Val**	sst_1	>1000
		sst_2	5.4
		sst_3	31
		sst_4	45
		sst_5	0.7
sst3-ODN-8	NH_2-CO-DCys-Phe-**Tyr**-N(CH$_3$)-CH(naphthyl)-CO-**Lys**-Cys-Phe-**Thr**	sst_1	>1000
		sst_2	>1000
		sst_3	8.6
		sst_4	>1000
		sst_5	>1000
Tyr^3-Thr^8-octreotide (TATE)	DTPA-DPhe-Cys-**Tyr**-**DTrp**-**Lys**-Thr-Cys-**Thr**	sst_1	>1000
		sst_2	1.3
		sst_3	>1000
		sst_4	>1000
		sst_5	>1000

Potential use of hsstr$_x$ is not restricted to target tumor cells. It has been found that various hsstr subtypes are expressed on proliferating endothelial cells[116,144]. Consequentially, the octapeptide D-Phe-c(Cys-Phe-D-Trp-Lys-Thr-Cys)-Thr(ol) (octreotide) has been found to inhibit angiogenesis[136] similar to the RGD motif. In fact, the inhibition of tumor growth by SST agonists may caused directly by hsstr on tumor cells or by suppression of growth factors. The role of SST analogues in cellular proliferation, tumor growth and angiogenesis has been recently reviewed[116,145]. Although the potential of SST analogues as anti-angiogenic drugs and for targeted therapy is not yet fully established, it is clear that the hsstr$_x$ family is an interesting target. Several other targets are discussed for specific delivery of drugs[13,140]. Additionally, a beneficial effect of combination of RGD and SST analog has been described recently[115,146] which is of great interest for a polymer therapeutic approach.

Melanocortin receptors and α-MSH

The melanocortins are a group of structurally related proteins which are formed from proopiomelanocortin by proteolysis. This group includes the adrenocorticotropic hormone (ACTH) and the melanocyte stimulating hormones (MSH, subtypes α, β and γ). In this section, α-MSH, its receptors and potential biomedical applications will be discussed shortly[147–151].

The melanocortin receptors (hMCxR, x = 1 - 5) are another example of seven-transmembrane domain GPCR. They play an important regulative role in a great number of processes, including feeding behavior (hMC3R and hMC4R)[147], tanning (hMC1R[152]), sexual function (hMC2R/hMC4R), immune response (hMC2R) and development of cancer (hMC1R/hMC4R, e.g. melanoma[153–155], pancreatic[156]). Similar to hsstr$_x$, hMC1R may dimerize[157][8] and be internalized upon ligand binding[158]. In comparison to the integrins, the number of these hormone receptors on cancer cells is limited with approximately 900 to 5700 receptors per melanoma cell[159].

ACTH and the MSHs all bind to hMC1R and hMCR 3 - 5 with variable affinities, while ACTH is the only natural ligand of high affinity for hMC2R (Table 2.3). Common to the four melanocortins is the four amino acid core sequence His-Phe-Arg-Trp which

[8] Please note: These dimers are already formed inside the cell, due to mutations, not on the plasma membrane after ligand binding as is the case for hsstr$_x$.

was identified as the minimal binding sequence[160, 161]. Table 2.3 also shows that the

Table 2.3: The melanocortin receptor family: Subtypes, natural ligands and function[162].

Subtype	Agonists and order of their affinity	Function
hMC1R	α-MSH = ACTH > β-MSH > γ-MSH	pigmentation
hMC2R	ACTH	steroid production, inflammation control
hMC3R	α-MSH = β-MSH = γ-MSH = ACTH	ingestion
hMC4R	α-MSH = ACTH > β-MSH > γ-MSH	ingestion, erectile activity
hMC5R	α-MSH > ACTH > β-MSH > γ-MSH	lipid secretion in tallow glands

various MSH peptides are not specific towards the various receptor subtypes (besides non-binding to hMC2R). In order to develop therapeutics based on interaction with hMCxR, it is important to have access to highly selective agonists or antagonists of high affinity. Accordingly, various investigators developed a number of potent synthetic agonists and antagonists with limited selectivity for the various subtypes like NDP-α-MSH (hMC4R)[163, 164], melanotan II (MTII) (hMC1R)[165], SHU9919 (hMCxR, x $\neq$ 2)[166] or HS401 (hMC1R)[167] by variation of the amino acids and/or the cyclic structure. Furthermore, current studies concentrate on *N*-methylation of amino acids[162] or di- or oligomerization[154] to increase selectivity or affinity, respectively. Just as RGD and SST-analogs, MSH-analogs are developed as therapeutics themselves, as well as carriers for therapeutic or diagnostic agents (Chapter 2.2.3).

CREKA, unknown target but effective homing

Very recently, *Ruoslahti* and co-workers[168] found a new tumor-homing peptide by phage-display technique. The short, linear sequence CREKA was identified to bind to breast cancer tissue. The peptide, as well as CREKA coated super paramagnetic iron oxide (SPIO) nanoparticles and liposomes (Figure 2.9) were found to accumulate in

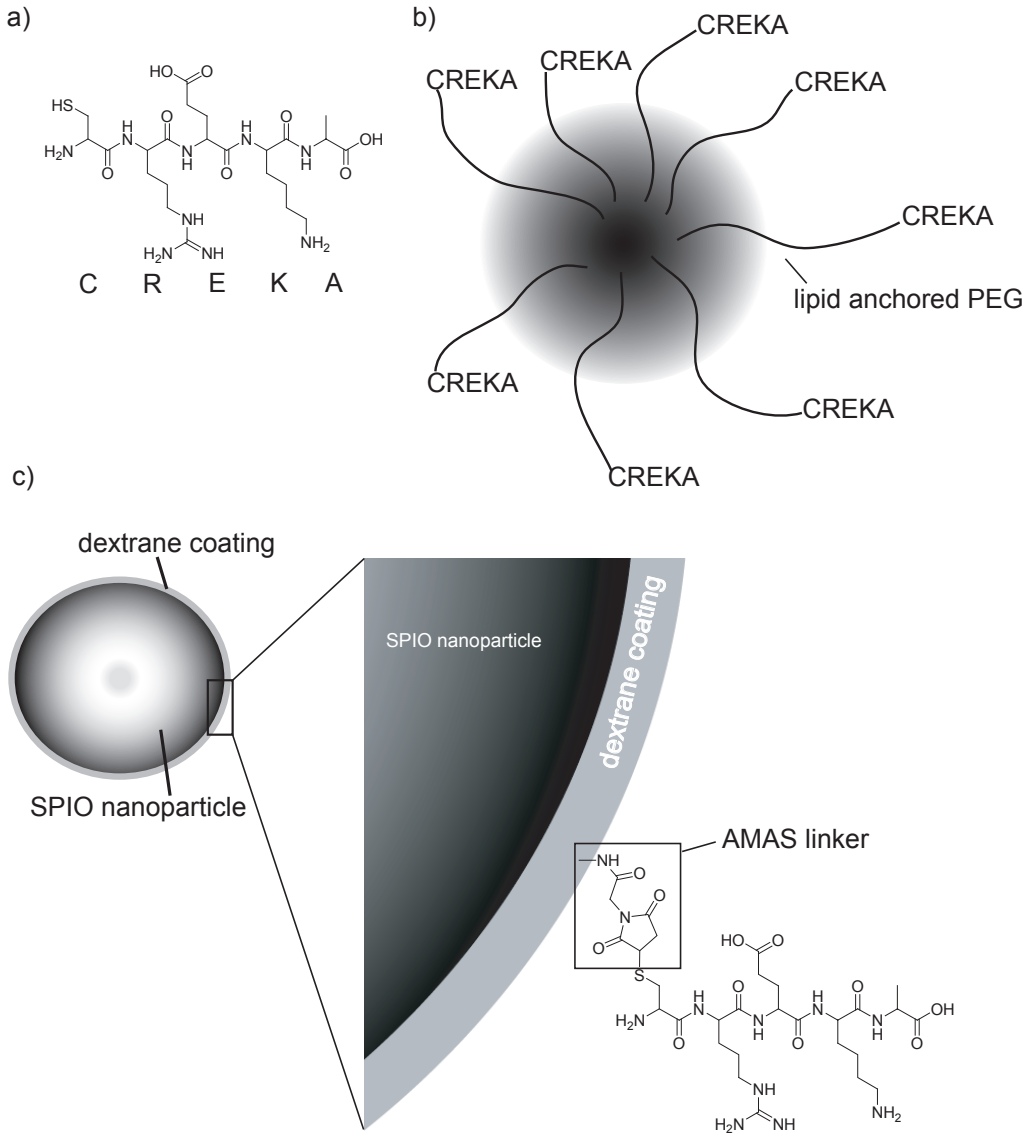

Figure 2.9: Structures of CREKA a), CREKA conjugated liposomes b) and super paramagnetic nanoparticles c). The nanoparticles are coated with a matrix of aminodextran and CREKA is attached to the amino groups via a linker (*N*-(a-maleimidoacetoxy) succinimide ester, AMAS).

tumor associated blood vessels, or more accurately, to clotted plasma proteins therein. The authors report a self-amplification of the homing effect to the tumors. Although the exact nature of the target CREKA remains unknown, evidence suggests that it binds to fibrin and/or fibrinogen which is present in the tumor vasculature. It was observed that both CREKA conjugated liposomes and nanoparticles are able to induce blood-clotting which, in turn, enhances binding of the conjugates. However, it has to be noted, that without appropriate pre-treatment of the mice[9], significant accumulation, especially of the SPIOs in tissues of the RETICULOENDOTHELIAL SYSTEM (RES) was observed. This might severely hamper application of such compounds in patients.

A number of other peptide receptors are currently evaluated in terms of their viability for targeted drug delivery. They are not discussed here, since they are not within the scope of this work. However, for PRRT in general they are intensely studied and in some cases even polymer conjugates already investigated[169–173]. Additionally other receptors, as the folate receptor are a subject of interest, as a great number of tumors actually overexpress this receptor[174,175].

2.2.2 Suitable radionuclides and chelators

After identifying suitable targets, this chapter will deal with the radionuclides which can be used for diagnosis and/or therapy when incorporated into peptides or peptide conjugates. The basal considerations if a nuclide is suitable for the use in nuclear medicine (diagnosis and therapy) include:

- **Physical properties of the isotope** like (physical) half-life, nature and characteristics of daughter nuclides as well as the nature and energy of the emitted particles and/or electromagnetic radiation. While the half-life determines the time interval in which a therapeutic or diagnostic effect can be elicited, the emitted energy designates the biological effect and range thereof within the body. While particle emitter (for therapy) typically have a high LINEAR ENERGY TRANSFER (LET), electromagnetic radiation (for diagnosis) displays limited interaction with

[9] the pretreatment consisted of preliminary injection of Ni^{2+} coated liposomes in order to deplet the plasma opsonins levels

Table 2.4: Physical properties of selected nuclides for radionuclide therapy

Nuclide	half life $t_{1/2}$/h	E_{Max}/MeV	mean biological range /mm	γ-energy /keV (percentage of γ-radiation)
^{32}P	342	1.72(β^-)	1.85	—
^{67}Cu	62	0.57(β^-)	0.27	92 (11), 185 (49)
^{90}Y	64	2.27(β^-)	2.76	—
^{131}I	193	0.61(β^-)	0.40	364 (81)
^{153}Sm	47	0.80(β^-)	0.53	103(28)
^{177}Lu	162	0.50(β^-)	0.28	113(6.4), 208 (11)
^{186}Re	89	1.07(β^-)	0.92	137(9)
^{188}Re	17	2.12(β^-)	2.43	155(15)
^{211}At	7.2	5.87(α)	0.06	670(0.3)
^{212}Bi	1.1	1.36(β^-) 6.09(α)	0.06	727(7)
^{213}Bi	0.76	5.9(α) 1.48(β^-)	0.07	440

biological tissue (low LET). If possible, the physical half-life should match the biological half-life (pharmacokinetics) of the administered conjugate to maximize effect and minimize side effects.

- **Chemical properties of the isotope** which determine how the nuclide can be incorporated into the carrier molecule. Obviously, the two modes are covalent incorporation (nonmetals) and chelation (metals). Stability *in vivo* of the nuclide-carrier linkage is crucial and can depend on pH or ionic strength of the solvent (body fluid) which might be prone to changes on the passage through the body.

A great number of isotopes of numerous elements have been investigated for their applicability in nuclear medicine. Table 2.4 shows a selection of therapeutic isotopes found in literature. The only type of emitter that is routinely used in clinical oncology are β^--emitters. Reasons for this are their availability via (n,γ) reactor processes and the broad spectrum of particle energies. The released energy of the applied radionuclide, however, is only one point that has to be considered. Some nuclides that possess favorable physical constants themselves are restricted in their use, as decay products shows unfavorable properties. For example, the non-metal ^{211}As is attached

covalently to its carrier molecule and upon conversion to its daughter ^{207}Bi, a metal, it is released. The latter is well known to accumulate in the kidneys.
Generally the particle energy and thus, the mean biological range should be chosen in respect of the size of the malignant lesion. It is of considerable interest in the case of solid tumors, if the whole lesion is accessible (e.g. necrotic parts are not or very limited accessed by blood vessels[176–178] and, in the case of targeted therapy, the target is distributed homogeneously in the tumor. Ideally, the mean biological range should be half the diameter of the lesion. This allows that the cells are hit a number of times from different directions (cross-fire effect) which increases the chance of fatal damage. Most β^--emitters do also emit γ radiation (Table 2.4). This is desirable to a certain extend, as this can be used for dosimetry and/or visualization and staging of the tumor.
The oldest and still one of the most common elements in nuclear medicine is iodine. Administration of iodine is used for the treatment of a number of thyroid diseases. Radioiodination of bioactive peptides can be easily performed at tyrosine moieties. However, the *in vivo* stability of the formed C-I bond is limited which leads to release of iodine and dose-limiting side effects. Of the large number of β^--emitters, two intensely investigated nuclides,^{90}Y and ^{177}Lu, should be mentioned. They vary significantly in the energy of the released particles. The mean biological range of ^{90}Y is 2.76 mm (Table 2.4), making this isotope suitable for larger malignant lesions, while ^{177}Lu is short-ranged with 0.28 mm of biological range. This makes it an ideal candidate for the treatment of smaller lesion and metastasis. α-emitters are very short ranged (Table 2.4). The helium nuclei dissipate their kinetic energy within a couple of cells diameters, also making this type very interesting for metastasis and especially non-localized (e.g. hematological) malignancies. Due to their high LET a few hits can effectively kill cells, whereas in the case of β^--particles a much higher number is required. This also explains why so far no α-particle emitter reach advanced clinical stages, since very fast and efficient delivery to the target cells and rapid clearance of all residual radionuclide from the body is importance, or systemic or organ-related toxicity would be prohibiting. Figure 2.10 illustrates the different biological ranges of ^{212}Bi, ^{177}Lu and ^{90}Y. The higher the particle range, the higher the chance that the particle related toxicity harms other cells or tissues (e.g. blood vessels) in the proximity.

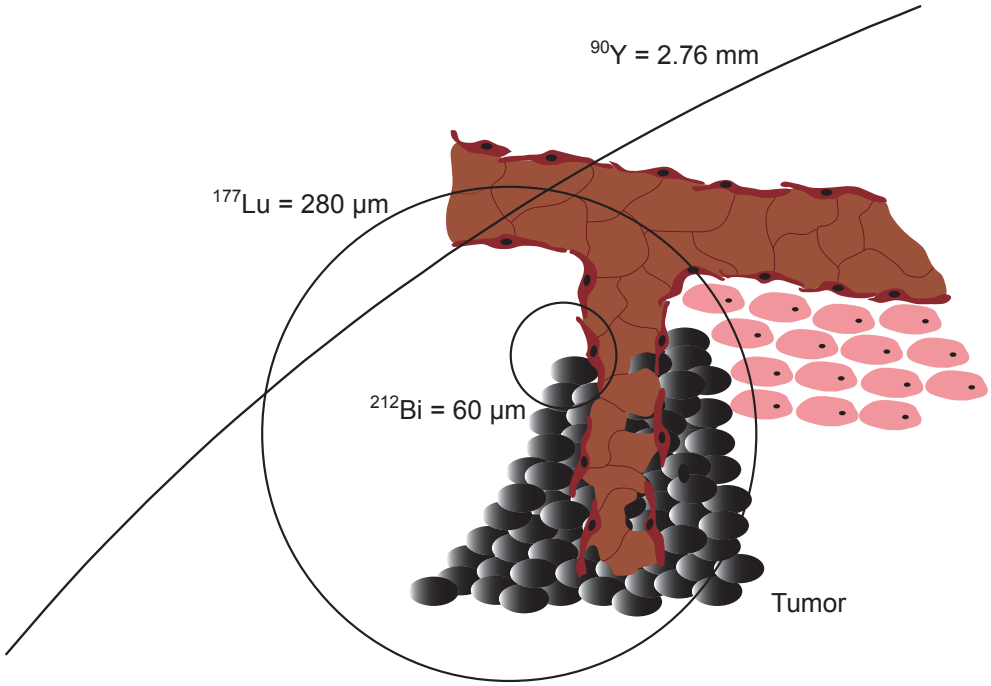

Figure 2.10: Illustration of the mean particle range of the three therapeutic radionuclides ^{212}Bi, ^{177}Lu and ^{90}Y in comparison with cells. Please note: the biological range is statistical and the black circles only roughly correspond with the mean biological range in proportion to cell diameter of approx. 30 μm.

Two major imaging methods in modern nuclear medicine are SINGLE-PHOTON EMISSION COMPUTED TOMOGRAPHY (SPECT) and POSITRON EMISSION TOMOGRAPHY (PET). One prominent example for SPECT is OctreoScan® (^{111}In-diethylentriamine pentaacetic acid^0-octreotide (^{111}In-DTPA^0-OC)) while PET is mainly performed with ^{18}F-fluorodeoxyglucose (FDG). Recently *Li*[179] reviewed the use of SST analogs for PET imaging.

The two chelators 1,4,7,10-tetraazacyclododecane-1,4,7,10-tetraacetic acid (DOTA) and DTPA are the most common chelators for radiometallation, with DTPA being already part of a commercial product, OctreoScan®. Besides DOTA and DTPA, also a number of derivatives are commercially available or have been described in literature (Figure 2.11) Recent research focuses not only on the development of new chelators to improve binding selectivity and affinity to metals of interest, but also to develop new derivatives to allow fast and effective coupling/incorporation of the chelators (in)to antibodies, peptides[180] or polymers via isothiocyanate coupling, oxime ligation[181–183] or 'click-chemistry'[183,184] (vide infra, Chapter 2.5), or incorporation into polymers[100]. *Liu* and *Edwards*[185] reviewed the design, synthesis and radiometallation of this type of bifunctional ligands for radiopharmaceuticals.

Both DOTA and DTPA can bind to a great number of nuclides, but affinity for different ions and kinetic factors of metallation differ strongly. This is of great importance, since *in vivo* stability of the chelator-metal complex must be high, but incorporation and purification should be fast. As can be seen in Table 2.5, fast and quantitative radiometallation of DOTA with a number of elements is possible under appropriate conditions.

Upon coupling of the chelator to the targeting molecule (especially in the vicinity of the binding motif), its binding profile towards their target can change significantly. Furthermore, the introduction of the metal can also change the pharmacokinetics, the rate of internalization of the ligand/receptor complex[190] and thus, tumor uptake. To complicate matters, also the site of DOTA attachment and nature of the used linker between the chelator and the peptide is of relevance. This can lead to the loss of subtype binding capacity as was reported recently in the case of the peptide sst$_2$-ANT after DOTA coupling[137]. Some further examples are given in Table 2.6. In literature, the IC$_{50}$ of the same peptides towards the same receptor subtype vary substantially[10]. The

[10]Compare IC$_{50}$ values of 0.07[135], 2.4[137] and 4.0 nM[138,191] for binding of SST-28 to hsstr$_5$.

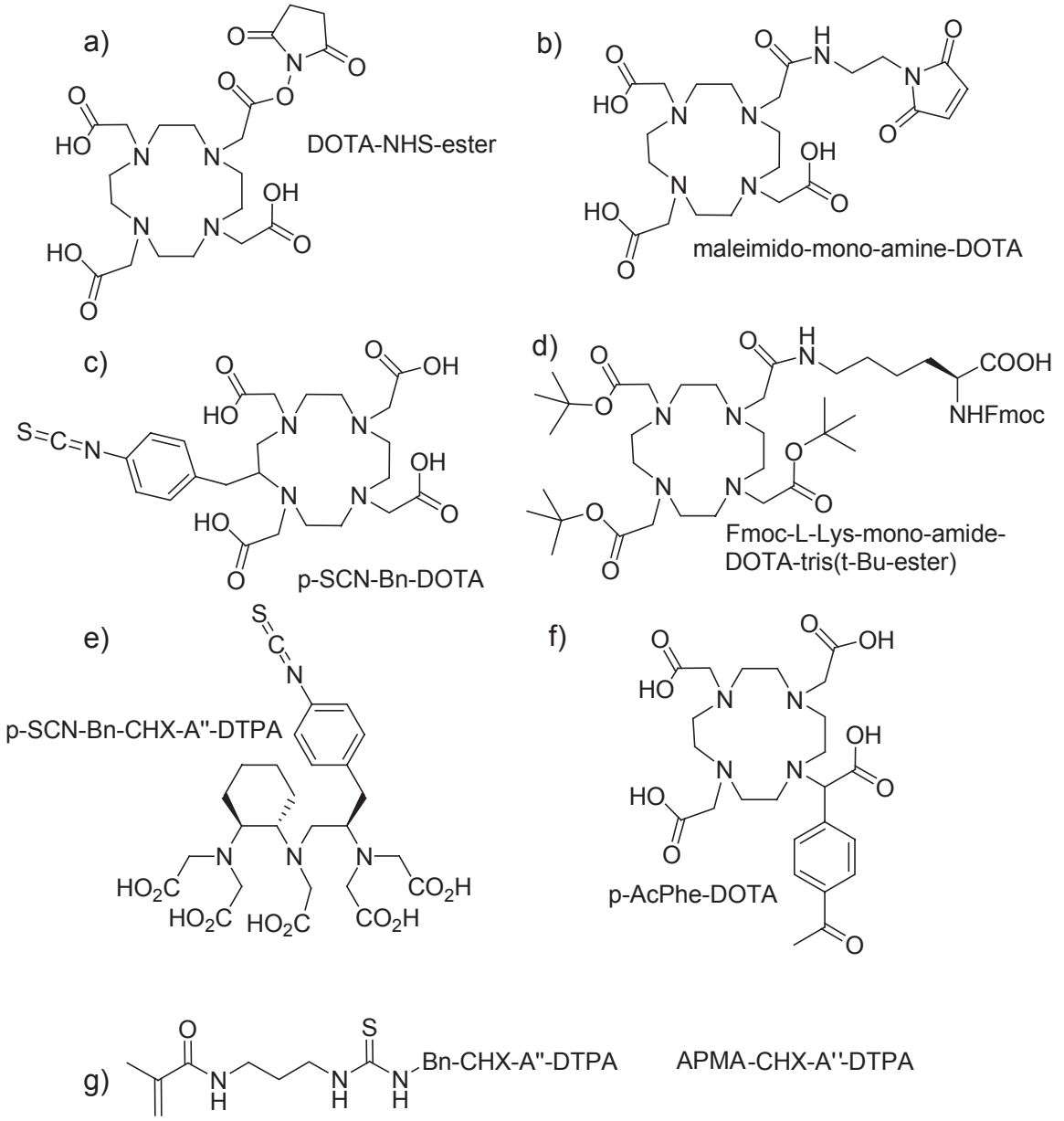

Figure 2.11: A selection of DTPA and DOTA derivatives. While a), c) and e) react with primary and secondary amine groups, b) can be coupled to free thiols, e.g. of cystein moieties of peptides. d)[180] can be used in solid phase synthesis (SPS) (Fmoc strategy) of peptides while f)[181] can react with aminooxy peptides under oxime formation (see Chapter 2.5). g)[100] can be directly incorporated during radical polymerization of acrylates/acrylamides. a) through e) can be purchased from Macrocyclics Inc., Dallas, Tx, USA.

Table 2.5: Comparison of parameters of radiometallation of DOTA conjugates of octreotide analogs with various elements[186–189].

Nuclide	Temperature [°C]	pH value	Time [min]	RCY [%]
^{68}Ga	90	4.2 - 4.6	1	100[a]
	90	4.2	15	95
	RT	4.2	5	60
^{64}Cu	50	5.5	45	100
^{90}Y	80	4 - 4.5	20	100
^{111}In	100	4 - 4.5	30	100
	80	4 - 4.5	20	60
^{177}Lu	80	4 - 4.5	20	100
^{213}Bi	100	6 - 7	5	100

[a] microwave heating

Table 2.6: Affinities (IC_{50} [nM]) of SST analogs with and without chelator as well as after radiometallation towards the five $hsstr_x$ subtypes[137, 191]; compare also with Table 2.2.

Peptide	$hsstr_1$	$hsstr_2$	$hsstr_3$	$hsstr_4$	$hsstr_5$
octreotide	>10,000	2.0 ± 0.7	187 ± 55	>1,000	22 ± 6
DTPA-octreotide	>10,000	12 ± 2	376 ± 84	>1,000	299 ± 50
^{111}In-DTPA-octreotide (OctreoScan®)	>10,000	22 ± 3.6	182 ± 13	>1,000	237 ± 52
DOTATOC	>10,000	14 ± 2.6	880 ± 324	>1,000	393 ± 84
^{90}Y-DOTATOC (OctreoTher)	>10,000	11 ± 1.7	389 ± 135	>10,000	114 ± 29
sst_2-ANT	>1,000	3.6 ± 0.4	>1,000	349 ± 30	276 ± 119
DOTA-sst_2-ANT	>1,000	1.5 ± 0.4	>1,000	287 ± 27	>1,000
In-DOTA-sst_2-ANT	>1,000	9.4 ± 0.4	>1,000	380 ± 57	>1,000

reason for this is unclear, but might be due to different experimental methods. The change in affinity between peptides, peptide-chelator and peptide-chelator-metal conjugates can be explained by the change in overall charge and/or hydrophilicity (DOTA carries four carboxylic acid moieties) as well as with induced steric hindrance. Not only the affinity *in vitro* can be subject to change, but also the pharmacokinetics may alter significantly[192]. Systematic investigation of the impacts of net charge, carbohydrate conjugation, hydrophilicity/lipophilicity, size, multimerization and structure has just started and the results of *in vitro* and *in vivo* experiments are not always conclusive.

2.2.3 PRRT

Clinical studies with hsstr$_x$ targeting

Clinical evaluation of PRRT is yet limited to the rare class of inoperable and/or metastasized neuroendocrine GASTROENTEROPANCREATIC hsstr$_x$ positive tumors. *Teunissen* et al.[191] recently reviewed the developments with radiolabeled SST analogs. First tests where performed with ^{111}In labeled SST analogs. However, the effective range of the Auger-electrons is very low («10 μm) so that internalization is crucial or better, DNA intercalation is desirable[193]. Additionally, in the common case of heterogeneous receptor distribution within the tumor mass, no bystander effect can be achieved, limiting the clinical response of ^{111}In radiopharmaceuticals[193].
Already in 1995, *Donoghue* et al.[194] used a mathematical model to predict the optimal size of tumor with respect of the used therapeutic radionuclide. For ^{90}Y a diameter of 34 mm was calculated, while tumors of 2 mm should respond best to treatment with ^{177}Lu. More recently, first preclinical results support this calculation as it could be shown that a combination of the two nuclides result in a higher response in tumor xenografts[195,196], while smaller lesions are more effectively treated with ^{177}Lu while bigger respond better to ^{90}Y[197,198].
Table 2.7 summarizes results of clinical trials with OctreoScan, OctreoTher and ^{90}Y-DOTATATE.

Table 2.7: Clinical studies of PRRT with different peptide-radiometal compounds[191].

Peptide-conjugate	# patients	Clinical response	
OctreoScan	64 (97 % PD)[a]	6 % PR	23 % PD
OctreoTher	200 (92 % PD)[a]	21 % CR + PR	13 % PD
^{90}Y-DOTATATE	75 (89 % PD)[a]	37 % PR	11 % PD

[a] prior to the treatment
CR = complete remission, no evidence of disease
PR = partial remission, >50 % reduction of tumor size
PD = progressive disease, >25 % increase in tumor size

Recent preclinical studies with hsstr$_x$ targeting

Hsstr$_x$ targeting was performed so far with agonists. This is thought to be preferable because internalization of the ligand receptor complex would increase the residing time of the nuclides at the tumor. However, after a very recent report of *Ginj* et al.[137], this paradigm might shift. *In vivo* experiments in a mouse model showed a markedly higher accumulation of antagonists of hsstr$_2$ and hsstr$_3$ in the tumor as compared to agonists. The hsstr$_3$ antagonist peaked 1 h after administration with over 60 % of the injected dose per gram of tissue (%ID/g, i.e. the weight normalized percentage of injected radioactivity in the respective organ) in the tumor and very high tumor/tissue ratios. The authors suggest that these results should be confirmed by further studies and that antagonists of other relevant peptide receptors should be examined in this respect.

α-Particle emitters are of high interest, but sufficient delivery systems are yet to be developed. SST analogs seem natural candidates for these studies, since the are known to accumulate very rapidly at the tumor site, reducing the toxic load to the body and especially to the blood[199]. A first study by *Norenberg* et al.[189] with ^{213}Bi-DOTATOC in an animal model showed an anti-proliferative effect on the tumor, accompanied by minimal organ toxicities. This makes this compound an interesting candidate for further studies.

Another approach that is set apart from the traditional approach of optimizing receptor affinity and pharmacokinetic profile was reported recently[200]. Trifunctional

compounds, bearing octreotide, chelator and a virus derived peptide that triggers transport to the nucleus were investigated. The transport to the nucleus is projected to increase the therapeutic effect of attached ^{111}In. It was shown that the compounds not only displayed an increased cellular uptake in comparison to ^{111}In-DOTATOC, but also has a pronounced uptake into the cell nucleus. However, these preliminary results now have to be examined in respect of cytotoxicity of this new class of trifunctional compounds.
Recent studies on combinations of different receptor-specific peptides suggest yet another paradigm shift. However, while the concept is intriguing, the presented experimental data show that the high renal uptake prohibits the use of these radiolabeled RGD-octreotate chimeras so far[146, 201].

Protecting the kidneys

Renal clearance is the favored mode of excretion in PRRT but can be also the dose-limiting factor. Several studies concerning this aspect have led to important insights of the mechanisms of reabsorption after glomerular filtration of peptides in the renal proximal tubules. While the mechanisms of this uptake are not yet clearly established, *de Jong* et al.[202] recently showed that the multiligand receptor megalin, a negatively charged endocytic (i.e. internalizing) peptide and protein receptor, is involved in the reabsorption process of OctreoScan. Furthermore, it has been found that administration of positively charged amino acids (Lys and Arg, L and D) and polycations significantly reduces the reabsorption[34, 203, 204]. Accordingly nephrotoxicity is reduced in the case of ^{90}Y labeled SST analogs by coadministration of Lys and Arg[205], while in the case of the α-emitter ^{213}Bi this positive effect was not observed[189]. The reduced reabsorption is generally attributed to the blocking of the negatively charged megalin. Incorporation of oligo-D-glutamic acids sequences led to a reduction of the kidney uptake of radiolabeled minigastrin, another peptide in development for PRRT. Interestingly, oligo(aspartic acid) does not exert this effect[206]. This suggests that the effect is not solely charge dependent.
While being the most prominent example, hsstr$_x$ positive tumors are not the only ones where progress in PRRT are made. As mentioned above, integrins, and in particular $\alpha_v\beta_3$ are overexpressed in a number of tumors, including melanoma, glioma, breast

and ovarian cancers and proliferating blood vessels. Therefore it seems logical to consider integrins as worthy targets for PRRT, especially in the case of rapidly growing solid tumors. *Liu* et al.[170] reviewed the use of RGD peptides and integrin antagonist peptidomimetics in this aspect. Also for analogs of α-MSH reports and preclinical advances can be found in the literature.

Preclinical evaluation of α-MSH analogs for PRRT

Various reports on the biodistribution of radiolabeled MSH analogs can be found, dating back from 1999. *Chen* et al.[207] observed up to 6.52 ± 1.11 %ID/g of radiolabeled (^{99m}Tc and ^{188}Re) NDP-α-MSH (30 min p.i.). However, the tumor retention was mediocre and the peptides were excreted to a high degree in the feces. The same group later evaluated DOTA-Re[Arg^{11}][Cys^{3,4,10},D-Phe^{7}]MSH$_{3-13}$ (DOTA-Re[Arg^{11}]-CCMSH) and similar rhenium cyclized MSH analogs. Some gave very promising tumor uptake accompanied with only very limited hepatobilliary uptake[208]. Interestingly, the performance *in vitro* was not reflected *in vivo* (tumor uptake and excretion), as comparison of IC_{50} values shows. The peptide with the highest affinity *in vitro* did not show the highest tumor uptake *in vivo*. Administration of therapeutic doses of ^{188}Re[Arg^{11}]CCMSH lead to prolonged survival rates, but no case of complete remission was reported[209]. It was hypothesized that the high-energy β-particles emitted from ^{188}Re deposited a majority of the decay energy outside the small-sized tumors present in this study.After administration of [^{212}Pb]DOTA-Re[Arg^{11}]CCMSH (α-emitter) the results were different. Uptake in the tumor was pronounced and prolonged (after 4 h, > 10 %ID/g), while the uptake in the kidney decreased comparably fast. The survival rates of tumor bearing mice were promising; up to 45 % of mice (200 μCi administered) survived disease-free[209]. Also with both ^{177}Lu and ^{90}Y labeled DOTA-Re[Arg^{11}]CCMSH, persistently high uptake was observed in the tumor. However, at the same time a markedly higher renal uptake in comparison with ^{212}Pb was observed[158]. Insertion of the negatively charged (at physiological conditions) amino acid glutamic acid between the peptide and the chelator helped to reduce the kidney uptake significantly, albeit accompanied by a minor reduction of the tumor uptake[210]. *Froidevaux* et al.[211] recently reported on the synthesis of another potential MSH analog [Nle^{4},Asp^{5},D-Phe^{7}]-α-MSH$_{4-11}$ (NAPamide), for imaging or therapy of hMC1R

expressing tumors. In comparison with CCMSH peptides, the tumor uptake was comparable or lower (depending on the CCMSH conjugate). At the same time, however, the kidney uptake was markedly reduced. A follow-up study, evaluating SAR, showed that Lys^{11} plays a critical role for the kidney uptake[212], similar as observed for CCMSH[208].

Most or all peptides that are in advanced stages of preclinical or in clinical studies for PRRT are monomeric. However, as discussed in Chapter 2.2.1, there is evidence that oligo- and multimers of cell recognition moieties can be superior to monomers, in terms of their specificity and/or biodistribution. Some of these oligo- and multimers will be discussed in the following chapter. In literature, the terms multivalency and polyvalency are used interchangeably for the interaction of several ligands bound to one molecule with their receptors. However, it becomes evident that also the combination of different ligands in multiple copies exerts special effects which are only observed if the ligands are bound to the same carrier. For the first example of multiple copies of ligands, the term polyvalency will be used in this work, whereas the latter case of different ligands on the same scaffold will be termed multivalent.

2.2.4 Polyvalency at work

Polyvalent and multivalent interaction are crucial in numerous biological situations. For the attachment of cells to the ECM, the integrins have already been mentioned and the cells bind with great numbers of integrins the RGD motif of e.g. fibronectin. On the other hand, e.g. viruses need to bind to different epitopes on cell surfaces in order to be able to enter and thus deliver their genetic material to the cells. For polyvalent and multivalent interactions both peptides and sugars (or the combination, glycoproteins) can be responsible[77]. In Figure 2.12, a number of binding mechanism of polyvalent and multivalent ligands to cell surface receptors are illustrated. The most simple effect is a statistical one, as upon binding of one ligand of a polyvalent construct, the other ligands are held in close proximity of the receptor. This can lead to a faster follow-up binding if the first ligand is released, resulting in a higher observed affinity of the polyvalent ligand (Figure 2.12a). In contrast to monomeric ligands, a number of binding modes are possible. These include the simultaneous binding of

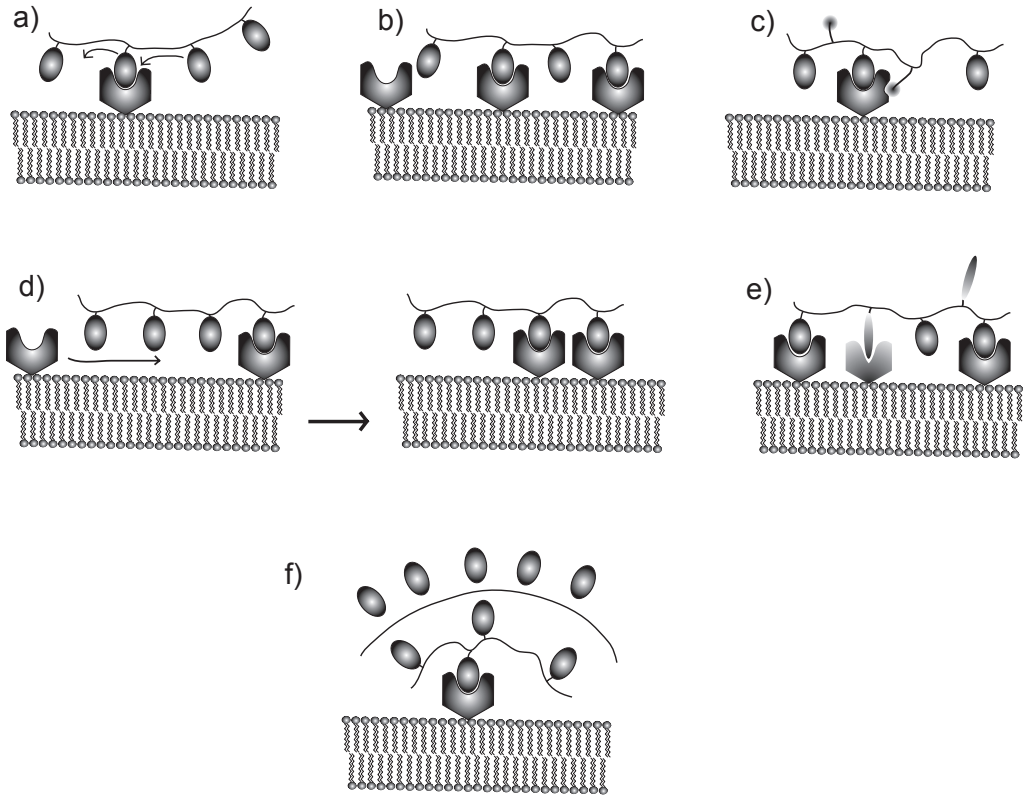

Figure 2.12: Simple illustration of various bindings modes of poly- and multivalent ligands: a) statistical effect, b) chelation of receptors, c) subsite binding, d) receptor clustering, e) simultaneous binding of different receptors and f) steric shielding.

ligands which decreases the overall off-rate (Figure 2.12b). Subsite binding offers a chelation effect at one receptor as the same or another type of ligand bound to the same scaffold binds to another epitope of the receptor (Figure 2.12c). Upon binding of one receptor a signal is induced that leads to receptor clustering, increasing the possibility of the chelation effect (Figure 2.12d). Scaffolds, that are polyvalent in different ligands (multivalency) can lead to simultaneous binding of two different receptors, which, in turn can lead to a different signal than binding of the receptors alone or independent binding of the two different receptors (Figure 2.12e). Finally, bulky ligand scaffolds can act as a barrier for other (monomeric) ligands, decreasing competitive binding (Figure 2.12f). In the past decade, much insight into this matter was gained by the use of synthetic polymeric scaffolds carrying multiple copies of ligands. For example, the effect of polyvalent galactose, prepared by ring-opening metathesis polymerization, on cell chemotaxis was studied by *Gestwicki* et al.[213]. It was shown that the cell response was dependent on the valency of the galactose multimers. A number of articles and reviews by *Whitesides*[77] and *Kiessling*[214–219] give more detail of this subject.

Multimers of SST analogs

In the case of SST analog oligo- or multimers, only limited studies are available. *Kessler* et al.[220] studied the effect on the binding affinity of dimers of c(D-Pro-Phe-Thr-Lys-Trp-Phe) linked by hydrocarbon chains of different length. A maximum binding affinity was found for spacers of 16 - 18 carbon atoms size. *Modlinger*[181] recently described various DOTA bearing TATE dimers and a tetramer. *In vitro* studies showed a decreased binding affinity for $hsstr_2$ in comparison to TATE for all multimers. *In vivo* biodistribution studies revealed a very high kidney uptake and only moderate to low tumor/background rations in comparison with the monomer.

RGD multimers

Since the interaction of cells with their surroundings via the integrin receptor family is typically multivalent and integrin clustering is an important aspect of the signal

cascade, it seems a logical step that RGD multimers are synthesized and compared in their affinity, specificity and biodistribution with monomeric RGDs. In fact, while SST analogs are much more routinely used in nuclear medicine and oncology than integrin antagonists, RGD oligo- and multimers are represented in much higher numbers in literature. In Figure 2.13 a number of oligo- and multimeric structures described in this section are depicted. Recently, *Ye* et al.[221] reported on the synthesis, *in vitro* and *in vivo* evaluation of arrays of multimeric linear RGD motifs, bound to a near infrared (NIR) fluorescent dye (cypate) (Figure 2.13a). It was shown that with increasing numbers of RGDs, the binding affinity increases. However, even a construct of 8 linear RGD units shows lower affinity than c(RGDfK). Additionally, it was shown that not only the number of RGD units influences the affinity, but that also their arrangement is relevant. Are all RGDs attached to one side of the cypate a lower affinity is observed than if the half the number is attached on either sides of cypate. Biodistribution studies showed that tumor uptake is better for higher affinity structures, but these linear oligomers show pronounced uptake in the liver and the kidney even 24 h post injection (p.i.). Additionally, only moderate tumor/organ ratios were observed.

In the group of Prof. *Kessler* recently a number of di-, tetra- and octamers of cyclic RGD with different types and length of spacers (hydrophilic and flexible hexaethylenglycol (HEG) and more hydrophobic and less flexible 6-aminohexanoic acid (AHX)) have been synthesized and evaluated (Figure 2.13b)[67,89,225]. It was shown, that tumor uptake of the dimer and the tetramer is higher as compared to the monomer and even higher as galacto-RGD (Chapter 2.2.1). Especially tumor/background ratios profits from multimerization and for most organs a trend can be observed from mono- over dimeric to tetrameric compounds (Figure 2.8c). Importantly, comparison of the biodistribution data of mono- and tetramers shows no effect of the higher molar mass on the blood pool retention[101,226].

These well defined oligomers are highly interesting compounds for integrin targeting, but the synthesis of these compounds is a tedious $\sim$20-step reaction and numerous HPLC purification steps are necessary.

Boturyn et al.[222] reported on a modular concept of preparing tetramers of c[RGDfK] via oxime formation. The application of this highly effective coupling reaction makes the overall preparation more feasible. Also *Dijkgraaf* et al.[91] were recently able to reduce the necessary numbers of steps to produce tetramers of c(RGDfK) significantly

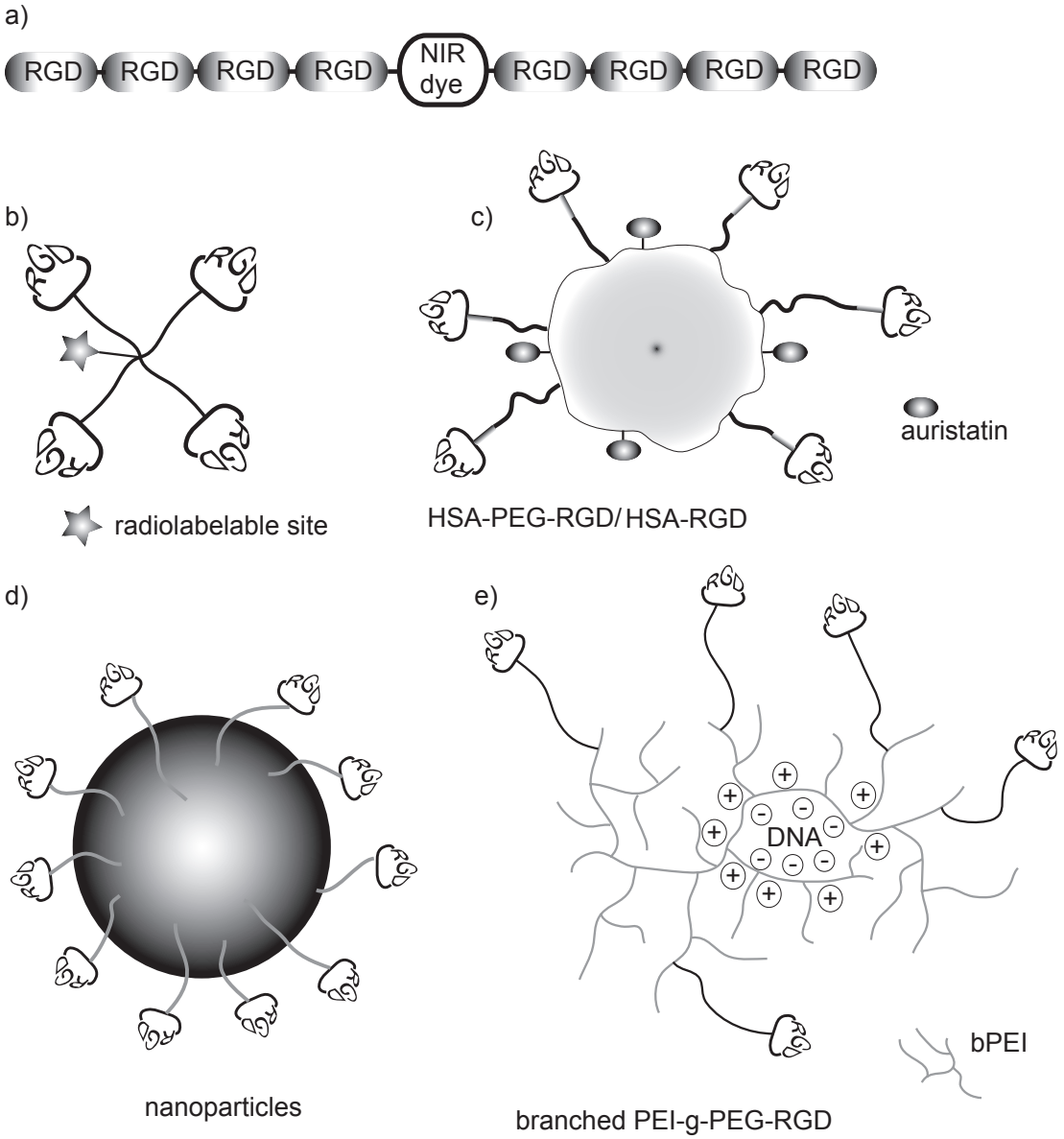

Figure 2.13: Structures of various RGD oligo- and multimers. *Ye* et al.[221] reported on oligomers of linear RGD units attached to a near-infra red (NIR) dye. b) Several groups prepared a number of oligomers (n $\leq$ 8) that can be radiolabeled or carry a fluorescent dye[89,91,92,101,114,222]. c) RGD attached to human serum albumin (HSA) has been reported by *Temming* et al.[223]. d) RGD coated nanoparticles by *Montet* et al.[96,103] showed a pronounced multivalency effect but also significant uptake in the organs of the RES while in the case of e) polyplexes with pending RGD moieties a negative effect of multiple copies of RGD on the biodistribution has been reported[224]. Please note: Sizes are not in scale.

by application of click-chemistry. *In vivo* screening revealed a significant increase in tumor accumulation and generally favorable tumor/organ rations. However, the reported tetramer showed a very high kidney uptake both at 2 h p.i. ($\sim$ 22 %ID/g) and 24 h p.i. ($\sim$ 20 %ID/g). In another study, the same group investigated the influence of the linker between the peptides on the biodistribution[92].

Temming et al.[223] recently reported on human serum albumin (HSA) functionalized with multiple copies (5 - 13) of c[RGDfK] and the cytostatic auristatin bound via a lysosomal labile linker in a 4-step reaction (Figure 2.13c). Attachment of the peptide was performed via short alkyl linkers and poly(ethylene glycol) (PEG) chains, alternatively. The number of attached copies of RGD, the linker and the additionally attached drug influenced the binding affinity. However, the size of the used PEG chains is not mentioned in the report and actual structure activity relationships (SAR) can not be deduced from the data presented. Some evidence suggests that both PEG and drug conjugation increase the IC_{50} values of the conjugates and increasing numbers of RGD decrease it. Additionally, the incorporation of ^{89}Zr by chelation with deferoxamine attached to HSA was reported. ^{89}Zr is an interesting nuclide due to its relatively long half-life of 78 h as compared to other β^+-emitter as this allows long term PET imaging.

Montet et al.[103] prepared RGD coated nanoparticles (Figure 2.13d) which show a pronounced multivalent effect. However, biodistribution data suggest a strong uptake in a number of organs, including liver, spleen, skin and intestine[96].

Kim and co-workers recently prepared branched poly(ethylene imine)-*graft*-[poly(ethylene glycole)-RGD4C] (bPEI-g-PEG-RGD) (Figure 2.13e) conjugates with plasmid DNA in order to block the vascular endothelial growth factor (VEGF) receptor, thus inhibiting tumor angiogenesis. It was shown that bPEI-g-PEG-RGD exhibits an enhanced gene delivery in comparison to bPEI-g-PEG and leads to increased survival in tumor bearing mice[224]. It was reported that the affinity of these constructs to human dermal microvascular endothelial cells (HDMEC) was decreased with increasing number of PEG-RGDs bound to the PEI. When only one PEG-RGD was attached, affinity was similar to the reference peptide but already 5 copies bound to PEI halved the relative affinity. Conjugates carrying 10 and 20 PEG-RGD chains showed no affinity at all. The authors attribute this to an aggregation effect. The charged peptides agglomerate within the bPEI-DNA core while the hydrophilic PEG surrounds it. Since the RGDs are then not presented on the surface of the micelles, no specific binding can occur[224, 227]. This demonstrates another problem of targeted delivery. Obviously,

targeting moieties must be presented in a manner that interactions with their target is not affected.

Multimers of α-MSH analogs

Similar to hsstr$_x$ and in contrast to integrins, hMCxR bind their ligands with high affinity. As discussed earlier, multimerization of high affinity ligands sometimes does not increase the binding to their targets and is not necessarily beneficial for the biodistribution.
Sharma et al.[228,229] reported on MSH and NPD-α-MSH multimers based on poly(vinyl alcohol) (molar mass 110,000 g/mol) as well as latex and polyamide beads as scaffolds. Their results suggested that these conjugates are suitable for the identification of melanoma cells *in vitro*. However, for *in vivo* studies these conjugates are not suitable due to size and solubility issues.
Well-defined NDP-α-MSH oligomers with up to six peptides were synthesized via oxime formation by *Brandenburger* et al.[230]. They reported on an up to 8 fold increase of the affinity to hMC1R of these oligomers in comparison to the native peptide.
Vagner et al.[154,231] reported on MSH(4) (His-D-Phe-Arg-Trp, low affinity) and NDP-α-MSH (high affinity) di- and trimers, linked by rigid and flexible linkers and studied their affinities towards hMC4R. They found a trend of increased affinity with increasing number of ligands only observed for the low affinity peptide MSH(4) (up to 23 fold increase).

2.2.5 Summary

Peptide receptor radionuclide therapy and imaging are rapidly developing fields in the context of targeted and individualized cancer therapy. Imaging methods are important in the assessment and staging of diseases. Of the numerous receptors which are under investigation for PRRT and PRI, the somatostatin receptor and the ligand octreotide are in advanced stages. OctreoScan® is already routinely used in the clinic and OctreoTher is currently investigated in clinical trials.

Despite substantial effort that is put into the investigation and development of suitable conjugates for PRRT and PRI, several limitations remain. Multimerization of the ligands via hydrophilic and biocompatible scaffolds seems to be a promising way to circumvent some problems. In a number of cases, this approach is working, whereas in other examples the oligomerization is not beneficial. However, SAR are rarely described or understood. In recent years, investigators started to take a look into polymer-peptide conjugates as candidates for PRRT. The concept of polymer therapeutics and these special considerations will be discussed briefly in the next chapters.

2.3 Polymer therapeutics

2.3.1 Biocompatibility of polymers

Substances, materials and assemblies are often called biocompatible if they do not have a negative influence on a biological system. However, presumably *no* material shows *no* negative influence in *all* living creatures in *all* possible assemblies. Therefore one has to keep in mind, that biocompatibility of a substance or material is typically only given in a certain, very specific context. Two examples shall clarify this point:

- An implant in the cardiovascular system (i.e. a stent) shall typically exhibit minimal interaction with substances within the blood, especially shall not lead to specific or unspecific adhesion of cells or proteins. A bone implant, in contrast, shall exhibit strong interaction between the bone and the surrounding tissue.

- The fate of intravenously injected soluble polymers depends on, among other factors, their hydrophilicity/hydrophobicity and their hydrodynamic radius (Chapter 2.1.2). If polymers are not degradable (e.g. having no hydrolysable bonds within the backbone), high molar mass fractions can eventually be deposited within the body. This may lead to pseudo tumors as described for poly(*N*-vinylpyrrolidone) (PVP), when used as blood plasma expander. Nevertheless, PVP is regarded as a biocompatible polymer in general and is widely used in pharmacy as well as health and personal care products[232].

Furthermore, the following subdivisions of the term biocompatible can be found[233]:

- **Biotolerant** components and compounds are only tolerated within the organism for some months to a couple of years. Minor deficiencies and interactions may be observed but no degradation, tissue alteration or toxicity shall be observed.

- A compound or substance is called **bioinert** when no chemical or biological interactions are observed. No toxic substances are released and, if implanted, only a non-adherent connective tissue capsule is formed around the implant. To this class some ceramics and polymers are attributed, along with most metals.

- Substances and implants are termed **bioactive** when a defined and pronounced interaction is observed. Implants typically need to be specifically designed and modified to be bioactive (for RGD-modified polymers see e.g. *Hersel* et al.[113]). This is especially important to ensure long-term and mechanical stability of implants.

2.3.2 Concepts and recent examples

The term 'Polymer therapeutics' is used for a variety of different constructs some of which are illustrated in Figure 2.14. Polymers that cause a therapeutic effect them-

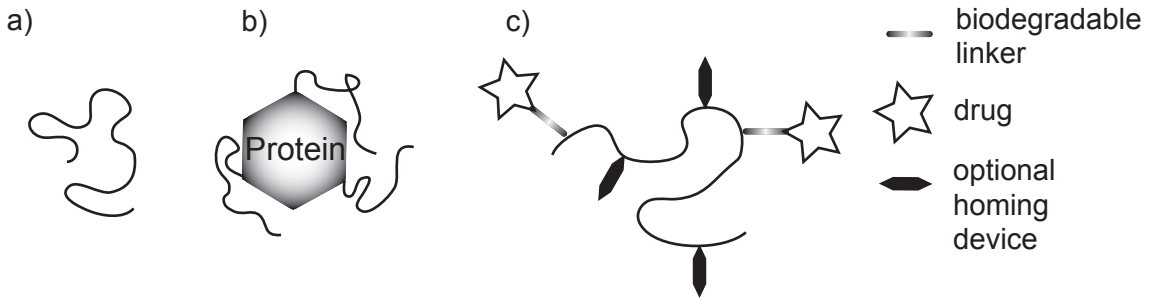

Figure 2.14: Illustration of the different types of 'polymer therapeutics'. a) Polymeric drugs, b) polymer-protein conjugates and c) polymer-drug conjugates (with optional peptide for e.g. active targeting)[42, 49].

selves are termed polymeric drugs (Figure 2.14a). Normally an additional entity is

involved to elicit a therapeutic effect. In this case the polymer is mostly regarded as the carrier, solubilizer/pharmacokinetic modifier or protective agent against degradation of the active substance. These entities can be proteins (Figure 2.14b), peptides and drugs or a combination thereof (Figure 2.14c). In addition polymer micelles, polymer decorated liposomes (Figures 2.5f, 2.7d) and polymer-DNA/RNA complexes (Figure 2.13e) (polyplexes) are under investigation.
The rationale for polymer therapeutics stems from a seminal paper of Prof. *Ringsdorf* which dates back to 1975. Therein the use of polymers as carriers for therapeutic substances and homing devices is hypothesized (Figure 2.15)[9]. The still valid basic

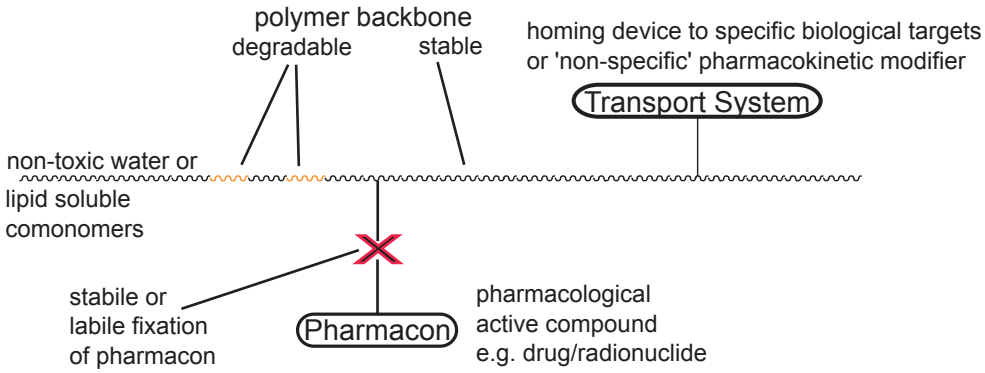

Figure 2.15: Illustration of *Ringsdorf*s concept for polymer therapeutics. Freely adapted from ref.[9].

considerations include the (biodegradable or biostable) non-toxic polymer backbone, built up from monomers which are largely responsible for the solubility of the entire compound (often via hydrophilic side chains, as the backbone of many polymers consists of a saturated alkyl chain). Additionally a pharmacon, typically a low-molar mass drug, is attached. The nature of the linker between the polymer and the drug usually has a major impact, as many drugs only become active on release from the polymer itself (prodrug concept). Finally a transport system can be present, either active (e.g. receptor binding peptide) or passive (pharmacokinetic modifier).
The object of this work is the peptide targeted delivery of radionuclides with relatively small polymers. Therefore a detailed discussion of the advances of 'classic' polymer therapeutics (passively targeted large polymers) is outside the scope of this work. A number of recent reviews can be found in literature[42, 43, 46, 48, 49].
In contrast to systems using drug encapsulation by polymers for controlled drug re-

lease, the drug/bioactive compound is covalently bound to the polymers (with the exceptions of polyplexes). This makes the compounds new chemical entities which normally leads to more difficult approval procedures. However, as a first step in the development, the assessment of the biocompatibility of the polymeric carrier is often regarded necessary, even though any modification of this carrier will invariably alter its behavior *in vivo*. Two major differences between polymer therapeutics and other macromolecular drugs can be identified. In contrast to antibodies, oligonucleotides or proteins, polymers are typically easily accessible on a multi-gram (or often multi-ton) scale. Various properties such as size, charge and solubility can be varied easily by altering the feed or adding different monomers. However, these large scale polymers are synthesized by e.g. radical or ionic polymerization, ROMP or polyaddition/condensation. These polymerization techniques always lead to polydisperse products. This problem hampers the otherwise rapid advance in the field of polymer therapeutics. Distinct polymer chains will differ in size and possibly charge and monomer composition, which is likely to lead to a different biodistribution and effect. Additionally, any chemical modification tends to change the pharmacokinetics of polymers. For example, indifferent of the nature of the chemical modification (anionic, cationic, peptidic or with doxorubicin) the retention in the bloodstream is significantly reduced in the case of *N*-(2-hydroxypropyl)methacrylamid (HPMA) copolymers[31,32]. In several cases the biodistribution becomes less favorable, as can be seen in an reduction of tumor/organ ratio for kidneys and liver in a prostate carcinoma xenotransplant rat model[32]. However, in the case of conjugation with the chemotherapeutic agent doxorubicin the biodistribution remains largely unaffected besides a significant higher *relative* accumulation in the kidneys. The reason for this general trend of reduced circulation time is unclear. It could be reasonably assumed that attachment of moieties like doxorubicin or peptides may lead to some kind of aggregation of these groups and contraction of the hydrodynamic radius in consequence (as aforementioned with the example of adverse effects of multiple copies of PEG-RGD chains on bPEI 2.2.4). However, introduction of charged side chains should not lead to a contraction of the polymers hydrodynamic radius, due to electrostatic repulsion and enhanced water solubility. In the case of the introduction of carboxylic acids into the side chain, one could anticipate an additional repulsion effect from the highly negatively charged filtration barrier in the glomerulus. However, the opposite is observed. This again shows the complexity of SAR in the interactions of polydisperse compounds and biological

systems.

The polymer architecture is an important aspect that can change the characteristics like biodistribution and blood retention of polymers. Besides linear polymers, hyperbranched polymers, dendrimers and bow-tie dendrimers as well as dendronized polymers are under investigation (Figure 2.16). Polyglycerols can serve as an ex-

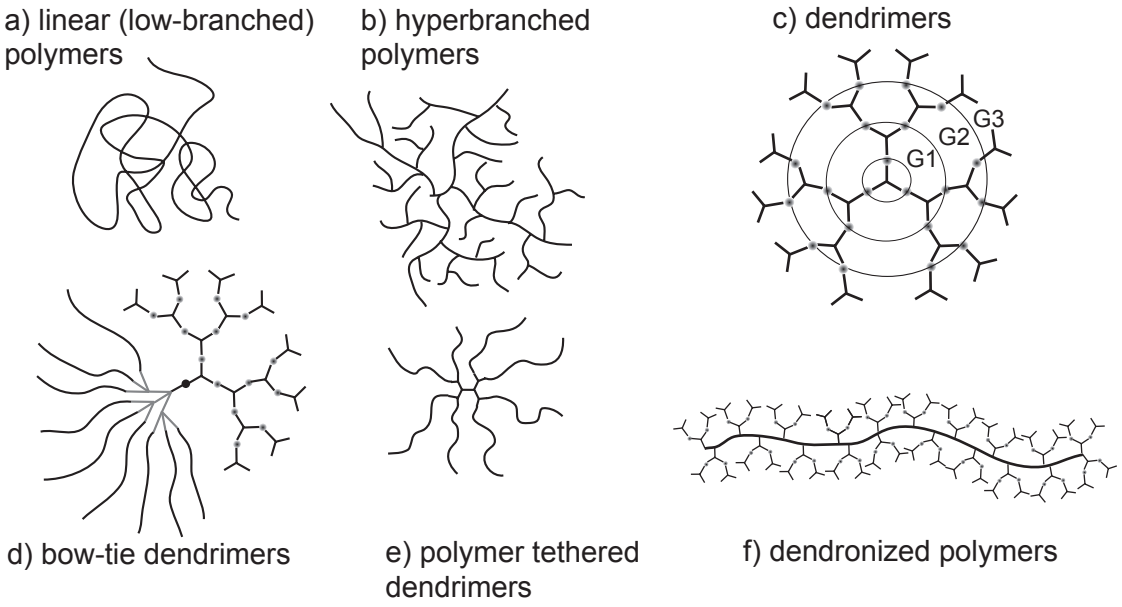

Figure 2.16: Schematic illustration of various polymer architectures available. Besides simple linear and branched polymers (a), hyperbranched (b), dendrimers (G3) (c), bow-tie dendrimers (d), polymer tethered dendrimers (e) and dendronized polymers (f) are under investigation.

ample to explain the rationale behind the change in architecture. PEG has been mentioned a number of times already. In fact, it is the most common polymer for polymer therapeutics. PEG conjugated (PEGylated) peptides were the first polymer therapeutics entering the markets starting from 1990 with PEG-adenosine deaminase being the first. Several reviews discussing recent developments in PEGylation can be found[234,235]. Albeit PEGylation has proven its usefulness in many examples, PEG has one major shortcoming. Chemical modification is only possible at the two chain ends. This is absolutely sufficient or even necessary in the typical case of polymer-protein conjugates as one protein is decorated with one or several PEG chains to enhance solubility, reduce immunogenicity or toxicity and prolong the biological half-life. However, if one thinks of more sophisticated protein/drug/peptide-polymer conjugates or

multimerization, linear PEG is often not an option. In contrast, dendritic (perfectly branched) polyglycerols offer a great number of modifiable sites on the exterior of the molecule (Figure 2.16)[43]. Unfortunately, the step by step synthesis of these perfectly shaped molecules is difficult and tedious. Moreover, modification of the exterior with more hydrophobic moieties (drugs like doxorubicin) can vitiate the solubility or lead to aggregation[236]. However, dendrimers are intriguing molecules. *Gillies* et al.[237] recently investigated the difference that architecture makes for biodistribution of otherwise similar polymers. They reported that dendrimers of the same molar mass show different blood circulation half-life, depending on the architecture. PEG side chains of different size were attached to first, second and third generation polyester dendrimers to obtain similar molar mass ($M_n \sim 40{,}000$ g/mol) products. The blood pool half-life increased from 1.4 h for G1, 26 h (G2) to up to 31 h for the G3 dendrimers. This example shows how sensitive pharmacokinetic characteristics can be in terms of the molecular architecture. The authors also propose a mechanism for the observed effect (Figure 2.17). Dendrimers of higher generations are typically described being more densely packed than linear polymers of the same molar mass, reducing their hydrodynamic radius. However, the coiled linear polymers can be assumed to be more flexible. Thus, their reptation through pores of a size significantly smaller than the hydrodynamic radius should be easier for linear coiled polymers than for dendrimers or hyperbranched structures. The design of dendrimers for biological applications has been recently reviewed be *Lee* et al.[238] and more examples of possible future applications can be found therein. Although dendrimers and bow-tie dendrimers are a relatively new and promising class of polymer architectures for biomedical applications, they again suffer from a disadvantage, their tedious step-by-step synthesis. Table 2.8 summarizes the advantages and disadvantages of the various types of polymer and dendrimer architectures described in literature. In preliminary studies *Lee* et al.[239] showed that a polyester bow-tie dendrimer conjugated with doxorubicin is a promising candidate for chemotherapy. It showed similar efficacy *in vivo* as Doxil®, an approved liposomal doxorubicin formulation. However, in contrast to Doxil® it is a monomolecular substance, so that formulation and stability issues do not arise. Furthermore, drug attachment is not limited to hydrophobic drugs as in the case of liposomes.

It has been briefly mentioned that also polymers were labeled with targeting moieties and radionuclides instead of drugs for imaging or therapeutic applications. This could

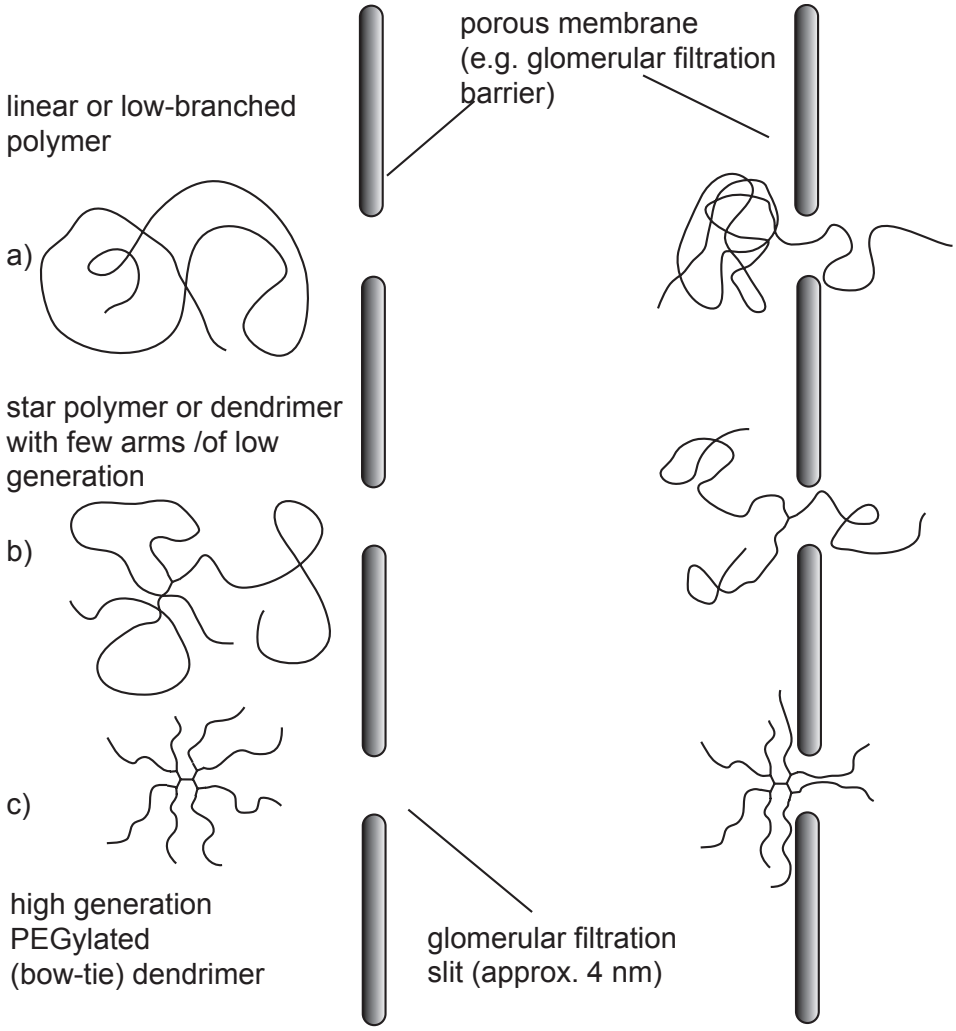

Figure 2.17: Schematic illustration of the permeation of polymers of different architecture through narrow pores like the glomerular filtration slit. Linear or low-branched polymers occupy a relatively large hydrodynamic volume, but can easily uncoil and reptate through the pores (a). Star polymers with a low number of arms or polymer tethered low generation dendrimers are similarly not hampered by steric hindrance and can also penetrate the barrier (b). In contrast, high generation dendrimers occupy a relatively small hydrodynamic volume but this can not be condensed much further, nor can such construct fully uncoil. Therefore reptation through pores is limited if the pores are considerably smaller then the hydrodynamic volume of the dendrimer. Adapted from ref.[238].

Table 2.8: Comparison of different polymer architectures.

Architecture	Advantages	Disadvantages
Linear and branched	facile synthesis via polymerization typically one step synthesis of scaffold great variety of monomers available	polydisperse products polymer analog reactions inefficient, analysis difficult
Dendrimers	well defined, high density of functionalities on periphery fine-tunable pharmacokinetics	multistep reaction functionalization may vitiate solubility
Bow-type dendrimers	analog to dendrimers additionally orthogonal functionalization possible	sophisticated multistep reaction
Hyperbranched	many advantages similar to dendrimers one step synthesis	limited reproducibility limited synthetic control polydisperse products
Dendronized polymers	high density of functionalities rigid polymer architectures accessible	limited synthetic control polydisperse products very difficult analysis typically multistep reaction

be termed polymer supported peptide receptor radionuclide therapy (^{P}PRRT). Some examples will be discussed in the next chapter as these are some of the few conjugates which are - at least to some extend - comparable with the compounds presented.

2.3.3 Polymer therapeutics in nuclear medicine

Recently, *Ghandehari* and co-workers[31] presented first contributions on radiolabeled HPMA copolymers. By free radical polymerization they obtained copolymers of HPMA and a monomer containing a chelator for ^{99m}Tc, an ideal radiolabel for *in vivo* imaging. However, the chelator *N*-ϵ-bis(2-pyridylmethyl)-L-lysine is not well suited for chelation of therapeutic nuclides. In addition, the passive tumor targeting via EPR is very slow. While this is no problem when polymeric prodrugs are used, slow accumulation unfavorable when cytotoxic radionuclides are to be delivered. Some minor adjustments are possible by choosing slowly decaying nuclides, but possibilities are limited. However, polymers bearing targeting peptides could be suitable for delivery of radionuclides to tumors.

Integrin targeted HPMA copolymers in nuclear medicine In the same group HPMA copolymers carrying RGD along with additional chelators suitable to bind diagnostic and therapeutic radionuclides were prepared[100,240,241]. The copolymers were synthesized from 5 different methacrylamide derived monomers by free radical polymerization. HPMA to provide the water solubility and biocompatibility, while carboxylic acid moieties in the side chains were used for the attachment of the homing peptide RGD4C. Other side chain modifications were introduced for radiolabeling with iodine, technetium and yttrium. A mean 15 to 16 units of RGD were reported to be incorporated in polymers of approximately 28 kDa (M_w).
Here, the shortcomings of analytical methods for polymer-peptide conjugates become apparent. The authors determined the RGD content by amino acid analysis in combination with gel permeation chromatography (GPC) data. While the molar mass of the conjugates should increase by approx. 16 kDa (M(RGD4C) = 1273.9 g/mol) the GPC grossly underestimates the values giving only an increase of 1.6 kDa[241]. This could be also an indication of the aforementioned aggregation of peptides at the inside of polymer-peptide conjugates. No synthetic or structural control is possible with free radical polymerization and the monomer content in the resulting polymer only vaguely resembled the feed composition, which points to a non-azeotropic polymerization behavior[31,240,241]. Consequently, one has to assume that the polymer composition changes, as the polymerization proceeds. It was shown by endothelial cell (HUVEC) adhesion assay that the polymer-peptide conjugates inhibit binding of the cells similar to the free peptide *in vitro*. *In vivo*, the HPMA copolymer-RGD4C conjugates exhibit enhanced tumor enrichment by combination of the effects of EPR and targeting via integrin since it is more active than RGD4C and than the polymer-peptide conjugate with the inactive peptide RGE4C. In Figure 2.18 the tumor to organ (T/O) ratios of the HPMA copolymer-RGD4C conjugates and the monomeric peptide RGD4C in a prostate cancer xenograft 24 h p.i. are compared. For all organs but the blood, the polymer conjugates gives rise to higher T/O values than the peptide. The pronounced difference for the muscle is important, since the muscles are by absolute weight the biggest tissues in an the mouse and in humans (approx. 30 - 50 % of total body weight). For this reason a very high T/O for the muscles helps to limit the whole body dose the patient would be objected to. Very recently, it could be shown that a similar conjugate, labeled with the therapeutic nuclide ^{90}Y, leads to arrest of tumor growth in a prostate cancer mouse xenograft[100]. However, a pronounced radioactivity concentra-

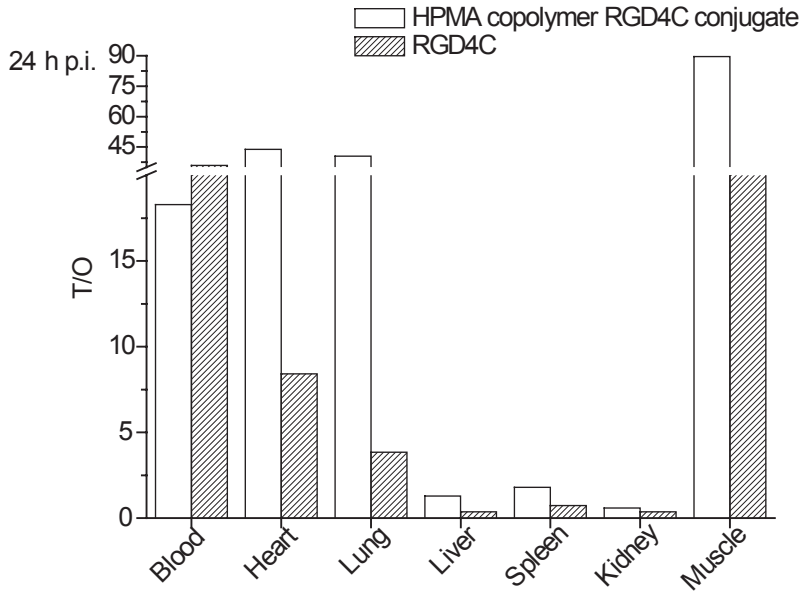

Figure 2.18: Comparison of the tumor to organ ratios of the integrin binding peptide RGD4C and a HPMA copolymer RGD4C conjugate. In all organs but the blood, this ratio is higher for the polymer conjugate than for the peptide.

tion in organs like liver, spleen and especially kidney as well as a rather slow targeting profile should be addressed. Only after approximately 48 hours the tumor/kidney ratio reaches 1. At this time point, already 41 % of the total dose administered has already decayed. Although no nephrotoxicity was observed, a faster delivery is desirable. An alternative could be application of a radionuclide with a longer half-life, such as ^{177}Lu ($t_{1/2} = 162$ h), delivering a greater fraction of the dose, when higher tumor/organ ratios are achieved. Although these results are very promising, it is desirable to enhance the synthetic and structural control of this type of conjugate and to obtain more consistent analytical information. In order to increase synthetic control, polymers obtained from multi-step reactions or polymers synthesized by living polymerization methods are possible approaches.

2.3.4 Summary

Polymer therapeutics are a relatively new but rapidly growing field. It can be already anticipated that this wide and diffuse group will have a big share in drug development in the future. Until now, the majority of applications are in combination with low molar mass molecules as active compounds, where the polymers ´only´ serve as a pharmacokinetic modifier. Here, PEGylation is the most prominent example which is already widely established for solubilization of poorly water-soluble drugs. Since many biologically active compounds are eliminated from further investigation in early stages of development due to poor solubility, polymer conjugation is a valuable tool to save highly active compounds from this fate.

Synthetic polymers suffer from a polydispersity which is highly unfavorable in a biomedical context. Recent developments in polymer chemistry allow the preparation of polymers of narrow molar mass distribution by various methods. However, these techniques also have limitations and limited information can be found on the use of e.g. controlled-radical polymerizates for biomedical application. All examples of HPMA copolymers described herein, were prepared by free radical polymerization allowing only limited control of the polymer architecture. In contrast, dendrimers can be build up to have perfectly controlled architectures. However, their sophisticated step-by-step synthesis is tedious and not always perfect. The community realizes more and more that the controlled polymer synthesis will be one of the most important problems to be addressed in the future of this field of research.

Despite a great number of polymers which are termed biocompatible at times, only few polymers are actually used in the development of polymer therapeutics, especially PEG, HPMA copolymers and poly-L-glutamic acid. In the following chapter, another polymer will be introduced and discussed, the poly(2-oxazoline)s (POx). These are the mainstay of this work and will be established as a promising, highly modular and versatile carrier system in polymer therapeutics.

2.4 Poly(2-oxazoline)s

2.4.1 2-Oxazolines

The five-membered ring system of 4,5-dihydrooxazoles is known since the late 19th century. While first mentioning of the oxazoline ring was in 1889, it took *Gabriel* and *Eschenbach* until 1897 to report the synthesis and isolation of pure 2-methyl-2-oxazoline which was then termed μ-methyloxazolin[242]. In literature it is repeatedly claimed that *Andreasch* described the oxazoline ring system first in 1884[243,244]. However, the cited reference[245] does not mention any oxazoline-like structure but deals with the synthesis of allyl urea.

While 4,5-dihydrooxazole is the name recommended by IUPAC, it is still more common to use the term 2-oxazolines for structures derived from this heterocycle (Fig. 2.19). 2-Oxazolines are of considerable interest in organic synthesis. Aldehydes, ketones, lactones, amino acids, thiirans, olefins as well as homologated carboxylic acid derivatives are accessible by appropriate reactions. Furthermore, the inertness to a variety of reagents and conditions makes the oxazoline ring system a valuable protection group for carboxylic acids[243]. Substitution at the 2, 4 and 5 position yields a great variety of derivatives. 2-Oxazolines and bisoxazolines are widely used as ligands in complex chemistry and complexes of (bis)oxazolines with numerous transition metals are known (e.g. Zr[246], Re[247], Ru and Rh[248], Pd[249], Cu[250,251], and Zn[252]). *McManus* and *Patrick*[253] reviewed the use of oxazoline containing ligands for asymmetric catalysis, first described in 1986[254].

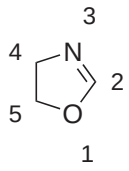

Figure 2.19: 4,5-Dihydrooxazole, commonly known as 2-oxazoline.

The oxazoline ring system is synthetically easily accessible and chirality can be introduced at the 4 and 5 position by chiral α-amino acids.

In Figure 2.20 five approaches for the preparation of 2-oxazolines are depicted. Route 1 is the aforementioned first synthesis of 2-methyl-2-oxazolin[242]. Route 2 and 3 are variations of this first procedure of *Gabriel* and *Eschenbach* by *Zarka*[255] and *Cesana*[256] respectively. An activated carboxylic acid derivative is reacted with 2-aminoethylchlorine. An often applicable facile one step synthesis, the addition of

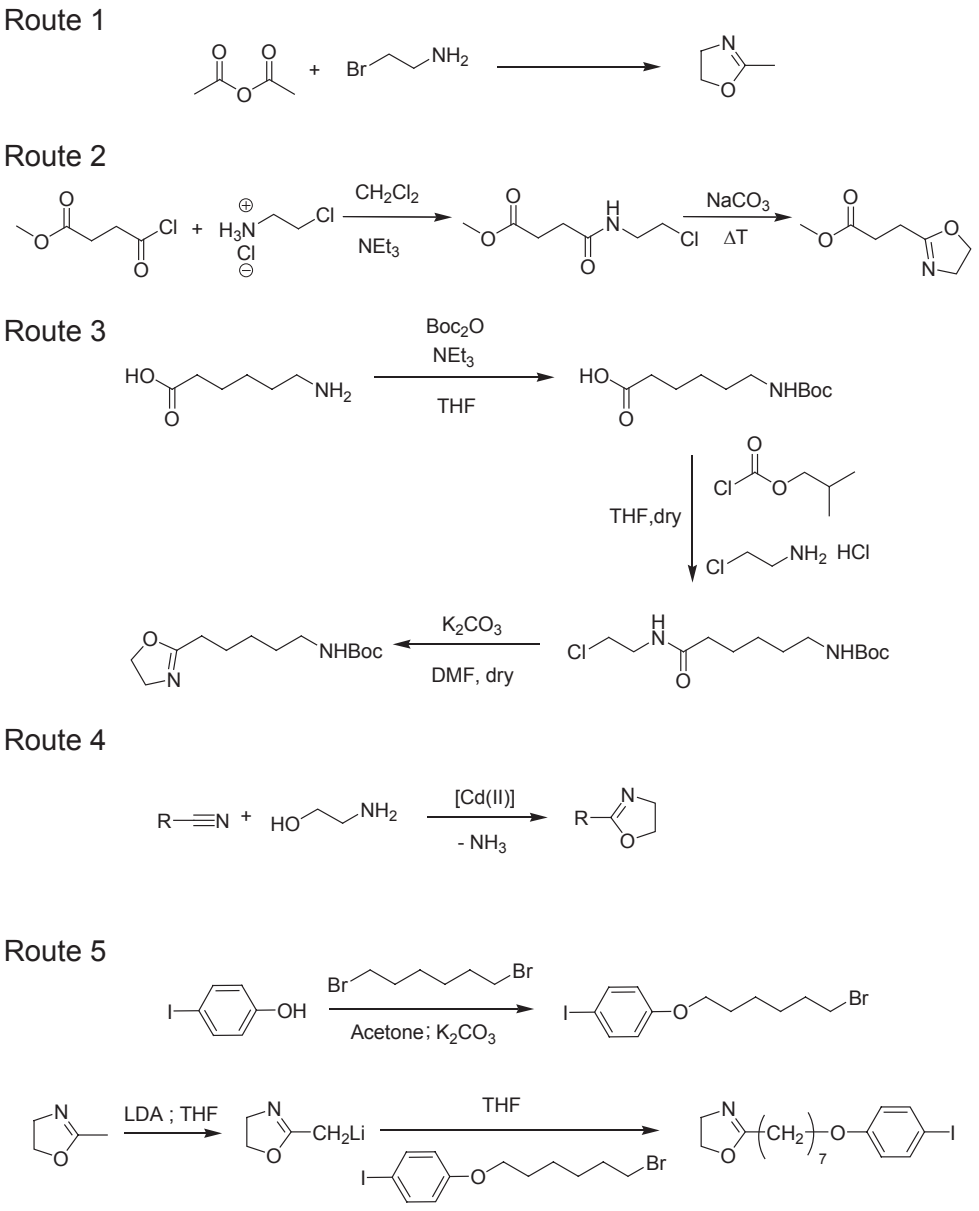

Figure 2.20: Five synthetic routes towards 2-oxazolines. In the first three the oxazoline ring is build up starting for carboxylic acid (derivatives), in the fourth nitriles and aminoethanol are used as educts. The fifth route starts from commercially available 2-methyl-2-oxazoline.

aminoethanol to nitriles is shown as Route 4[257]. Route 5 was developed by *Persigehl*[258] and was also applied for the synthesis of 2-[3-(1,3)-dioxolan-2-ylpropyl]-2-oxazoline[259] (DPOx), used in this work. More examples of synthetic routes towards 2-oxazolines can be found by *Aoi* and *Okada*[260]. Besides the aforementioned applications, 2-oxazolines substituted only at position 2 are mainly known for their use in living cationic ring-opening polymerization (CROP).

2.4.2 Living polymerization of 2-oxazolines

In the middle of the 1960s four groups independently reported on the CROP of 2-oxazolines[261–266]. Figure 2.21 shows the initiation, propagation and termination reactions, while in Figure 2.22 possible chain transfer and repolymerzation reactions, as described by *Litt* et al.[267] are depicted. Several reviews can be found in literature that deal with the polymerization of 2-oxazolines in detail[244, 260, 268, 269].
Electrophiles, such as Lewis and Brønsted acids, or alkylating agents can attack the nucleophilic nitrogen of the oxazoline ring with the rate constant k_i. The resulting oxazolinium cation can be attacked by a second oxazoline under ring-opening (Figure 2.21, Route A, $k_{P,i}$) or ring-open under formation of a linear covalent amide structure (Fig. 2.21, Route B, k_X). Both species are electrophilic and can react with additional 2-oxazolines. On which side the equilibrium between covalent and ionic species lies, depends on various factors. Increasing nucleophilicity of the initiator counterion and of the monomer decreases the tendency of the reaction to be ionic. With the non-nucleophilic trifluoromethylsulfonate (triflate, OTf) as counterion, the propagating species is the cation with any type of 2-oxazoline[260] and the propagation rate increases[270]. The solvent also exerts considerable influence. Acetonitrile (ACN) stabilizes the propagating cation due to its polarity and donor properties. Methyltriflate (MeOTf) as initiator has another, very valuable advantage. Due to its high reactivity it reacts very fast with 2-oxazolines even below room temperature, while polymerization starts at temperatures above $\sim 40\,^{\circ}\mathrm{C}$. This is utilized in the synthesis of initiator salts[271]. Quantitative and fast initiation of polymerization (in comparison with the propagation) is a crucial factor when well-defined polymers with narrow molar mass distributions are to be obtained. Since the initiation is nearly instantaneous and the

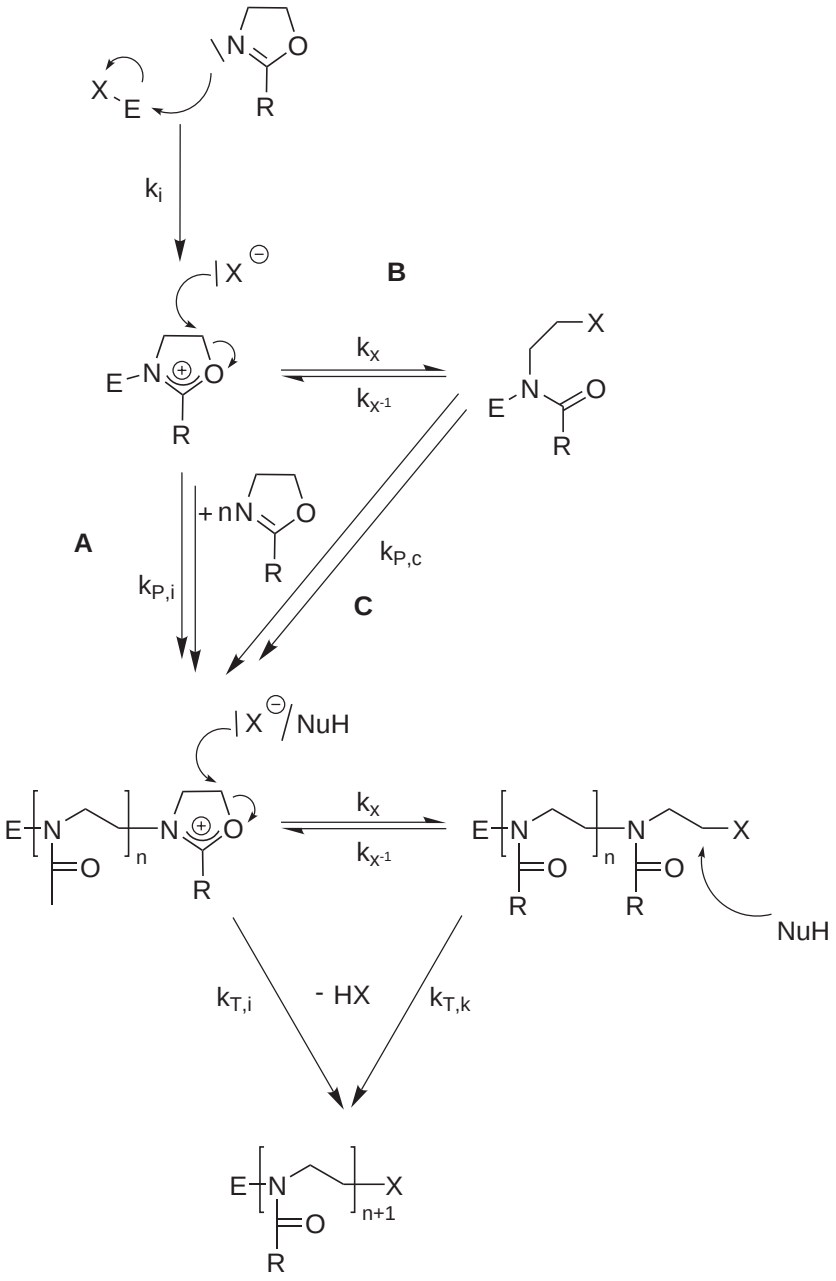

Figure 2.21: Mechanism of living cationic polymerization of 2-oxazolines (X-E = electrophilic initiator, e.g. methyltriflate and NuH = nucleophilic terminating reagent, e.g. piperidine or piperazine).

formed oxazolinium triflate is sterically and electronically similar to the propagating polymer chain end, poly(2-oxazoline)s can be prepared with very low polydispersity indices (M_w/M_n) of $\sim$ 1.02 to 1.20. Due to the moderately slow propagation of the polymerization of 2-oxazolines facile on-line investigation of the reaction is possible, e.g. by proton nuclear magnetic resonance (^{1}H-NMR) spectroscopy or gas chromatography (GC). Although the polymerization of 2-oxazolines is regularly termed a living

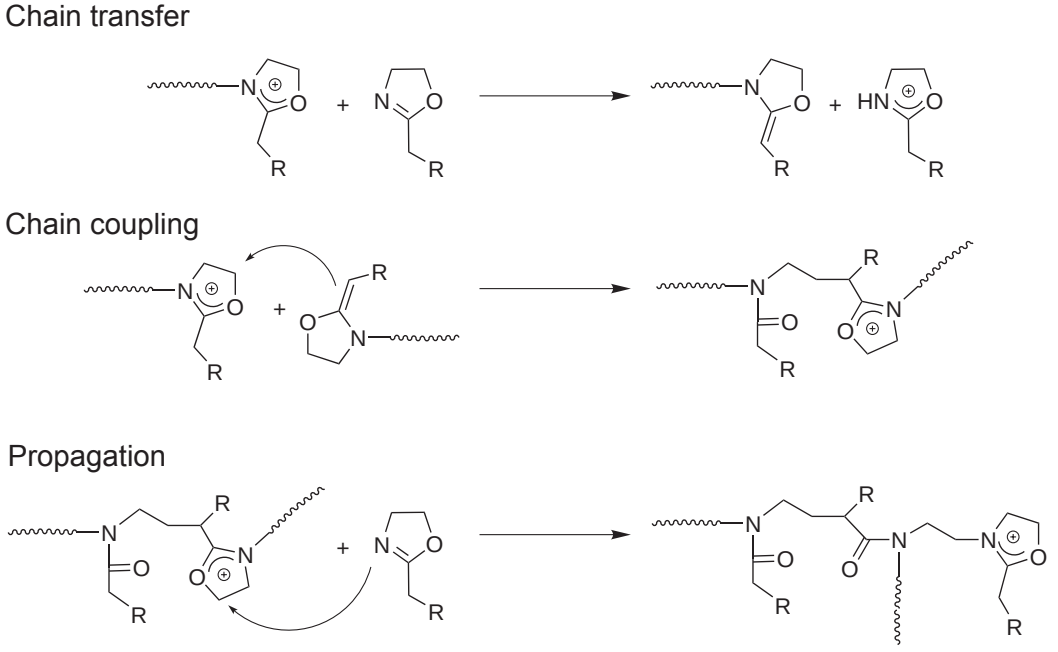

Figure 2.22: Proposed mechanism of chain transfer, chain coupling and repolymerization during the cationic ring-opening polymerization of 2-oxazolines[267].

one, the investigations of *Litt* et al.[267] done in the early 1970s should be considered. Experimental findings which can be explained by chain transfer reactions, suggest that side reactions can occur. However, these studies where mainly performed with bulk polymerization experiments at high temperatures ($T > 120\,°C$) and at very high $[M]_0/[I]_0$ ratios. *Hoogenboom* et al.[272] recently accounted the appearance of a high molar mass shoulder in the GPC traces of poly(2-ethyl-2-oxazoline)s to this transfer and subsequent chain coupling, when the polymerization was carried out at high monomer concentration ($[M]_0 > 5\,M$). In conclusion, poly(2-oxazoline)s can be synthesized with high structural control and definition. However, this generally is restricted to a degree of polymerization(DP) of around 50, although in some cases, higher DPs have been reported while polydispersities were still low[272,273].

The frequently used 2-oxazolines include 2-methyl- and 2-ethyl-2-oxazolines (MeOx and EtOx) which yield hydrophilic polymers, 2-alkyl-2-oxazoline (especially nonyl, NonOx) and 2-phenyl-2-oxazoline to obtain hydrophobic polymers as well as 2-*iso*-propyl-2-oxazoline (iPOx). Poly(2-isopropyl-2-oxazoline)s (PiPOx) are water-soluble and show an interesting phenomenon, the lower critical solution temperature (LCST) at a temperature interesting for biomedical applications[274–278]. Concentration dependent, an upper temperature limit (cloud point, CP) can be found, above which the polymer is no longer soluble in aqueous solution[273,279–281]. By copolymerization with the hydrophobic NonOx, *Huber* and *Jordan*[282] could recently show that polymers with a CP below room temperature are accessible.
Due to the living character of the polymerization of 2-oxazolines, blockcopolymers are accessible and a number of reports can be found where multifunctional initiators were applied in order to obtain star-like homo- and blockcopoly(2-oxazoline)s[283–292] while by initiation with lipid-triflates lipopolymers can be obtained[293,294]. This architectural variability is interesting also for biomedical applications. Blockcopolymers of hydrophilic and hydrophobic monomers result in amphiphilic polymers and can form micelles. A prominent example of this type of polymer is pluronic® series (generally structure: poly(ethylene glycole-b-propylene glycole-b-ethylene glycole), PEG-PPG-PEG) which is widely used, e.g. from metal processing to biotechnology and drug delivery. Additionally, amphiphilic blockcopolymers are highly interesting for the emerging field of polymer genomics. In this area of research, the influence of amphiphilic polymers on the gene expression of cells are investigated[295].
The living CROP allows specific and orthogonal functionalization of both chain ends of the resulting polymer. While this is also widely applied for PEG, in POx additional side chain modifications are possible.

2.4.3 Chemistry on poly(2-oxazoline)s

Two main possibilities pendant group chemistry of POx can be found in literature. The somewhat more common, facile and versatile approach is the (partial) saponification of e.g. poly(MeOx) (PMeOx) and subsequent capping of the produced ethylene imine groups with functional isocyanates and carboxylic acids. Hereby *Chujo* et

al.[285,296–300] produced a number of stimuli sensitive hydrogels which will be discussed later (Chapter 2.6.2). However, this type of polymer analog modification allows only limited control over the amount of functional side chains, quantitative conversion is unlikely and residual ethylene imine groups, being cationic species, are not necessarily desirable for a biomedical application. Furthermore, no control over the microstructure of the polymers is possible.

The second strategy is the incorporation of functional monomers via copolymerization. Due to the living character of the CROP, direct analysis of the polymer microstructure is possible. If both monomers are consumed at the same rate, random copolymers are obtained. On the other hand, if the monomer consumption rates differ significantly, gradient or even block copolymers are the result. Figure 2.24 shows a number of described side chain functionalities which can be introduced directly by polymerization. The first example, 2-vinyl-2-oxazoline was described already in 1959 in a patent, however there the radical polymerization of the vinyl group was described, leaving the oxazoline ring intact[301], while some 7 years later the CROP of this monomer seems[11] to have been reported[265] and studied in detail afterwards[302–306]. Protected hydroxyl and carboxylic acids were introduced in 1968[307]. These moieties remain up to date among the more regularly employed side chain functionalities and were used extensively in the context of micellar catalysis[255,308,309]. *Hsieh* and *Litt* reported on carbazole derivatives[310,311] while *Persigehl* et al.[258] introduced iodoaryl bearing oxazolines. *Binder* and *Gruber*[312] introduced the dialkyne and azide bearing monomers and more recently, ligands for catalysis[313] and even Pd-catalysts[314] could be introduced directly. Finally, a protected aldehyde bearing monomer was suggested[315] and introduced[259] as well as a protected amine moiety[256,316] for chemoselective reactions. Figure 2.24 shows a number of possible reactions on the side chains of poly(2-oxazoline)s. Recently, first poly(2-oxazoline)-peptide conjugates were prepared in this group (Figure 2.25). *Cesana*[317] prepared poly(2-oxazoline)-c(RGDyK) conjugates for *in vivo* diagnosis of integrin expressing tissue, especially neovasculature of tumors (vide supra, Chapter 2.2.1). In another preceding work, a first poly(2-oxazoline)-octreotate conjugate was prepared, which carried also the chelator DOTA[315]. In both cases the peptide attachment at the polymer side chains were performed with standard peptide coupling protocol using protection groups. Thus, attaching both ´homing-device´ as

[11] the author is illiterate in japanese and thus, was unable to read the respective original contribution

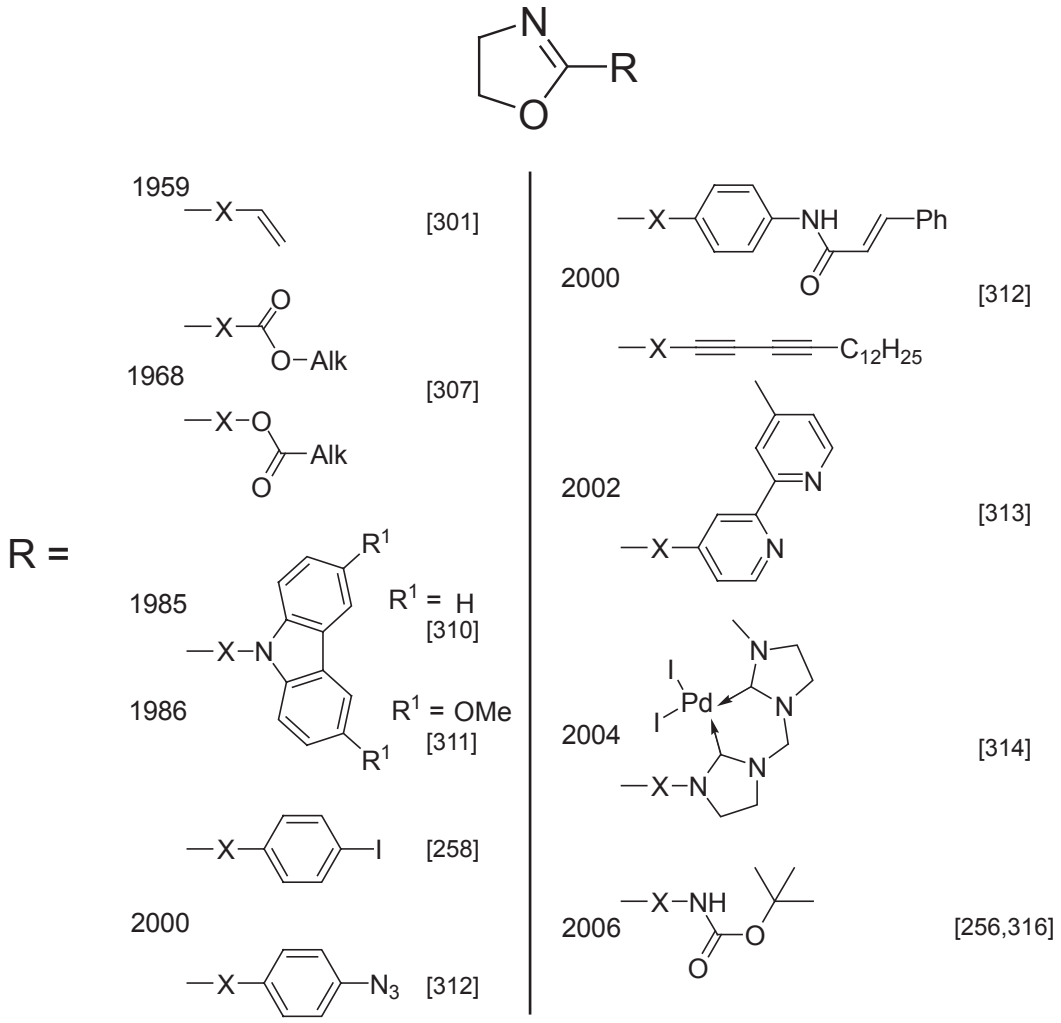

Figure 2.23: Simplified representation of 2-substituted 2-oxazolines (and the year of their introduction) that allow to introduce side chain functionalities by (co-)polymerization. In recent years a more pronounced interest in functional poly(2-oxazoline)s, especially in our group, led to a number of new functional monomers. Please note: X stands for an eventual alkyl chain spacer.

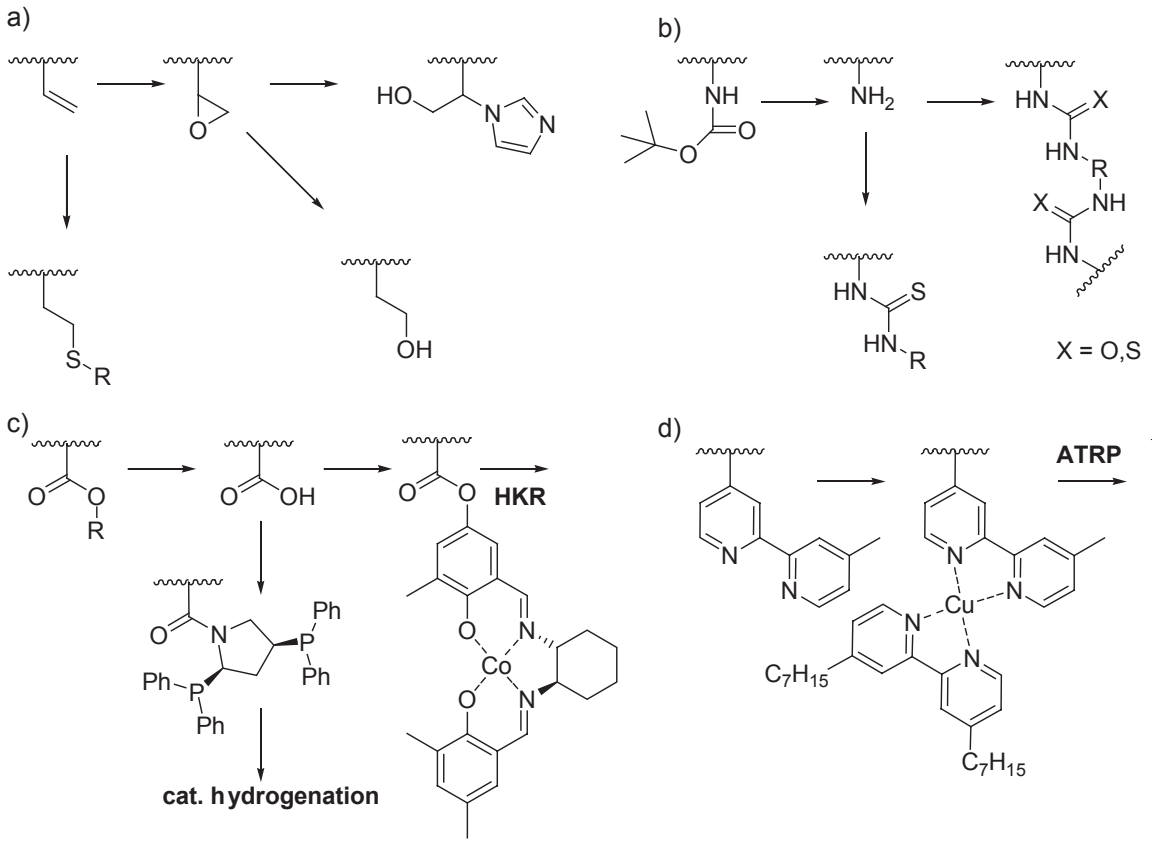

Figure 2.24: Polymer analog reactions on poly(2-oxazoline)s allow attachment of chemical moieties incompatible with CROP, e.g. catalysts, peptides or fluorescent dyes.

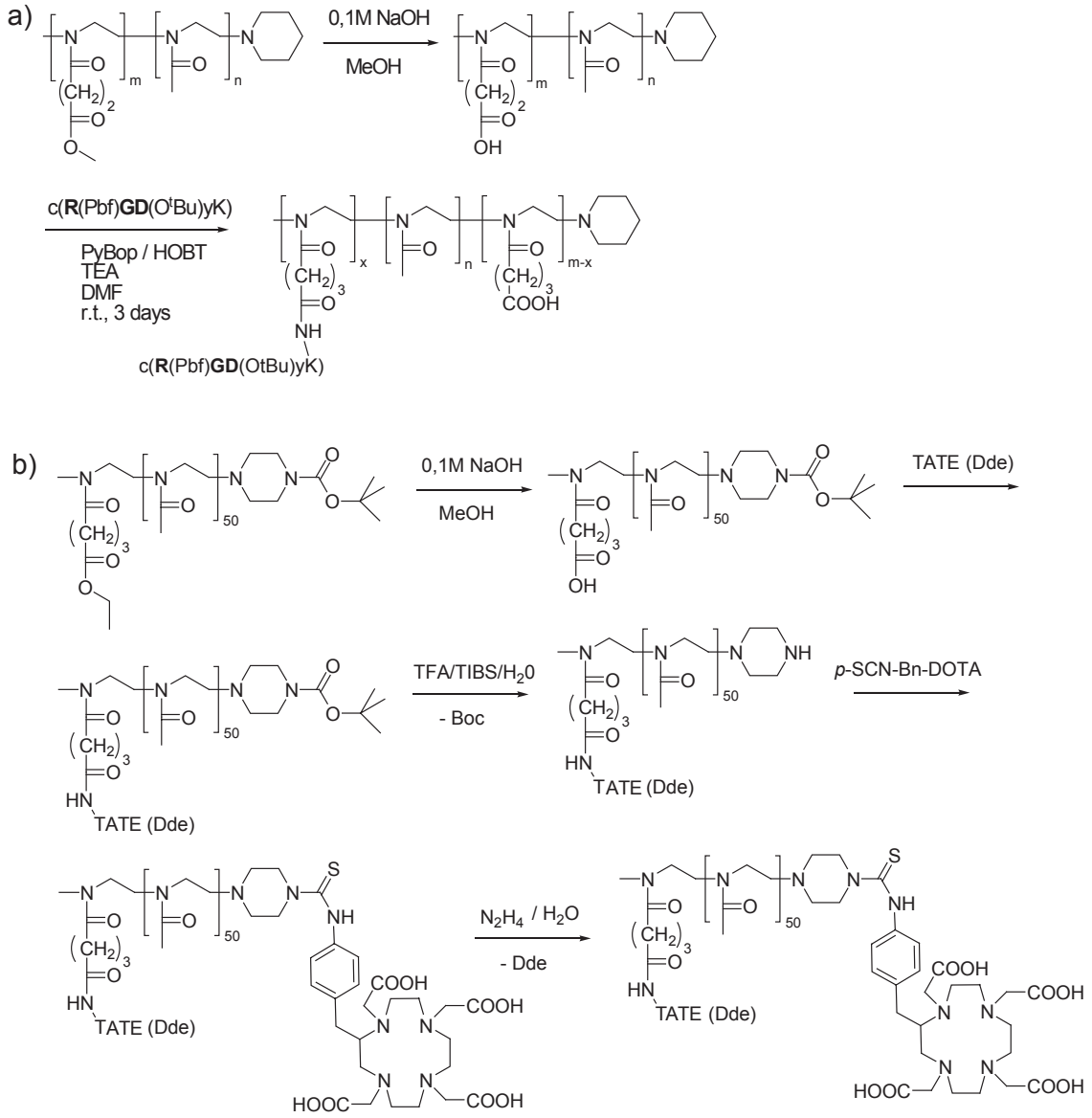

Figure 2.25: Preliminary work performed to prepare poly(2-oxazoline)-peptide conjugates. a) The attachment of the peptide in both cases was performed by coupling polymer bound carboxylic acid with a free amine on the peptide[317]. In the second case (b) with additional attachment of DOTA via the polymer N-terminus, five polymer analog steps were necessary, crippling the efficiency of this approach[315].

well as chelator required a tedious series of five polymer analog steps (Figure 2.25b). The coupling reaction with the peptide was not quantitative and thus, subsequent purification via HPLC was necessary. The overall yield was very poor. When attempting to attach multiple copies of peptide a reasonable HPLC separation may be even more difficult. For these reason it is highly desirable to introduce side chain functionalities which allow facile and quantitative modification.

2.4.4 Biocompatibility of poly(2-oxazoline)s

Poly(2-oxazoline)s still seem to be considered somewhat exotic in polymer chemistry even though they are known for a considerable time. Although there is already a patent application involving POx as carrier for peptides[318] only limited data about the biocompatibility of POx can be found in literature as compared to PEG or PHPMA. However, a number of publications concerning the biocompatibility and biomedical applications of poly(2-oxazoline)s exist[319–322]. While data are limited, there is no evidence for considerable toxicity or incompatibilities related to neither PMeOx nor PEtOx. In general it seems that PMeOx and PEtOx show a similar behavior *in vivo* as PEG. *Goddard* et al.[319] reported on the biodistribution of radioiodinated poly[(MeOx)-co-(2-(4-hydroxyphenyl)-2-oxazoline)] (PMeOxHPhOx) after i.v. administration. They found no significant accumulation in organs other than skin and muscle. However, the reported amounts of detected radioactivity in the various organs seems not to have been standardized to the mass of the organs. Therefore it is not surprising that the skin and muscles, which add most to the total mass in the body, contain significant amounts of radioactivity, while the value of %ID/g might by actually quite low for these organs. Importantly, only a low accumulation of the polymer in the RES, in liver and spleen has been found. This would make POx a potential candidate for biomedical applications. However, the reported polymers were obtained by bulk polymerization and more importantly, the pendant free hydroxyl group certainly leads to branched products. Subsequent fractionation into different, relatively narrow batches of different molar masses reduced the broad polydispersity, but branched and linear polymers were not separated by this method. This could, as already elaborated, lead to significantly different pharmacokinetics in comparison

with well defined and linear POx of low polydispersity.
Zalipsky et al.[321] compared the biodistribution of PEtOx, PMeOx and PEG (DP ~ 40) grafted liposomes in mice. While PEtOx-liposomes showed a slightly faster blood clearance as compared to PEG, PMeOx was cleared slightly slower. Both POx led to a higher uptake in the liver. PEtOx was found more in the spleen, while PMeOx was less accumulated than the PEG derivative in this organ. Overall, the authors showed that the two hydrophilic POx give rise to a similar distribution *in vivo* as PEG if grafted on liposomes. In conclusion, albeit data is limited concerning the biocompatibility of hydrophilic POx, it is promising.

2.4.5 Summary

Poly(2-oxazoline)s are a family of chemically and structurally versatile polymers which have shown no adverse biological effects up to date. Since they can be produced with high definition and a number of different terminal and side chain functionalities. Additionally lipopolymers, blockcopolymers and star-like polymers are accessible. High-priced monomers, the delicate polymerization and thus far, little or no significant superiority in properties of the product appalled industry and, in parts, academia to study and apply this class of polymers in detail and broadness. However, the rapidly emerging and developing field of polymer therapeutics asks for well-defined, biocompatible and functionalizable polymers. Here, for many application, the price of the carrier material will be of no or little significance. Other parts like therapeutic or target homing moieties exceed the production cost of any POx by orders of magnitudes. Thus, POx seems a promising candidate for the development of polymer therapeutics following the rationale of *Ringsdorf*[9] (Figure 2.15.

2.5 Chemoselective coupling reactions

Chemoselective coupling reactions are recently coming into focus as a valuable tool to realize chemical entities which were difficult, or impossible to synthesize even with sophisticated synthetic procedures, such as *Merrifield*s solid phase peptide synthesis (SPPS). When peptides larger than 100 amino acids are to be synthesized, usually chemoselective couplings are applied. This is not only because of the effectiveness and ease of those reactions, but also their tolerance of functional groups present in unprotected peptides. Large, fully protected peptide fragments have typically only limited solubility.
In polymer chemistry, chemoselective reactions are enticing for another reason, as two points are of paramount importance biomedically applicable conjugates. Reduction of polymer analog steps and maximization of modification yield. This shall be explained by an arithmetic example. If one assumes an average of 10 functional groups pending at the polymer and an average conversion efficiency of 90 % one ends up with only 35 % of polymer that is quantitatively converted. The rest consists of polymer with variable ratios of functionalized side chains. Adding to the natural polydispersity of a polymer, this functional dispersity will make it very difficult to isolate the desired polymer conjugate. Even with 99 % coupling efficiency per functional moiety, only 90 % of the polymer will be fully converted. In many cases it will be possible to use an excess of (low molar mass) reagent for the modification (similar to SPPS), allowing to push the modification yield. However, it is still important to apply highly efficient coupling reactions which exhibit no or only very limited side reactions.
In this work, different ways to use chemoselective coupling reactions should be elucidated. After a thorough look into literature three reactions (Figure 2.26) where considered to be interesting candidates for our purposes.

2.5.1 Aldehyde-aminooxy Coupling

The reaction between aldehydes and aminooxy compounds gives oximes (Figure 2.26a) with good efficiency in aqueous solution over a wide pH range. The formed bond is reasonably stable under physiological conditions against hydrolysis[226] and for in-

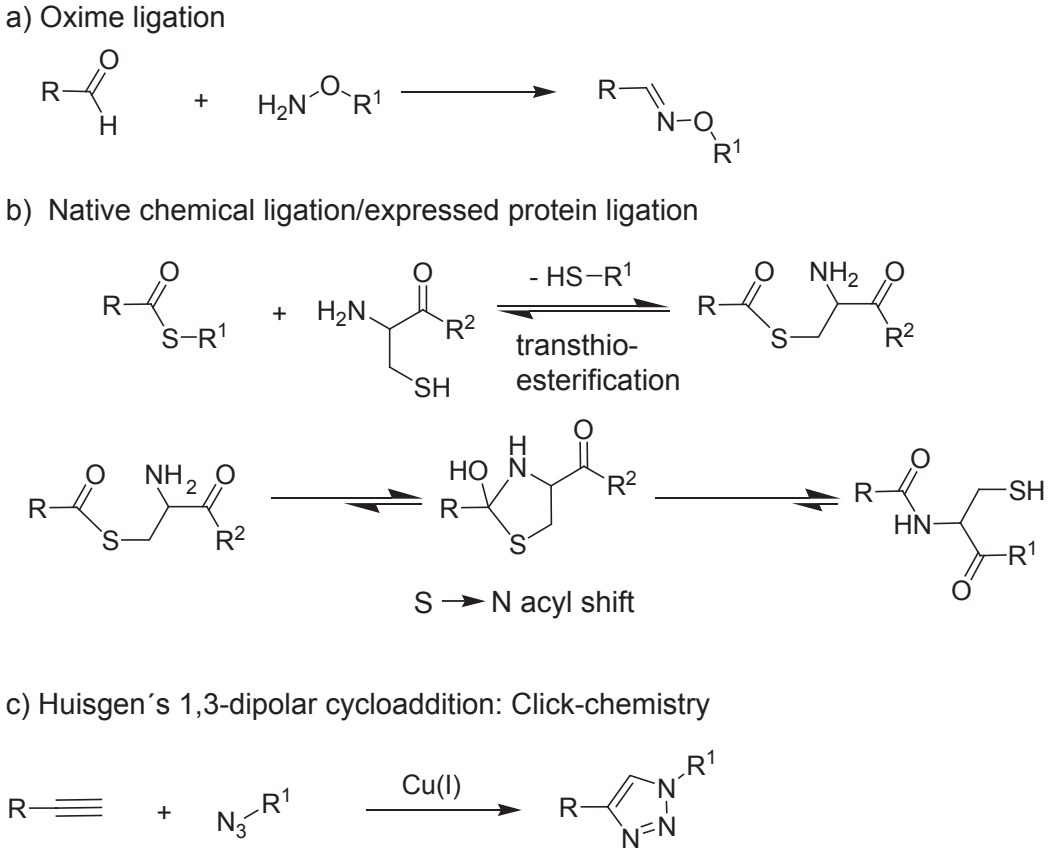

Figure 2.26: Three examples of chemoselective reactions. a) The oxime formation can be performed in aqueous media over a wide pH range. b) The native chemical or expressed protein ligation is performed at or around neutral pH in water. c) Click-chemistry is typically performed under basic conditions in water, aqueous media or organic solvents.

troduction of aldehydes and aminooxy groups a number of synthetic procedures are described and established. *Poethko* et al.[226] have shown that under appropriate conditions a number of unprotected amino acids do not significantly interfer with the oxime formation. Before that, a series of papers in the early nineties described the use of oxime ligation for coupling of radionuclide chelators to antibodies[323–326], while *Mikola* et al.[327] reported on the steroid modification.
Soon afterwards, *Rose*[328] described the highly efficient synthesis of peptide multimers. Since then, a number of peptides/peptide conjugates, glycoconjugates and oligonucleotides have been synthesized by this method[222, 329–332]. In addition this coupling methods are used in nuclear medicine for rapid attachment of short-lived nuclides[333]. A review by *Lemieux* and *Bartozzi*[334] covers the aminooxy ligation and similar chemoselective ligations.
Finally this reaction was also applied in polymer chemistry to realize highly effective and chemoselective polymer analog modifications[259, 335].

2.5.2 Native chemical ligation

Peptides carrying cystein at the N-terminus can be coupled chemoselectively to thioesters (Figure 2.26b). The coupling is performed readily in aqueous solution around neutral pH. The first step is a reversible transthioesterification followed by an almost[12] irreversible S→N acyl shift via a thiazolidine intermediate[337]. This reaction is termed native chemical ligation (NCL) and the resulting connection is a (native) peptide bond[338–340]. NCL has only little limitations and has been developed in the meanwhile also for SPPS[341] and protein engineering[342–346]. As long as it is possible to introduce a thioester moiety and a N-terminal cystein the two fragments will couple rapidly at room temperature. Importantly, other cystein moieties within either peptide fragments do not interfer with the reaction because all but the N-terminal cystein cannot undergo the irreversible acyl shift. *Kalia* and *Raines*[347] developed a route, utilizing reversed NCL for C-terminal introduction of functionalities into proteins. They introduced an alkyne which was subsequently used for the 1,3-dipolar cycload-

[12] this acyl shift is not entirely irreversible but the reversed reaction is thermodynamically highly unfavorable and often regarded as irreversible. However, in protein splicing this N→S acyl shift is crucial[336]

dition with an azide (Huisgen cycloaddition) bearing fluoresceine, a third candidate of chemoselective reaction applied in the present work.

2.5.3 Click-chemistry

The term click-chemistry, coined in the group of *Sharpless*, originally denominated coupling reactions that:

- must be modular, wide in scope, give very high yields
- generate only inoffensive byproducts that can be removed by non-chromatographic methods
- are stereospecific (but not necessarily enantioselective)

The required process characteristics should include:

- simple reaction conditions (ideally, the process should be insensitive to oxygen and water)
- readily available starting materials and reagents
- the use of no solvent or a solvent that is benign (such as water) or easily removed
- simple product isolation
- the product should be stable under physiological conditions[348].

However, the term 'click-chemistry' became more and more synonymous with the Cu(I)-catalyzed Huisgens 1,3-dipolar cycloaddition between azides and alkynes (Figure 2.26c). The first systematic investigation of this reaction and application in peptide synthesis was reported by *Tornøe* et al.[349] followed shortly after by a more mechanistic investigation by *Sharpless* and co-workers[350–352], revealing the step-wise formation of the triazole ring (Figure 2.27). Since then, an immense interest in click-chemistry

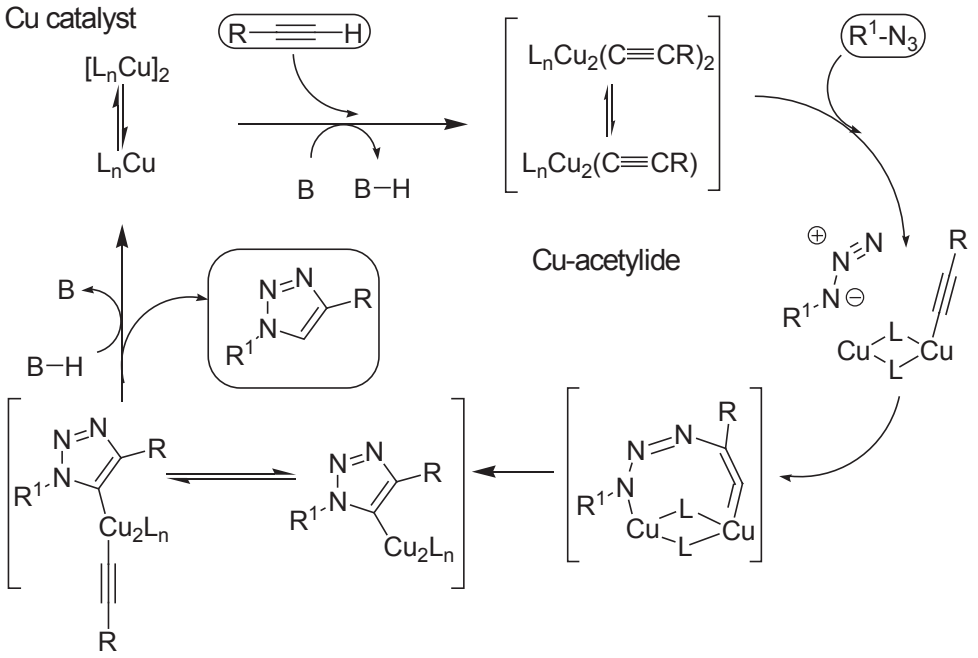

Figure 2.27: Schematic illustration of the mechanism of the copper catalyzed Huisgen 1,3-dipolar cyclo addition between azides and alkynes[351,352].

evolved (Figure 2.28) and the copper catalyzed Huisgen cycloaddition appeared in many areas of chemistry, from material science[353,354] over organic synthesis[91,355,356], biochemistry[357–361], supramolecular chemistry[362–364] and polymer science[99,365–374]. Since numerous and very recent reviews are available in literature[375–377], no detailed discussion of this reaction is necessary here.

2.6 Hydrogels

Hydrogels are highly hydrated three-dimensional networks of hydrophilic polymers. Due to the, cross-linking hydrogels are insoluble but swell in water (or other polar solvents). Several different types of hydrogels can be differentiated:

- Ionic and non-ionic hydrogels: Ionic hydrogels contain numerous charged units (normally in the monomer unit, e.g. poly(acrylic acid-co-sodium acrylate) and regularly show a higher swelling degree ($\frac{\text{m(swollen)-m(dry)}}{\text{m(dry)}} = S_W D$) in water (super-

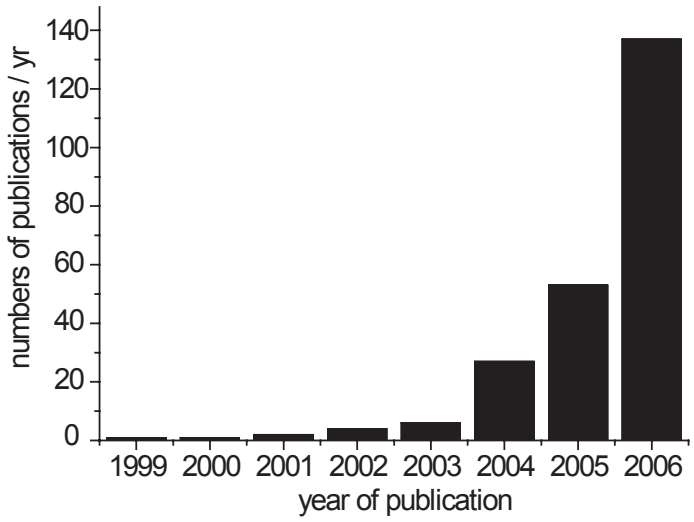

Figure 2.28: The increase in publications on 'click-chemistry' shows the growing interest in this field. Please note: the numbers were obtained from SciFinder®Scholar 2006 and for the search term "click chemistry" after removal of duplicates.

absorbant polymers (SAP), S_WD up to 1000), but are generally stronger affected by the ionic strength of the solvent than non-ionic hydrogels.

- Physically and chemically cross-linked hydrogels: Polymers can be cross-linked by physical interactions (hydrophobic interactions, ionic interactions, polymer chain entanglement or hydrogen bonds) or covalently. Covalent cross-linking is sometimes regarded as more stable and permanent, but that is not necessarily the case.

- Hydrogels from natural polymers, synthetic polymers or recombinant protein-polymers: Many different hydrophilic polymers such as gelatin[250,378,379], chitosan[380], alginates[250,381] and other natural polysaccharides have been used to prepare hydrogels. For synthetic polymers PEG[382] (or polyglycerols[335]), PHPMA[383], POx[297], PMMA[384] and poly(phosphazene)s[385] can serve as examples. Recently also recombinant proteins like elastin-like polymer (ELP) come into the focus of research[386–390].

- Permanent and temporary (reversible) hydrogels: Chemically cross-linked hydrogels are often referred to as permanent while physically cross-linked ones are

referred to as temporary or reversible. However, numerous examples showed that it is possible to form labile covalently cross-linked hydrogels (pH-, temperature-, light- or enzymatically labile).

- Inert and stimuli responsive hydrogels: Hydrogels can be inert or stimulus sensitive. Not only the breakdown of the whole gel, but also the degree of hydration can be responsive to stimuli such temperature[386, 387, 391], pH[392] or other parameters.

2.6.1 Hydrogels for biomedical applications

Hydrogels in biotechnology or for biomedical applications are often envisioned as scaffolds for cells. Without the information that they are in an appropriate surrounding, cells tend to undergo apoptosis (Chapter 2.2.1). In the natural surrounding, this information is given by the ECM or other cells. It comprises not only of the mere interaction of cell bound receptors with their ligands, but also the mechanical stress that is mediated thereby. These physical/mechanical properties affect the differentiation of cells as well as their movement (haptotaxis).
Traditional cell culture, however, lack these factors and cell propagation is therefore limited. Scaffolds in tissue engineering can be regarded as a special type of cell culture. In order to ensure appropriate cell growth and thus, tissue regeneration, the scaffold should mimic the natural environment of the respective cells. Cells need adhesion points, such as the already discussed RGD motif in the ECM. If such adhesion motifs are present in the scaffold, enhanced proliferation of the cells is observed. But hydrogels should also mimic to some extend the mechanical properties of the tissue microenvironment. The mechanical input is of great importance for the differentiation of cells, and the mechanical conditions vary for different tissues, as e.g. neuronal tissue demands a different environment than cartilage or bone.
Additionally, nutritional aspects are of significance. While free and efficient diffusion/transport of small molecules and gases is important for the use in cell culture (transport of nutrients to the cells and waste from the cells), hydrogels for controlled release should offer control over transport characteristics.
Furthermore, the degradation should be controllable and degradation should not re-

lease toxic fragments nor influence the environment undue[13]. The influence of the mechanical properties of the hydrogel should be diminished *in concert* with the increasing mechanical influence of the newly formed ECM. It is desirable to decouple the degradation and mechanical properties of the materials. Recently, with hydrogels cross-linked by matrix-metalloproteases (MMP) labile peptide sequences promising candidates to solve this problems have been found. A recent review by *Brandl* et al.[393] covers the rationale of the design of hydrogels for tissue engineering.

2.6.2 Poly(2-oxazoline) based hydrogels

In 1978 Dow Chemicals Co. patented a hydrogel which strongly resembles an PEtOx hydrogel. It was, however, derived of poly(ethyleneimine), subsequently acylated and cross-linked with diisocyanates. It was intended to be used as kraft pulp decolorant and as a water absorber as it could absorb 13 times its mass of water ($S_WD = 13$)[394]. The first hydrogels chemically derived from poly(2-oxazoline)s were reported by *Chujo* et al.[296,298,395,396]. Here, partial hydrolysis of PMeOx was used to obtain poly(MeOx-co-ethylene imine)s. These were subsequently cross-linked with diisocyanates or diacylchlorides yielding hydrogels ($S_WD \leq 72$). However, this high swelling degree was partially due to residual free amine groups which lead to a strongly reduced swelling in aqueous salts[395]. The same approach led to hydrophilic POx with pending furan and maleimide (thermoreversible Diels-Alder cross-linking, $S_WD \leq 15$)[296], bipyridyl (cross-linked by M^{2+}, thermo- and oxidation sensitive, $S_WD \leq 66$)[299,397], coumarin and anthracene (photo cross-linkable, $S_WD \leq 21$)[300,398,399] and sulfhydryl (oxidative cross-linking, $S_WD \leq 24$)[300,399].

As a second approach to prepare POx hydrogels, the copolymerization of MeOx with a bis-2-oxazoline has been reported. This leads directly to hydrogels ($SD \leq 45$), which show no reduction of S_WD in up to 20 wt % $NaCl_{aq}$. Kinetic studies showed that the bis-2-oxazoline reacted much faster than MeOx, so that a relatively short distance between branching points and long pending poly(2-oxazoline) chains can be expected[396]. The same methods was applied for the preparation of amphigels (copolymerization with EtOx) and lipogels (copolymerization with 2-*n*-octyl-2-oxazoline, $S_WD = 10$ in

[13] e.g. pH decrease by the degradation of polyesters may lead to inflammatory reactions

toluene).

Additionally, the preparation of hydrogels from telechelic PMeOx and pluriisocyanates was reported. Star-like[285] and linear[297] PMeOx yielded hydrogels with a $S_WD = 9$ and 12, respectively. Similarly, POx with amine groups in the side chains were cross-linked with phenyl diisocyanate. However, their swelling properties were not reported[256].

Finally, and relevant for eventual biomedical applications, *Uyama* and *Kobayashi*[279] reported on thermo sensitive hydrogels, consisting of a copolymer of a PiPOx macromonomer and ethylene glycol dimethacrylate. As shortly discussed in Chapter 2.4.2, PiPOx shows LCST behavior. This leads to a strong decrease of the swelling degree of the PiPOx containing hydrogels when the temperature is above the CP ($S_WD \leq 100$, if $T < CP$; $S_WD < 20$, if $T > CP$).

2.7 Summary

The specific delivery of diagnostic and therapeutic compounds to diseased cells and tissue is a rapidly developing field and an important part of the prospected individualized medicine where the patient is treated specifically according to the needs of his or her individual disease pattern. Passive and active mechanisms can be exploited for the targeting and the targets may be the diseased cells or related tissue or cells. As targeting compounds antibodies or fragments thereof, oligonucleotides (aptamers), peptides, peptidomimetics other small molecules, micelles, liposomes and polymers are exploited (Chapter 2.1).

The targeted delivery of therapeutic radionuclides, typically α- or β-emitters bound to peptides, is the principle of peptide receptor radionuclide therapy (PRRT). While diagnostic application with OctreoScan® is already in clinical routine for the detection and staging of neuroendocrine tumors, therapeutic approaches (e.g. OctreoTher) are still in clinical trials. Multimerization of targeting moieties is an intensely investigated alternative and it was shown in a number of examples that multimerization leads to an enhanced tumor uptake of radionuclides and to improved tumor to organ ratios (Chapter 2.2).

Polymers can exhibit a passive targeting for certain diseases (e.g. arthritis, cancer) due to their size or can be decorated with moieties for active targeting. However, polymers are naturally polydisperse unless they have been prepared in a step-wise fashion. This polydispersity is their biggest disadvantage in biomedical applications. As a material this polydispersity can improve e.g. its mechanical properties, but in a complex organism, polymers of different size, shape or chemical composition regularly show significantly different pharmacokinetics. PEGylation has been very successful in the recent years and numerous PEGylated drugs have been approved. Among other alternative polymers, HPMA copolymers are investigated extensively and several promising drug conjugates are in clinical trials. However, these polymers are synthesized by free radical polymerization, hence only very little synthetic control is

possible. It is desirable to find polymeric carriers which allow to combine biocompatibility, synthetic and structural control and multifunctionality (Chapter 2.3).

Poly(2-oxazoline)s are synthesized by living cationic ring-opening polymerization. This allows a good control over the molar mass and narrow polydispersities can be obtained. Furthermore, different structures such as telechelic, block- or random copolymers as well as star-like (co-)polymers can be prepared. A number of studies showed that the water-soluble poly(2-methyl-2-oxazoline)s and poly(2-ethyl-2-oxazoline)s show excellent biocompatibility, similar to PEG. However, in contrast to PEG, functional side chains can easily be introduced. Attachment of multiple copies of, e.g. peptides which specifically bind to tumor cells to poly(2-oxazoline)s should allow the preparation of relatively well-defined polymer-peptide conjugates for targeted drug delivery (Chapter 2.4).

For the attachment of targeting moieties a number of pending side chain functionalities in poly(2-oxazoline)s are available. However, these functionalities, e.g. carboxylic acids or hydroxyl- groups do not allow for highly efficient and selective coupling methods. Therefor, new side chain functionalities for chemoselective coupling reactions, e.g. oxime formation, native chemical ligation and click-chemistry are desirable. These reactions have been shown to be of high efficiency and selectivity in difficult conceptual formulations and their application is promising for the projected use, the efficient attachment of multiple homing devices to poly(2-oxazoline) side chains (Chapter 2.5).

Poly(2-oxazoline) based hydrogels have been shown to be accessible as stimuli responsive (reversible and irreversible) hydrogels. Due to their good biocompatibility, these hydrogels are an intriguing alternative as scaffolds for tissue engineering related applications (Chapter 2.6).

3 Aim of this work

Upgrading of the modular kit of poly(2-oxazoline) chemistry A great variety of 2-substituted 2-oxazolines have been described in Chapter 2.4.3, but they generally lack applicability for chemoselective and effective coupling reactions. The first and primary aim of this work was to introduce new side chain functionalities for chemoselective coupling reaction (Chapter 2.5). For the oxime ligation, an aldehyde is to be introduced, protected as a dioxolane, due to good commercial availability of the educts (Figure 3.1a). Secondly, a thioester in the side chain of the polymers is desirable, accessible either by polymer analog transthioesterification or coupling reaction of a suitable bifunctional reagent (Figure 3.1b). Finally, alkyne bearing side chains are needed for click-chemistry. Again, two possible routes are shown in Figure 3.1c. Besides the successful introduction of the functionalities, the respective coupling reactions need to be evaluated. Following the concept of *Ringsdorf* (Figure 2.15), these reaction are to be used for the preparation of well-defined poly(2-oxazoline)-peptide conjugates bearing additionally a chelator for radionuclides.

Defined and functional linear and star-like poly(2-oxazoline)s Preliminary experiments[315] gave some insight into copolymerization of MeOx and an ester functionalized monomer (methyl-3-(oxazol-2-yl)propionate, MOP). This work showed that the two monomers do not copolymerize statistically, but gradually, implying that the peptides, which are attached subsequently via peptide chemistry are situated to a greater extend at one end of the chain. However, it is desirable that the homing devices are evenly distributed along the polymer chain. Functional monomers that undergo random copolymerization are therefor of interest. As mentioned before in Chapter 2.4, at a DP > 50 it is often difficult to obtain well-defined POx. However, for some aspects

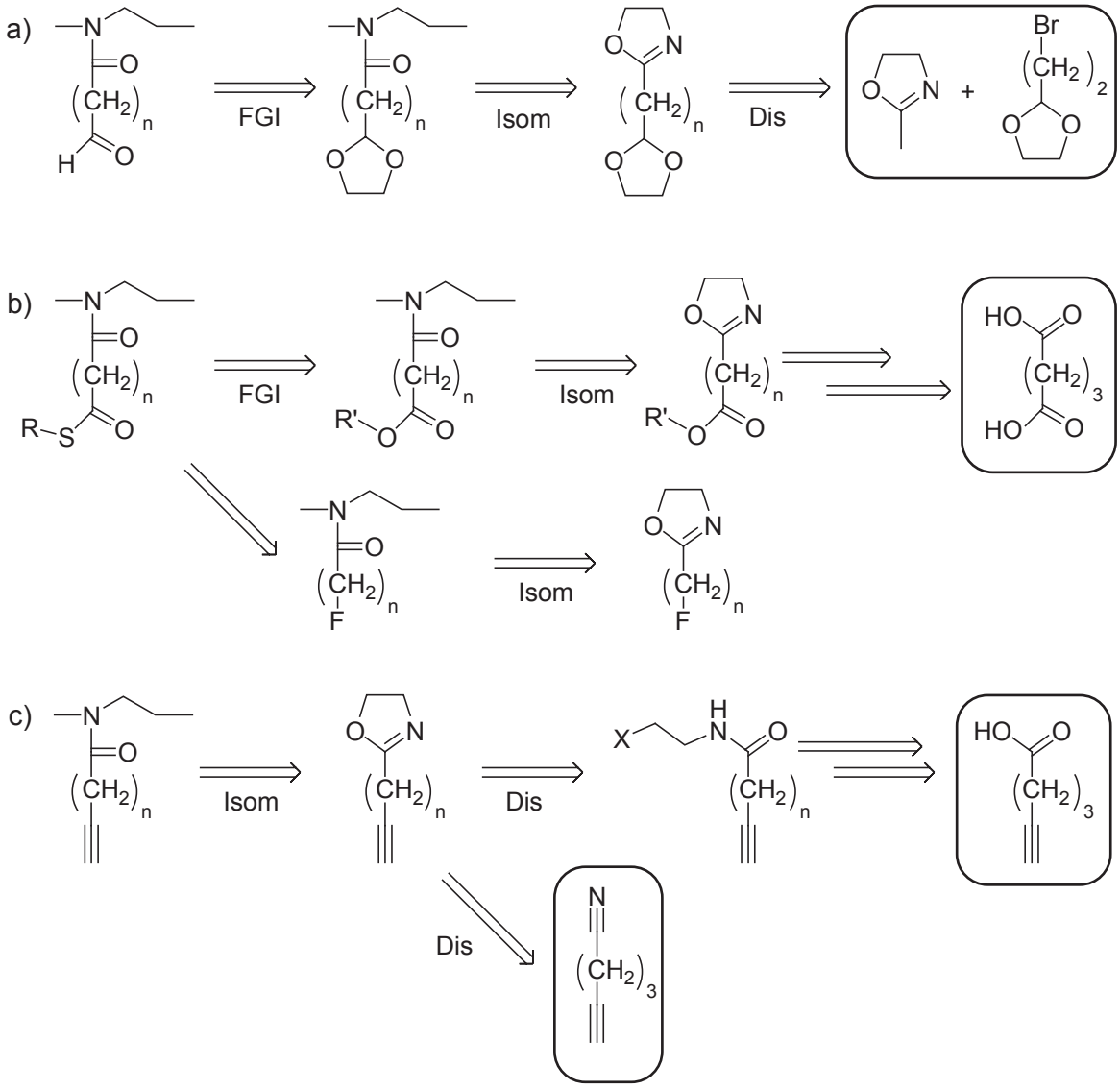

Figure 3.1: Retrosynthetic considerations for poly(2-oxazoline) bearing functional side chains for chemoselective ligations. The necessary monomers can be derived in few steps to commercially available educts (circled compounds). Dis, Isom and FGI stand for disconnection, isomerization and functional group interconversion in retrosynthetic terms.

of the desired biomedical application it is of interest to increase the molar mass. With star-like copolymers (with several arms of a DP $\sim$50), higher molar masses could be obtained and the branched architecture (Figure 2.17) is expected to influence the biodistribution. However, again here the question of definition is important and kinetic investigations will be necessary in order to elucidate whether controlled synthesis of star-like POx is feasible. It will be especially of interest to what extend a multifunctional initiator shows fast and quantitative initiation of all initiator functionalities and homogeneous growth on all arms of the star.

From Functionality to Function - Strategies After the introduction of new functional monomers, the evaluation of their copolymerization behavior with MeOx and EtOx and the establishment of high-yielding coupling procedures, one has to consider strategies for the preparation of polymer-peptide conjugates useful for our intended purpose, ^{P}PRRT. Two consideration suggest that the DP of the polymers and the numbers of to be attached peptides are kept low to start with. A rather low DP (thus molar ass) is typically beneficial for analysis of the polymers. NMR spectroscopy tends to be more accurate and mass spectrometry may be more readily performed and analyzed. In addition, it might seems reasonable to start with polymers which can be (at least roughly) compared with existing compounds, e.g. the RGD-oligomers of *Kessler* and co-workers. The rather low molar mass should also theoretically ensure a rapid distribution and blood clearance in comparison to high-molar mass conjugates, a point of special interest when therapeutic nuclides are to be applied. Thus an overall mass of 5 - 15 kDa and a functional group content (thus homing peptides) of approx. 2 - 5 units is projected. The attachment of different peptides by the various coupling methods should demonstrate the modularity of the presented system.

4 Results and Discussion

4.1 Monomers and linkers

Modifying a described procedure of *Persigehl*[258], 2-[3-(1,3)-dioxolan-2-ylpropyl]-2-oxazoline (DPOx, **1**) was prepared from 2-methyl-2-oxazoline and 2-(2-bromoethyl)-1,3-dioxolane with *n*-buthyllithium (*n*BuLi) and *N*,*N*,*N*',*N*'-tetramethylethylendiamine (TMEDA) in tetrahydrofuran (THF) by *Taubmann* (Figure 4.1) as described in literature[259,400]. This facile one-step one-pot synthesis from commercially available educts gave good yields after silica chromatography and distillation. The use of *n*BuLi and TMEDA instead of lithium diisopropylamide (LDA) as described in literature for a similar reaction, increased the yield to 84 %.
The one step synthesis of 2-(pent-4-ynyl)-2-oxazoline (**2**) from 5-hexynenitrile and

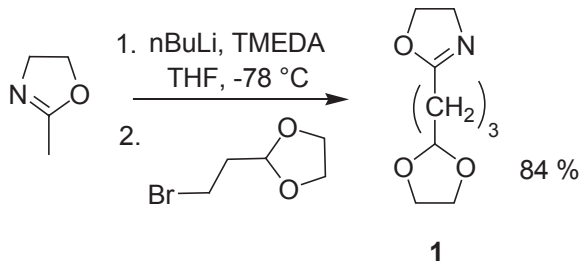

Figure 4.1: Schematic synthesis of 2-[3-(1,3)-Dioxolan-2-ylpropyl]-2-oxazoline (**1**). TMEDA activates the *n*BuLi and thus increases the yield[259].

2-aminoethanol with cadmium acetate according to *Witte* and *Seeliger*[257] failed, presumably due to the cross-reactivity of the alkyne group. However, two other approaches towards alkyne bearing monomers were successful (Figure 4.2). Both demanded several steps but reasonable overall yields could be obtained. Methylation of

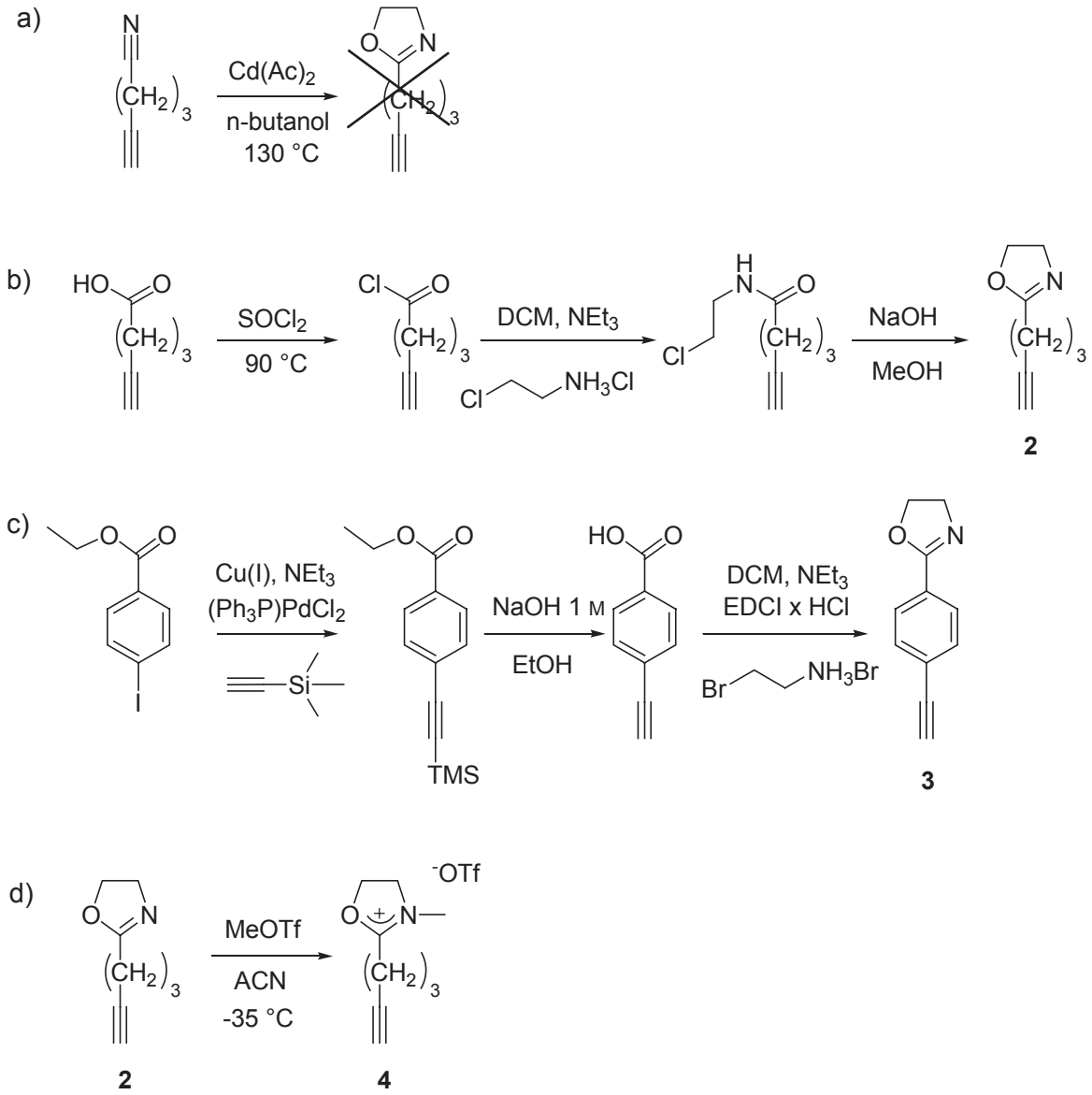

Figure 4.2: Approaches towards alkyne bearing 2-oxazoline monomers. The direct one-step synthesis according to *Witte* and *Seeliger* failed (a). Three-step synthesis of 2-(pent-4-ynyl)-2-oxazoline (PynOx, **2**) as described in literature (b)[401], and three-step synthesis of 2-(4-ethynylphenyl)-2-oxazoline (**3**)(c). Reaction of **2** with methyl triflate (MeOTf) gave the initiator salt **4** in excellent yield (d).

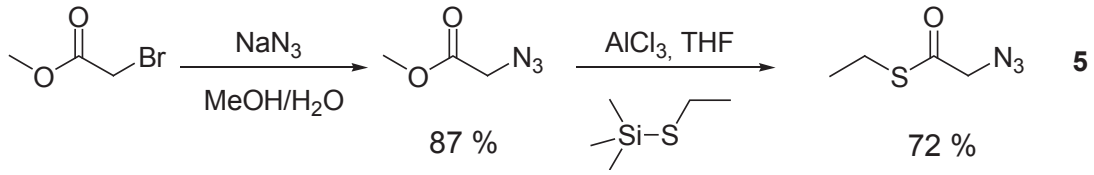

Figure 4.4: Reaction scheme for the facile two-step preparation of a linker for the introduction of a thioester into poly(2-oxazoline) side chains.

2 yielded the initiator salt *N*-methyl-2-(pent-4-ynyl)-2-oxazolinium triflate (PynOx-OTf, **4**). This reaction was performed in acetonitrile or diethylether as solvents. In both cases the colorless solid obtained at $\leq$ -35 °C liquefied at higher temperatures. A look at the structure of the obtained salts (Figure 4.3) might explain this tendency to deliquesce. It resembles the structure of a class of ionic liquids, the imidazolinium salts quite closely.

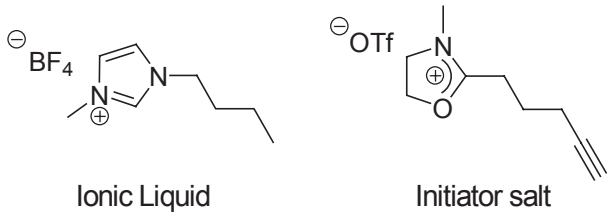

Figure 4.3: Structure of a typical ionic liquid compared to **4**.

The monomer 2-(4-ethynylphenyl)-2-oxazoline (**3**) could successfully be prepared by a facile three-step synthesis in moderate overall yield (32 %, unoptimized). Both alkyne monomers would have two distinct advantages in comparison to **1**. The alkyne moiety is not protected and can be directly used for click-chemistry, saving one polymer analog step. Additionally, if alkyne moieties remain unreacted, the physiological effect is expected to be low as compared to free aldehyde groups.
Attempts to transthioesterificate polymers with pending esters were not successful. Therefore, it was decided to synthesize a bifunctional reagent to introduce a thioester via click-chemistry. Starting with methyl bromoacetate the azide was introduced by substitution of the bromine and transthioesterification finally yielded ethyl(2-azido)thioacetate (**5**)(Figure 4.4). It should be mentioned, that this class of small organic azides (number of C-atom $\leq$6 per azide) should be handled with great caution, since several members of this class are highly explosive, although no violent

reaction has been observed with the prepared azides, neither on blow nor with an open flame.

4.2 Polymerizations and kinetic investigations

4.2.1 Linear poly(2-oxazoline)s

The polymerization carried out in this work are summarized in Figure 4.5 and Table 4.1. Polymer carriers for *in vivo* applications should be well-defined as outlined already. A thorough discussion of the prepared polymers seems therefore reasonable

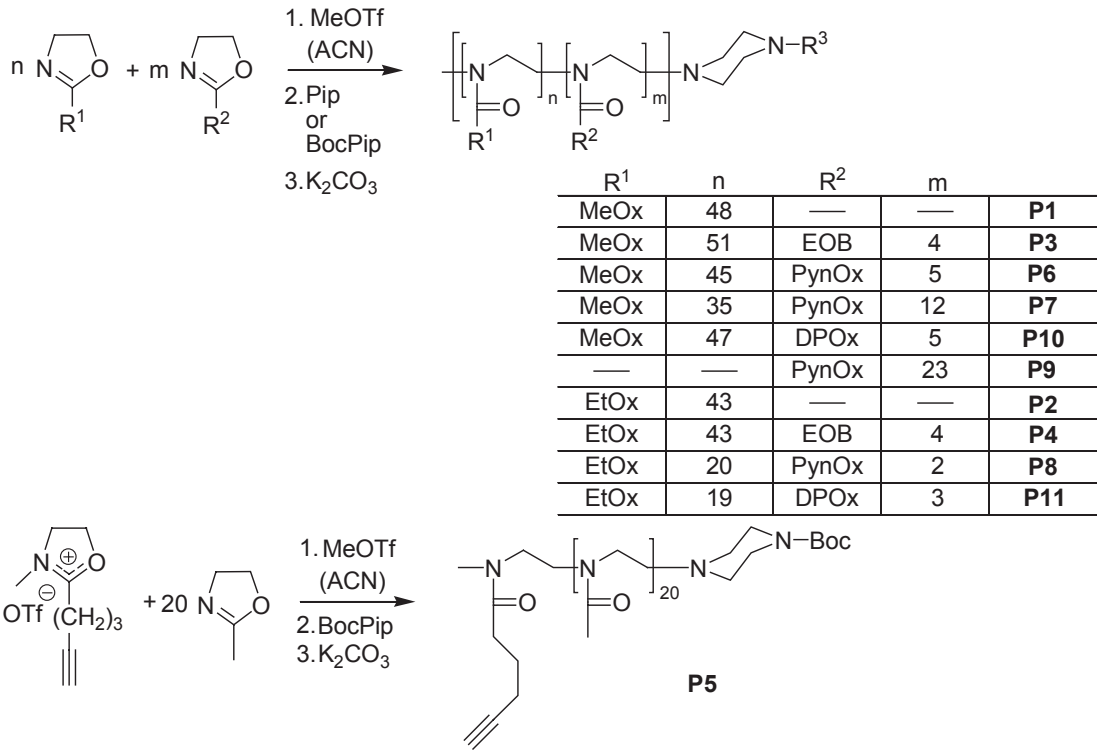

R^1	n	R^2	m	
MeOx	48	—	—	**P1**
MeOx	51	EOB	4	**P3**
MeOx	45	PynOx	5	**P6**
MeOx	35	PynOx	12	**P7**
MeOx	47	DPOx	5	**P10**
—	—	PynOx	23	**P9**
EtOx	43	—	—	**P2**
EtOx	43	EOB	4	**P4**
EtOx	20	PynOx	2	**P8**
EtOx	19	DPOx	3	**P11**

Figure 4.5: Reaction schemes of the preparation of the presented polymers.

to evaluate if the functional poly(2-oxazoline)s can actually be prepared with high definition, also in terms of their functional side chain content.

As a first step in the evaluation of a polymer for biomedical application, its fate

Table 4.1: Synthesized homo- and copolymers with respective selected analytical data.

	Polymer	$M_{n,calcd}$[a] [g/mol]	$M_{n,NMR}$[b] [g/mol]	$M_{n,GPC}$[c] [g/mol]	PDI[d]	Yield [%]
P1	P($MeOx_{48}$)BocPip	4290	5300	6600	1.16	84
P2	P($EtOx_{43}$)BocPip	4460	5700	6200	1.15	88
P3	P($MeOx_{51}EOB_4$)Pip	5180	5300	6800	1.16	95
P4	P($EtOx_{43}EOB_4$)Pip	5100	5700	6500	1.23	60
P5	PynOxP($MeOx_{20}$)BocPip	2040	2220	3190	1.06	99
P6	P($MeOx_{45}PynOx_5$)BocPip	4710	5820	7890	1.06	94
P7	P($MeOx_{35}PynOx_{12}$)BocPip	4830	6650	6960	1.17	83
P8	P($EtOx_{20}PynOx_2$)BocPip	2460	2450	4000	1.04	92
P9	P$PynOx_{23}$BocPip	3490	3630	6160	1.09	70
P10	P($MeOx_{47}DPOx_5$)Pip	5030	6550	9430	1.09	99
P11	P($EtOx_{19}DPOx_3$)Pip	2540	2550	3560	1.06	75

[a], as calculated from $[M]_0/[I]_0$

[b], as calculated from end-group and side chain analysis based on ^{1}H-NMR

[c], as obtained from gel permeation chromatography (solvent DMAc)

[d], obtained from GPC, M_w/M_n

upon administration to an organism has to be studied. All available data suggest a very good biocompatibility of poly(2-oxazoline)s. However, up to date, neither well-defined nor well characterized polymers of low molar mass of MeOx and EtOx have been investigated in that respect. Therefore, two homopolymers of MeOx and EtOx were prepared. The targeted molar mass was approx. 5 kDa. Consulting the literature on PEG of similar size, we assumed that polymers of this size should behave different from low-molar mass substances, but do not exhibit an EPR effect. The first two entries in Table 4.1 show selected analytical data of these two polymers, P$MeOx_{48}$BocPip (**P1**) and P$EtOx_{43}$BocPip (**P2**). In order to allow future evaluation of the influence of negative charges on the side chains of poly(2-oxazoline)s, copolymers with ester bearing ethyl-4-(oxazol-2-yl)butanate (EOB), P($MeOx_{51}EOB_4$)BocPip (**P3**) and P($EtOx_{43}EOB_4$)BocPip (**P4**) were prepared. As has been outlined already, biodistribution and blood pool retention data on (negatively) charged polymers are contradictory. It might be interesting how poly(2-oxazoline)s contribute to this issue. The following entries (**P5** - **P9**) show the analytical data of a MeOx homopolymer initiated with the initiator salt **4** and copolymers of **2** with MeOx and EtOx and a

homopolymer of **2**. Thus, the ratio of MeOx or EtOx and **2** within the polymer ranges from 3/1 to 20/1. On these polymers the efficiency of polymer analog click-chemistry will be investigated. Additionally, the thioester linker **5** is supposed to be attached through the alkyne moiety. The last two entries (**P10** and **P11**) denominate copolymers of **1** with MeOx and EtOx on which attachment of aminooxy-functionalized peptides will be evaluated.

Several efforts to homo- or copolymerize the novel alkyne bearing monomer **3** were not successful. These experiments were performed at 85 °C in acetonitrile. *Hoogenboom* et al.[270] showed that 2-phenyl-2-oxazoline does polymerize, albeit very slowly, at this temperature. Since with MeOx or EtOx only blockcopolymers could be expected (due the obvious strong difference in reactivity), this issue was not investigated further for the moment. For the copolymerization with, e.g. 2-phenyl-2-oxazoline, **3** might be interesting for the introduction of functional groups into hydrophobic poly(2-oxazoline)s.

For all polymers (all but **P8**) the molar masses obtained from end-group analysis (^{1}H-NMR) and GPC are higher than expected from $[M]_0/[I]_0$. Such a discrepancy of GPC values are observed commonly, since the actual calibration standards used were not poly(2-oxazoline)s. Therefore, it can not be expected that the GPC gives accurate data due to differences in the interaction of the polymer analyte and the stationary phase. The use of GPC is that the value for the polydispersity index (PDI) can be readily obtained. These values are, for all but one polymer below 1.2. End-group analysis based on ^{1}H-NMR data gave 5 - 20 % higher values for the molar mass as expected. In contrast, the integral values of the different side chains signals of copolymers are in good accordance with $[M_1]_0/[M_2]_0$. Typically, the DP is calculated from the integrals of the terminal methyl group, originating from the initiator, and the backbone methylene signals' integral. In the case of *N*-*tert*-butyloxycarbonylpiperazine (BocPip) terminated polymers, the 3 methyl groups can serve as an additional probe for this method of quantification. In most cases the end-group analysis with the two different termini give values for DP in reasonable accordance. However, three points have to be considered when NMR is used for quantification. The intensity of the signal of the terminal methyl group (CH_3, 3H) is very low in comparison to the backbone methylene signals (e.g. 200H for DP = 50). In some cases this weak signal can not even be observed in the spectrum. In any case, the relation of the signals (thus the calculated DP) is strongly dependent on the integration limits chosen and an error of 10 % can be assumed. It has been shown that piperidine and piperazine are fast

and effective terminating reagents[402]. Non-quantitative termination could lead to an additional overestimation of the DP when the terminal Boc group is used for quantification.

Additionally, the integrals of ^{1}H-NMR spectra do vary significantly in different solvents. The reason for this are e.g. different aggregation behavior of the polymers and varying relaxation of the nuclei of different parts of the polymer (side chain vs. backbone) depending on the solvent. Therefore, comparison of integrals obtained from NMR spectra in different solvents has to be performed with caution.

The ^{1}H-NMR spectrum of **P6** is shown in Figure 4.6. All signals can be assigned

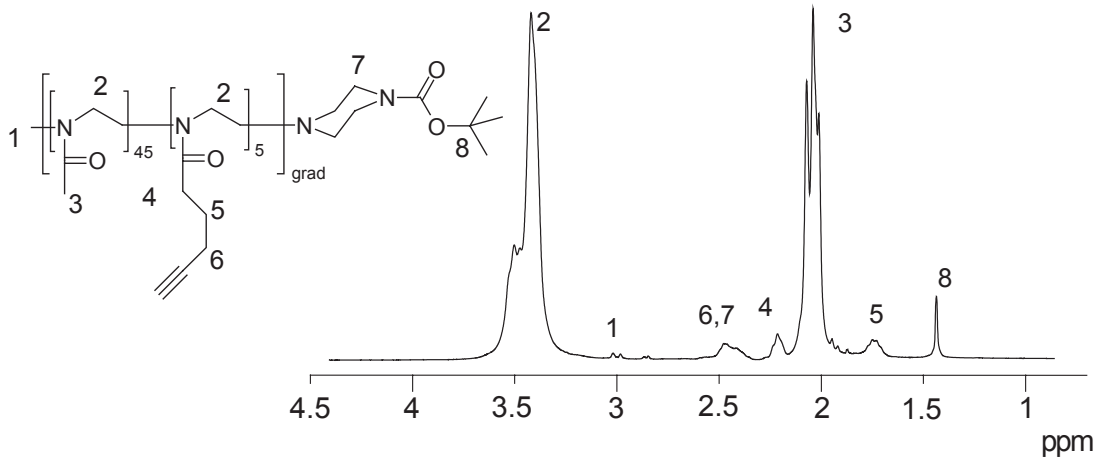

Figure 4.6: ^{1}H-NMR (D_2O, 250 MHz) of **P6**. All signals can be assigned as depicted. Please note, while the end-group analysis gives a somewhat higher DP than expected from $[M]_0/[I]_0$ values for both monomers, the relative intensities of the two monomers are in excellent accordance with the expected values.

and the overall DP is somewhat overestimated. The relative intensities of the two monomers are in excellent accordance as expected from $[MeOx]_0/[\mathbf{2}]_0$. However, the signal of the alkyne proton of **2** can not be found in the spectrum of **P6**. This is actually valid for all copolymers containing **2**. However, as will be seen in Chapter 4.4.2, this proton is detected in ^{1}H-NMR spectrum after 'clicking' the alkyne.

A closer look into the microstructure of some of the prepared polymers will be taken, to address the issue of gradient vs. random copolymers.

Kinetic investigations of the copolymerization with functional monomers

Gas chromatography can be used for kinetic investigations of the polymerization behavior of volatile 2-oxazolines. The polymerization is carried out in a vial sealed with a septum and the GC automatically collects samples at the set time intervals. The apparent propagation rate for the polymerization (k_p^{app}) is expressed in equation 4.1. The monomer consumption depends on the polymerization rate, the concentration of active chain ends ([P*]) and the monomer concentration [M]. For a rapid and quantitative initiation, which can be expected with triflates, [P*] equals $[I]_0$ and stays constant throughout the polymerization (equation 4.2).

$$-\frac{d[M]}{dt} = k_p^{app}[P^*][M] \tag{4.1}$$

$$-\frac{d[M]}{dt} = k_p^{app}[I]_0[M] \tag{4.2}$$

Integration gives equation 4.3. Since k_p^{app} and $[I]_0$ are constant (in the absence of chain termination) a linear plot of $\ln\frac{[M]_0}{[M]_t}$ vs. t should be observed for a living polymerization.

$$\ln\left(\frac{[M]_0}{[M]_t}\right) = k_p^{app}[I]_0 t \tag{4.3}$$

From the slope of this plot, $k_p^{app}[I]_0$, one can calculate the apparent propagation rate for a given monomer concentration.

Figure 4.7 shows the monomer consumption versus time for the polymerizations of **P8** and **P11**. In the case of **P8** (Figure 4.7a), the monomer consumption for both monomers is fast and proceeds at the same rate. The polymerization is completed after approx. 15 h.

The polymerization of MeOx and **1** to give **P11** is even faster. However, the conversion does not reach 100 % for **1**, but stops at approx. 90 %, while until 75% conversion both monomers react at the same rate.

What is the reason for this observation? First and most importantly, chain termination can be ruled out as a significant reason for this deviation. If some, or even all chains would be terminated, obviously one would expect a slower, or altogether halt in the monomer conversion for both monomers. A close look to the GC chromatograms gives a possible explanation. As the intensities and the integrals of the monomers de-

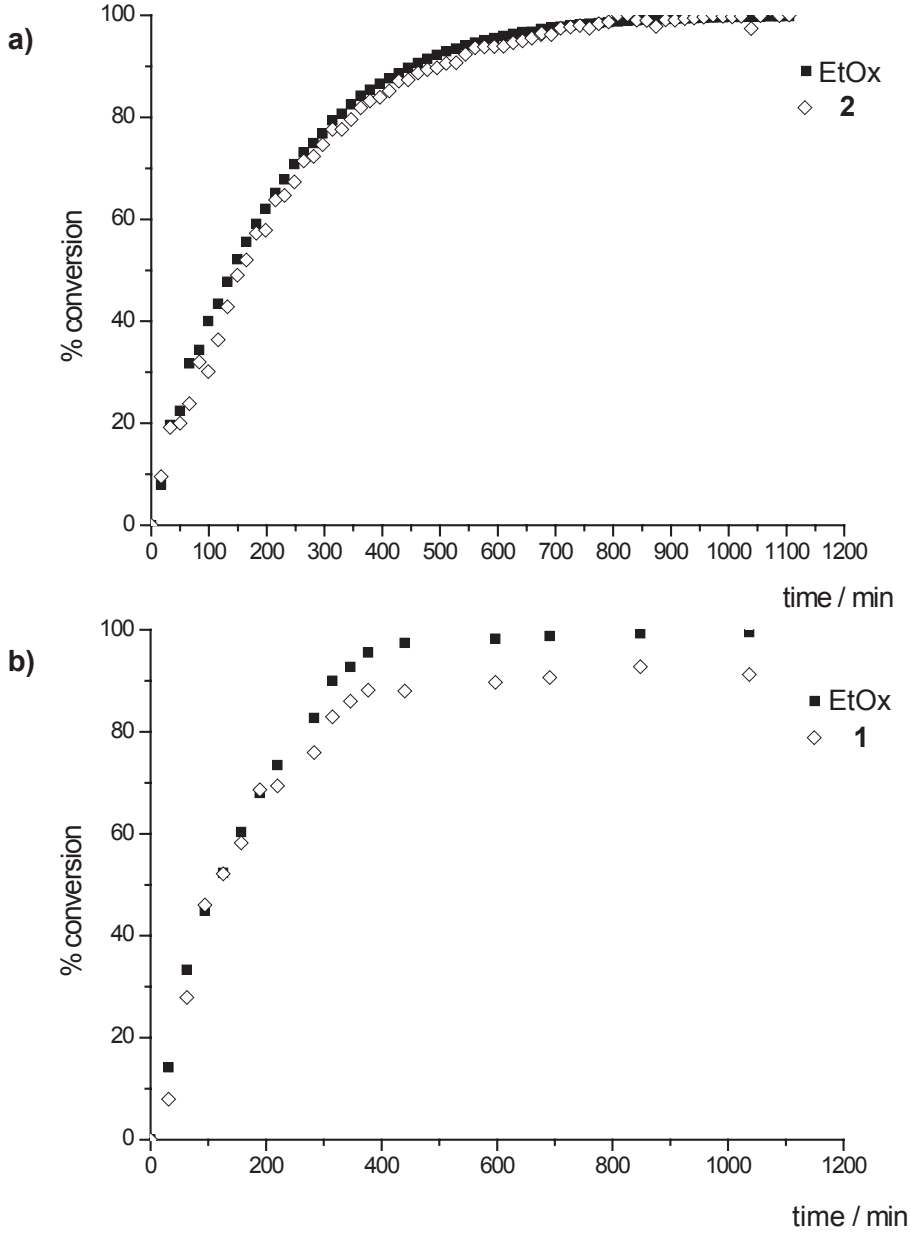

Figure 4.7: Plot of monomer consumption vs. time for the polymerization of **P8** (a) and **P11** (b). Please note, while monomer conversion occurs faster in the case of **P11**, the polymerization rates are faster for **P8** due to a lower $[I]_0$ in the latter case (Table 4.2).

crease, the automatic integration algorithm is not able to discern correctly between the monomer peak and a weak but broad tailing of unknown origin in the case of **1**. This tailing becomes dominant as the concentration of **1** decreases, feigning a monomer content which is actually much lower. However, for the calculation of the rate constant the slope in the beginning of the polymerization can be used (Figure 4.8). For

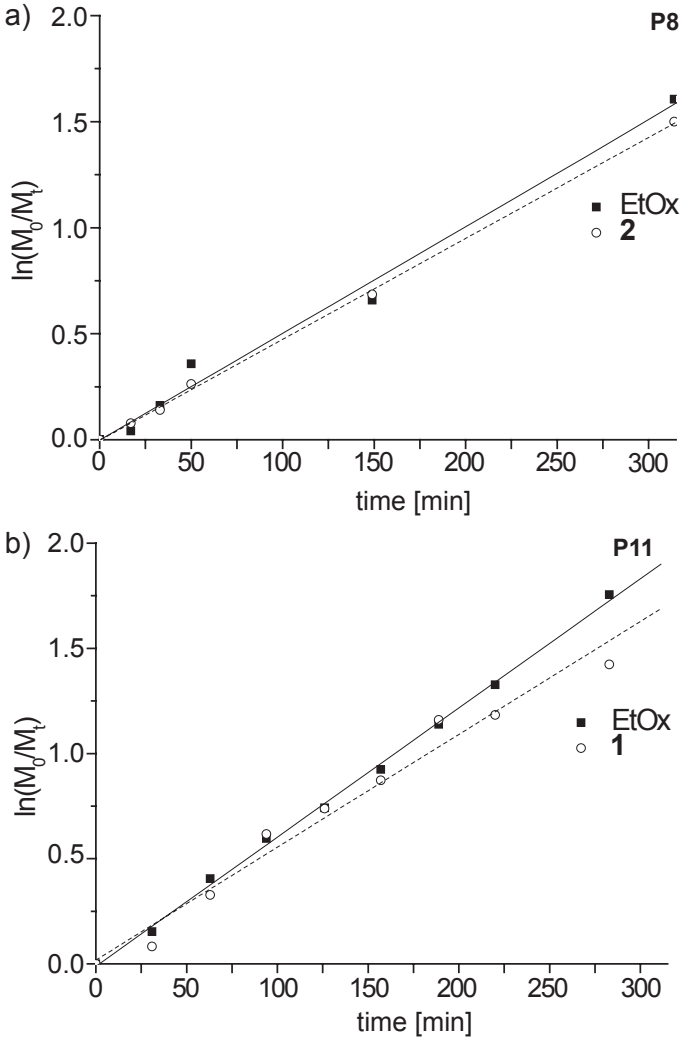

Figure 4.8: First order kinetic plots for **P8** (a) and **P11** (b), which show a linear development. Both monomers are consumed at a similar rate. Due to a slightly higher concentration the slope is steeper for **P11** while the actual rate is lower.

the copolymerizations of MeOx or EtOx with **2**, the plots are reasonably stable to very high conversions (Figure 4.9). Evaluation of the linear first order kinetic plots

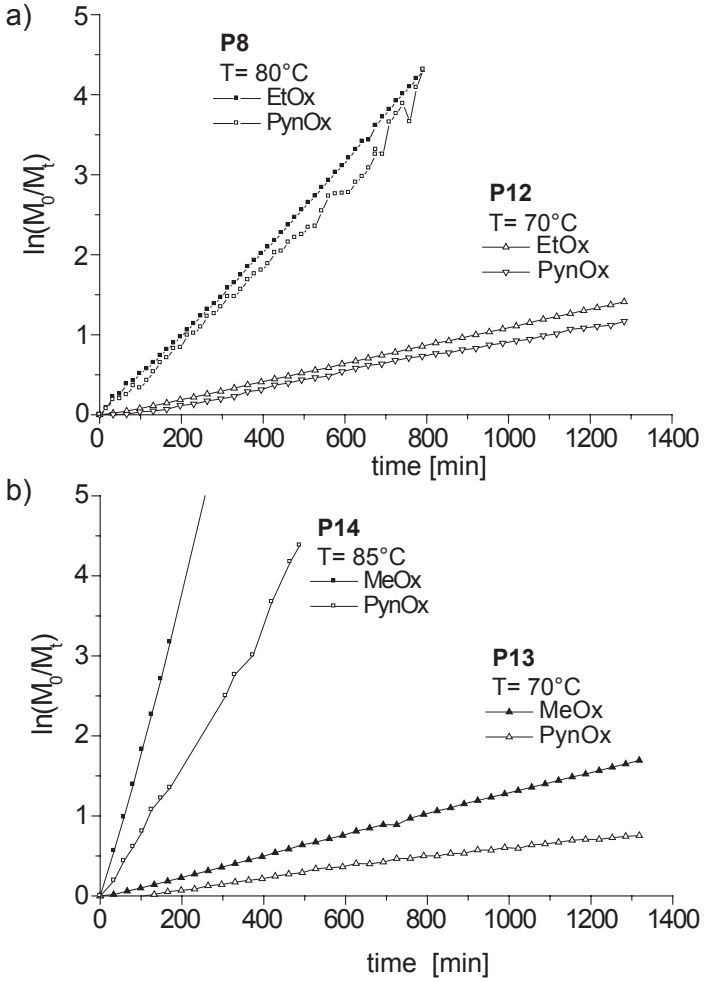

Figure 4.9: Linear first order kinetic plots for **P8** (a) and **P12** (a) through **P14** (b). The strong influence of 10 °C is clearly seen in a much faster propagation at higher temperature as expected, while the in both cases the differences between the monomers stays indifferent of the temperature. Both **P8** and **P12** are obtained as almost perfect random copolymers (a) while **P13** and **P14** give a pronounced gradient character (b).

gives the respective values for k_p^{app} (Table 4.2). The first three entries show that **P8**, **P11** and **P12** are nearly perfect random copolymers, as the apparent polymerization

Table 4.2: Calculation of apparent rate constants k_p^{app} of the copolymerization of **P8** and **P11** through **P14**.

	$[I]_0^a$	$[EtOx]_0^b$	$[MeOx]_0^b$	$[\mathbf{1}]_0^b$	$[\mathbf{2}]_0^b$	$slope_{M_1}^c$	$slope_{M_2}^c$	$k_{p,M_1}^{app\ d}$	$k_{p,M_2}^{app\ d}$
P8	35.8	0.72	—	—	0.08	9	8.5	2.5	2.4
P11	41.7	0.78	—	0.11	—	10	9.7	2.4	2.3
P12^e	17.5	0.34	—	—	0.034	1.8	1.7	1.0	0.97
P13^e	18.2	—	0.34	—	0.035	2.2	1	1.2	0.55
P14^f	48.1	—	0.98	—	0.23	33	15	6.9	3.1

^{a} mmol/L, ^{b} mol/L, ^{c} $10^{-5}\,s^{-1}$, ^{d} $\frac{L}{mol*s}\times 10^{-3}$, ^{e} T = 70 °C, ^{f} T = 85 °C

rates of the monomers are almost identical. This is contrasted by the copolymerization of MeOx and **2**. Here, the values for $k_{p,MeOx}^{app}$ and $k_{p,\mathbf{2}}^{app}$ differ significantly, having a ratio of $\frac{k_{p,MeOx}^{app}}{k_{p,\mathbf{2}}^{app}} = 2.2$. This indicates a pronounced gradient character of the resulting copolymer, indifferent of the temperature.

It is noteworthy that this temperature indifference for the copolymerization behavior is not necessary the case as demonstrated by *Hoogenboom* et al.[270]. While the ratio of the polymerization rates between MeOx and EtOx were independent of the temperature (80 °C vs 100 °C) and the initiators, this was different when compared with 2-nonyl-2-oxazoline (NonOx). While the $k_{p,EtOx}^{app}$ was 1.6 $\frac{L}{mol*s}\times 10^{-3}$ compared with $k_{p,NonOx}^{app} = 2.2\ \frac{L}{mol*s}\times 10^{-3}$ at 80 °C, EtOx polymerized faster then NonOx at 100 °C (6.8 $\frac{L}{mol*s}\times 10^{-3}$ vs 5.6 $\frac{L}{mol*s}\times 10^{-3}$, all initiated with MeOTf). If these differences are not within the experimental error, these results indicate that one can influence the microstructre of POx only by changing the polymerization temperature.

Particularly interesting is the comparison of entries **P12** and **P13**. The temperature and the concentrations for all participating species are virtually identical. The consumption rate for MeOx is slightly higher than the rate for EtOx, but the difference is not as pronounced as expected when compared with literature ($\frac{k_{p,MeOx}^{app}}{k_{p,EtOx}^{app}} = 1.2$ compared to ~ 1.5[270]). This difference might be due to a different concentration (0.8 M vs 1.25 M) and solvent (ACN vs. DMAc) used in the reference experiments. More striking is the comparison of the values for $k_{p,\mathbf{2}}^{app}$. In the copolymerization with EtOx a rate of $k_{p,\mathbf{2}}^{app} = 0.97\ \frac{L}{mol*s}\times 10^{-3}$ is calculated while in the copolymerization with MeOx only roughly half of this value is obtained with $k_{p,\mathbf{2}}^{app} = 0.55\ \frac{L}{mol*s}\times 10^{-3}$.

Since all polymerization parameters were kept constant, this indicates that **2** is less reactive towards the propagating cationic species (predominantly 2-methyl-2-oxazolinium) in the latter case and more reactive towards the 2-ethyl-2-oxazolinium chain end present during polymerization of **P12**. Another explanation would be that the difference is within the experimental error.
In conclusion, it was shown that the copolymerization of EtOx with **1** and **2** yields nearly perfect copolymers, while in the case of the copolymerization with MeOx a pronounced gradient character of the resulting copolymer was obtained. The experiments performed during this work showed for the first time that it is possible to obtain gradient and random copolymers of water-soluble 2-oxazolines (MeOx and EtOx) and chemically functional 2-oxazolines(**1** and **2**).

MALDI-TOF mass spectrometry

Matrix assisted laser desorption/ionization time-of-flight mass spectrometry (MALDI-TOF-MS) is a valuable method for the analysis of polymers. In comparison with other mass spectrometrical methods, no or little fragmentation of the analyt is observed. Thus, molecules with larger molar masses like polymers and peptides are ideally analyzed using this technique.
A general trend that was observed during this work was that EtOx containing polymers gave better MALDI-TOF spectra then MeOx polymers. Similarly piperazine terminated polymers (or deprotected ones) gave a better resolution of the spectra. Detailed analysis of signals obtained from MALDI-TOF spectra allows the determination of M_w ($\frac{\sum_i^i n_i \times M_i^2}{\sum_i^i n_i \times M_i}$), M_n ($\frac{\sum_i^i n_i \times M_i}{\sum_i^i n_i}$) and thus, the polydispersity as determined by MALDI, PDI_{MALDI} ($= M_w/M_n$). This procedure, however, becomes complicated for copolymers. Starting from a homopolymer, the possible mass signals increase rapidly with increasing comonomer content for copolymers until the point where different copolymer compositions have virtually the same molar mass. This has been discussed recently in detail for **P6**[401].
Figure 4.10 shows the MALDI-TOF mass spectrum of **P2**. The distribution is narrow and symmetric. The two most intense signals at $m/z = 4485$ and 4584 can be attributed to polymers of 2-ethyl-2-oxazoline associated with a sodium ion. The respective DP is

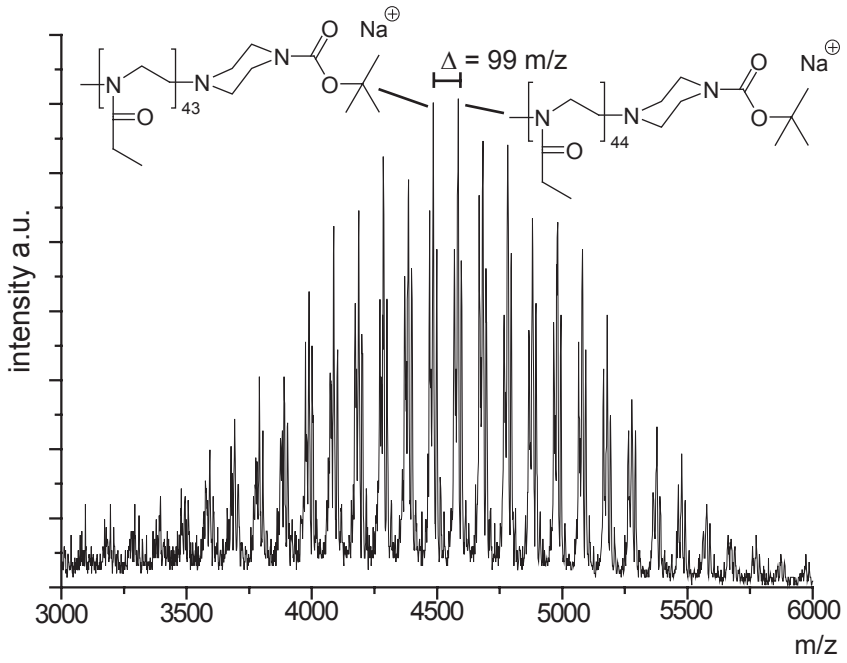

Figure 4.10: MALDI-TOF spectrum of P(EtOx$_{43}$)BocPip (**P2**).

43 ($m/z_{calc} = 4485.9\,g/mol$) and 44 ($m/z_{calc} = 4585.0\,g/mol$), respectively, which is in excellent accordance with the value expected from $[M]_0/[I]_0$ (43). Along with these, signals can be found which are assignable to lithium and potassium associated polymer species. Signals that correspond to polymer chains with DP = 29 to up to 58 can be found, no unassignable signals are observed. The intensities of the signals were obtained and the average masses of the **P2** were determined. For M_n a value of $4546\,g/mol$ is calculated while $M_w = 4605\,g/mol$ ($PDI_{MALDI} = 1.01$). Together with the data obtained from GPC and ^{1}H-NMR spectroscopy it can be stated that **P2** was successfully prepared with a high definition and with a molar mass as projected.
Another homopolymer of MeOx, but initiated with the initiator salt **4** is **P4**. In Figure 4.11 the MALDI-TOF mass spectrum of **P4** is shown. In this case, four different distributions can be discerned. The two most intense distributions are highlighted in green and red. These signals can be attributed to polymer species of PynOxP(MeOx$_n$)BocPip with a potassium or a hydrogen counterion. The maximum of both distributions is found at values around $m/z = 2000$, in excellent accordance with the molar mass of the projected PynOxP(MeOx$_{20}$)BocPip ($M = 2040\,g/mol$). Two additional, minor distributions are observed, one assignable to polymer species lacking

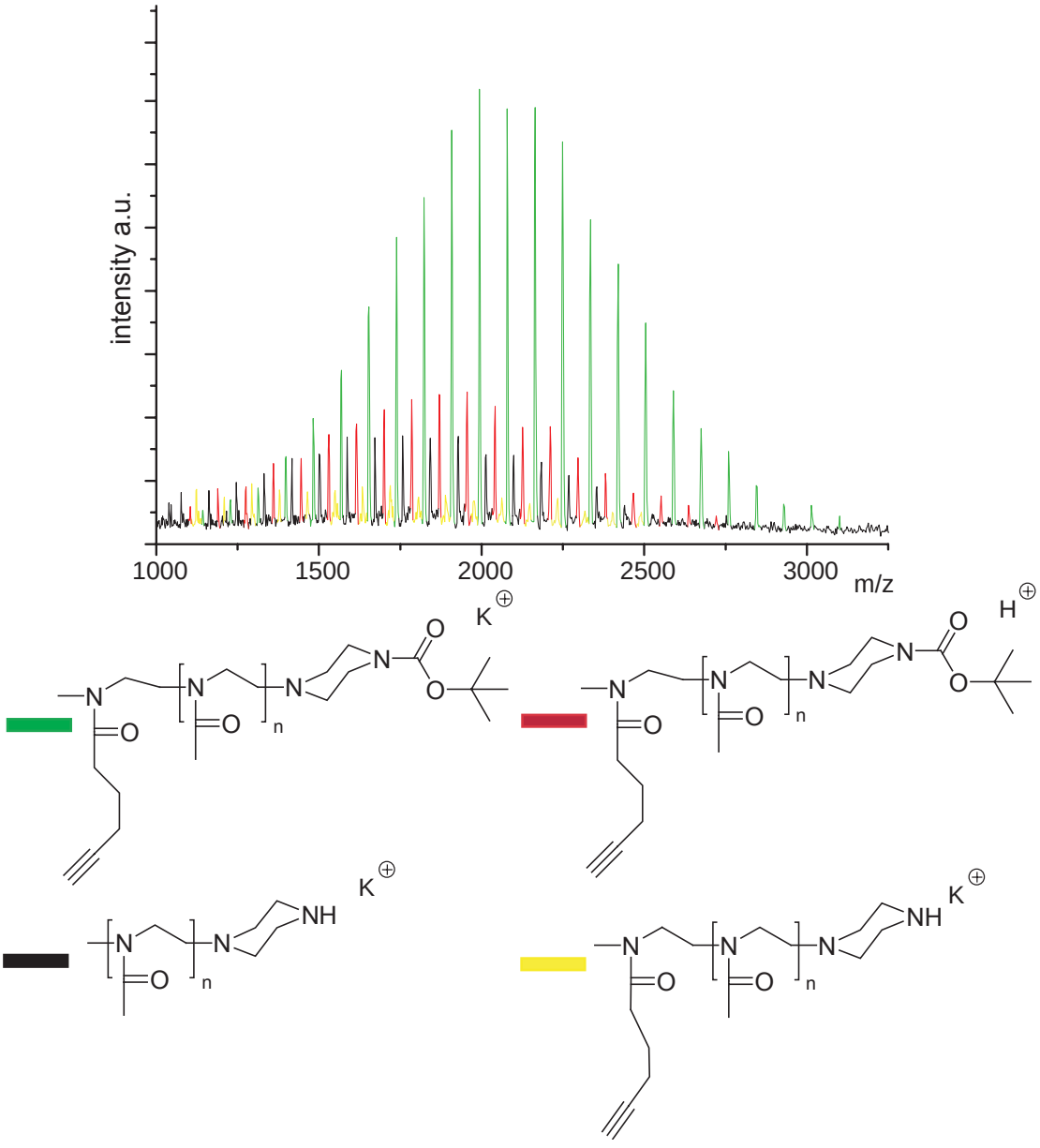

Figure 4.11: MALDI-TOF spectrum of PynOxPMeOx$_{20}$BocPip.

the terminal PynOx moiety and the Boc protection group at the other terminus (black signal distribution). This could be explained by some residual methyltriflate in the initiator which initiated the homopolymerization of MeOx, although no evidence for substantial amounts of MeOTf could be found in the analytical data of **4**. Another possibility would be the reversed fragmentation of **4** accompanied by the release of methyl triflate. In this case one would expect the incorporation of then available monomer **2** into the growing chain during polymerization of **P4**. Since no signals could be found assignable to polymer species containing more then one unit of **2**, this possibility can be ruled out.

Finally, the forth distribution (yellow) present in the mass spectrum of **P4** could originate from species of **P4** also lacking the terminal Boc-group. It was already mentioned that polymer species with free piperazine gave MALDI-TOF spectra of much better quality, i.e. higher intensity. It might well be that the actual amount of the two lower intensity distributions (black, yellow) is overestimated due to far better ionizability of these species. Quantification by ^{1}H-NMR spectroscopy, however, is not accurate enough to rule out even 5 - 10 % of polymer chains lacking a terminal PynOx group.

Another possibility is that water, especially under basic conditions, can lead to chain termination. Unfortunately, the molar mass of the resulting polymer species would be similar to the one of BocPip terminated species. In Figure 4.12 the theoretically calculated isotopic distributions of two polymer species are illustrated and compared with the experimental values. The molar mass of [PynOxP(MeOx$_{19}$)BocPip + K]$^+$ is M = 1993.54 g/mol while for [PynOxP(MeOx$_{21}$)OH + K]$^+$ M = 1995.51 g/mol is calculated. The observed maximum at 1993.8 is in very good agreement with the calculated mass for [PynOxP(MeOx$_{19}$)BocPip + K]$^+$. But things are a bit less obvious, when the isotopic distribution is taken into account (compare Figure 4.12, series A and B). It can be seen that the two distributions overlap significantly and the third most intense signal of [PynOxP(MeOx$_{19}$)BocPip + K]$^+$ is observed at an almost identical m/z value as the second most intense signal of [PynOxP(MeOx$_{21}$)OH + K]$^+$. However, also this analysis corroborates that the polymer species that gives rise to the observed peak in the mass spectrum, is actually a member of the distribution of **P4** than of the possible side product (PynOxP(MeOx$_n$)OH). This comparison should mainly serve as an example how difficult it can be to obtain ultimate proof over the identity and definition of polymers, also by MALDI mass spectroscopy. Especially for copolymers, it typically possible to calculate molar mass of theoretical side products and their associates

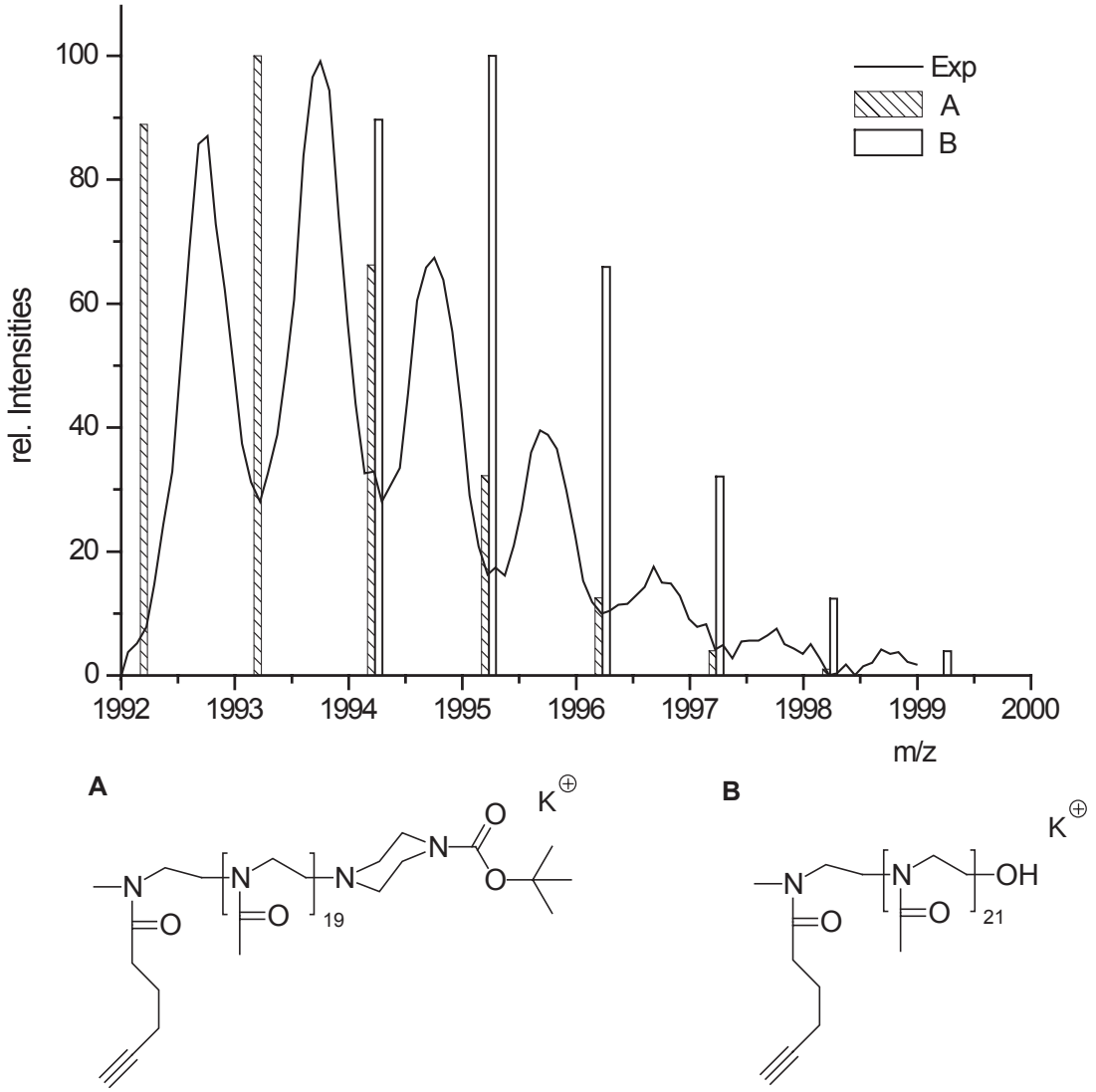

Figure 4.12: Comparison of the theoretical isotopic distribution of polymer species A (**P4**) and B (possible sideproduct of **P4**) with the observed signal distribution in the MALDI spectrum of **P4**. Please note, the isotopic abundances are calculated with ChemDraw® Ultra for one decimal.

with salts with the same or a very similar molar mass as the actually desired product. However, in combination with other analytical techniques, especially ^{1}H-NMR spectroscopy, where functional groups can be easily identified, one can come to well founded assumptions whether the desired product has been obtained.
In the same manner, MALDI mass spectra of the copolymers **P6**, **P8** and **P11** were obtained and analyzed. In all cases, the most intense signals can be found at values of m/z as expected from $[M]_0/[I]_0$. In the case of **P11** a slight deviation in respect to the content of DPOx in the resulting polymer was observed. Signal distributions can be found that correspond to polymer species that contain between 0 (EtOx homopolymer) to 6 units of **1**. The most abundant peak distributions can be assigned to species containing 3 to 5 units of DPOx each having a maximum at 17 units of EtOx, whereas 2 to 3 units of **1** and 19 of EtOx was the targeted content.
In contrast to this, the mass spectrum of **P8** and especially its unprotected counterpart P($EtOx_{20}PynOx_2$)Pip (**P24**), will serve as an example that it is possible to obtain copolymers with high definition, also in respect of the monomer content (vide infra, Chapter 4.3.1).

4.2.2 Star-like poly(2-oxazoline)s

Several reports on star-like homo- and blockcopoly(2-oxazoline)s can be found, starting from the early 1980s[283–292]. Only two of those reports investigated whether all functionalities of a multifunctional initiator are of equal reactivity. In these cases a step-wise initiation of the multi-initiators (halogen and tosylate) was observed[284, 285].
Since it is well established that triflates are highly reactive initiators for the 2-oxazoline polymerization, it is of interest, if fast and complete initiation can be achieved with triflate multimers. This would be necessary if the various arms of the stars are supposed to be homogeneous for the same reasons that account for the low polydispersity of linear polymers. Therefore, the polymerization reactions of MeOx in the presence of bis-, tris- and tetrakistriflates (Figure 4.13) were investigated and compared with the polymerization initiated by methyl triflate. Especially pentaerythritol tetrakis(trifluoromethylsulfonate) (**I3**) appears sterically crowded which could lead to a step-wise initiation.

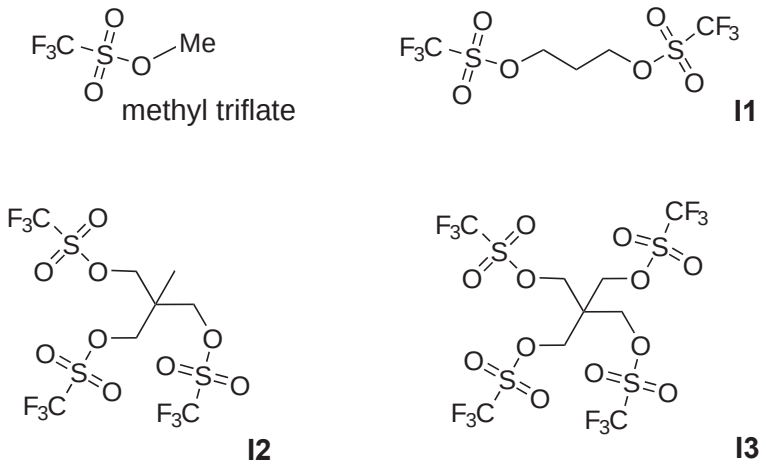

Figure 4.13: Structures of methyl triflate and three prepared triflates for the synthesis of linear (**I1**) and star-like poly(2-oxazoline)s (**I2**,**I3**).

The first order kinetic plots of the polymerization of MeOx at a concentration of $[\text{MeOx}]_0 \sim 0.8\,\text{mol/L}$ at 85 °C, initiated by the four different triflates are shown in Figure 4.14. The initiator concentration for all experiments was constant ($[\text{I}]_0$) and thus the concentration of triflate groups ($[\text{I}]_0^f$) varied, depending on the initiator. All four plots are linear, indicating a living character of the polymerization. The polymerization reactions proceed to quantitative monomer conversion. It can be seen, that the slope of the plots increases with increasing numbers of triflate groups per initiator molecule. The calculated apparent polymerization rates are shown in Table 4.3. Actually, two rates were calculated for each experiment. First, the apparent rate (k_p^app) and, second, the apparent rate per initiating group ($\frac{k_\text{p}^\text{app}}{\#\text{ of triflate groups}} = k_\text{p}^\text{app,f}$).
According to the increasing slope in the first order plots, the values for k_p^app increase

Table 4.3: Calculation of apparent rate constants k_p^app of the polymerization of MeOx with MeOTf and multifunctional initiators **I1**, **I2** and **I3**.

	$[M]_0/[I]_0^f$	$[\text{I}]_0^a$	$[\text{I}]_0^{fa}$	$[\text{MeOx}]_0^b$	slope^c	k_p^app	$k_\text{p}^\text{app,f}$
P15	80/1	8.69	8.69	0.695	4.48	5.16	5.16
P16	80/4	8.63	34.5	0.690	14.5	16.8	4.20
P17	80/4	8.77	35.1	0.693	19.7	22.5	5.61
P18	80/2	8.75	17.5	0.690	8.99	10.3	5.14
P19	80/3	8.20	24.6	0.661	12.6	15.4	5.12

^{a} mmol/L, ^{b} mol/L, ^{c} $10^{-5}\,\text{s}^{-1}$, ^{d} $\frac{\text{L}}{\text{mol*s}} \times 10^{-3}$

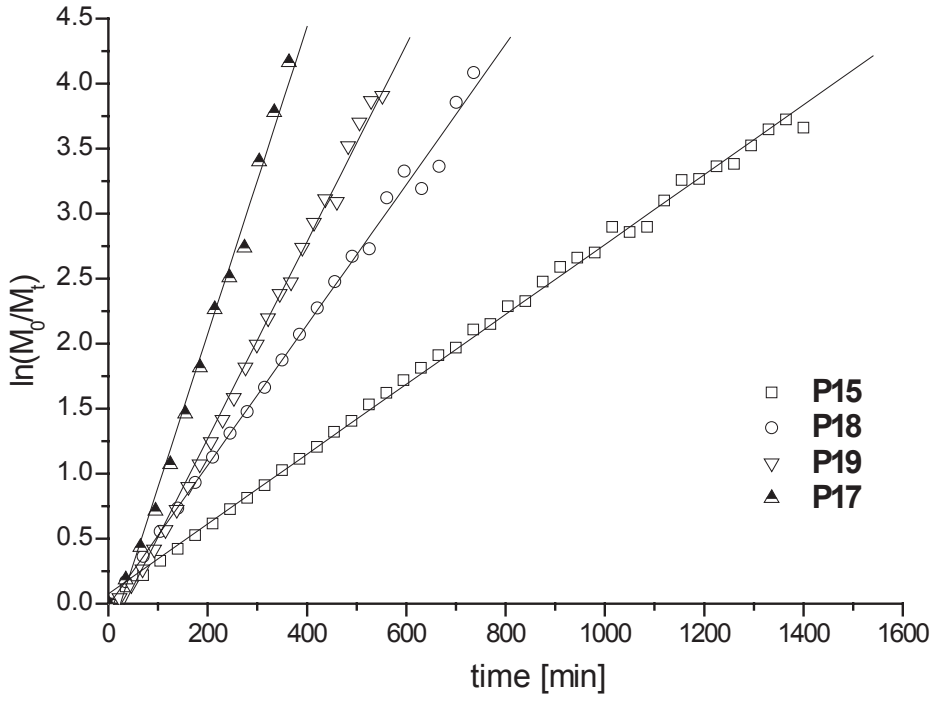

Figure 4.14: Linear first order kinetic plots for the polymerizations of **P15** and **P17** through **P19**.

with the numbers of initiating functions. The rate observed for **P15** is somewhat lower compared with the rate observed with **P14** (vide supra, Table 4.2). This is possibly due to the lower monomer concentration in this case or lies within the experimental error of the measurement. The rates for the polymerization initiated with the bis- and tristriflate (**P18**, **P19**) are approximately twice and thrice the value of **P15**, respectively. The experiment with **I3** was performed in duplicate (**P16**, **P17**) which led to differing polymerization rates. The arithmetic average, however, is in good accordance with the values for the three other initiators. With a medium value of $19.6 \times 10^{-3} \pm 4.03 \frac{\mathrm{L}}{\mathrm{mol*s}}$ the polymerization initiated with **I3** is approx. four times faster than the polymerization initiated by methyl triflate. The similar values of $k_{\mathrm{p}}^{\mathrm{app,f}}$ for the different initiators indicate that all triflate groups of **I1**, **I2** and **I3** show comparable reactivity. Additionally, in Figure 4.15 the number of initiating functions are plotted against k_p^{app} and an linear increase is observed. Extrapolation to 0 triflate units gives a rate of zero as expected.

These results are in contrast to earlier reports of *Chujo* et al.[285] and *Kobayashi* et

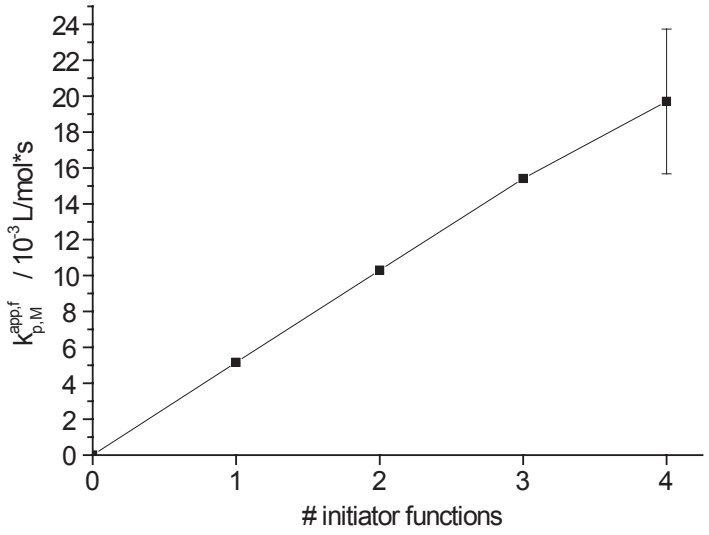

Figure 4.15: Development of the apparent polymerization rates of triflates of different multiplicities. The polymerization rate increases with the number of initiating functions in a linear dependence. This proves that all initiator functionalities exhibit the same activity as MeOTf and no steric hindrance even in the case of the bulky tetrafunctional initiator **I3** exists.

al.[284] and suggest that it is possible to obtain star-like poly(2-oxazoline)s with evenly sized arms using small and crowded initiators like **I3**. However, linear first-order ki-

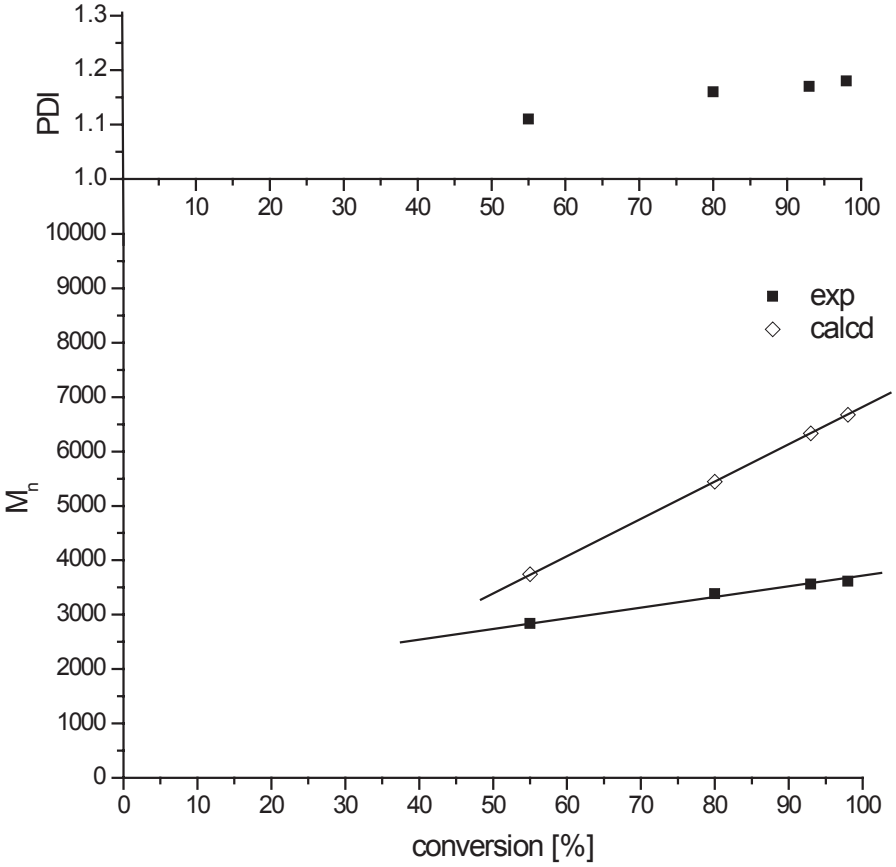

Figure 4.16: Calculated and observed (GPC) development of molar mass and polydispersity with conversion of the star-like polymerization with **I3**.

netic plots, only show that the concentration of living chain ends remain constant over the course of the polymerization. Chain transfer can not be ruled out on the basis of these experiments. Therefore an additional polymerization with **I3** as an initiator was performed and samples where taken at different time points and analyzed by GPC (Figure 4.16). As can be seen, the molar masses, as obtained from GPC, are lower than calculated. This, however, is expected with star-like polymers and RI-detection. However, a linear increase for M_n with the conversion is observed (indication the absence of chain transfer) and the polydispersities are reasonable low with values below 1.2 for all samples.

Unfortunately, no MALDI-TOF mass spectra of any samples of star-polymers could be obtained.

In another experiment, the star-like block copolymer **P20** (Figure 4.17), consisting of EtOx as the main monomer and **1** and **2** as two different functional monomers in the two blocks was prepared. The polymerization was followed by GC and GPC

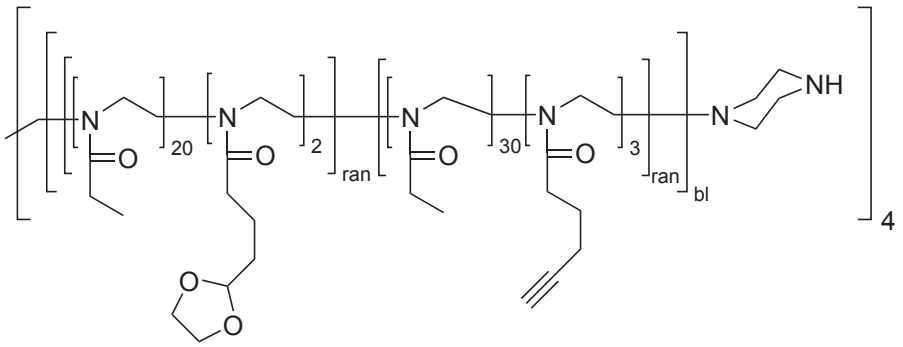

Figure 4.17: Structure of star-like diblockterpolymer **P20**.

and additionally a ^{1}H-NMR spectrum was obtained from the product. In Table 4.4, the calculated rate constants of the monomers for the two different blocks are shown. While in the first block, the values for k_p^{app} of EtOx and **1** are identical and a random

Table 4.4: Calculation of apparent rate constants k_p^{app} of the polymerization of the star blockcopolymer **P20**.

	$[I]_0^{f\,a}$	$[\mathrm{EtOx}]_0^b$	$[\mathbf{1}]_0^b$	$[\mathbf{2}]_0^b$	$\mathrm{slope}^c_{\mathrm{EtOx}}$	$\mathrm{slope}^c_{\mathrm{M_2}}$	$k^{app}_{p,\mathrm{EtOx}}$	$k^{app}_{p,\mathrm{M_2}}$
First block	39.6	0.83	0.077	—	8.3	8.2	2.1	2.1
Second block	35.4	1.07	—	0.107	16	14	4.5	4.0

^{a} mmol/L, ^{b} mol/L, ^{c} $10^{-5}\,\mathrm{s}^{-1}$, ^{d} $\frac{\mathrm{L}}{\mathrm{mol}*\mathrm{s}} \times 10^{-3}$

copolymer is obtained, the rate constants for EtOx and **2** differ by 13 %, resulting in a weak gradient character of the second block.

Of both blocks, samples have also been analysed by GPC. A pronounced shoulder at higher molar mass is present, a phenomenom observed regularly with poly(2-oxazoline)s. In both cases the values for the peak average molar mass (M_P) of the high molar mass shoulder is approx. twice the value of M_P (first block M_P = 4000 and 7700 g/mol; second block M_P = 9100 and 17300 g/mol), the intensity of the higher molar mass signal is approx. half the lower molar mass signal and in both cases no baseline separation is observed. The signal shape is very similar for both blocks and no shoulder at M_P of the first block is observed in the GPC trace after polymerization of the second block (**P20**). Therefore, termination can be ruled out as reason for the

bimodal trace of the first block and that the preparation of the star blockterpolymer was successful, despite the bimodal GPC trace. The reason for the occurrence of the high molar weight shoulder remains unclear, but may be due to some aggregation taking place during GPC measurement or other type of artifacts of the GPC measurement (as also observed later, see Chapters 4.4.1 and 4.3.2). Alternatively, one could assume that this shoulder is due to polymer chain coupling. However, it appears unlikely that a pronounced fraction of the stars undergo chain coupling to dimers, whereas any hint of trimers or higher multimers is absent. The overall polydispersity of **P20** is reasonably low with PDI = 1.22. Similar to star-like homopolymers, the absolute values of M_n are considerably lower than calculated from $[M]_0/[I]_0$. Integration of the signals in the ^{1}H-NMR spectra of **P20** gives monomer ratios which are in excellent accordance with the expected values, and the value of DP as calculated from ^{1}H-NMR is slightly higher ($\sim$10 %) as would be expected.

4.2.3 Summary

In the preceding chapters the preparation and analysis of the polymers **P1** - **P20** has been described and discussed. Performing kinetic studies by online GC measurements of the monomer consumption, the microstructure of the polymers could be identified and it has been shown that both new functional monomers **1** and **2** can be copolymerized with MeOx and EtOx to give gradient and random copolymers respectively. All prepared polymers are of low polydispersity of PDI $\leq$ 1.23 (GPC). Furthermore, characterization of the polymer products by MALDI-TOF MS and ^{1}H-NMR spectroscopy corroborated that well-defined polymers were obtained.

4.3 Modifications at the polymer terminus

4.3.1 Removal of the Boc protection group

Before the terminal amine group is available for the attachment of the radionuclide chelator, the protection group Boc must be removed. While this is generally a trivial reaction, e.g. in peptide chemistry and would be not worth mentioning, polymer analog modifications should always be investigated with scrutiny. Figure 4.18 shows the general reaction scheme for this deprotection. It was performed in a 95/2.5/2.5 (v/v/v) mixture of trifluoroacetic acid (TFA), water and triisobutyl silane (TIBS). Table 4.5

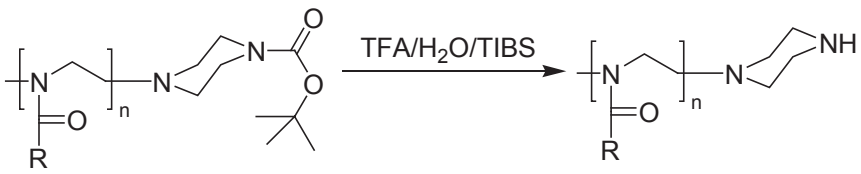

Figure 4.18: Reaction scheme for the removal of the Boc protection group at the terminal piperazine.

shows selected analytical data of polymers after terminal Boc removal. Analog to the analytical data of the respective educts, ^{1}H-NMR and GPC slightly overestimate the DP. However, again it can be shown by MALDI-TOF MS that the actual molar masses are in good agreement with the expected values from $[M]_0/[I]_0$. ^{1}H-NMR spectroscopy

Table 4.5: Selected analytical data of polymers after removal of terminal Boc protection group.

Polymer		$M_{n,calcd}$[a] [g/mol]	$M_{n,NMR}$[b] [g/mol]	$M_{n,GPC}$[c] [g/mol]	PDI[c]	Yield [%]
P21	P($MeOx_{48}$)Pip	4190	5200	6360	1.22	66
P22	P($EtOx_{43}$)Pip	4360	5700	6670	1.18	88
P23	P($MeOx_{45}PynOx_5$)Pip	4620	7000	7130	1.04	92
P24	P($EtOx_{20}PynOx_2$)Pip	2360	2350	3990	1.06	93

[a], as calculated from $[M]_0/[I]_0$

[b], as calculated from end-group and side chain analysis based on ^{1}H-NMR

[c], as obtained from GPC (solvent DMAc)

can serve as a relatively sensitive method for the quantification of the Boc group, due

to the appearance of the sharp and relatively intense singlett originating from the three methyl groups at 1.4 ppm. Accordingly, ^{1}H-NMR spectroscopy is also suitable to verify the removal of Boc.

Figure 4.19 depicts the comparison of the ^{1}H-NMR spectra of **P1** and the deprotected P(MeOx$_{48}$)Pip (**P21**). The sharp singlett at 1.4 ppm (Signal 5) in the spectrum of **P1** is no longer observed in the spectrum of **P21**. Accordingly, successful deprotection was confirmed for the polymers **P22** - **P24**. The molar mass of the polymers should

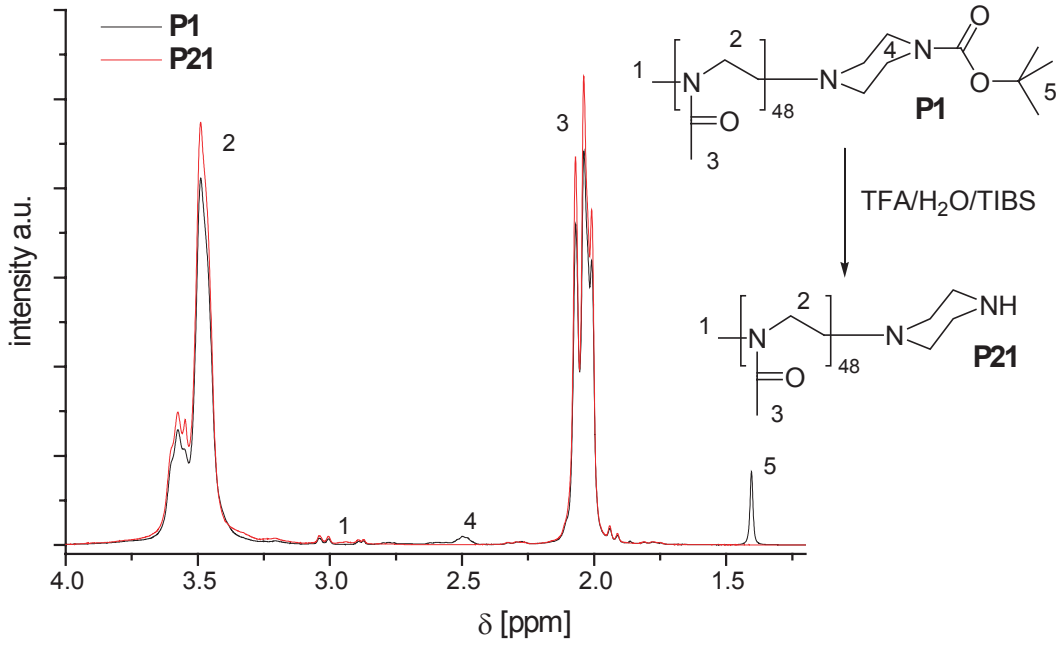

Figure 4.19: Comparison of ^{1}H-NMR (D_2O, 300 MHz) spectra of **P1** and **P21**. The disappearance of the signal at 1.4 ppm indicates the quantitative removal of the terminal protection group.

be reduced by 100 g/mol through the removal of the Boc group. GPC is not exact enough for this minuscule change in molar mass, since 100 g/mol is less then the typically observed intrinsic error of GPC (approx. several hundred g/mol). As an additional analytical method to corroborate the results from ^{1}H-NMR, MALDI-TOF MS was performed. Figure 4.20 shows the comparison of the MALDI-TOF mass spectra of **P2** and **P22**. While the overall shape of the peak distributions does not change significantly upon deprotection it can be easily seen that it shifts to lower m/z values by Δm/z = 100 - 200.

Finally, HPLC was performed to prove unambiguously the successful removal of the

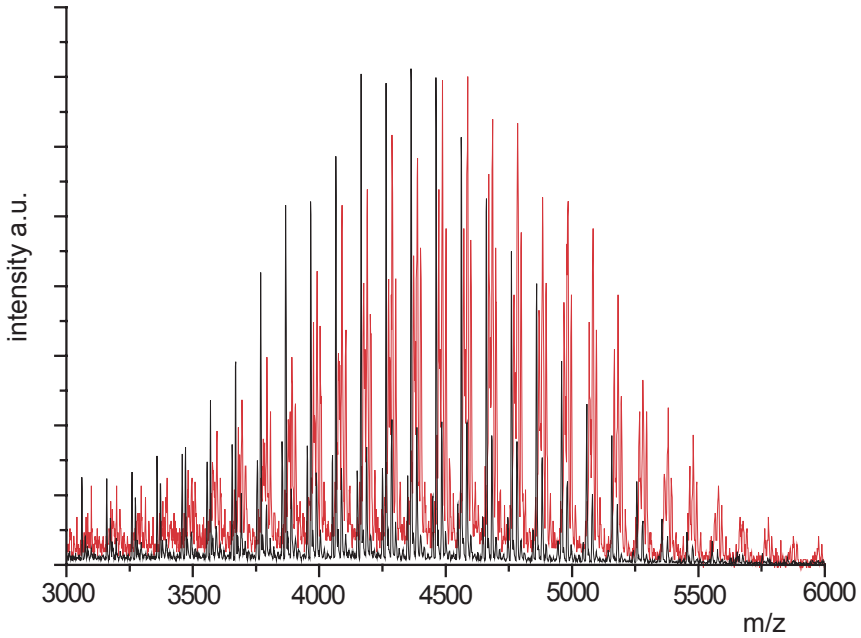

Figure 4.20: Comparison of MALDI-TOF mass spectra of **P2** (red) and **P21** (black). The shift to lower m/z values after the removal of the Boc group can be easily observed.

protection group. In contrast to GPC, this chromatographical method does not discern by the size of the solute but by interaction of the solute with the stationary phase, an effect more determined by chemical composition. The comparison of the HPLC elugrams of **P6** and the deprotected P($MeOx_{45}PynOx_5$)Pip (**P23**) is shown in Figure 4.21. Both polymers give rise to a broad elution peak but although only a small moiety at one polymer terminus is removed, the retention time does change by almost 2 min. Similar shifts are observed for the other deprotected polymers. In conclusion, the removal of the Boc protection group at terminal piperazine is facile and quantitative.

MALDI-TOF MS analysis of the content of functional side chain content in P24

The functional group distribution can not be analyzed by GPC, neither by HPLC or ^{1}H-NMR spectroscopy. The latter can serve for quantification, but will only be able to give average values. Although it has been shown be GC analysis that, random copolymers of e.g. EtOx and **2** can be obtained, it is desirable to know the actual deviation from the average content of functional groups within the polymer. To this end, the

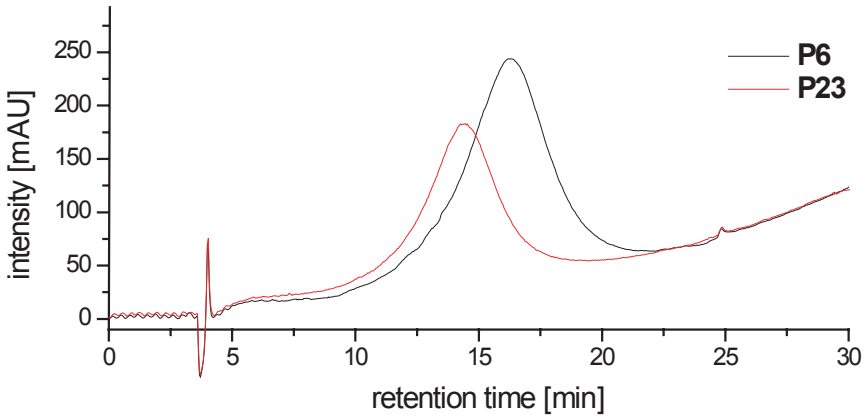

Figure 4.21: Comparison of HPLC chromatograms of **P6** and **P23** at 220 nm. The removal of the protection group leads to a shift of approx. 2 min to earlier elution time.

MALDI-TOF MS of **P24** was analyzed in detail (Figure 4.22). **P24** was used instead of its parent compound **P8** since the MALDI-TOF mass spectrum of **P24** was much better resolved than the one of **P8**. This might be attributed to the free terminal amine group, which should lead to an increased ionizability of **P24** as compared to **P8**.

The most intense signals are found at m/z values as expected from $[M]_0/[I]_0$, the spectrum is symmetrical and the polydispersity as calculated from the MALDI-TOF MS spectrum is low ($PDI_{MALDI} = 1.02$). After a close inspection of the spectrum, one can eventually distinguish five different signal distributions, which are shown as five different peak groups highlighted in red with the respective remainder of the spectrum in black in Figure 4.22. The two most intense signals at m/z = 2456.4 and 2494.4 can be assigned to $[P(EtOx_{21}PynOx_2)Pip+H]^+$ and $[P(EtOx_{20}PynOx_3)Pip+H]^+$ ($m/z_{calc} =$ 2456.7 and $m/z_{calc} = 2494.7$ respectively). The two most intense peak distributions can be assigned to the respective polymer species that contain two ($[P(EtOx_nPynOx_2)Pip + H]^+$, Figure 4.22b) and three ($[P(EtOx_nPynOx_3)Pip + H]^+$, Figure 4.22c) units of **2** with varying amounts of EtOx. This corresponds excellently with the monomer feed ratio of the precursor polymer (**P8**) of $[\mathbf{2}]_0/[I]_0 = 2.2$. A peak distribution assignable to polymer species containing four units of **2** can be found with a slightly lower intensity (Figure 4.22d). Finally, two distributions with m/z values that correspond with polymer chains containing one (Figure 4.22a) and five copies (Figure 4.22e) of PynOx can be identified, albeit of significantly lower intensity than for the former signal groups.

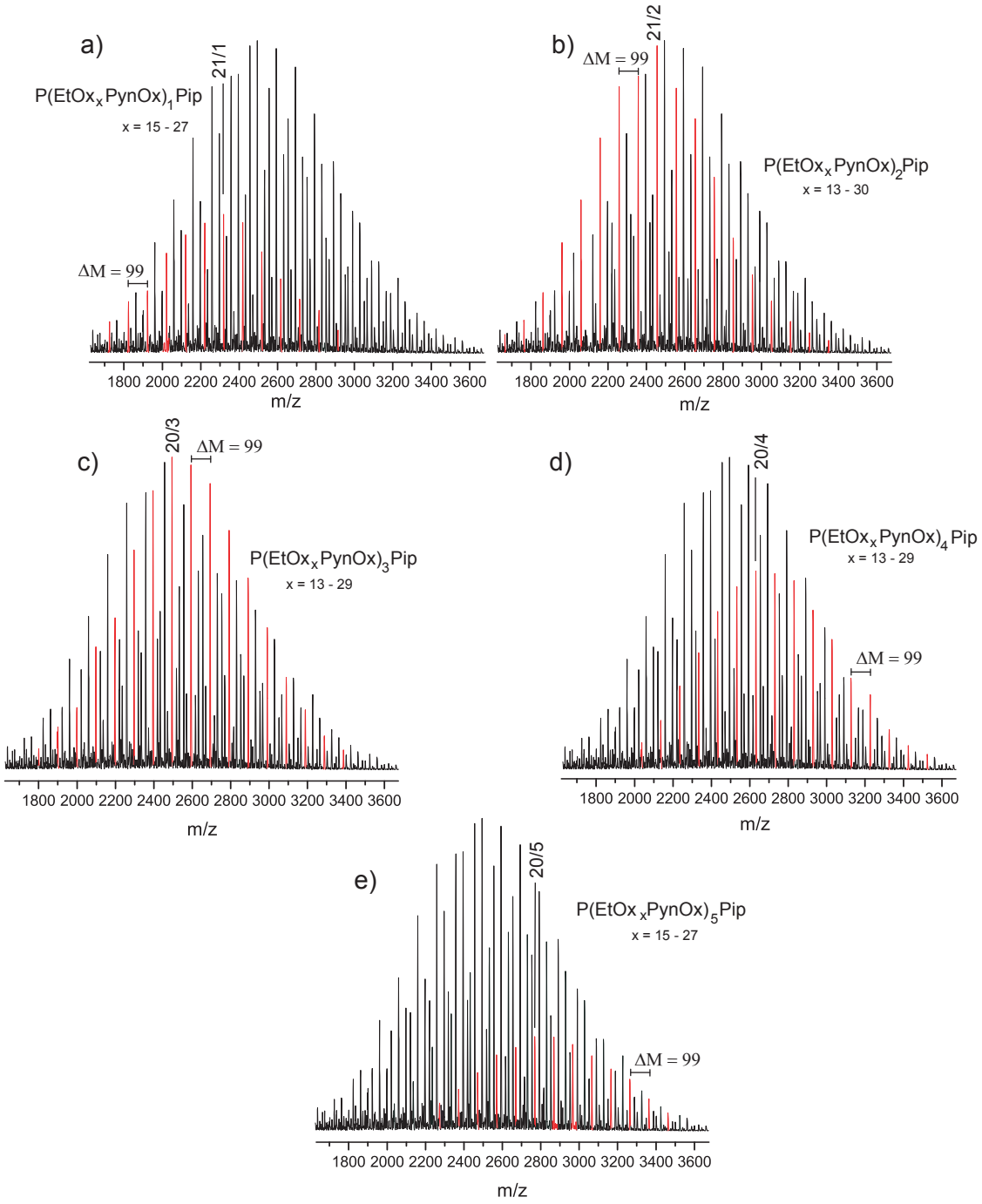

Figure 4.22: MALDI-TOF spectrum of **P24**: Highlighted in red are the 5 different distributions for the content of the functional comonomer **2**. It can be seen, while the content of EtOx spans from about 13 to 29 in the mixture of polymer chains, no signals could be assigned to polymer chains containing more than six units of **2** or less than one.

No signals could be reasonably assigned to polymer species containing no, or more than five copies of PynOx. This MALDI-TOF analysis suggests that it is possible to control the amount of a functional monomer units in a copolymer within close limits. For all five mentioned distributions, the amount of EtOx varies between 13 and 30 with a maximum around 20 in all five cases. This is also in excellent agreement with the initial ratio of $[EtOx]_0/[I]_0$ for the polymerization of **P8**.

4.3.2 Attachment of the radionuclide chelator

The amine group of the terminating reagent piperazine can be used for the attachment of a fluorescent dye as shown recently[403–405]. These labeled polymers have been used in fluorescence correlation spectroscopy for the study of the aggregation behavior of amphiphilic poly(2-oxazoline)s. Fluorescent dyes can be also valuable to study the fate of polymers within the body. Fluorescence microscopy is regularly applied to visualize cellular uptake and compartimentation of labeled compounds down to the subcellular level. This can be of considerable importance to analyze the fate and distribution of drugs e.g. within the kidney.
In this work, the primary interest was to study the overall *in vivo* biodistribution of water-soluble poly(2-oxazoline)s and poly(2-oxazoline)-peptide conjugates. For this purpose analog labeling with radionuclides is preferable, as it allows *in vivo* imaging and quantification. The macrocycle DOTA chelates a number of interesting nuclides for biomedical applications, e.g. ^{111}In and ^{68}Ga, as already mentioned (Chapter 2.2.2). The commercially available derivative of DOTA, 2-(4-isothiocyanatobenzyl)-1,4,7,10-tetraazacyclododecane-1,4,7,10-tetraacetic acid (*p*-SCN-Bn-DOTA) is widely applied for the attachment of the chelator to amine groups of, e.g. antibodies. Figure 4.23 depicts the coupling reaction of amine terminated polymers with *p*-SCN-Bn-DOTA and Table 4.6 shows elected analytical data. The attachment was performed in methanol as a solvent and potassium carbonate as a heterogenous base. The reactions were stirred for typically 3 days at RT and the solvent was subsequently removed by a stream of nitrogen. The residual solid was collected with water for subsequent gel filtration. Thus, not only potassium carbonate and HCl could be removed easily, but also unreacted chelator.

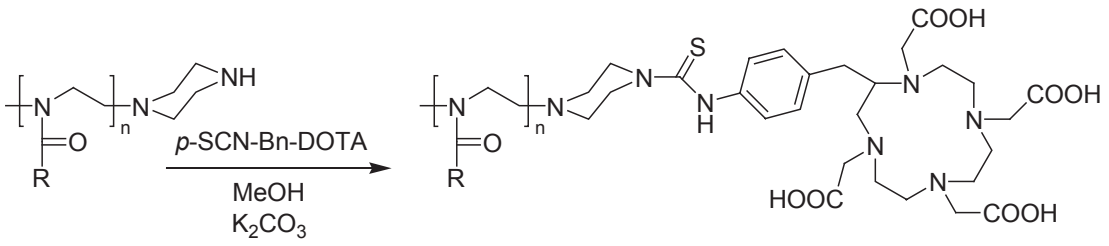

Figure 4.23: General reaction scheme for the coupling of the chelator *p*-SCN-Bn-DOTA to the terminal piperazine.

Table 4.6: Selected analytical data of polymers after attachment of the chelator DOTA.

Polymer	$M_{n,calcd}$[a] [g/mol]	$M_{n,NMR}$[b] [g/mol]	Coupling yield [%][b]	Coupling yield [%][c]	$M_{n,GPC}$[d]/PDI[d] [g/mol]	Yield [%]
P30	4480	5300	75	n.d.	7282/1.45	60
P31	4910	6600	100	n.d.	8093/1.45	62
P32	5170	5100	100	77	6772/1.03 22705/1.03	54
P33	2910	2710	75	n.d.	3895/1.05	68
P34	5580	6500	75	29	n.d.	81
P35	2820	2600	30	20	n.d.	58
P36	3200	3100	25	29	n.d.	61

[a], as calculated from $[M]_0/[I]_0$

[b], as calculated from end-group and side chain analysis based on ^{1}H-NMR

[c], as determined by UV/Vis

[d], as obtained from GPC (solvent DMAc)

The coupling efficiencies, as determined by ^{1}H-NMR spectroscopy, vary from approx. 100 % to only 25 %. The reason for the broad variance for the coupling efficiencies remains unclear. In a number of attempts, no coupling at all was observed. A major contributor to this problem may be the quality of the commercial product *p*-SCN-Bn-DOTA. Different batches obtained from Macrocyclics Inc. differed strongly in appearance, e.g. from a slight to a bright yellow in color, and from powder to crystalline. An inquiry at Macrocyclics Inc. revealed that different batches of the product actually differ significantly in the content of water and HCl.

A comparison of the HPLC elugrams of **P21** and PMeOx$_{48}$PipBnDOTA (**P30**) shows that the retention time of the polymer was unaffected by the conjugation with DOTA (Figure 4.24). However, the observed difference at in the elugrams of **P21** and **P30**

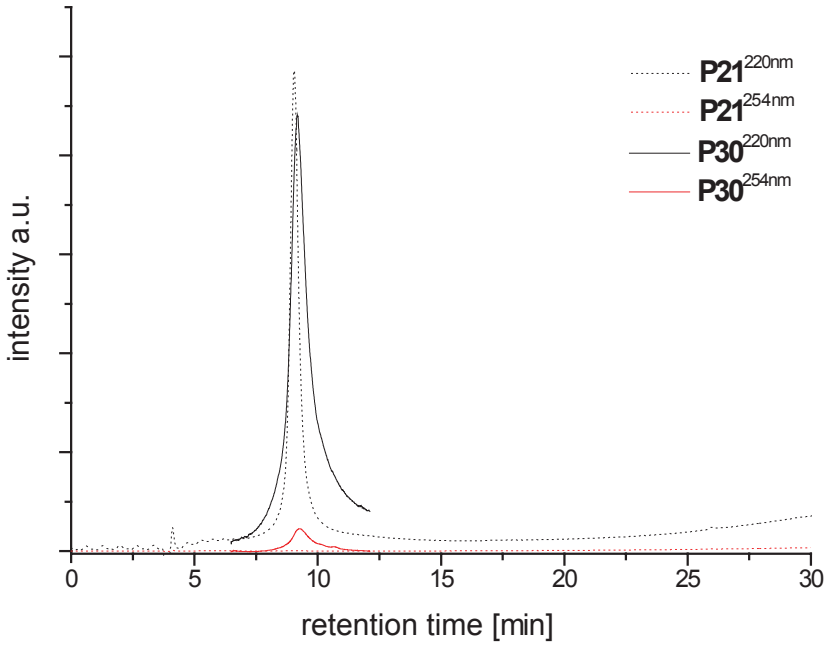

Figure 4.24: Comparison of HPLC chromatograms of **P21** and **P30**. While the retention time remains virtually unaffected upon conjugation of DOTA onto the polymer terminus, the successful attachment is verified by the absorption at 254 nm which is absent in the educt **P21**.

recorded at 254 nm proves the successful coupling of the chelator. While the polymer precursor **P21** contains no chemical moiety that absorbs at this wavelength, a phenyl ring with an strong absorption at 254 nm was introduced by *p*-SCN-Bn-DOTA. Since only one phenyl ring was introduced per polymer chain, the absorption is low. More-

over, the absorption is broad, indicating that the signal is derived from a polymer analyt.

For quantification, ^{1}H-NMR spectroscopy was applied. Figure 4.25 shows the comparison of the spectra of **P21** and **P30** along with the signal assignment . Four new

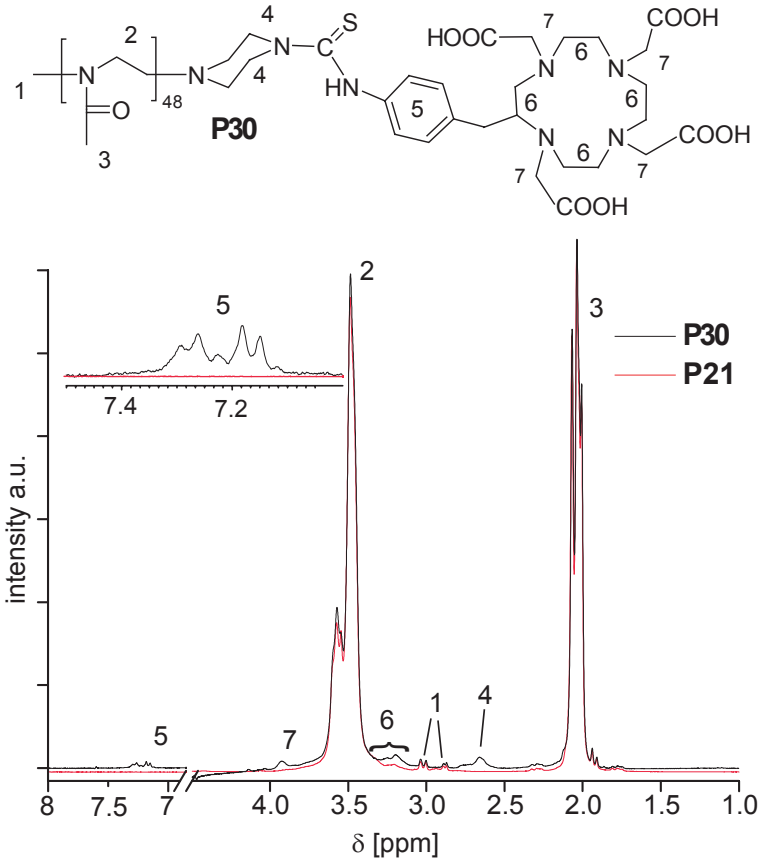

Figure 4.25: Comparison of the ^{1}H-NMR spectra of **P21** (D_2O, 300 MHz) and **P30** (D_2O, 250 MHz). After conjugation with the radionuclide chelator four new signals, 4 - 7 are observed and can be assigned. Signal 5 originates from the phenyl ring in *p*-SCN-Bn-DOTA and can be used for quantification, thus determination of the coupling yield.

signals can be identified (4 - 7) after the coupling reaction. Signal 4 already appears in the spectrum of **P1** but is absent in the spectrum of **P21**. Assuming that the attachment of the Boc and DOTA groups does not only influence electronically the adjacent methylene groups of the piperazine ring, but also sterically stabilizes the ring, forcing the ring into the chair conformation with the bulky substituents in an equatorial position. As a result, the signals of the respective protons are narrowing

and are observable in the ^{1}H-NMR spectra of **P1** and **P30** but absent for **P21**. The protons originating from the ring ethylene groups of DOTA give rise to signal 6, which overlaps with the backbone protons (2), as does signal 7. Only signal 5 is isolated and is therefore used for the quantification. The amount of DOTA attached to the polymers, as judged from ^{1}H-NMR spectroscopy can be found in Table 4.6. For **P30** it was determined that 70 % to 80 % of the polymer chains contain the chelator DOTA. Figure 4.26 shows another example of the HPLC elugrams after DOTA functionalization of **P23** resulting in P(MeOx$_{45}$PynOx$_5$)PipBnDOTA (**P32**). While in the unconjugated polymer **P23** no absorption at 254 nm could be found, the product showed a very broad elution peak concomitant with the strong polymer band observed at 220 nm. In contrast to the results of HPLC analysis of **P30**, the elution peaks are

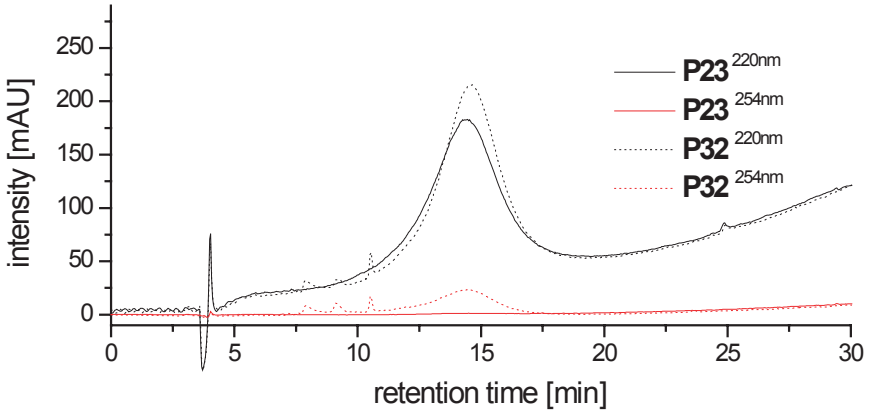

Figure 4.26: Comparison of HPLC chromatograms of **P23** and **P32**. While the retention time remains unaffected upon conjugation of DOTA to the polymer terminus, the successful attachment is verified by the absorption at 254 nm which is absent in the educt (**P23**).

broader and it is more clearly observed that the moiety giving rise to the new band at 254 nm (the phenyl ring of *p*-SCN-Bn-DOTA) must be polymer bound.

Selected samples of the polymer-chelator conjugates have also been analyzed by GPC. Here, the obtained results are inconsistent. The additional mass by the introduction of DOTA is 550 g/mol. This increase is reflected reasonably well in the GPC elugrams of **P30**, **P31** and **P33**. However, the polydispersity increases strongly in the case of **P30** and **P31**, while it remains very low in the case of **P33**.

The precursor of **P32**, **P23** shows monomodal elution profile with a narrow molar mass distribution while the product **P32** is separated in two different peaks, one hav-

ing an apparent mass of M_n = 22705 g/mol (PDI = 1.03), the other located at M_n = 6772 g/mol (PDI = 1.03). The reason for this is unknown. No chemical reaction seems possible that would lead to any di- or oligomerization or cross-linking of the polymer at the reaction conditions. It seems possible that physical interaction via the carboxylic acid moieties resulting in aggregation of the polymer-DOTA conjugates can occur. However, this behavior is only observed for **P32** and not for other samples. In the next chapter we will find another case of the appearance of a high molar mass elution signal for a DOTA bearing polymer sample.
In conclusion, HPLC is useful for a first and rapid evaluation whether the coupling with DOTA was successful, but for a sound quantification the samples are to be purified by gel filtration (quality control by HPLC to check for residual free chelator) and analyzed by ^{1}H-NMR spectroscopy. The combination of HPLC and ^{1}H-NMR spectroscopy serves as a reliable combination for the evaluation of a polymer analog modification. GPC in contrast seems not to be reliable. Presumably, aggregation can occur for these polymers giving rise to elution peaks which can not be explained by the chemical modification. In addition, the amount of sample necessary for GPC is substantially higher than for HPLC and in contrast to ^{1}H-NMR samples the polymer is not easily recoverable.

4.4 Modification of polymer side chains

4.4.1 Removal of the dioxolane protection group

The protection of an aldehyde functionality during CROP of 2-oxazolines is necessary since aldehydes are not compatible with the living polymerization[259]. Recently the polymerization of the protected aldehyde 2-oxazoline monomer **1** was described and the polymers were used in an oxime coupling for the first time. Before a coupling reaction can occur, the dioxolane group has to be converted to the reactive aldehyde (Figure 4.27). Various attempts of a quantitative conversion to free aldehyde failed. Only when the reaction was performed within a dialysis membrane, the corresponding aldehyde bearing polymers were obtained. The reaction was a purification at the

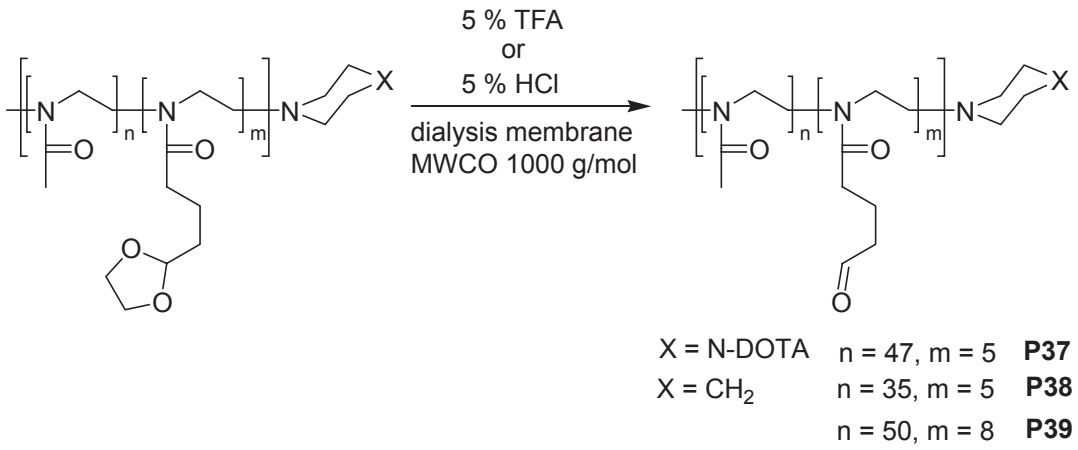

Figure 4.27: Reaction scheme of the removal of the dioxolane protection group.

same time, since low molar mass impurities (including the released ethylen glycole) are removed during the dialysis. The deprotection was performed in 5 % TFA_{aq} or 5 %HCl_{aq}.

Table 4.7 summarizes selected analytical data of the aldehyde bearing polymers **P37**-**P39**.

The first two entries show analytical data for P($MeOx_{35}DPOx_5$)Pid and P($MeOx_{50}$-$DPOx_8$)Pid for comparison[316]. These two polymers were dialyzed/reacted 2 h in 5 % HCl_{aq} against 5 % HCl_{aq} and twice for 2 h against Millipor® to give P($MeOx_{35}OBOx_5$)-Pid (**P38**) and P($MeOx_{50}DPOx_8$)Pid (**P39**), respectively. As shown by HPLC analysis (Figures 4.28 and 4.29), the reaction was quantitative. The elution time shifts to lower values upon the polymer analog conversion. No residual polymer was observed. Interestingly, the integration of the aldehyde signal in the ^{1}H-NMR spectra (solvent D_2O) gave lower values than expected from the dioxolane content of the precursor polymers, while an unaccounted signal around 4.9 ppm was observed. This could not originate from the proton geminal to the dioxolane ring, since the signals of the dioxolane ethylene protons around 3.9 ppm were absent. Only after thorough freeze-drying and recording of spectra in $CDCl_3$, this unassignable signal disappeared and the signal integral originating from the aldehyde at 9.7 ppm had the expected values. Exemplary, the ^{1}H-NMR spectrum of **P39** is shown in Figure 4.30. It is assumed that in the presence of water, a significant amount (approx. 50 %) of the aldehyde is present in its hydrated form and the geminal proton appears at a similar chemical shift (4.8 ppm) as the dioxolane proton signals.

Table 4.7: Selected analytical data polymers with pending dioxolane and aldehyde side chains.

	Polymer	$M_{n,calcd}$[a] [g/mol]	$M_{n,NMR}$[b] [g/mol]	$M_{n,GPC}$[c] [g/mol]	PDI[c]
	$P(MeOx_{35}DPOx_5)Pid$[316]	4000	4000	5245	1.18
	$P(MeOx_{50}DPOx_8)Pid$[316]	5840	5840	7518	1.25
P37	$P(MeOx_{47}OBOx_5)PipDOTA$	5360	5600	7205	1.06
				26492	1.05
				97657	1.06
P38	$P(MeOx_{35}OBOx_5)Pid$	3780	5800	6946	1.22
P39	$P(MeOx_{50}OBOx_8)Pid$	5480	5800	11980	1.25

[a], as calculated from $[M]_0/[I]_0$

[b], as calculated from end-group and side chain analysis

[c], as obtained from GPC (solvent DMAc)

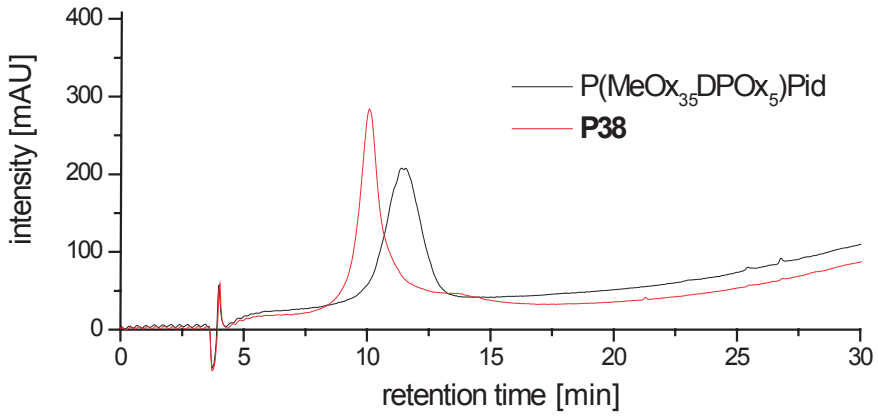

Figure 4.28: Comparison of HPLC chromatograms of $P(MeOx_{35}DPOx_5)Pid$ and **P38**. The retention time shifts significantly to lower values values as the dioxolane group is removed.

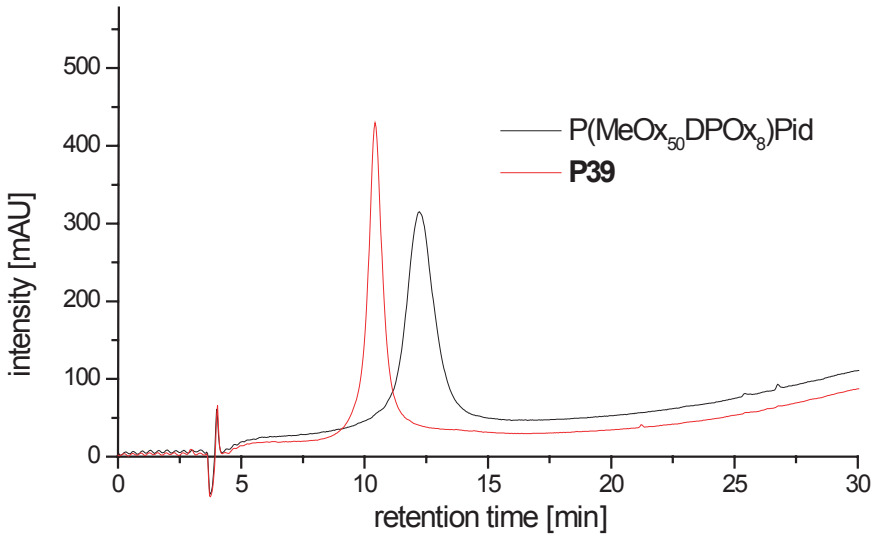

Figure 4.29: Comparison of HPLC chromatograms of P($MeOx_{50}DPOx_8$)Pid and **P39**. The retention time shifts significantly to lower values values as the dioxolane group is removed

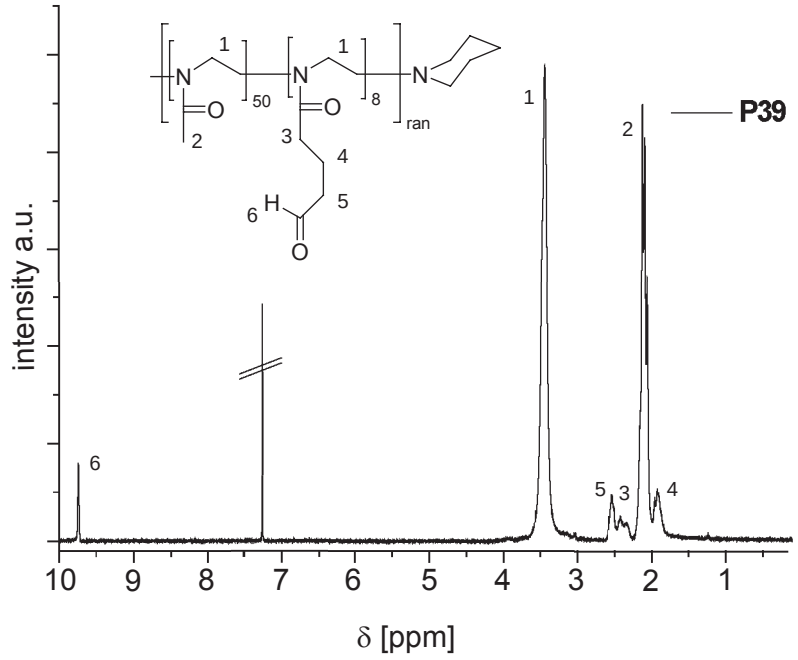

Figure 4.30: ^{1}H-NMR of **P39** ($CDCl_3$, 250 MHz). In contrast to the NMR in D_2O, the integral value of the aldehyde proton at 9.7 ppm is in excellent agreement with the expected value.

Again GPC analysis gave interesting values. Deprotection decreases the molar mass of these two polymers, but GPC data show a pronounced increase to approximately twice the molar mass as expected. Since the molar mass must decrease, this shows the limitations of GPC and the major effect that chemical modification of only approx. 15 % of the polymer side chains can have. Furthermore, for **P37** instead of one, three well separated and narrow elution peaks were found. Similar as for **P32**, one signal appears at an elution time corresponding to a molar mass of around 25.000 g/mol. In addition a very narrow, albeit weaker peak is observed around 100.000 g/mol (PDI 1.06). It seems unlikely that any kind of side reaction could lead to such well-defined high molar mass oligomers or aggregates of the **P32**. Therefore it must be assumend that these high molar mass elution signals are artefacts caused by specific polymer-stationary phase interactions.

4.4.2 Chemoselective coupling reactions on the polymer side chains

The novel polymer bound aldehyde functionality has been coupled to a model aminooxy compound, *O*-benzylhydroxylamine by *Taubmann* et al.[259] as described previously (Figure 4.31). It was shown that the coupling reaction was quantitative as judged from ^{1}H-NMR spectroscopy. Accordingly, it was necessary to evaluate if it

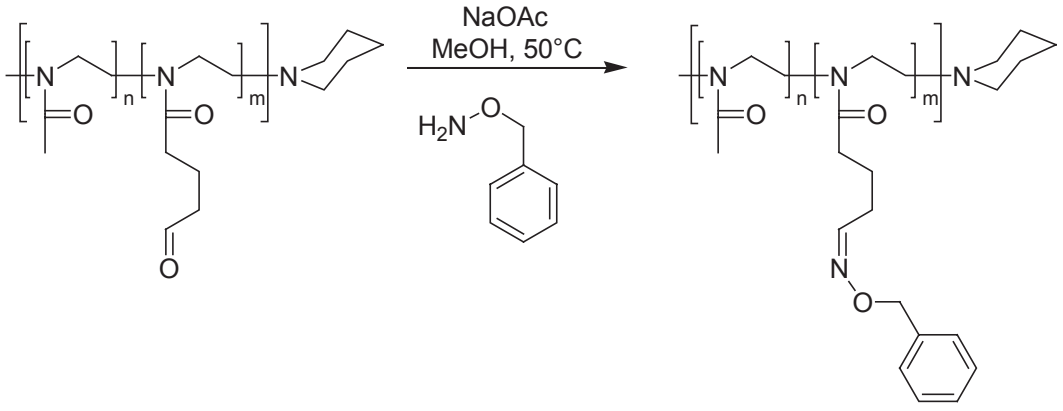

Figure 4.31: Reaction scheme of the polymer analog chemoselective oxime formation[259].

is also possible to convert the pending alkyne functionalities with azides to triazoles with high or maybe quantitative yield. For this purpose two small azides, ethyl(2-azido)acetate and (trimethylsilyl)methyl azide, were coupled to the pending alkynes. Moreover, the coupling of the linker **5** for subsequent native chemical ligation was used to allow the attachment of N-terminal cystein containing peptides (Figure 4.32). The

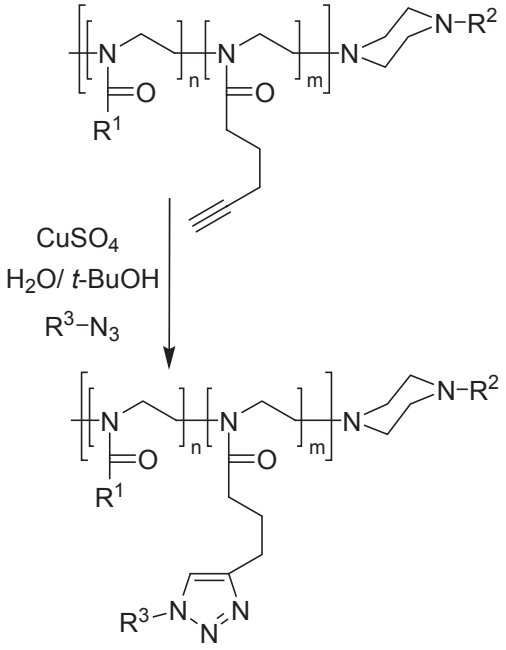

R^1	n	R^2	m	R^3	
CH_3	45	BocPip	5	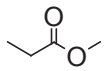	**P25**
CH_3	45	BocPip	5	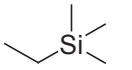	**P26**
CH_3	45	BocPip	5	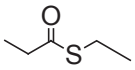	**P27**
C_2H_5	20	Pip	2	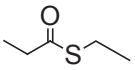	**P28**

Figure 4.32: Reaction scheme for the polymer analog chemoselective coupling reaction via Cu(I) catalyzed Huigens' cycloaddition ('click-chemistry')[401].

coupling reactions were performed in aqueous media. The catalytic Cu(I) was generated *in situ* by reduction of $CuSO_4$ by sodium ascorbate as described previously[366]. Table 4.8 shows analytical data for the polymers **P25** - **P28** after side chain modification. The recovered yields were reasonably high, only the (trimethylsilyl)methyl azide coupled polymer was obtained in a moderate yield. The trimethylsilyl (TMS) side chains presumably lead to hydrophobic products, which accounts for some loss of polymer during work-up. The reason to apply click-chemistry on poly(2-oxazoline)s was the reported high coupling efficiency for this reaction. In order to evaluate this aspect, HPLC and ^{1}H-NMR spectroscopy were performed.

The ^{1}H-NMR spectra of **P6** and P($MeOx_{45}{}^{Triaz}TMS_5$)PipBoc (**P26**), along with the signal assignment is shown in Figure 4.33. The proton signals 4, 5 and 6 are assigned to the alkyne side chain methylene groups. Upon side chain modification, it is expected

Table 4.8: Selected analytical data of polymers after ´clicking´ of small organic azides.

	Polymer	$M_{n,calcd}$[a] [g/mol]	$M_{n,NMR}$[b] [g/mol]	$M_{n,GPC}$[c] [g/mol]	PDI[d]	Yield[e] [%]
P25	P($MeOx_{45}$-$^{Triaz}Ac_5$)BocPip	5291	6700	7.74	1.07	73
P26	P($MeOx_{45}$-$^{Triaz}TMS_5$)BocPip	5362	7800	8430	1.06	48
P27	P($MeOx_{45}$-$^{Triaz}ThioAc_5$)BocPip	5442	5200	7031	1.15	70
P28	P($EtOx_{20}$-$^{Triaz}ThioAc_2$)Pip	2648	3000	3276	1.11	84

[a], as calculated from $[M]_0/[I]_0$ and for 100 % conversion of the polymers
[b], as calculated from end-group and side chain analysis
[c], as obtained from gel permeation chromatography (solvent DMAc)
[d], obtained from GPC, M_w/M_n
[e], recovered product, quantitative functionality conversion according to analysis

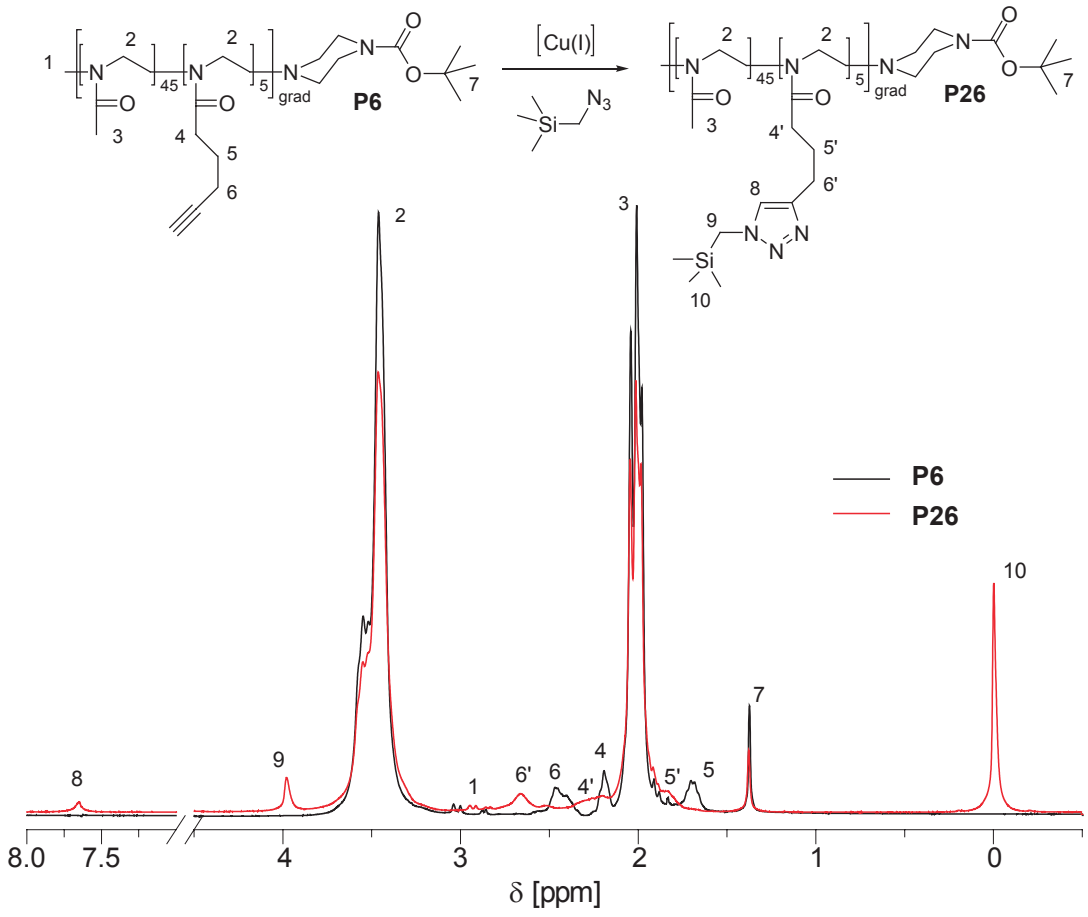

Figure 4.33: ^{1}H-NMR spectra (D_2O, 300 MHz) of **P6** and **P26**. The proton signals originating from the alkyne side chains shift quantitatively, indicating full side chain conversion.

that these signals shift, while the rest of the polymer signals should remain unaffected. Indeed, signals 5 and 6 shift low-field to signals 5' and 6' by about 0.2 ppm. Signal 4, originating from the methylene group adjacent to the polymer acyl group, shifts to a lower degree and broadens to become signal 4'. While these 3 signals change, the other signals of the polymer remain unaffected. Furthermore, 3 new signals are observed, at 7.6 ppm (aromatic proton of the triazole ring), 4.0 ppm (methylene group between the triazole and the TMS group), and 0.0 ppm (TMS). The integrals of these new signals are as expected when related to the signals arising from the terminal groups (Boc and methyl). More importantly, the complete shift of the alkyne side chain signals indicates a high degree of conversion $> 95\,\%$ (coupling efficiency per alkyne chain $> 99\,\%$). The backbone ethylene signals are of higher intensity as expected and a DP of around 80 is calculated. A more detailed discussion of this coupling reaction, along with additional IR analysis and coupling reactions of a polymer of higher alkyne content can be found in literature[401]. In accordance with the analytical procedure described in the recent chapters, HPLC can also be used to evaluate the polymer analog coupling efficiency (Figure 4.34). The shift to earlier elution times comparing **P24** and **P28**

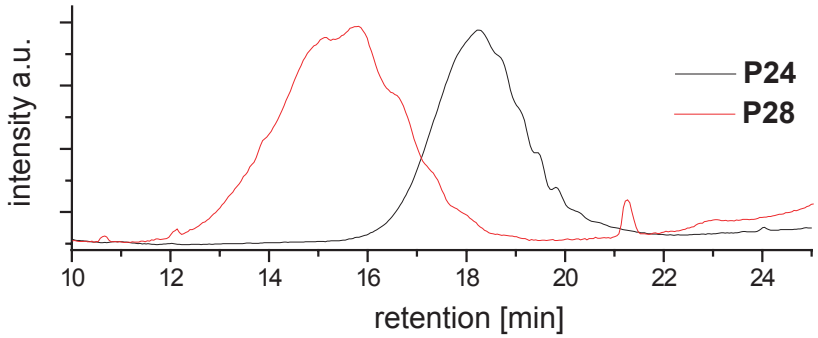

Figure 4.34: Comparison of HPLC elugrams of **P24** and **P28**. After the attachment of ethyl (2-azido)thioacetate the retention time is shifted for approx. 3 min.

can be explained by the 'exchange' of the rather hydrophobic alkyne moiety with the triazole ring and the introduction of the thioester, both relatively polar groups. The complete shift of the peak corroborates the earlier finding that the side chain conversion by click-chemistry is quantitative.

In conclusion, the coupling reaction between the pending alkyne groups with small azides was successful. Within the analytical limitations the conversion was found to be quantitative after a reaction time of several hours at room temperature. The next

chapter will deal with the attachment of bioactive peptides via click-chemistry, oxime ligation and native chemical ligations.

4.4.3 Coupling of peptides

Click chemistry

The copper(I) catalyzed coupling reaction between azides and alkynes has been applied for preparation of a tetramer of cyclic RGDs as reported recently[91]. Accordingly, first attempts to couple P($EtOx_{20}{}^{P}ynOx_2$)PipBnDOTA (**P33**) and c[RGDfK(N_3)][1] were performed with $CuSO_4$ and sodium ascorbate in water or water/*t*-BuOH. However, according to HPLC analysis no coupling of peptide and polymer was achieved. Instead increasing the reaction temperature to 100 °C as described by Dijkgraaf et al.[91], further attempts to obtain P($EtOx_{20}{}^{Triaz}RGDfK_2$)PipBnDOTA (**C1**) were performed using a Cu(I) salt (CuBr) and a hydrophobic chelator, 4,4´-dinonyl-2,2´-dipyridyl (dinonylbipy) in 60 % aqueous THF (v/v) as a solvent (Figure 4.35). This reaction mixture is very sensitive to air. Thus, the solid reagents were combined in a GC vial in the glove-box, the vial was sealed, and the degassed solvents were added. Instantly, an intense dark-brown color was observed. The mixture was stirred for 3 days at RT, upon which the color remained unchanged[2]. After solvent exchange, **C1** was purified by repeated precipitation in cold diethyl ether. In order to remove the copper from the polymer conjugate, it was necessary to add additional dinonylbipy to the polymer conjugate solution prior to re-precipitation. While adding the conjugate solution drop-wise to Et_2O, the lipophilic, thus ether soluble Cu-dinonylbipy complex remained dissolved in the organic phase, while the **C1** precipitated. After several precipitation and dissolution steps, the polymer was obtained as a colorless solid and finally freeze-dried from water. Figure 4.36 shows an HPLC elugram of **P33** and **C1**. Since the t_r of the two peaks differ (at 220 and 254 nm) only slightly and do have a strong overlap, a mixture of **P33** and **C1** was also analyzed by HPLC. The signal in the elugram of this mixture broadens in comparison to the two respective

[1] all RGD peptides used in this work were prepared by Dr. *López-García* in the group of Prof. *Kessler*.

[2] the color immediately changed from brown to green as oxygen was allowed to the mixture.

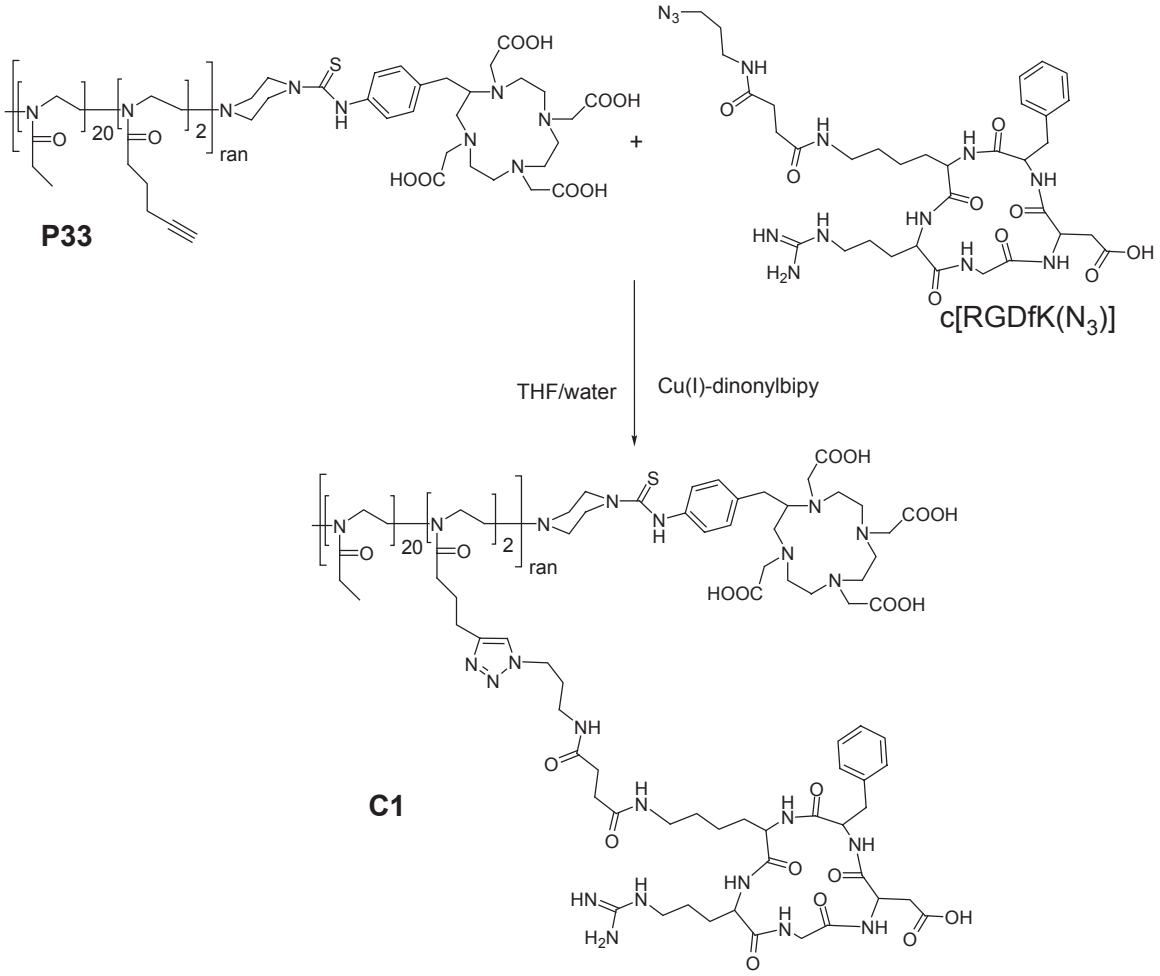

Figure 4.35: Synthesis of poly(2-oxazoline)-RGD conjugate **C1**. The reaction was performed in aqueous THF as a solvent with CuBr and 4,4´-dinonyl-2,2´-dipyridyl as the catalyst and approx. 1.5 equivalents c[RGDfK(N_3)] per alkyne functionality.

elugrams and the signal maximum is found in between the two distinct peaks of the **P33** and **C1**, proving that **P33** and **C1** are two distinct polymeric analytes. No free peptide was observed by HPLC, showing that the purification was sufficient not only to remove residual copper, but also excess peptide. The HPLC data suggest that the

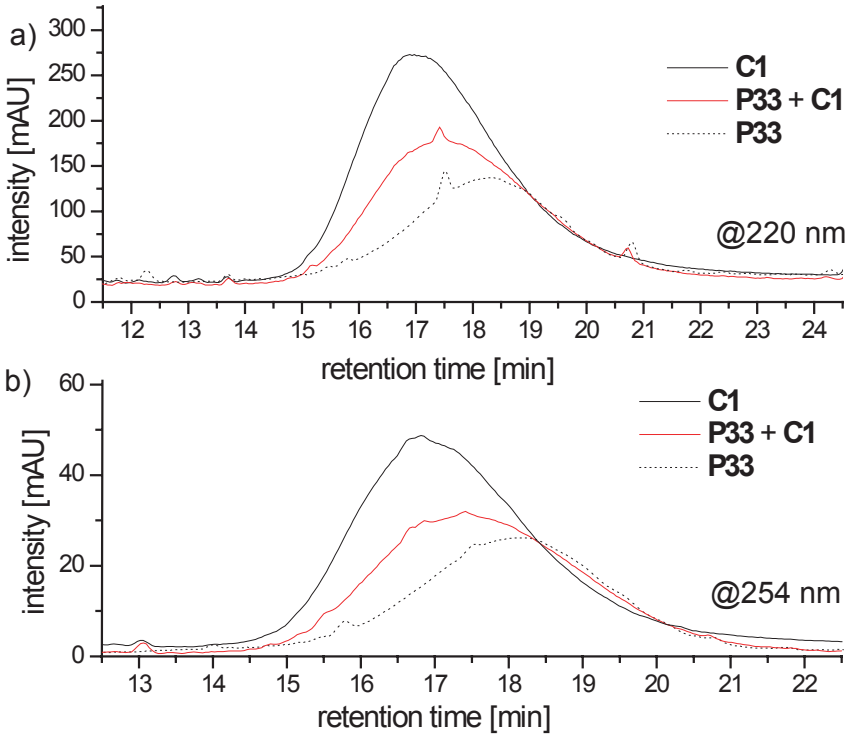

Figure 4.36: Comparison of HPLC chromatograms of **P33** and **C1** with the UV absorbance at 220 (a) and 254 nm (b). Additionally a mixture of **P33** and **C1** was injected to prove that **P33** and **C1** show distinct elution profiles.

conversion of **P33** was quantitative. Additionally, a ^{1}H-NMR spectrum was recorded of **C1** and compared the spectrum of **P33** (Figure 4.37). The analysis of th spectrum of **C1**, however, is somewhat inconsistent. The signals of the proton of the triazole ring and the methylene group adjacent to the triazole (on the peptide side), as well as the central methylene group of the polymer side chain can be identified and the chemical shifts and the integrals are in accordance with the experiments discussed in the previous chapter. However, no signals with significant intensities originating from the peptide can be identified. The reason for this is unknown. Apparently a triazole was formed, but the respective signals of, e.g. the C-H$^{\alpha}$ are not observed. Residual copper(II), being paramagnetic could induce paramagnetically enhanced nuclear re-

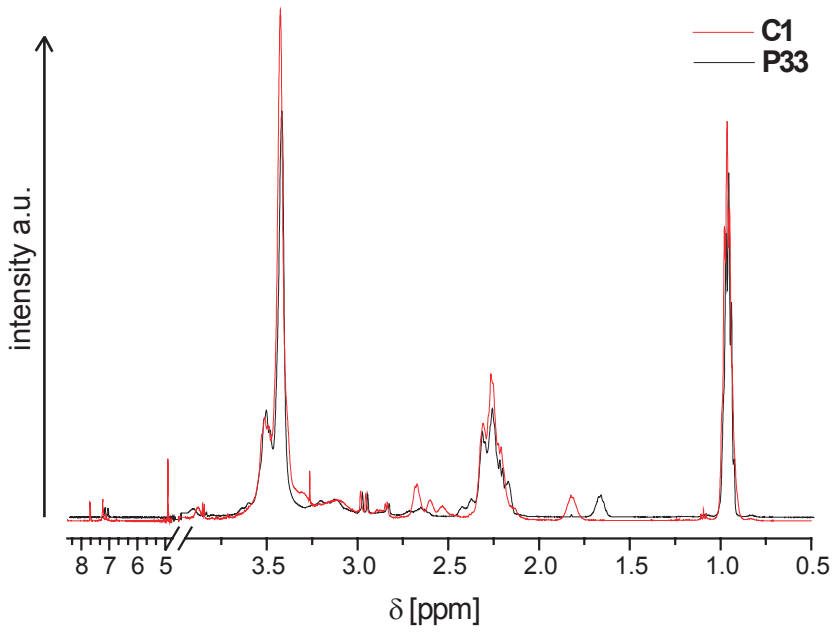

Figure 4.37: ^{1}H-NMR (D_2O, 500 MHz) of **P33** and **C1**. While the specific signals of the alkyne and the triazole ring confirm the formation of triazole. However, little evidence for the peptide can be found in the NMR.

laxation which leads to a broadening of signals of adjacent nuclei[406,407]. However, this seems rather unlikely, since no CuS could be precipitated from the conjugate solution. Alternatively, aggregation effects could lead to the effacement of the signals of the peptide.

Oxim ligation

RGD conjugates with poly(2-oxazoline)s via oxime ligation. Two approaches have been evaluated for the coupling of aminooxy peptides to aldehyde bearing poly(2-oxazoline)s. The aminooxy moiety is highly reactive towards carbonyl compounds, especially ketones and aldehydes. For this reason, several researchers found it difficult to obtain pure aminooxy bearing peptides. During work-up and purification it was regularly observed that products of aminooxy peptides and ketones, especially acetone, are formed[408]. For this reason, it was evaluated, whether it is possible to deprotect the peptide *in situ* and couple it directly to aldehyde bearing poly-

mer, without prior isolation and purification. For this purpose, c[R(Pbf)GD(tBu)fK-(BocAOAC)] (c[ṘGḊfK(Boc-AOAc)]) was dissolved in a mixture of TFA/TIBS/H_20 (91/7/2, v/v/v). After 3 h at RT, a solution of **P37** in buffer was added. The mixture was allowed to react for 3 days at RT. Purification and removal of excess peptide was performed by gel filtration. HPLC analysis of the resulting **C2** shows that the peptide conjugation leads to shift of approx. 2 min to higher values of t_r as compared to **P37** (Figure 4.38). Additional analysis of the polymer-RGD conjugate was performed by

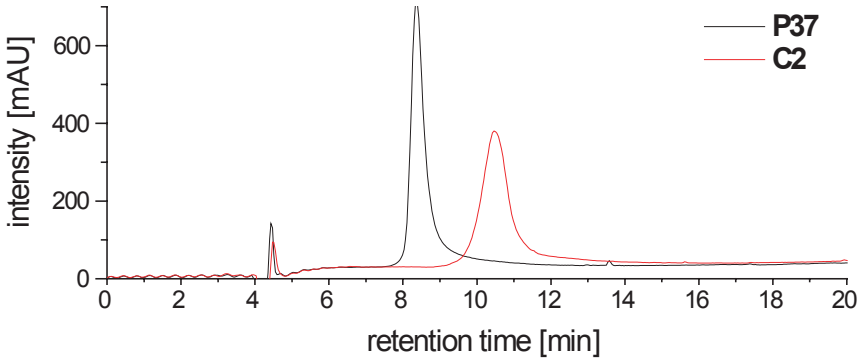

Figure 4.38: HPLC elugrams of **P37** and **C2**. The pronounced shift to higher retention times shows the quantitative conversion of the polymer precursor **P37**.

^{1}H-NMR (Figure 4.39) and ATR-IR spectroscopy. Broad signals of low intensity in the spectrum of **C2**, assignable to amide protons (between 7.2 and 8.3 ppm) and C-H^{α} (between 4.3 and 4.7) are observed. Furthermore, the aldehyde protons observed in the spectrum of **P37** are no longer observed. The integrals of the new signals are in good accordance with approx. 5 peptides per polymer as expected. The comparison of the IR spectra of **P34**, **C2** and the peptide also corroborates that the coupling of the RGD was successful (Figure 4.40). A broadening of the intense carbonyl stretch band of the polymer at 1631 cm^{-1} is observed which can be attributed to the additional amide I and amide II band of the peptide centered at 1658 and 1547 cm^{-1}, respectively. Additionally, two new weak bands at 1159 and 1109 cm^{-1}, related to the peptide can be found in the IR spectrum of **C2**.

In summary, HPLC, ^{1}H-NMR and ATR-IR spectroscopy indicate that the attachment of c[RGDfK(AOAc)] to P(MeOx_{47}OBOx_5)PipBnDOTA **P37** to form P(MeOx_{47}-^{Oxim}RGD$_5$)PipBnDOTA **C2** was successful and integration of the ^{1}H-NMR data is consistent with the amount of approx. 5 copies of c[RGDyK] per polymer chain in average and complete consumption of the side chain aldehyde functionalities. The

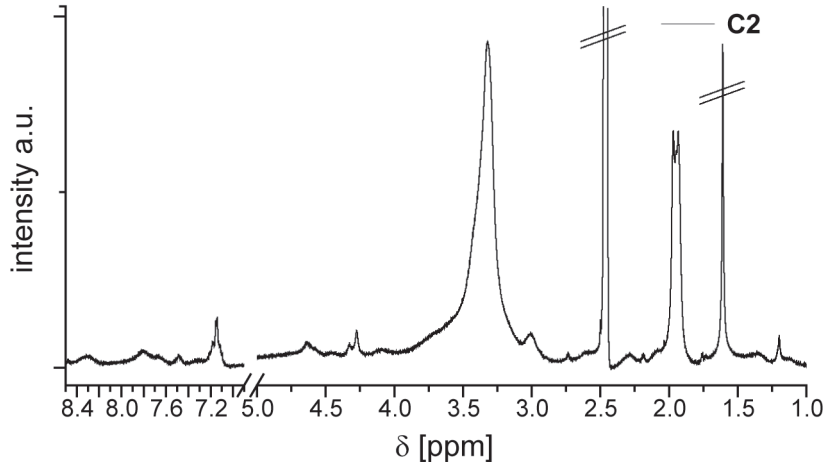

Figure 4.39: ^{1}H-NMR (D_2O, 250 MHz) of **C2**. While the aldehyde signal of the **P37** is no longer observed, a number of broad and weak signal are observed assignable to the peptide.

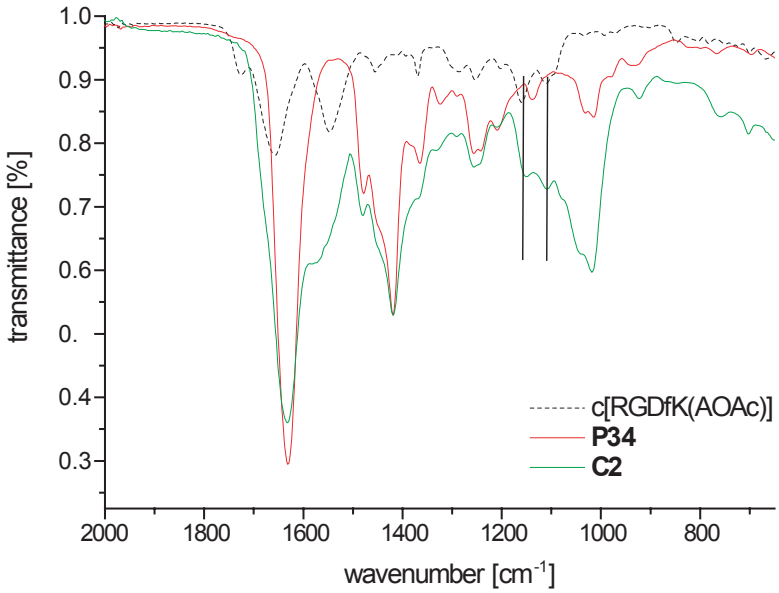

Figure 4.40: Comparison of the ATR-IR spectra of **P34**, c[ṘGḊfK(Boc-AOAc)] and **C2**. Broadening of the amide I band of the polymer by amide I and amide II and the additional weak signals at 1159 and 1109 cm^{-1} (indicated by lines) suggest successful attachment of the peptide to the polymer.

hydrophilicity of **C2**, as judged from HPLC, is high and therefore **C2** is a good candidate for a first *in vivo* evaluation in tumor bearing mice.

The chelator for radionuclides DOTA can have in impact on the receptor affinity or biodistribution of attached peptides, as the introduction of the radionuclides, as already discussed (vide supra, Chapter 2.2.2). To allow radioiodination, a RGD derivative with a tyrosine moiety was used for the preparation of another poly(2-oxazoline)-RGD conjugate (Figure 4.41). In this case the deprotected peptide c[RGDyK(AOAc)] was directly used for the coupling reaction. Figure 4.42 shows the HPLC elugrams of

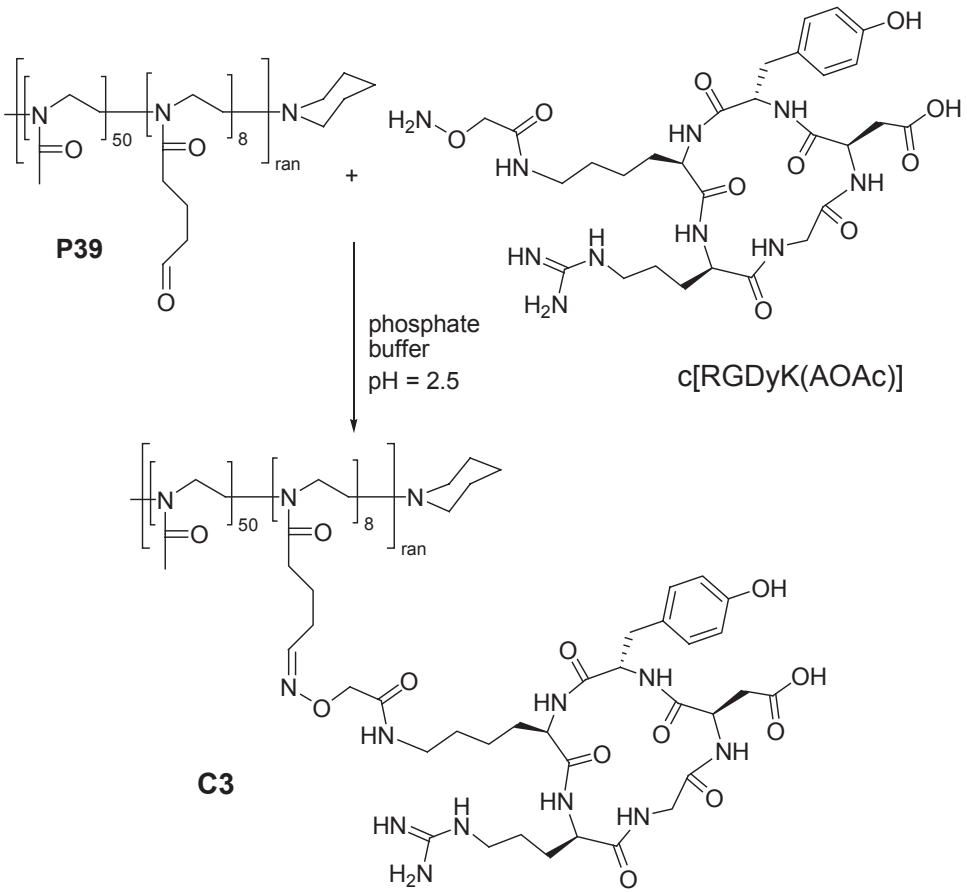

Figure 4.41: Reaction scheme for the preparation of **C3** from **P39** and c[RGDyK-(AOAc)]. The reaction was performed in pH 2.5 phosphate buffer.

the reaction mixture at 220 and 254 nm in comparison with the elugrams of the educt **P39** and the conjugate **C3**. The retention time increases slightly by approx. 30 s. The relatively narrow signal of the polymer shifts quantitatively upon conjugation

with c[RGDyK(AOAc)] and again purification from free peptide was successful by gel filtration as no free peptide can be detected in the purified product. The minor shift

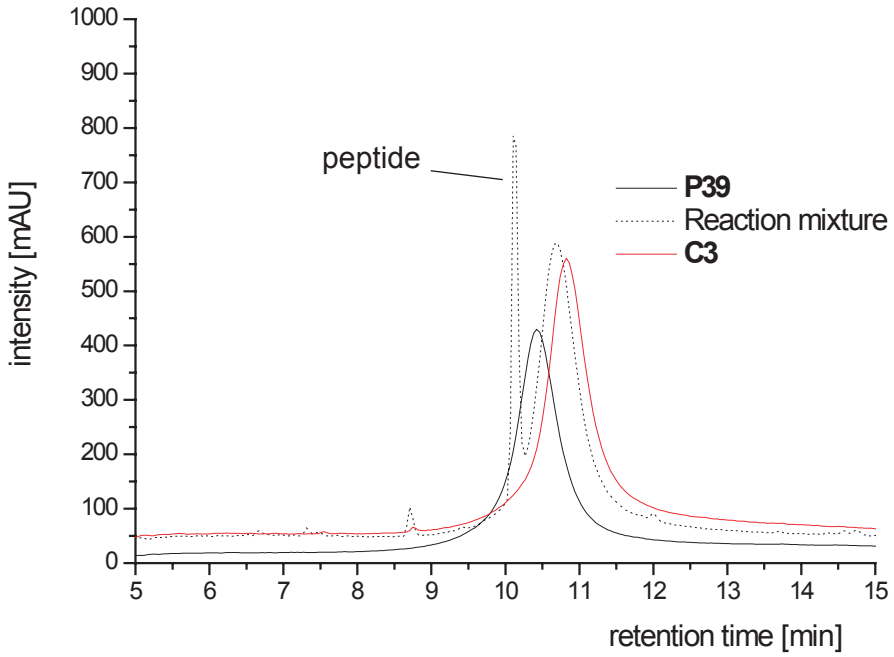

Figure 4.42: Comparison of HPLC chromatograms of **P39** and **C3** at 220 nm. The HPLC of the reaction mixture was taken after 3 h at room temperature. It can be seen that the purified product contains no residual peptide.

of t_r can be also observed in the elugram obtained at 254 nm, as can be seen in Figure 4.43. Additionally, an increase in UV activity can be observed comparing **P39** and **C3**. While the polymer precursors has a low absorbance at that wavelength, the tyrosine residue of c[RGDyK(AOAc)] leads to some absorption at 254 nm. However, the absorbance of Tyr is maximal at 275 nm in comparison with 257 nm in Phe. Therefore, UV spectra of **P39**, c[RGDyK(AOAc)] and **C3** (Figure 4.44) were recorded in order to evaluate if the weak band at 254 nm observed in the HPLC in fact originates from c[RGDyK]. The UV spectrum of **C3** resembles both the absorption characteristics of the polymer (strong absorbance $<$ 220 nm) and the peptide (local absorption maximum at 275 nm) which proves the attachment of c[RGDyK] to the polymer.
In summary, the two peptides c[RGDfK] and c[RGDyK] were successfully attached via an oxime bound to poly(2-oxazoline)s. This reaction is interesting as no catalyst is needed as for click-chemistry. On the other hand, one additional polymer analog reaction is necessary and aminooxy peptides are prone for side reactions in contrast to

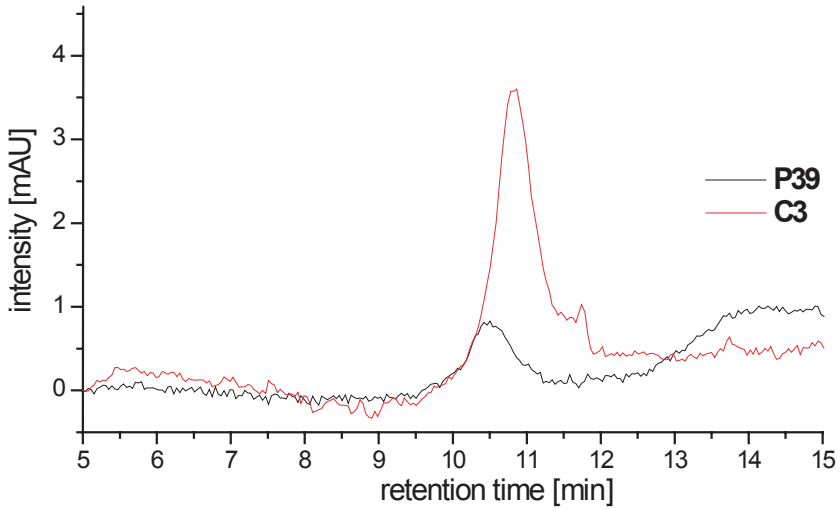

Figure 4.43: HPLC elugrams at 254 nm of **P39** and **C3**. Although the absorption of the peptide RGDyK is not pronounced at 254 nm, the additional absorption in the product can be observed in comparison with **P33**.

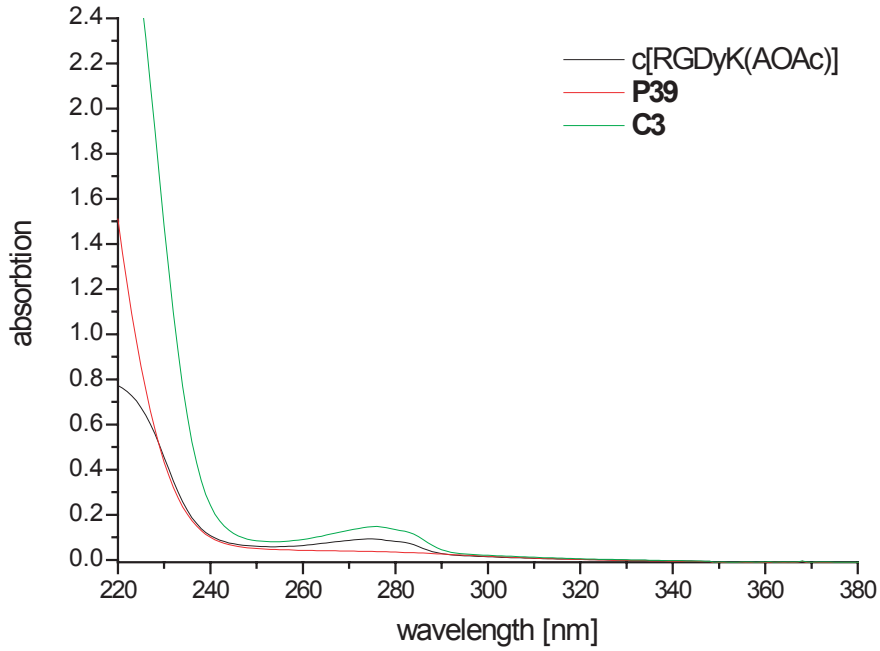

Figure 4.44: UV spectra of **P39**, c[RGDyK(AOAc)] and **C3**. A new maximum at 274 nm in **C3**, originating from the tyrosine residue attached to the polymer is observed, since no free peptide was observed by HPLC.

azide bearing peptides. Additionally, the coupling of another bioactive peptide, MTII, was investigated to evaluate if this reaction is modular as conceived.

MTII conjugates with poly(2-oxazoline)s via oxime ligation. The oxime ligation was also applied for the preparation of three poly(2-oxazoline) peptide conjugates (P($MeOx_{20}{}^{Oxim}MTII_2$)Pid, P($MeOx_{35}{}^{Oxim}MTII_5$)Pid and P($MeOx_{50}{}^{Oxim}MTII_8$)Pid (**C4** - **C6**), carrying the melanocortin receptor binding peptide MTII (Figure 4.45). $AOAc^0$-MTII was synthesized by *Opperer* in the group of Prof. *Kessler*. Attachment

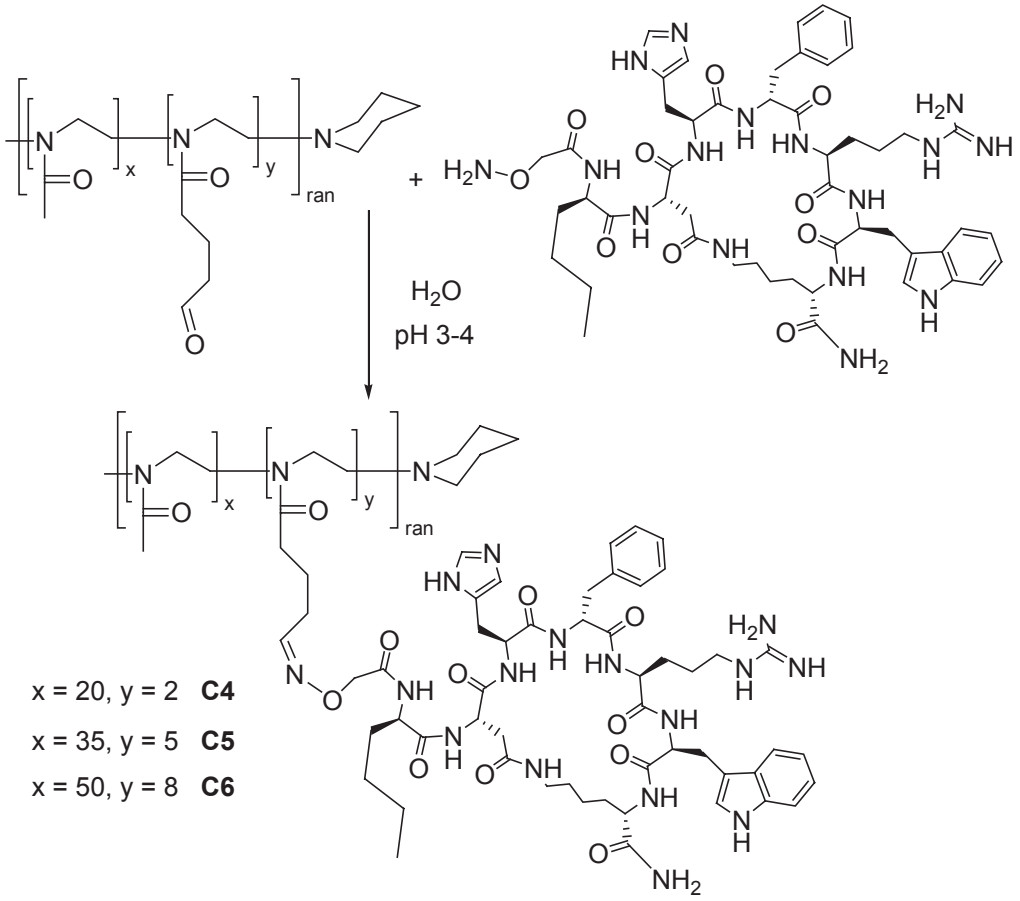

Figure 4.45: Reaction scheme of the preparation of the poly(2-oxazoline)-MTII conjugates **C4** - **C6**. The coupling was performed in acidic aqueous media (pH 3-4).

was performed in aqueous buffer at pH 3-4. Purification and removal of excess peptide was performed by gel filtration. For *in vitro* binding affinity studies to the four receptors hMC1R, hMC3R, hMC4R and hMC5R no radionuclide incorporation is necessary.

Thus, $AOAc^0$-MTII was coupled to piperidine terminated polymers. For further *in vivo* studies, however, coupling to DOTA bearing polymers, according to the preparation of **C2** is possible. Alternatively, radioiodination of one of the aromatic amino acids can be used to directly label **C4** - **C6**.
MTII is more hydrophobic than the cyclic RGD peptides. As a consequence, t_r in HPLC elugrams of the resulting conjugates are higher (14.4 min (**C6**) vs. 10.8 min (**C3**)) than for respective RGD conjugates (Figure 4.46, compare Figure 4.42). The

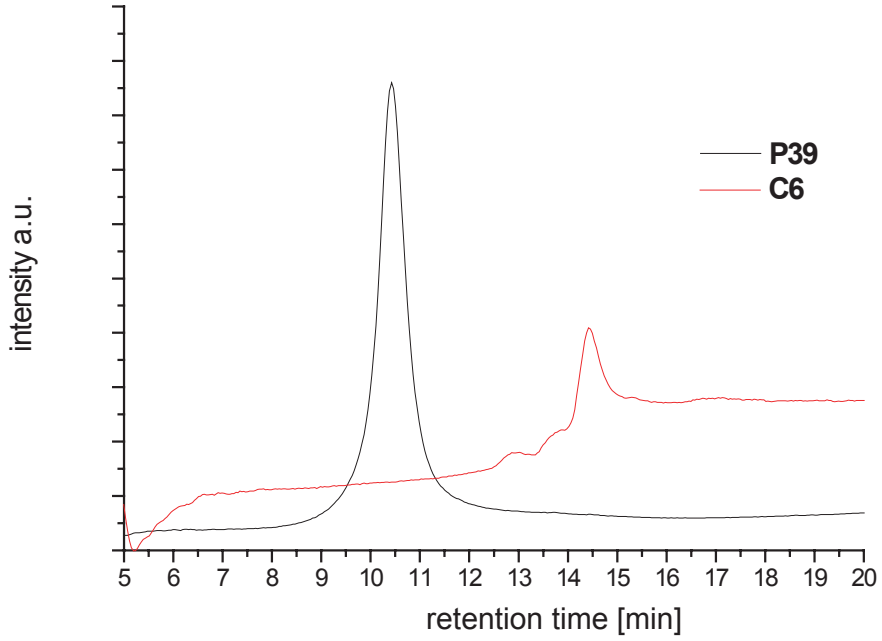

Figure 4.46: Comparison of HPLC chromatograms of **P39** and **C6**.

signal shifts for about 4 min to later elution times in the case of the reaction of **P39** to **C6**. In contrast to the HPLC evaluation of **C3**, no elution peak is observed at 254 nm in the case of the conjugates **C4** to **C6**. This can be explained by the difference in the UV absorption of MTII as compared to c[RGDfK] or c[RGDyK]. The absorbance maximum of MTII is located around 280 nm and only very low absorbance is found at 254 nm (local minimum, Figure 4.47) More evidence for successful attachment of MTII to **P37** - **P39** and quantification can be obtained by ^{1}H-NMR spectroscopy. In the case of the MTII conjugates this is facilitated since more aromatic protons are present as compared to RGD. In fact, broad and intense signals originating from aromatic protons can be found in the ^{1}H-NMR spectra of **C4**, **C5** and **C6**, exemplary shown for **C6** in Figure 4.48. While the aldehyde protons at 9.7 ppm are no longer

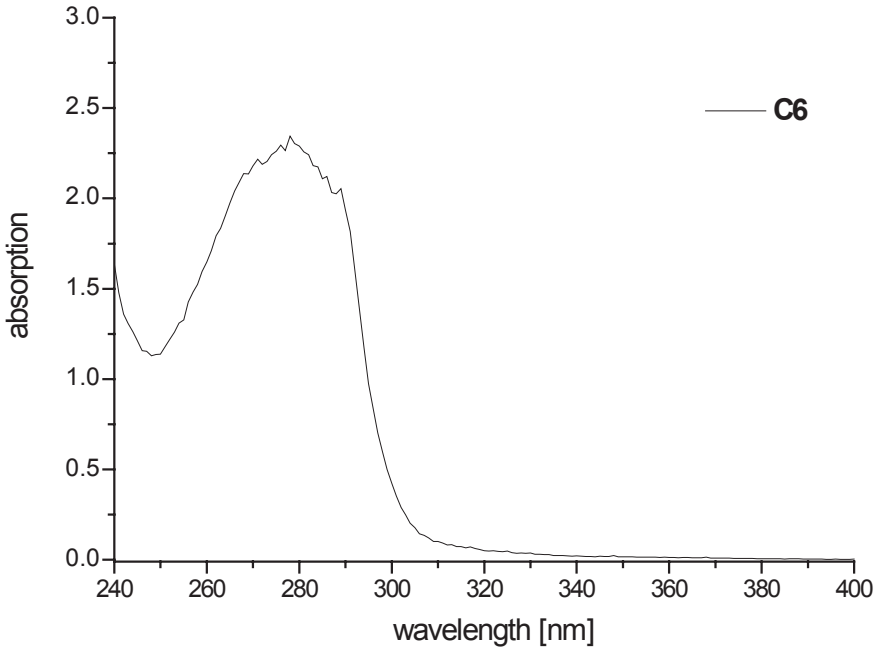

Figure 4.47: UV spectrum of **C6**. The local maximum at 277 nm is absent in the polymer precursor.

observed, the signals originating from the naphthyl, imidazolyl, phenyl groups are observed between 7.5 and 6.7 ppm in accordance with the expected chemical shifts of these aromatic moieties. Additionally, new broad signals are observed around 4 (C-H$^{\alpha}$) and 3 ppm and between 2 and 1 ppm (aliphatic protons). For quantification, the signal originating from the polymer methyl side chains (2.0 ppm) are related to the isolated aromatic peptide signals. Calibration of the signal at 2.0 ppm to 150 protons (according to 50 units of MeOx) gives 102 aromatic protons. This is in good accordance with the expected value of 8 to 9 MTII peptides per polymer chain (12H per MTII). Although the error for this estimation might be significant, it is obvious that substantial amounts of peptide were successfully coupled to **P39**. Accordingly, the expected integral value for signals originating from MTII can be found in the spectrum of **C5**, while in the case of **C4** only an average of one MTII seem to be attached to the peptide. However, in all three cases, ^{1}H-NMR, UV-Vis spectroscopy as well as HPLC analysis indicate successful oxime ligation between aldehyde bearing poly(2-oxazoline)s and AOAc^{0}-MTII. As discussed before, the incorporation of an aminooxy moiety is an additional step in peptide synthesis and the high reactivity of the aminooxy group towards ketones and aldehydes can be problematic at times.

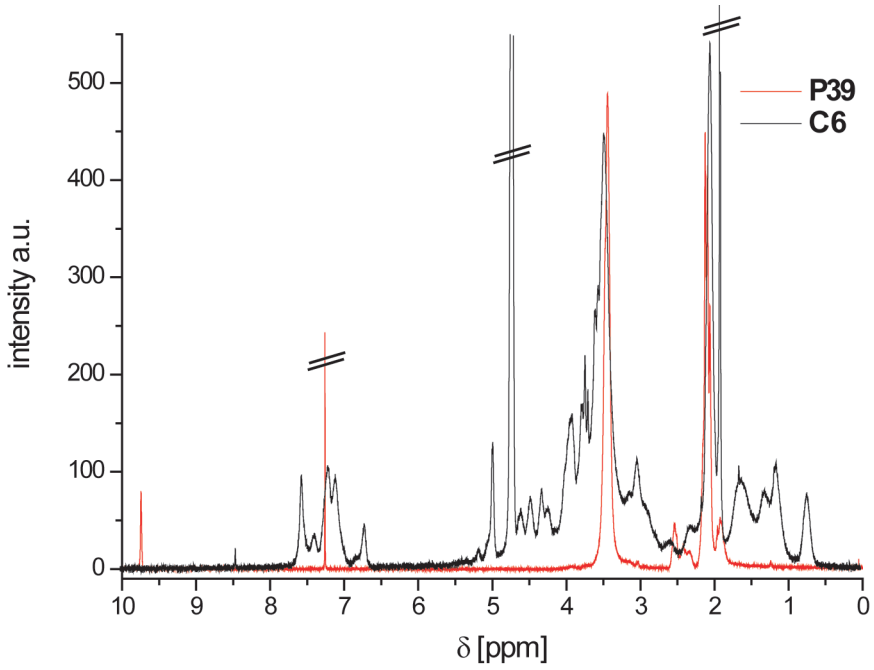

Figure 4.48: ^{1}H-NMR spectra of **P39** and **C6**. While the signal originating from the aldehyde is no longer observed, aromatic signal originating from MTII are found in the conjugate.

The third chemoselective ligation investigated in this work, the NCL, does not need peptide modification and shows no cross-reactivity.

Native chemical ligation

The NCL between a thioester bearing polymer and a peptide with a N-terminal cystein was performed with P($EtOx_{20}{}^{Triaz}ThioAc_2$)PipBnDOTA (**P36**) and the linear pentapeptide CREKA. To inhibit a possible cross-linking of either CREKA or the product via the thiol groups before, during or after the coupling reaction, the reaction was performed in degassed buffer (pH = 7.2)(Figure 4.49). Work-up (gel filtration) was also performed with degassed water and under a nitrogen atmosphere in order to prevent oxidative crosslinking.
P($EtOx_{20}CREKA_2$)PipBnDOTA (**C7**) was analyzed by HPLC (Figure 4.50), ATR-IR (Figure 4.51) and ^{1}H-NMR spectroscopy (Figure 4.52). CREKA is a highly hydrophilic (hygroscopic) peptide. In HPLC, **C7** is eluted approximately 4 min earlier than the educt **P36**. However, it could be assumed that the polymer would also be eluted at significant earlier times, if the thioester is merely hydrolyzed to form free pending carboxylic acid. This could not be ruled out as judged by HPLC, although a shift of 4 min seems unlikely pronounced for the introduction of approx. two carboxylic acids. Comparison of the IR spectra of **P36**, CREKA and **C7** give evidence of a successful polymer-peptide conjugation. Similar as in the IR spectrum of **C2**, a broadening of the carbonyl stretch band at 1630 cm^{-1} is observed for **C7**. Similar as observed in the IR spectrum of **C2**, a pronounced shoulder at the position of the amide II band (1550 cm^{-1}) is observed for **C7**. The shoulder corresponding to amide I of CREKA is relatively weak.
Unambiguous evidence for the successful native ligation can be found by ^{1}H-NMR spectroscopy. From comparison of the spectra of **P36** and **C7** (Figure 4.52) it can be concluded that several new signals, originating from the peptide, are observed. Additionally, the triplett at 1.1 ppm (originating from the thioester) is no longer observed, while at 1.2 ppm a duplett appears, also present ^{1}H-NMR spectrum of CREKA. Comparison of the integrals gives a CREKA content in **C7** which is in good accordance with the expected value of two.
Moreover, since ethanethiol is released during the reaction (Figure 4.49) a simple ol-

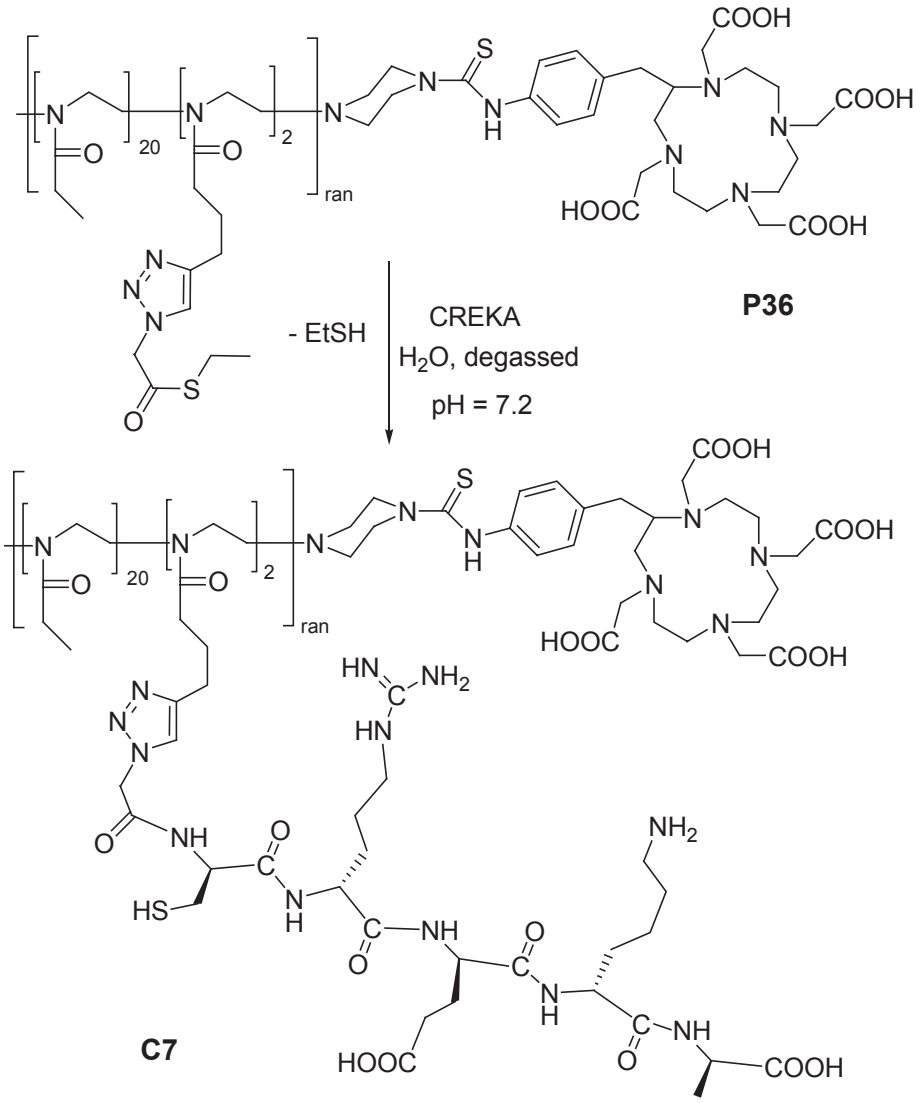

Figure 4.49: Reaction scheme for the NCL between **P36** and CREKA to form **C7**. In order to suppress oxidation and thus, formation of CREKA dimers or cross-linked **C7**, the reaction and work-up was performed in degassed solvent.

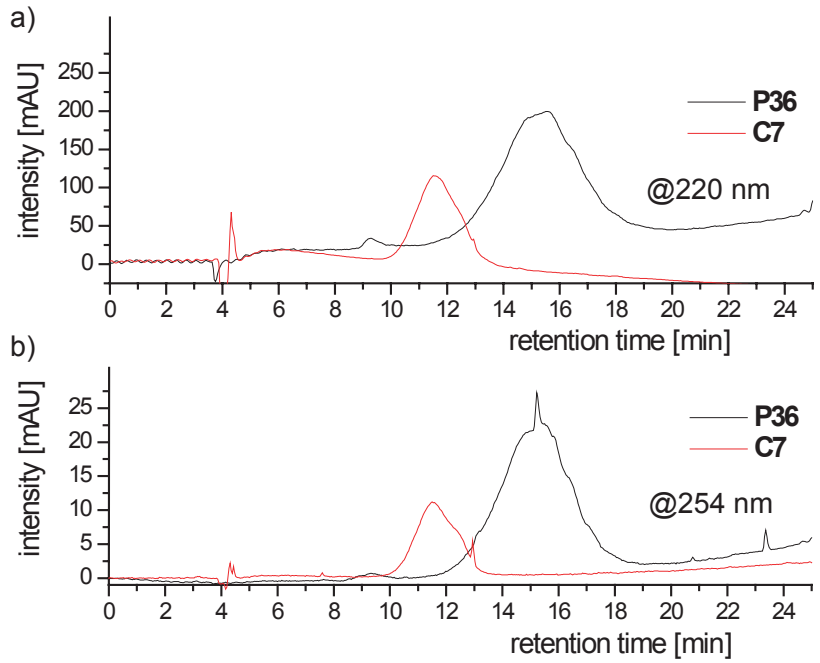

Figure 4.50: Comparison of HPLC chromatograms of **P36** and **C7**. The broad signal of **P36** shifts for approx. 4 min upon CREKA conjugation to lower elution time, reflecting the high hydrophilicity of CREKA.

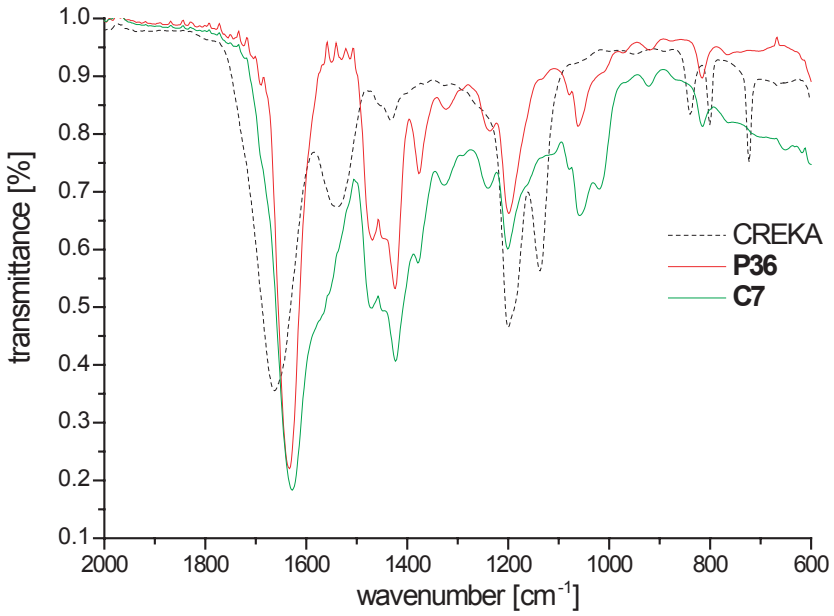

Figure 4.51: ATR-IR spectra of CREKA, **P36** and **C7**. The broadening of C=O str band of the polymer upon conjugation with CREKA is observed, especially around 1550 cm^{-1}, corresponding with the amide II band of the peptide.

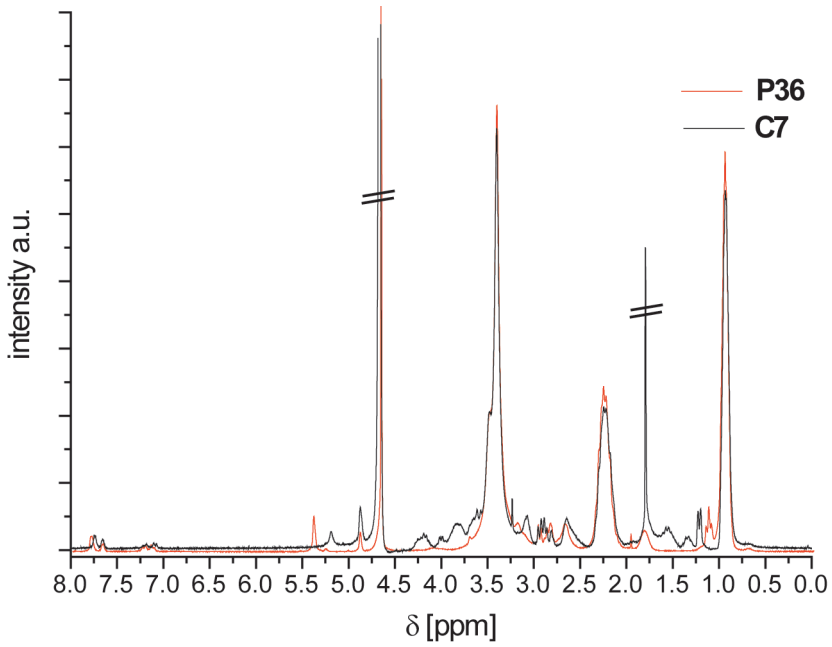

Figure 4.52: ^{1}H-NMR spectra (D_2O, 250 MHz) of **P36** and **C7**. New signals, originating from the peptide CREKA can be observed.

factory test upon opening of the reaction vessel proved the production of the extremely pungent smell of a thiol.[3].

Summary

The goal of this work was to introduce a novel, modular polymer carrier based on poly(2-oxazoline)s for biomedical applications, in particular for the polymer based peptide receptor radionuclide therapy ^{P}PRRT. In the recent chapters the conjugation of three bioactive, tumor targeting peptides with poly(2-oxazoline)s with pending side chains for different chemoselective ligations has been described. In Table 4.9 all presented poly(2-oxazoline)s peptide conjugates are summarized and it is indicated whether the various analytical methods confirm the successful coupling or not. In the case of click-chemistry it remains somewhat unclear if indeed the azide bearing peptide has been successfully attached to the polymer due to inconsistent ^{1}H-NMR

[3]the odor threshold for EtSH is 2.8 ppb and ethanethiol entered the *Guiness Book of Records* in 2000 as the "smelliest substance" in existence[409].

Table 4.9: Synthesized poly(2-oxazoline)-peptide conjugates. Whether coupling was confirmed by the various analytical techniques is indicated with √ for positive, ⊗ for unclear, n.d. for not determined and n.a. for not applicable.

Conjugate	HPLC	NMR	IR	UV
P($EtOx_{20}$-^{Triaz}RGDfK_2)PipBnDOTA **C1**	√	⊗	⊗	n.a.
P($MeOx_{47}$-^{Oxim}RGDfK_5)PipBnDOTA **C2**	√	√	√	n.a.
P($MeOx_{50}$-^{Oxim}RGDyK_8)Pid **C3**	√	n.d.	n.d.	√
P($MeOx_{20}$-^{Oxim}MTII$_2$)Pid **C4**	√	√	n.d.	√
P($MeOx_{35}$-^{Oxim}MTII$_5$)Pid **C5**	√	√	n.d.	√
P($MeOx_{50}$-^{Oxim}MTII$_8$)Pid **C6**	√	√	n.d.	√
P($EtOx_{20}$-^{NCL}CREKA_2)PipBnDOTA **C7**	√	√	⊗	n.a.

data. For the oxime-ligation, analytical data are unambiguous. It has been shown that protected aminooxy peptides can be deprotected *in situ* and coupled directly to aldehyde bearing peptides. Alternatively, also three unprotected aminooxy-peptides were successfully used in oxime ligation. Both, RGD and MTII peptides were successfully incorporated and the removal of excess peptides was facile by gel filtration. Furthermore, the attachment of CREKA, as an example of a bioactive *N*-terminal cystein bearing peptide has been performed by simple combination of peptide and thioester bearing poly(2-oxazoline) in neutral buffer.

4.5 Radiometallation

Before biodistribution studies can be performed, the incorporation of suitable radionuclides had to be established. Various protocols can be found in literature for the introduction of different nuclides into DOTA. The chelation of different metals is dependent on kinetic and thermodynamic factors. For the incorporation of gallium it is reported, that heating to 90 - 100 °C for 10 to 20 min is sufficient to obtain radiochemical yields (RCY) $> 95\,\%$[187, 190, 211]. Alternatively, heating by microwave allows for the reduction of the reaction time to 1 min. The chelation is typically performed in buffer at or around pH 4.2. Two different buffer systems can be found in literature, HEPES and sodium acetate. While the incorporation of Ga into DOTA is typically faster in HEPES, sodium acetate has the advantage of a low toxicity in contrast to

HEPES and must not be removed prior to administration.
For the chelation, **C2** was dissolved in buffer and the $^{68}GaCl_3$ solution was added. The mixture was heated for different time intervals and an aliquot was taken for HPLC analysis. The remainder of the solution was fractionated through a Sep-Pak C_{18} cartridge for purification. While free $GaCl_3$ could be washed out with water, the labeled conjugate remained on the column and was eluted subsequently with ethanol (quality control by HPLC). The ethanol was evaporated and the residual was collected with PBS buffer. Table 4.10 summarizes the attempts of chelation of ^{68}Ga into **C2**. Even at 95 °C and a reaction time of 25 min, only 50 % of ^{68}Ga was chelated using HEPES buffer. When acetate buffer was used, the RCY was even lower (Table 4.10,entry #5). Also the use of microwave heating did not increase the RCY (data not shown). Only longer reaction times increased the RCY to 70 %, but this is problematic with short-lived nuclides such as ^{68}Ga. The reason for this very low chelation yield remains unknown. For further experiments, a more systematic approach should be taken. This was not possible so far, since only limited time was provided for the preliminary chelation evaluation. However, the obtained activity of purified [^{68}Ga]**C2** was sufficient for first *in vivo* biodistribution experiments. Labeled and unlabeled peptides can normally be separated by HPLC. This was not possible for [^{68}Ga]**C2** as the broad elution band of the polymer does not shift markedly upon radiolabeling. Furthermore, no purification by gel filtration is possible since the molar mass change is only minute. To increase the specific activity, separation via an ion exchange column might be feasible.

Table 4.10: Evaluation of incorporation of ^{68}Ga into **C2** at various temperatures and reaction times.

#	Conjugate [mg]	Buffer [μL]	$^{68}GaCl_3$ [μCi]	T [°C]	time [min]	RCY[a] [%]
1	60	140 HEPES	245	65	15	0
2	120	140 HEPES	484	65	20	30
3	200	140 HEPES	230	95	25	50
4	60	140 HEPES	440	85	40	70
5	60	40 acetate	9500	95	20	22[b]
6	60	40 acetate	1150	95	20	15[a]

[a] as determined by HPLC radioelugrams
[b] after purification

4.6 *In vivo* and *in vitro* studies

4.6.1 Biodistribution of hydrophilic low molar mass poly(2-oxazoline)s

Several biodistribution studies concerning MeOx and EtOx containing polymers or liposomes have been briefly discussed before (Chapter 2.4.4). No studies on the biodistribution of well-defined homopolymers of MeOx and EtOx can be found in literature. In contrast, a great number of reports on linear PEG were published[410–416]. Therefore, the biodistribution of the prepared radiolabelable homopolymers of MeOx (**P30**) and EtOx (**P31**) of molar masses of $\sim$5000 g/mol was studied. The radiolabeling and biodistribution experiments were performed by *Gärtner* and *Blechert* in the Nuklearmedizinische Klinik und Poliklinik at the Klinikum rechts der Isar München in the group of PD Dr. *Essler*[417].

The In-111 labeled polymers-DOTA conjugates PMeOx$_{48}$PipBn[^{111}In]DOTA ([^{111}In]-**P30**) and PEtOx$_{43}$PipBn[^{111}In]DOTA ([^{111}In]**P31**) were injected i.v. into female CD1 mice. The mice were sacrificed after 30 min, 3 h or 24 h and the amount of radioactivity in various organs was determined. The amount of the radioactivity was calculated as %ID/g (Tables 4.11 and 4.12). For both polymer samples, the amount of radioactivity, which is proportional to the amount of polymer, is low in all dissected organs and the blood clearance is fast. The amount of [^{111}In]**P30** and [^{111}In]**P31** in the organs reflects the normal blood pool values and no significant organ uptake was observed. The uptake into the brain is particularly low, which indicates that these water-soluble, low molar mass POx are not able to cross the blood-brain barrier. The highest accumulation was found in the kidneys. This is explained by the fast renal excretion of the polymers. Only very limited radioactivity was found in the liver and spleen. These two organs represent a major fraction of the RES and the liver is an important organ for alternative excretion. Only 0.31 and 0.51 %ID/g were found in these organs combined after 30 min for [^{111}In]**P30** and [^{111}In]**P31**, respectively. The lung is, after the kidney and the blood pool, the organ with the highest amount of radioactivity found in the case of [^{111}In]**P30** (30 min p.i.). Similarly for [^{111}In]**P31**, the radioacitivity content found in the lungs is relatively high, but is exceeded by the uptake in

Table 4.11: Biodistribution data of [^{111}In]**P30** in organs after resection at indicated time points p.i. .

Organ	30 min	3 h	24 h
Blood	0.637 ± 0.121	0.228 ± 0.026	0.077 ± 0.022
Heart	0.192 ± 0.048	0.075 ± 0.016	0.056 ± 0.006
Lungs	0.443 ± 0.046	0.230 ± 0.077	0.137 ± 0.014
Kidneys[a]	1.526 ± 0.132	1.114 ± 0.098	0.964 ± 0.170
Liver	0.165 ± 0.036	0.118 ± 0.014	0.136 ± 0.026
Spleen	0.147 ± 0.037	0.091 ± 0.030	0.125 ± 0.025
Pancreas	0.139 ± 0.022	0.068 ± 0.003	0.060 ± 0.007
Muscle	0.121 ± 0.050	0.032 ± 0.006	0.027 ± 0.004
Skin	0.362 ± 0.138	0.081 ± 0.014	0.070 ± 0.012
Fat tissue	0.054 ± 0.009	0.025 ± 0.002	0.017 ± 0.007
Stomach	0.234 ± 0.066	0.071 ± 0.012	0.059 ± 0.007
Jejunum	0.147 ± 0.034	0.068 ± 0.026	0.108 ± 0.015
Colon	0.192 ± 0.041	0.073 ± 0.022	0.094 ± 0.014
Bone with marrow	0.110 ± 0.011	0.093 ± 0.009	0.109 ± 0.049
Brain	0.020 ± 0.002	0.013 ± 0.003	0.010 ± 0.003

values %ID/g ± SD, n = 3, [a] n = 6

Table 4.12: Biodistribution data of [^{111}In]**P31** in organs after resection at indicated time points p.i. .

Organ	30 min	3 h	24 h
Blood	1.267 ± 0.014	0.368 ± 0.023	0.085 ± 0.008
Heart	0.325 ± 0.022	0.125 ± 0.020	0.071 ± 0.005
Lungs	0.731 ± 0.111	0.278 ± 0.110	0.114 ± 0.006
Kidneys[a]	3.643 ± 0.225	2.394 ± 0.147	2.380 ± 0.217
Liver	0.312 ± 0.019	0.193 ± 0.013	0.274 ± 0.026
Spleen	0.198 ± 0.032	0.132 ± 0.005	0.155 ± 0.062
Pancreas	0.211 ± 0.040	0.101 ± 0.021	0.103 ± 0.016
Muscle	0.183 ± 0.009	0.055 ± 0.005	0.043 ± 0.014
Skin	0.927 ± 0.176	0.185 ± 0.028	0.192 ± 0.043
Fat tissue	0.146 ± 0.023	0.041 ± 0.009	0.059 ± 0.007
Stomach	0.318 ± 0.018	0.094 ± 0.016	0.086 ± 0.007
Jejunum	0.260 ± 0.050	0.097 ± 0.015	0.154 ± 0.025
Colon	0.291 ± 0.027	0.091 ± 0.019	0.142 ± 0.043
Bone with marrow	0.495 ± 0.094	0.222 ± 0.034	0.353 ± 0.132
Brain	0.049 ± 0.009	0.015 ± 0.002	0.007 ± 0.001

values %ID/g ± SD, n = 3, [a] n = 6

the skin (analog to the skin uptake as described by *Goddard* et al.[319]) and in the liver and spleen after 24 h. The slight increase of radioactivity in liver, spleen and the intestine between 3 h and 24 h indicates a minor uptake of radiolabeled [^{111}In]**P30** and [^{111}In]**P31** in the RES and hepatobiliary excretion to some extend. However, the absolute values of activity found in these organs are very low and almost negligible. The findings of the organ distribution data are corroborated by *in vivo* γ-camera imaging. In Figure 4.53 the obtained images 30 min and 3 h p.i. of [^{111}In]**P30** are

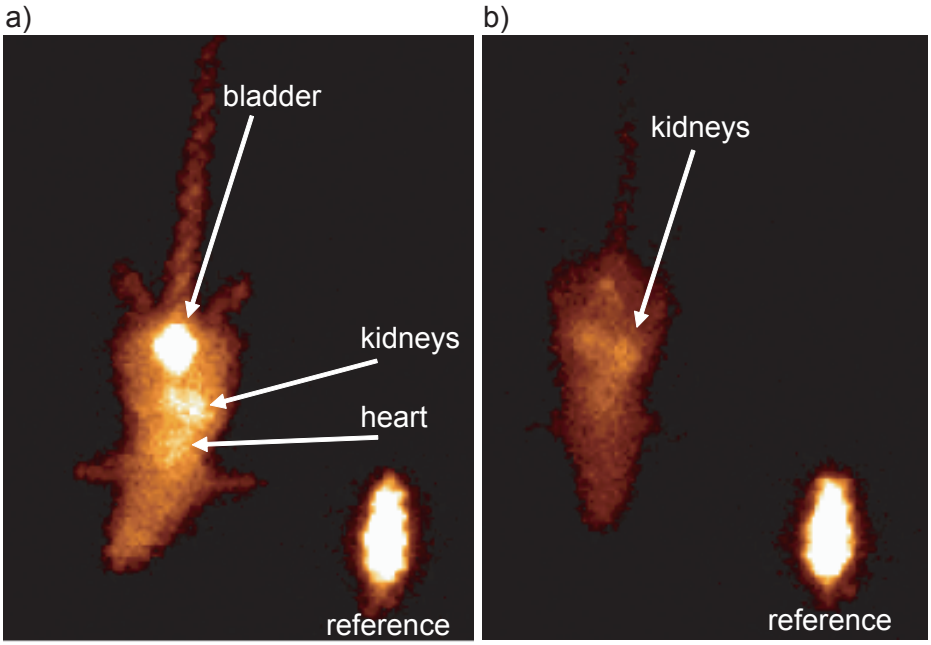

Figure 4.53: *In vivo* γ-camera imaging of biodistribution of [^{111}In]**P30** at 30 min (a) and 3 h (b) p.i. in a mouse. The reference is 10 % of the injected dose and was acquisited simultaneously to allow quantification. At both timepoints the predominant, albeit small, accumulation can be seen in the kidneys and the heart (blood pool). The pronounced uptake in the bladder shows the fast and effective renal clearance[417].

compared. The activity is evenly distributed throughout the body. Only the bladder, kidneys and, to some extend, the heart (blood pool) can be discerned. Already after 30 min the majority of activity has accumulated in the bladder (Figure 4.53a). These images show no significant accumulation occurs in organs not taken into account for the biodistribution study. After 3 h only very limited activity is left in the mouse as compared with the reference (i.e. 10 % of injected dose)(Figure 4.53b). The majority

of the remaining radioactivity found in the γ-camera image can be attributed to the bladder, kidney and heart. A region of interest (ROI) analysis of the two images revealed that only 11 %ID are left in the body after 30 min (excluding bladder activity), while after 3 h only 4.5 %ID remain. This also confirms earlier studies that PMeOx are comparable in their excretion and blood retention pattern with PEG. *Furuichi* et al.[414] found that 93.2 ± 2.26 % of i.v. administered PEG-4000 was excreted via the urine after 24 h in rats. Similarly, *Shaffer* et al.[410] found a 96 % excretion of PEG-6000 i.v. administered in men after 12 h. Interestingly, the lower molar mass PEG-1000 was excreted only by 85 % in the same time interval. Certainly, these values can not be compared directly, not only due to the different species but also due to the difference in the compounds used. However, two different studies have shown that for PEG, the threshold, from which a reduced glomerular filtration can be observed, is found between PEG-4000 and PEG-6000 in dogs, rabbits and rats[411,413].
The blood retention and the kidney uptake of [^{111}In]**P30** and [^{111}In]**P31** were additionally compared with [^{99m}Tc]DTPA and [^{99m}Tc]mercaptoacetyltriglycine ([^{99m}Tc]MAG3). While [^{99m}Tc]DTPA is routinely used as a tracer for the glomerular filtration rate, MAG3 is additionally secreted in the tubuli after the glomeruli. Thus, the excretion of MAG3 from the blood stream corresponds almost completely with the renal plasma flow. Both control substances clear rapidly and quantitatively from the blood in contrast to the polymers (Figure 4.54). While at 30 min the blood pool activity of [^{111}In]**P30** is equivalent to that of [^{99m}Tc]DTPA, the clearance slows thereafter. This difference might be due to a number of reasons. Small amounts of ^{111}In might have been co-injected or liberated from the complex. Free remains ^{111}In is known to have a high blood retention. Alternatively, higher molar mass fractions would be expected to accumulate in the blood stream while smaller fractions are excreted rapidly. As a third possibility, some small fraction of the injected polymer might adsorb to large plasma proteins and therefore be partly inaccessible to renal filtration. In the case of [^{111}In]**P31**, this last possibility can serve as an explanation for the higher blood pool retention as compared to [^{111}In]**P30**. PEtOx have a pronounced amphiphilic character in comparison to PMeOx. This could lead to a enhanced interaction with plasma proteins, which possess hydrophilic and hydrophobic compartments. However, the higher plasma level of [^{111}In]**P31** is only observed after 30 min. After 3 h p.i., the amount of [^{111}In]**P30** and [^{111}In]**P31** start to level out and show no difference after 24 h p.i.. Thus, if an increased plasma protein absorption is the reason for the higher

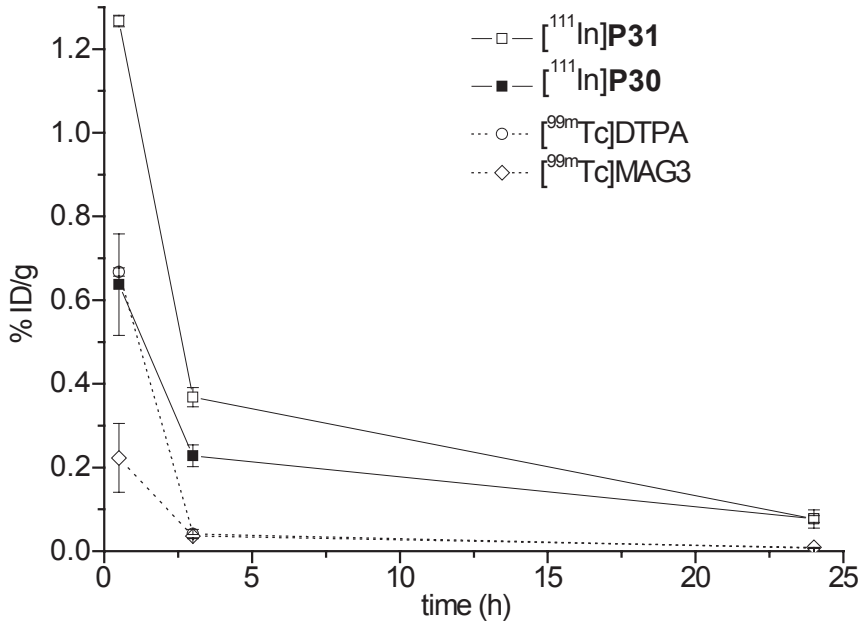

Figure 4.54: Development of radioactivity levels with time in the blood after i.v. administration of [^{111}In]**P30**, [^{111}In]**P31** and [^{99m}Tc]DTPA and [^{99m}Tc]MAG3, respectively. The polymer samples remain at higher levels in the blood in comparison to the low molar mass tracers.

amount of [^{111}In]**P31** in the blood at early time points, this absorption is reversible. Comparison with the previous study of *Goddard* et al.[319] shows that [^{111}In]**P30** and [^{111}In]**P31** are removed much faster from the blood pool. This can be attributed in parts to the higher molar mass of the described P(MeOx-co-HPhOx). For a polymer of M_w = 15 kDa, 7 %ID of the activity was still found in the blood after 24 h while for a M_w = 29 kDa sample 28 %ID were measured[4]. In this study the molar masses of the polymers were determined by two different calibrations methods for the GPC; calibration to PEG and PHPMA, resulting in strongly differing molar masses for identical polymers. The obtained values for M_w, calibrated against PHPMA were 3 - 4 fold higher as compared to the M_w obtained with PEG calibration. This shows the necessity for appropriate calibration standards for GPC, alternative analytical methods, or application of a number of different analytical methods to obtain reliable molar masses of polymers for biomedical applications. Up to date, no GPC calibration standards for POx are available. In addition, another factor might contribute to a longer blood

[4]these values are %ID not %ID/g and the values for M_w are obtained from GPC with PEG calibration.

retention of P(MeOx-co-HPhOx). This polymer is presumably partially branched due to the present, unprotected phenol moiety. As discussed earlier, branched polymers are known to exhibit a longer blood retention as compared to linear polymers of comparable hydrodynamic radius.

Figure 4.55 shows the development of the values for %ID/g of [^{111}In]**P30**, [^{111}In]**P31** along with [^{99m}Tc]DTPA and [^{99m}Tc]MAG3 in the kidney. As expected, the amount of the tracers peak at very early times p.i. and decrease to very low values thereafter. The measured activity of [^{111}In]**P30** was comparable with that of [^{99m}Tc]DTPA at

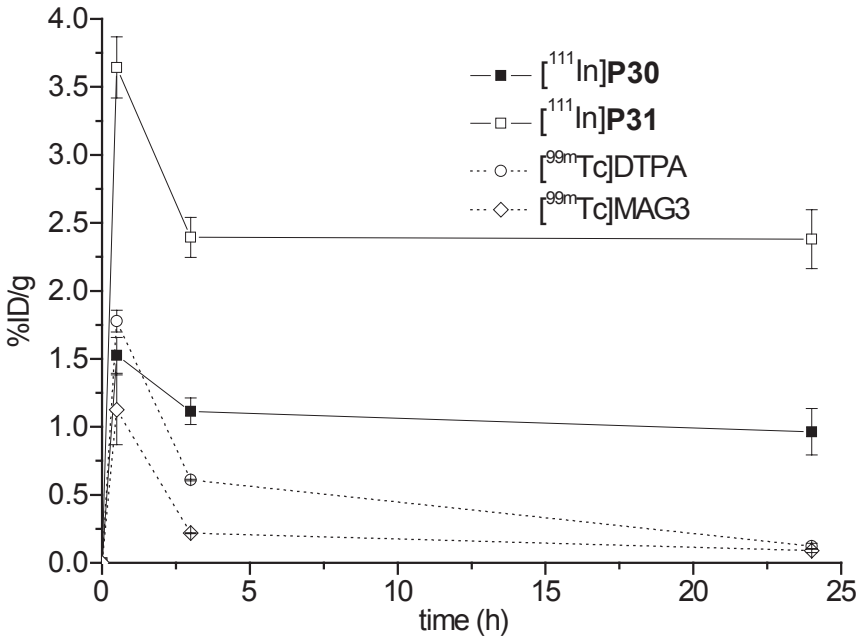

Figure 4.55: Development of radioactivity levels with time in the kidneys after i.v. administration of [^{111}In]**P30**, [^{111}In]**P31**, [^{99m}Tc]DTPA and [^{99m}Tc]MAG3, respectively. Both polymers remain at significantly higher levels in the kidney as compared to the two low molar mass renal clearance tracers.

30 min p.i.. However, in contrast to [^{99m}Tc]DTPA, the amount of [^{111}In]**P30** found in the kidney remains at around 1 %ID/g. The decrease of the amount of [^{111}In]**P31** is also limited and remains at even higher values (2.4 %ID/g).

While the amount of radioactivity found in the kidney and the blood for [^{111}In]**P30** and [^{111}In]**P31** is high in comparison with the low molar mass tracers [^{99m}Tc]DTPA or [^{99m}Tc]MAG3 it is low as compared to radiolabeled copolymers of HPMA of similar molar mass. Figure 4.56 compares the values of %ID/g 24 h p.i. for i.v. administered,

[^{99m}Tc] labeled HPMA copolymer (P(HPMA)[^{99m}Tc]DPK) of a molar mass of M_w = 7 kDa in mice with that of [^{111}In]**P30** and [^{111}In]**P31** ($M_w \sim 8$ kDa by GPC, ~ 6 kDa by MALDI-TOF MS). The blood pool activity of P(HPMA)[^{99m}Tc]DPK after 24 h is ap-

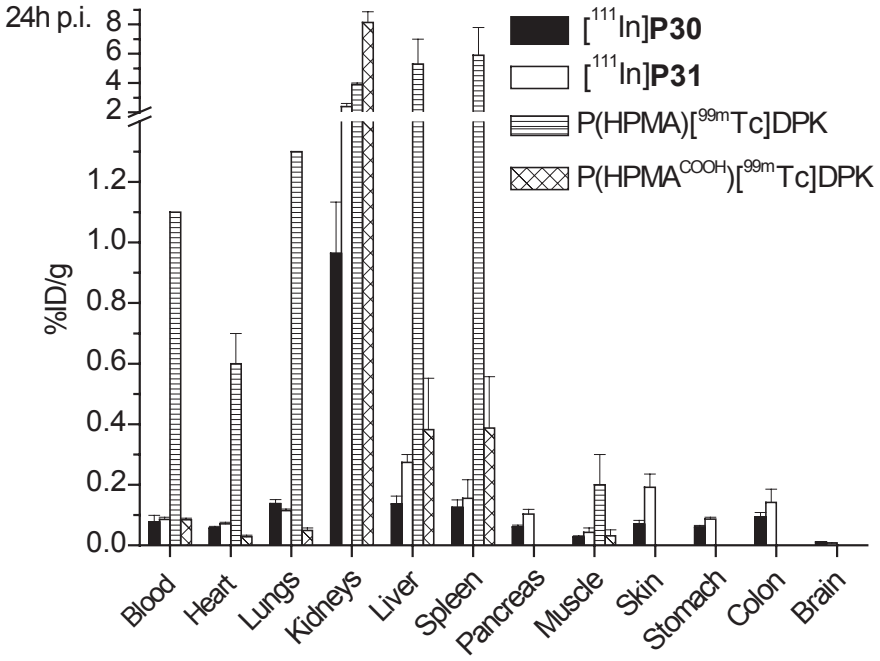

Figure 4.56: Comparison of %ID/g for i.v. administered ^{99m}Tc or ^{111}In labeled water-soluble polymers in various organs 24 h p.i.. Both POx, [^{111}In]**P30** and [^{111}In]**P31** show a markedly lower uptake in all organs as compared to P(HPMA)[^{99m}Tc]DPK. Introducing carboxylic acid side chains into the HPMA copolymer (P(HPMA^{COOH})[^{99m}Tc]DPK) reduces uptake in most organs to levels as compared with the neutral poly(2-oxazoline)s while the amount in the kidneys increases. Values for HPMA copolymers are taken from *Mitra* et al.[31]. Please note the break in the y-axis.

proximately 1.1 %ID/g while for the presented POx only approx. 0.08 %ID/g are found at this time point. The difference for the kidneys is less pronounced. Interesting, however, is the difference for the liver and the spleen. With 5.9 and 3.9 %ID/g ([^{111}In]**P30** and [^{111}In]**P31**, respectively) remaining radioactivity in the spleen and liver respectively, the uptake P(HPMA)[^{99m}Tc]DPK is 47 and 29 times higher in these organs as compared to [^{111}In]**P30** and 38 and 14 times higher as compared to [^{111}In]**P31**.

It has been noted in Chapter 2.1.2, that introduction of charged moieties into a polymer often alters its biodistribution pattern, also in the case of HPMA copolymers

(Figure 4.56). The introduction of a pending carboxylic acid moiety (P(HPMA^{COOH})-[^{99m}Tc]DPK)[5] markedly reduced the blood pool retention of and uptake in all organs but the kidney. For the latter the uptake was increased by more than 2 fold, possibly due to an increased renal clearance. Uptake in spleen (0.387 ± 0.17 %ID/g) and liver (0.382 ± 0.17 %ID/g) is reduced significantly for P(HPMA^{COOH})[^{99m}Tc]DPK. However, the mean values of %ID/g are still higher than the values observed for [^{111}In]**P30** (0.125 ± 0.025 %ID/g and 0.136 ± 0.026 %ID/g) or [^{111}In]**P31**(0.155 ± 0.062 and 0.274 ± 0.026 %ID/g).

This comparison has to be taken with caution, since the different polymers have been analyzed in different ways. Moreover, the molar masses are not directly comparable and thus, their biodistribution data. However, these polymers mentioned are the only polymers that can be found in literature which are at least similar to some extend and it is necessary to put the presented results into the context of literature reports. It is clear that the two presented water-soluble low molar mass poly(2-oxazoline)s **P30** and **P31** display no accumulation in any tissue or body compartment and are excreted rapidly via the kidneys. Therefore, this type of polymers may serve as a well-defined polymeric carrier for biomedical application of injectable drug-conjugates. The attachment of bioactive compounds will naturally change the biodistribution of the respective conjugates. However, the poly(2-oxazoline) backbone might be able to exert positive effects on the biodistribution of the attached bioactive compounds. This will be evaluated in the next chapter, where the biodistribution of the first radiolabeled poly(2-oxazoline)-RGD conjugate will be discussed.

4.6.2 Biodistribution of [^{68}Ga]C2 in tumor bearing mice

Experimental procedure

Besides a patent application by *Ansari* et al.[318] little can be found in literature about poly(2-oxazoline) peptide conjugates for targeted drug delivery. In this chapter the first result on the biodistribution of [^{68}Ga]**C2**, a radiolabeled water-soluble PMeOx-RGD conjugate are presented and discussed. These experiments were performed in

[5] 0.95 mmol COOH per g polymer, M_w = 8.3 kg/mol, $\rightarrow \sim 7$ COOH/polymer chain

the radiopharmaceutical laboratory of Prof. Dr. *Wester* in the Nuklearmedizinische Klinik and Poliklinik at the Klinikum rechts der Isar München under supervision of Dr. *Poethko*. The biodistribution was evaluated in a nude mouse model. The mice were transplanted subcutaneously with a M21 human melanoma. Seven mice were injected with approx. 80 μCi of P(MeOx$_{47}$^{Oxim}RGDfK$_5$)PipBn[^{68}Ga]DOTA ([^{68}Ga]**C2**) through the tail vain (under diethyl ether anesthesia) of which three mice were co-administered with an excess ($\sim$ 18 mg/kg) of unlabeled peptide (blocking experiment). One hour after the administration, the mice were sacrificed by CO_2 asphyxia and the blood was collected by heart puncture. An aliquot of the blood was taken for blood pool radioactivity measurement (0.05 - 0.26 g), while the remainder was centrifuged in order to collect the plasma (0.08 - 0.4 g). The other organs were resected, weighed and the activity of all collected organs was counted. After decay correction, the value for the radioactivity in the tail of the mice was subtracted[6] from the administered activity and the values of %ID/g for the various organs were calculated.

Tumor and organ uptake of [^{68}Ga]C2

In Table 4.13 the average values with the standard deviation for the different organs for unblocked and blocked mice are shown. Along with the values for %ID/g, the average values for the tumor to organ (T/O) ratios are depicted. Additionally, the values of %ID/g and T/O are plotted in Figures 4.57 and 4.58.
Generally, organ uptake is much higher than for the homopolymers [^{111}In]**P30** and [^{111}In]**P31** described in the previous chapter. This is possibly due to a combination of the higher molar mass of the conjugate (M_{calcd} = 8650 g/mol) and the attached peptides. However, without an control experiment with inactive peptide, e.g. RAD or RGE attached to the polymeric carrier, it is not be possible to distinguish between the two contributions. *Line* et al.[241] reported that for HPMA-RGD4C conjugates a significant increase in the tumor uptake (DU145 prostate tumor xenograft) is observed comparing to free peptide and copolymer labeled with inactive RGE4C even though no increased *in vitro* binding inhibition of $\alpha_v\beta_3$ HUVEC cells was observed for these polymer conjugates[240].

[6] this is regarded as remainder of the injection site and has not reached the circulation

Table 4.13: Biodistribution data and T/O of [^{68}Ga]**C2** in organs after resection 1 h p.i. in mice. Blocking experiments were performed by additional administration of an excess of unlabeled c[RGDfK].

	[^{68}Ga]**C2**		[^{68}Ga]**C2** + c(RGDfK)	
Organ	%ID/g[a]	T/O[a]	%ID/g[b]	T/B[b]
Blood	3.52 ± 0.54	0.52 ± 0.066	3.14 ± 0.70	0.43 ± 0.168
Heart	1.81 ± 0.27	1.00 ± 0.076	1.40 ± 0.33	0.97 ± 0.396
Lung	2.78 ± 0.65	0.67 ± 0.149	2.01 ± 0.30	0.65 ± 0.195
Liver	2.66 ± 0.33	0.68 ± 0.087	1.56 ± 0.17	0.83 ± 0.211
Stomach	1.45 ± 0.20	1.25 ± 0.125	0.81 ± 0.08	1.58 ± 0.310
Spleen	1.90 ± 0.27	0.96 ± 0.093	0.96 ± 0.23	1.39 ± 0.470
Intestine	1.91 ± 0.11	0.95 ± 0.064	1.11 ± 0.11	1.16 ± 0.180
Kidney	7.70 ± 0.33	0.23 ± 0.020	6.61 ± 0.58	0.19 ± 0.044
Adrenal glands	4.38 ± 1.22	0.43 ± 0.072	1.24 ± 0.11	1.04 ± 0.221
Muscle[b]	0.38 ± 0.06	3.45 ± 0.475	0.46 ± 0.12	2.90 ± 0.921
Tumor	1.81 ± 0.16	—	1.27 ± 0.17	—
Plasma	7.10 ± 0.75	0.26 ± 0.031	5.89 ± 1.20	0.23 ± 0.084

[a] n = 4

[b] n = 3, one value for %ID/g in the muscle was discarded since it was an obvious outlier (3.23 %ID/g).

The value of %ID/g for the plasma is considerably higher than that for the blood.

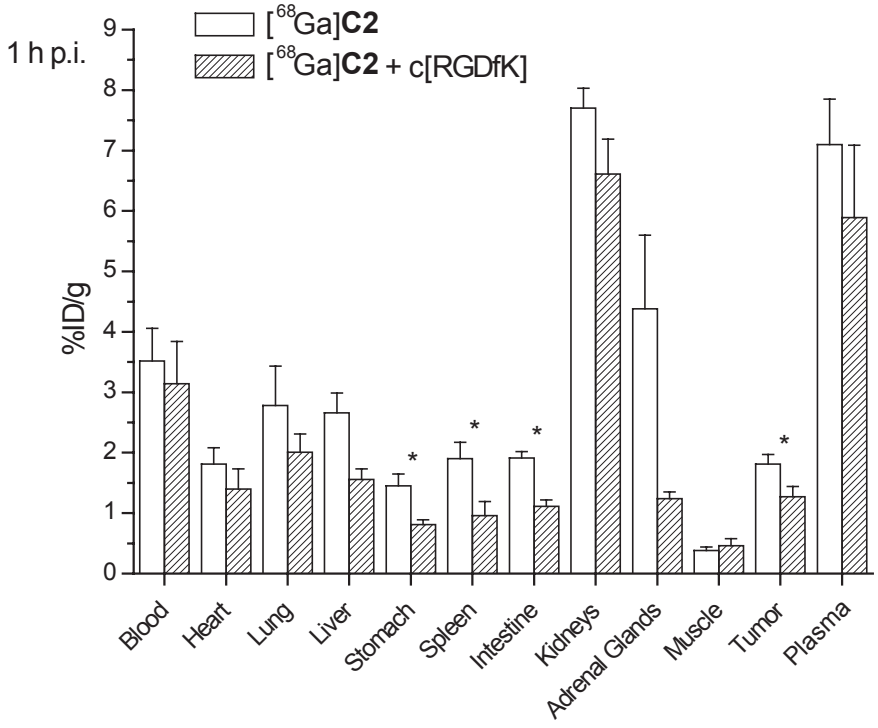

Figure 4.57: Uptake of the radioactivity in various organs 60 min p.i. of 80 μCi [^{68}Ga]**C2** in M21 melanoma bearing mice with and without co-administration of 18 mg/kg unlabeled c(RGDfK). Particularly high levels are found in the kidneys and the serum. Also the blood, lung and liver contain more than 2 %ID/g while in the tumor 1.81 ± 0.16 %ID/g where accumulated. Blocking of the receptors with an excess of unlabeled c(RGDfK) reduces the uptake in all observed organs and the tumor, indicating specific binding of [^{68}Ga]**C2** to $\alpha_v\beta_3$. * indicates statistical significance in decrease between unblocked and blocked experiment ($p < 0.01$).

Blood contains cellular compounds suspended in the plasma, in which numerous proteins, salts and other solutes are present. By volume, blood consists of approx. 55 % of plasma, which contributes with approx. 53 % of the mass to the blood. Therefore, the value of the %ID/g for the blood should be 53 % of the value of the plasma[7]. If less is found in the plasma, the radioactivity is bound to cellular components of the blood (e.g. leukocytes). The obtained mean values of 49.42 ± 4.02 % for the unblocked mice, and 53.22 ± 1.31 % for the blocked mice are in good accordance with

[7] $\rho_{\text{blood}} = 1.06$ mg/mL, $\rho_{\text{plasma}} = 1.03$ mg/mL[418–420]. Activity per gram blood $\hat{=}$ activity per 0.53 g plasma

the expected value for completely plasma bound activity. The mean tumor uptake at 1 h p.i. of [^{68}Ga]**C2** is with 1.81 ± 0.16 %ID/g good as compared to the value for a HPMA-RGD4C conjugate (1.05 ± 0.03 %ID/g)[100].
Comparison of the tumor uptake of [^{68}Ga]**C2** with galacto-RGD, one of the most advanced low-molar mass RGD compounds for $\alpha_v\beta_3$ imaging, shows that [^{68}Ga]**C2** is competitive in terms of its tumor uptake. In the same tumor model, galacto-RGD reaches with 1.56 ± 0.15 %ID/g 60 min p.i. a comparable, but somewhat lower value[101]. On the other hand, the dimer (c(RGDfE)HEG)$_2$-K-Dpr-[^{18}F]FBOA (Figure 2.8) shows a higher tumor uptake of 2.48 ± 0.15 %ID/g. Comparing to a large number of radiolabeled RGD peptides or peptide conjugates[421], the obtained value for [^{68}Ga]**C2** is reasonably competitive. Comparing the blood pool activity after one hour shows that there is a pronounced difference between these two peptides and the polymer conjugate [^{68}Ga]**C2**. The blood pool activity of [^{68}Ga]**C2** is 10 - 20 times higher when compared to galacto-RGD and the RGD dimer[101]. This hints to an effect of the size of the conjugate, a prolonged circulation time and might actually lead, to some extend, overestimation of radioactivity in well perfused organs, such as spleen, liver and lung. Alternatively, the high blood pool activity could stem from free ^{68}Ga, released from [^{68}Ga]**C2** or originating from insufficient purification. However, the stability of [^{68}Ga]**C2** in serum or blood has not been investigated in this context. Investigations by Lendvai et al.[422] showed that injection of [^{68}Ga]DOTA does not lead to such prononounced blood retention. In contrast, it is reported that injection of free $^{68}GaCl_3$ leads to a prominent uptake in most organs and that blood retention is high.
For the control experiment, additionally unlabeled c(RGDfK) was administered to the mice. Table 4.13 shows that in all organs and the tumor, the uptake was decreased. This seemed a good indication for a specific binding of [^{68}Ga]**C2**, since unspecific binding should not be affected by the addition of free and unlabeled peptide. However, the reduction varies and is statistically significant (one-way ANOVA, $p < 0.05$) only for the stomach, spleen, intestine and the tumor. The group sizes where small ($n = 4$ and 3), so that for a number of organs (especially kidney, liver) it can be expected that the difference becomes significant with larger number of mice (the p-values are close to 0.05).

Tumor to organ ratios of [^{68}Ga]C2

Besides the absolute amount of tumor uptake, high tumor to organ ratios (T/O) are crucial for imaging purposes and therapy by PRRT.
The well-defined and smaller conjugates galacto-RGD and (c(RGDfE)HEG)$_2$-K-Dpr-[^{18}F]FBOA show similar tumor uptake as [^{68}Ga]**C2**. In contrast, the T/O for both compounds are much higher than for [^{68}Ga]**C2**. For the latter, only for the stomach, muscle and the heart values $T/O > 1$ are observed. These results are somewhat discouraging as compared to the two low molar mass compounds. For galacto-RGD only in the liver and the kidney values of $T/O < 1$ were measured at 1 h p.i. and the dimer shows a higher uptake in the tumor compared to all organs dissected. Comparison of

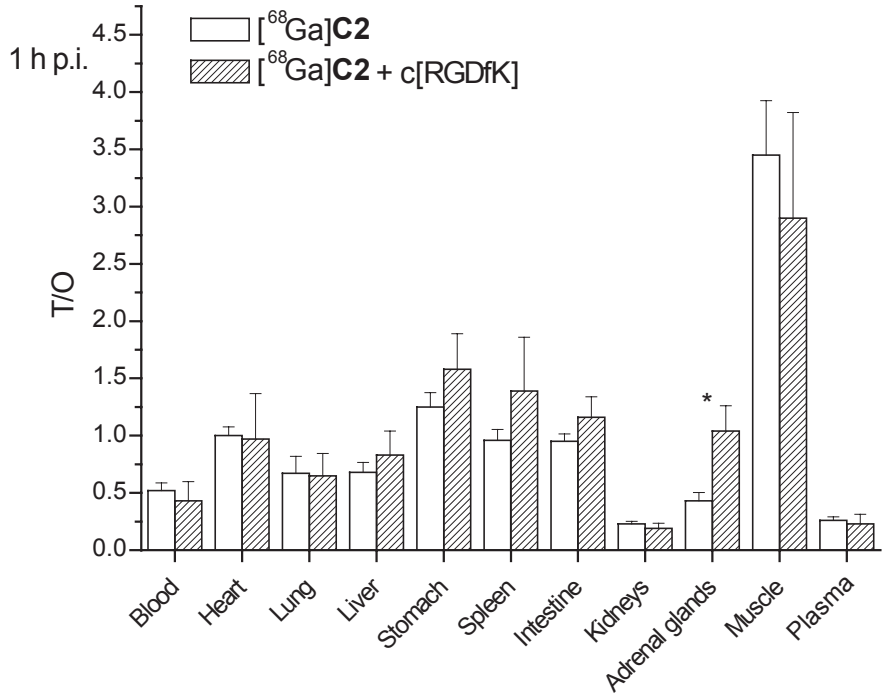

Figure 4.58: T/O ratios 60 min p.i. of 80 μCi [^{68}Ga]**C2** in M21 melanoma bearing mice with and without co-administration of 18 mg/kg unlabeled c(RGDfK). While the ratio seems largely unaffected in a number of organs (e.g. blood, heart, lung, kidneys and muscle), the T/O raises in the liver, stomach spleen and the adrenal glands. This might indicate a multivalency effect, since the reduction in the integrin overexpressing tumor is reduced less in relation then in those organs. * indicates statistical significance in increase between unblocked and blocked experiment ($p < 0.01$).

the obtained T/O values with the values of the HPMA-RGD conjugates of *Ghandehari* and co-workers[100,240,241] in contrast is encouraging. The two compounds were not tested on the same tumor model, nor do they target with the same peptide but a qualitative comparison will help to understand and interpret the obtained biodistribution data of [^{68}Ga]**C2**. Figure 4.59 shows the plots of the T/O ratios of [^{68}Ga]**C2** and [^{99m}Tc]HPMA-RGD4C one hour p.i. in mice. For the heart, lung and muscle, higher

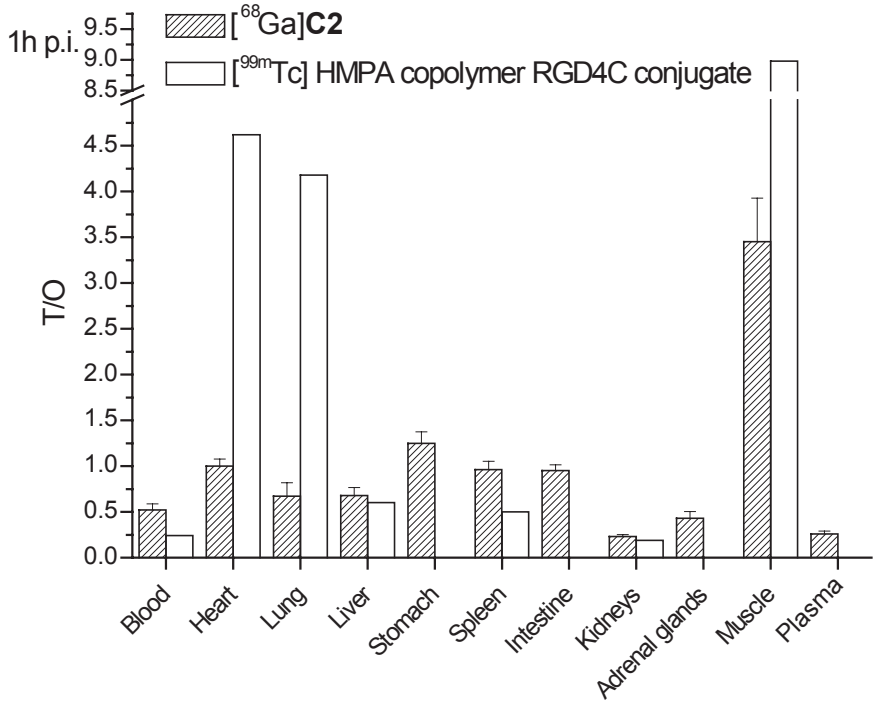

Figure 4.59: Comparison of T/O values of radiolabeled HPMA-RGD4C and [^{68}Ga]**C2** 1 h p.i. in DU145 prostate cancer and M21 melanoma xenograft, respectively. While T/O values of HPMA-RGD4C are much higher for heart, lung and muscle, they are lower for the other organs examined in comparison to [^{68}Ga]**C2**. Values for the HPMA conjugate taken from *Mitra* et al.[100]

T/O are obtained for the HPMA-RGD4C whereas for the blood and the spleen higher values are calculated for [^{68}Ga]**C2**. For the liver and the kidney, the obtained values were comparable. Importantly, *Mitra* et al.[100] report an increase of all T/O ratios over the time and an increase to 4.32 ± 0.32 %ID/g in the tumor after 72 h.
The same group of researchers reported on a different conjugate, lacking the chelator DTPA but with pending carboxylic acid moieties. This conjugate reached approx. 5 %ID/g in the tumor already at 24 h p.i.[241] . In this case, the two different conju-

gates behaved opposite then would be expected from the previous reports of the same group. The conjugates bearing RGD4C and carboxylic acids exhibited an approx. two fold higher uptake in liver, spleen, kidney and the tumor after 24 h compared to the HPMA-RGD4C conjugates bearing DTPA and without the free carboxylic acid side chains. Each DTPA contributes five -COOH residues, but these are largely blocked and neutralized upon conjugation with ^{99m}Tc. These two reports can serve as another example of the difficulties to identify SAR with complex polymer-conjugates.

The molar mass of [^{68}Ga]**C2** is significantly smaller than of HPMA-RGD4C (approx. 10 kDa vs. 40 kDa) which might explain the lower blood pool activity of [^{68}Ga]**C2** as compared to HPMA-RGD4C (1 h p.i.). This indicates a faster renal clearance and possibly, faster increase of T/O ratios. An optimal behavior of any compound for PRRT would be a fast and pronounced accumulation in the tumor, accompanied with a rapid wash-out in the residual organism. Additionally, maximization of tumor retention is desirable to increase the duration of radiation exposition of the tumor (Figure 4.60). Oriented on actual tumor uptake values of galacto-RGD, the RGD-dimer or tetramer and a HPMA-RGD4C conjugate, a comparison of the total exposition of the tumor to radioactivity is shown. The larger the integral is in Figure 4.60 (termed regularly area-under-the-curve, AUC) is, the higher the exposition and the therapeutic effect. The same accounts for the AUC for other organs, which would be responsible for potential side effects. The AUC for the polymer conjugate is much higher compared to the low molar mass compounds. Certainly, also the AUC for the other organs will be comparably higher. Balancing these contribution is crucial for the development of successful compounds for PRRT. Reducing the actual requirements for a compound in PRRT, one could claim: Maximize the AUC for the tumor and minimize the AUC for all other organs.

Despite numerous studies on radiolabeled RGD peptides and RGD peptide conjugates, a comprehensive SAR is a matter of considerable conjecture. A modular kit of a well-defined polymer carrier for the attachment of RGD peptides, such as that presented for poly(2-oxazoline)s, could be valuable to help to elucidate this issue.

In order to evaluate **C2** and the other presented poly(2-oxazoline) conjugates, it would be necessary to perform biodistribution studies at later time points. Evaluation at 6 h p.i. could already show a marked difference, but certainly 24 and 48 h p.i. would be of interest. For these later time points, however, Ga-68 would not be suitable due to its short half-life. In-111 has already been introduced to polymer bound DOTA and

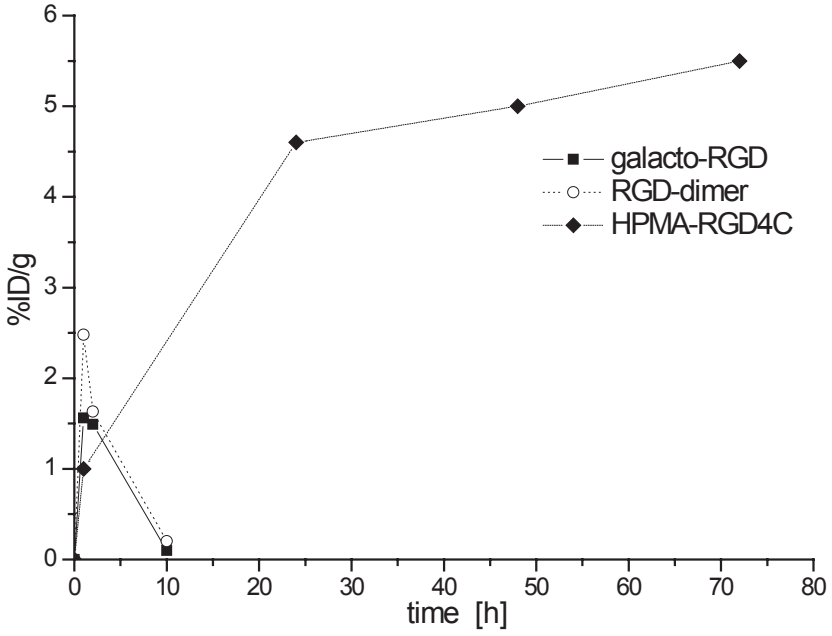

Figure 4.60: Development of tumor uptake of galacto-RGD, an RGD-dimer/tetramer and an HPMA-RGD4C. While the tumor uptake 1 h p.i. is lower for the polymer conjugate, it increases with time and leads to a much higher overall delivery of therapeutic radioactivity to the tumor in comparison to the low molar mass compounds. Values are taken or estimated from graphical presentations from *Mitra* et al.[240] and *Poethko* et al.[101,226]. Please note, the 10 h values of galacto-RGD and the RGD-dimer are estimated from similar low molar mass compounds.

is suitable for long-time measurements due to its relative long half-life ($t_{1/2} = 2.8\,d$). Therefore, follow-up experiments with **C2** should be performed with this nuclide.
As another source of error, the blood content of the dissected organs should be considered. For the small cyclic RGD peptides used so far in the group of Prof. *Wester*, the blood pool activity is very low after 1 h, therefore, no significant mistake must be considered from blood 'contaminated' organs. In contrast, a considerable amount of activity was found in the blood at the time of measurement for [^{68}Ga]**C2**. This might lead to an overestimation of radioactivity uptake.
Since **C2** was stored in aqueous solution for a prolonged period of time (> 5 months) prior to administration, partial degradation of the peptide might have occurred. Quality control by HPLC has been performed and no change in the chromatogram was observed. However, it can not be ruled out that the RGD peptides in **C2** degraded without perceptible change in the HPLC elugram of **C2**. Due to the high tumor uptake of [^{68}Ga]**C2**, it is safe to assume that no complete degradation occurred, but it is conceivable that the administered polymer conjugate did not bear the assumed 5 copies of c[RGDfK]. Alternatively it could be possible, that the peptides were not fully accessible, similar as reported for RGD bearing hyperbranched polymer polyplexes[224].

In conclusion, the uptake of [^{68}Ga]**C2** in the tumor of M21 bearing mice is with 1.81 %ID/g 1 h p.i. slightly higher than the value reported for HPMA-RGD4C and galacto-RGD, the most advanced imaging probe for $\alpha_v\beta_3$. However, T/O ratios are not satisfactory, partially due to a remaining high blood pool activity. It is necessary that later time points after injection of labeled **C2** are evaluated. These experiments will commence in the near future. Additionally, it might be of interest to introduce carboxylic acid polymer side chains into this type of conjugate.

4.6.3 *In vitro* evaluation of poly(2-oxazoline)-MTII conjugates

The three novel poly(2-oxazoline)-MTII conjugates **C4**, **C5** and **C6** were tested for their affinity towards the melanocortin receptors hMC1R and hMC3R - hMC5R by Dr. *Xu* in the group of Prof. *Gillies* at the University of Arizona, Tucson, AZ, USA.

In Table 4.14 values, taken from literature for MTII[423–425] are compared with the obtained values. The values for the IC_{50} of MTII to the four receptor show a pronounced scattering, either due to the markedly large errors for the values, or because different cell lines were used for the experiments.
The results showed that **C4** displays a low affinity to all four receptors (in the μM range), with the highest affinity for hMC1R. Instead of binding enhancement, the affinity is reduced in comparison to MTII. Actually, the obtained values are comparable with dimers of the low-affinity linear core peptide MSH(4)[154]. It seems that either the introduction of the 2-(aminooxy)acetic acid moiety, or the attachment to the polymer greatly diminishes the affinity of the peptide towards all receptors. This effect, however, is compensated in the case of the multimers **C5** and **C6**. In contrast

Table 4.14: Competitive binding MTII against NDP-α-MSH in hMC1R, hMC3R, hMC4R and hMC5R expressing cell lines.

	IC_{50} [nM]			
Conjugate	hMC1R	hMC3R	hMC4R	hMC5R
MTII[423–425]	0.25 - 0.686	8.56 - 34.1	0.72 - 6.60	43.6 - 46.1
C4	226.0 ± 27.0[a]	933.7 ± 324.9[b]	2202.5 ± 638.9	1015.0 ± 232.5
C5	6.2 ± 1.3	24.5 ± 5.0	12.6 ± 3.5	29.4 ± 13.9
C6	4.7 ± 0.9[b]	16.6 ± 5.6	8.5 ± 1.9	24.7 ± 9.8

experiments with **C4** - **C6** were performed 4 times in quadruplicate unless,
[a] 2 independent experiments, [b] 3 independent experiments

to **C4**, the affinities of **C5** and **C6** were found to be in the low nanomolar range. For all four receptors the order of affinity is **C4** < **C5** ≃ **C6** (Figure 4.61). The differences between the pentamer **C5** and the octamer **C6** are not significant. The order of the subtype affinity is hMC1R > hMC4R > hMC3R > hMC5R for **C5** and **C6**. No specificity was observed, which is not surprising since the mother peptide MTII has no specificity towards either receptor, but the order of subtype affinity of MTII is resembled by the conjugates **C5** and **C6**. Although no multivalency effect of the prepared conjugates compared to MTII is observed, the trend among the conjugates is clear. The observed affinities are in the low nanomolar range. In comparison with the MTII, however, a number of differences of these conjugates, especially considering a possible use in cancer diagnosis or therapy, should be addressed.

- Conjugation with the hydrophilic polymer increases the hydrophilicity of the

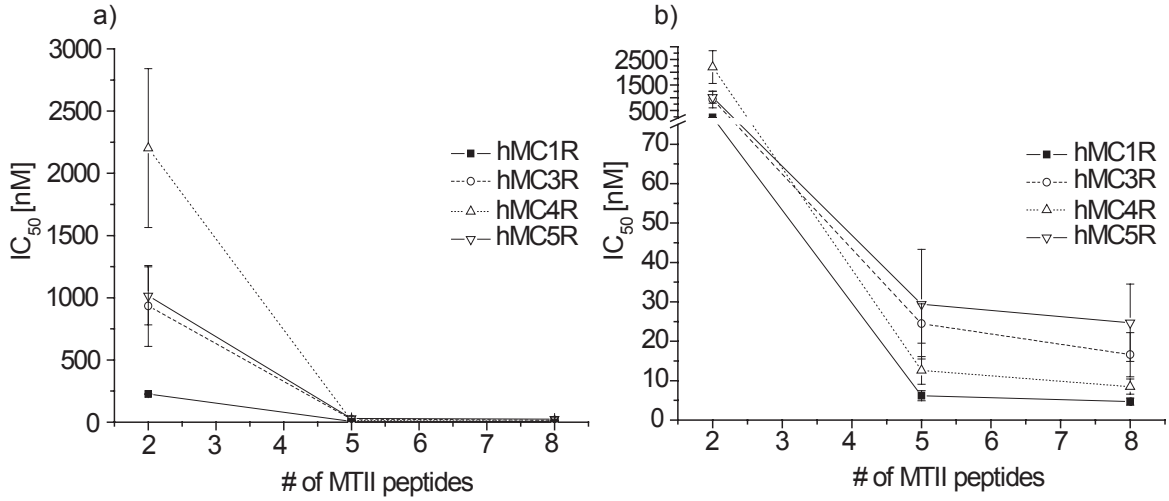

Figure 4.61: Development of the binding affinity of the poly(2-oxazoline) MTII conjugates with the number of attached peptides. Please note, both plots show the same values, but the y-axis in b) is broken for better visualization.

conjugates significantly in comparison with the peptide. Even **C6**, carrying 8 copies of the hydrophobic MTII is eluted at relatively low t_r in the HPLC. This could lead to a increased bioavailability and could eventually decrease liver uptake.

- The introduction of a chelator or a fluorescent dye can be performed at the distal polymer terminus with little influence on the binding affinity of the conjugated peptides.

- The attachment of MTII to the polymer should reduce or completely diminish transition of the peptide conjugate through the blood-brain barrier, which would rule out the binding to hMC3R and hMC4R. Thus, targeting of hMC1R expressing melanoma could be feasible.

- The significant increase in molar mass should influence the biodistribution and prolong blood and body retention of polymer-MTII conjugates. This could lead to an increased delivery of an attached drug or radionuclide as compared to the peptide.

Similar affinities for other MSH analogs (IC_{50}(DOTA-NAPamide) = 1.37 nM[211] and IC_{50}(DOTA-Re[Arg^{11}]MSH) = 2.1 nM[208]), discussed as promising candidates for diagnostic and therapeutic purposes, suggest that the presented conjugates **C5** and **C6** are candidates for *in vivo* evaluation. It might be of interest to attach low affinity peptides (e.g. linear MSH(4)) and evaluate the affinity profiles of their poly(2-oxazoline) bound multimers. These peptides could be produced much cheaper and in larger scale. Furthermore, the alteration of the aminooxy moiety on the MTII (attachment via various linkers) might help to prevent the pronounced decrease of affinity of the peptide.

4.7 Poly(2-oxazoline) hydrogels

The focus of this work was to evaluate the synthesis of well-defined poly(2-oxazoline) peptide conjugates and their feasibility as injectable drug-delivery systems. The presented new side chain functionalities, however, seemed to be also suitable for the preparation of reversible and permanently cross-linked hydrogels. Therefore, preliminary studies were performed to evaluated the preparation and properties of hydrogels based on polymers already described in this work.

4.7.1 Azine hydrogels

Aldehydes are highly reactive towards hydrazine. Monoaddition leads to a hydrazone, while addition of two aldehydes to one hydrazine gives an azine (particularly an aldazine vs. ketazines derived from two ketones). The reaction of hydrazine with polymers bearing multiple aldehydes leads to cross-linking (Figure 4.62).
Preliminary tests showed that the addition of hydrazine hydrate to 20 %wt and 30 %wt solutions of **P38** at room temperature (0.5 equiv hydrazine per aldehyde) leads to rapid (< 2 min) solidification of the mixture. However, after covering the hydrogels with deionized water over night (to allow swelling) the hydrogels liquified again.
Subsequently, the hydrogels were cross-linked and/or swollen in various buffers (Table 4.15) The gelation and swelling has been evaluated in aqueous buffers ranging from

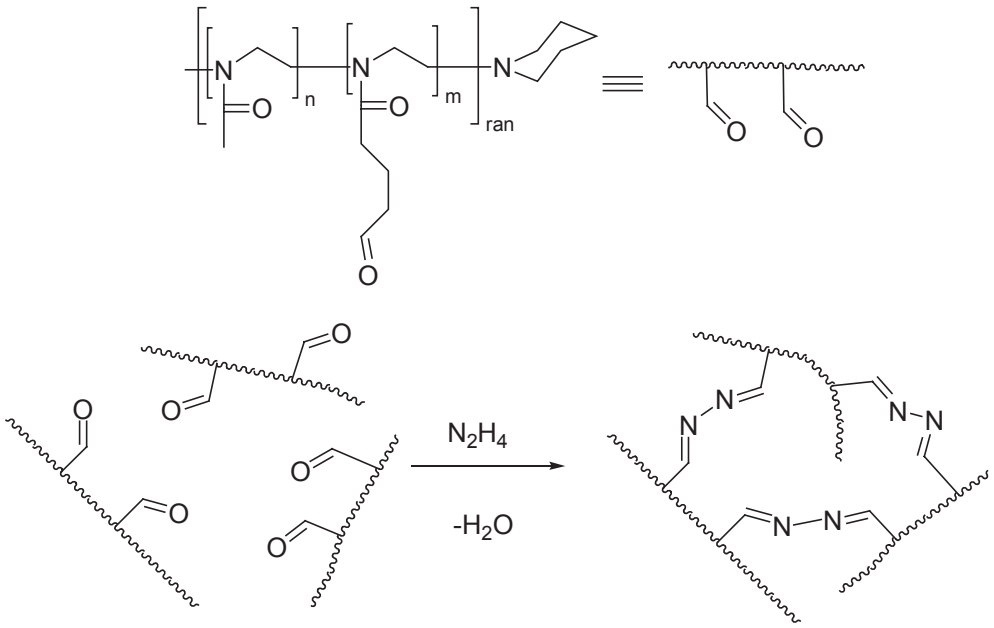

Figure 4.62: Illustration of the cross-linking of aldehyde bearing polymers with hydrazine.

Table 4.15: Azine hydrogels from hydrophilic poly(2-oxazolines) at various pH.

Hydrogel	Polymer	% wt[a]	Solvent	Yield[b]	SD[c]
H1	**P39**	10	pH4	86 %	13.1
H2	**P39**	20	pH4	87 %	4.2
H3	**P39**	20	pH6	90 %	4.2
H4	**P39**	20	pH8	117 %	2.7
H5	**P38**	30	pH4	61 %	4.2
H6	**P39**	30	pH5	79 %	2.3
H7	**P39**	30	pH6	49 %	2.5
H8	**P39**	30	pH7	54 %	2.2
H9	**P39**	30	pH8	65 %	1.4
H10	**P38**	30	pH9	0 %	—
H11	P($MeOx_{50}DPOx_8$)Pid	20	2 M HCl	59 %	5.3

[a] concentration of polymer solution

[b] recovered polymer after drying

[c] $\frac{\text{m(swollen)-m(dry)}}{\text{m(dry)}}$

pH 4 to pH 9. The yields of gels were moderate to excellent. In the case of **H4** a yield greater 100 % has been found, presumably due residual water or salt from the buffer. It should be noted that the gels have not been extracted (e.g. with DCM) and residual entrapped polymers could feign a higher yield than actually accomplished.
The swelling degree roughly correlates with two parameters. The %wt of the precursor polymer solution and the pH of the solvent. **H1** shows with $S_WD = 13$ the highest degree of swelling of all prepared azine hydrogels. Considering the relative high functional density, this value is high as compared with literature values[395]. Since the same polymer **P39** gives different values depending on the concentration of the precursor solution, it is assumed that the different swelling behavior stems from different degrees of cross-linking. At low concentrations, intramolecular reactions are favored. The resulting lower intermolecular cross-link density allows the hydrogel to expand further, thus swelling to a higher degree.
For the polymers prepared from 20 %wt solution, swelling and drying was performed repeatedly. The amount of recovered hydrogel in the second cycle (swelling in H_2O) was 35 % for **H2** and 44 % for **H3** and the swelling degree was reduced to 3.6 for both samples. The reduced amount of hydrogel can be explained by washout or decomposition (explaining the loss of 60 % and 51 % of dry hydrogel), but the reduction of S_WD points at an additional cross-linking which occured during drying of the gels. This assumption is corroborated by the fact that the loss of hydrogel in a third cycle was much lower (approx. 10 %). A strong increase of recovered amount of hydrogel in the case of **H4** in the second cycle is presumably an outlier as in the third cycle the values correspond again with the values for **H2** and **H3**.
From these first results it is clear that azine hydrogels can be formed under acidic conditions. Therefore, direct cross-linking of dioxolane bearing polymers and hydrazine under acidic conditions should be possible. Four 20 %wt solutions of P($MeOx_{50}DPOx_8$)-Pid in different solvents (pH 4, pH 2.5 buffer, 0.1 N HCl and 2 M HCl) were prepared. The hydrazine was added to the polymer solution and the mixture was taken up with a syringe for mixing and directly injected into a mold. However, before all of the solution could be injected to the mold, approx. a quarter of the solution solidified within the syringe in the case of 2 M HCl as a solvent, although the whole process of addition of hydrazine and mixing did not take longer than 2 s. In the other solvents, no gelation occurred within 2 d.
Subsequent swelling of the remainder of the gel in 2 M HCl resulted in 187 mg of **H11**

(29.7 mg after drying, S_WD = 5.3). The same hydrogel was afterwards allowed to swell in 0.1 N HCl (S_WD = 8.8), pH 4 (S_WD = 3.4) and pH 6 (S_WD = 3.7) buffer and deionized water (S_WD = 4.7). Over the course of repeated swelling and drying, the hydrogel broke down mechanically, but without hydrolysis (relatively stable values for the amount of dry gel).

4.7.2 Imine hydrogels

During the course of this work a novel amine-bearing 2-oxazoline monomer has been developed by *Anselment*[316]. It seemed a obvious choice to combine aldehyde and amine polymers to form imine cross-linked hydrogels. Therefore P($MeOx_{35}OBOx_5$)Pid and MeOxP($EtOx_{51}AEOx_4$)Pip where combined to a 20 %wt polymer solution in pH 4 (**H12**) and pH 9 buffer (**H13**) (Figure 4.63). The water was removed by slow evap-

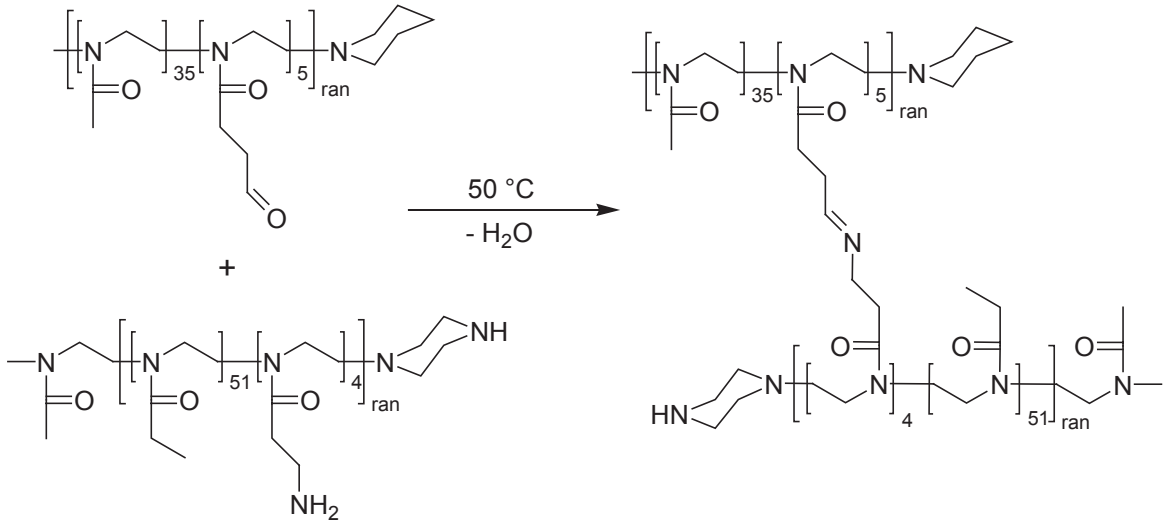

Figure 4.63: Preparation of the imine hydrogels **H12** and **H13**.

oration at 50 °C. Both polymers were subsequently immersed in the respective buffer and allowed to swell. For **H12** $S_WD = 5.9$ and for **H13** $S_WD = 7.2$ was obtained. Considering the high density of cross-linking groups, these values are reasonably good.

4.7.3 Urethane cross-linked hydrogel

A poly(2-oxazoline) hydrogel cross-linked via urethanes has been already described as mentioned earlier[285]. Due to the high reactivity of isocyanates towards water, the hydrogel preparation had to be performed in the absence of water. As a good and water compatible (for subsequent swelling) solvent for poly(2-oxazoline)s acetonitrile was chosen. The cross-linker was directly added to the solvent which was subsequently added to the lyophylized polymer (P($MeOx_{20}AEOx_5$)Pid. After 10 min 1.5 mL of water was added upon which the hydrogel (**H14**, Figure 4.64) immediately swelled (125 mg). After drying (17.2 mg, S_WD = 6.3) the procedure was repeated (106 mg/18.4 mg, S_WD = 4.7).

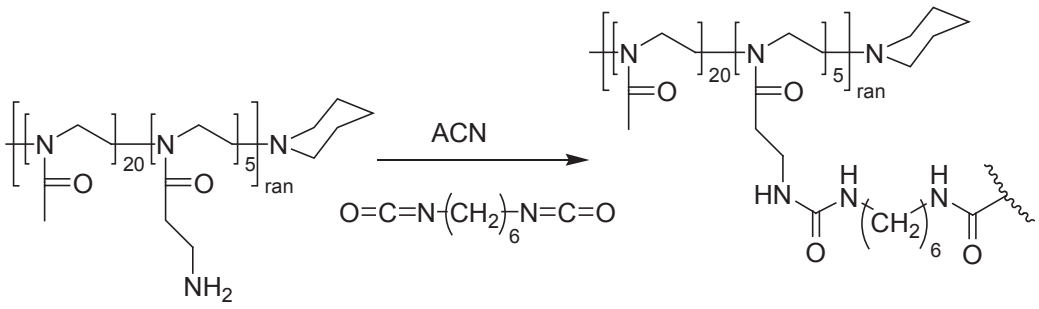

Figure 4.64: Preparation of the urethane cross-linked hydrogel **H14**.

4.7.4 Oxidative cross-linking

In this work the attachment of N-terminal cystein bearing peptides via NCL was described. The oxidative cross-linking of these conjugates is a concern during synthesis, work-up and storage. On the other hand, the oxidative disulfide formation has been applied for the preparation of hydrogels[300, 399]. Therefore, **P27** was dissolved in pH 7 buffer and cystein was added (equimolar to thioester groups). It is assumed that the cystein undergoes NCL and polymer **P40** is formed (Figure 4.65). The resulting solution was allowed to dry slowly at air and 50 °C. Upon addition of deionized water a hydrogel (**H15**) was immediately formed.Of the mechanically instable **H15**, 83.8 mg could be recovered and dried (4.8 mg, S_WD = 16.5). In a second cycle, 38.7 mg hydrogel

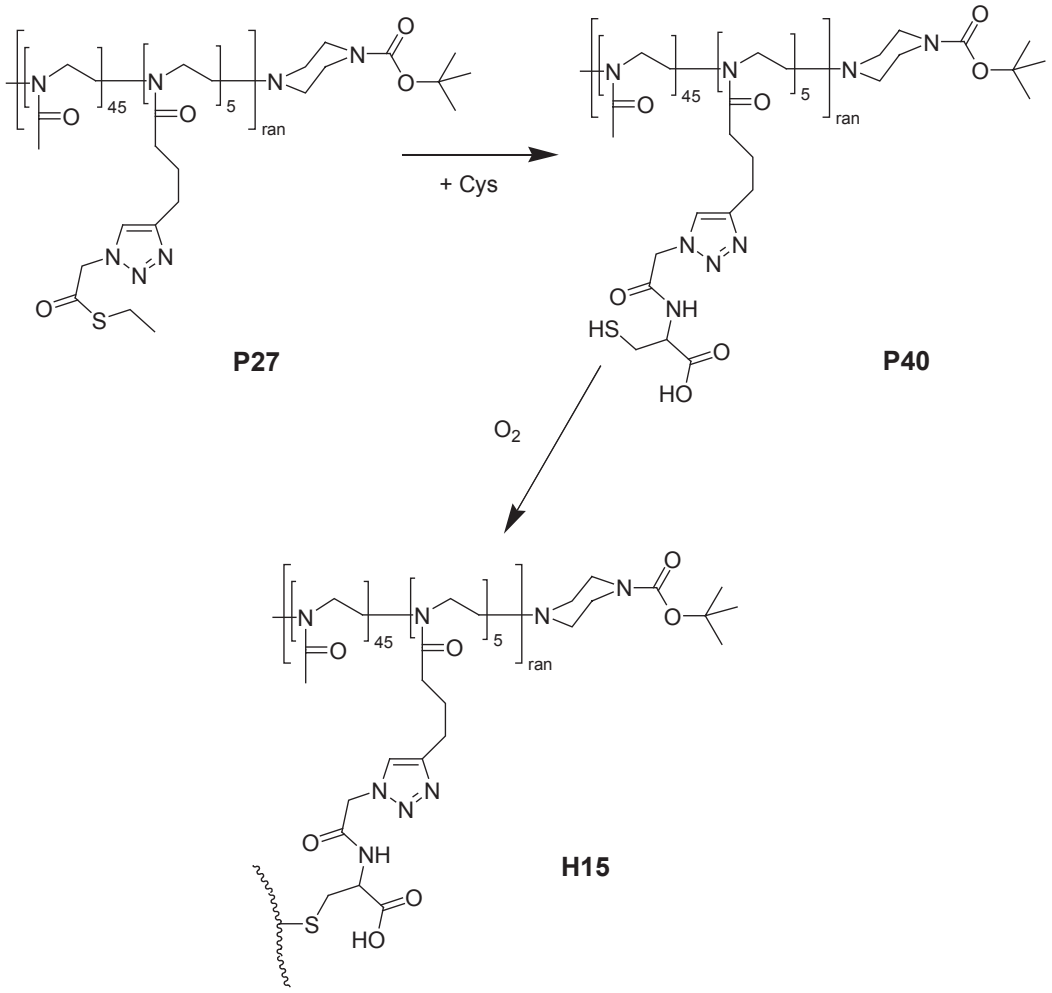

Figure 4.65: Formation of the oxidative cross-linked hydrogel **H15** from **P27**.

of 2.4 mg dry polymer (S_WD = 15.1) were obtained. To show whether cross-linking indeed occurred via disulfide bridges, 4.6 mg 1,4-dithio-DL-threitol (Clelands reagent, known to break down disulfide bridges) was added to the hydrogel immersed in water and immediately decomposition of the gel started. After approx. 3 hours, no more hydrogel was observed in the clear solution. Thus, NCL of the cystein and subsequent oxidative crosslinking has been proven.

4.7.5 Summary

Preliminary studies on the first azine and imine cross-linked poly(2-oxazoline) hydrogels are presented. The gelation of aldehyde bearing polymers with hydrazine occurs rapidly at room temperature. The observed swelling degrees were dependent on the concentration of the precursor polymer solution and on the method of cross-linking. The values of S_WD were mediocre for hydrogels in general, but good concerning the low DP of the used polymers and the high degree of cross-linking. Both azine and imine cross-linked hydrogels are expected to undergo pH dependent hydrolysis. Furthermore, changing the cross-linker (e.g. diaminooxy-compounds) will influence the hydrolysis behavior of respective hydrogels. However, detailed studies on the degradation behavior could not be matter of this work. While urethane cross-linked hydrogels will be much more stable towards hydrolytic degradation rapidly degradable hydrogels can be prepared by oxidative cross-linking as shown with the example of the disulfide bridged **H15**.

Since no accounts on poly(2-oxazoline) based hydrogels for tissue engineering could be found in literature, the presented first results should be only a starting point for the evaluation and development of sophisticated stimuli responsive POx hydrogels for biomedical applications.

5 Summary

The presented work aimed towards the development of a modular system of well-defined polymeric carriers based on poly(2-oxazoline)s, for the application in radionuclide cancer therapy. Therefore, functional polymers had to be synthesized and characterized. Subsequently, bioactive peptides and a chelator for radionuclides needed to be attached. Preliminary *in vivo* and *in vitro* screening suggest that the presented conjugates are feasible candidates for future developments.
In preceding works, polymer peptide conjugates have been prepared via standard peptide coupling protocols. In the presented work the use of effective and selective coupling methods for the attachment of bioactive peptides and the radionuclide chelator 1,4,7,10-tetraazacyclododecane-1,4,7,10-tetraacetic acid (DOTA) to water-soluble and well-defined poly(2-oxazoline)s has been realized for the first time.
Three highly effective and selective coupling reactions were utilized:

- The aminooxy ligation between *O*-hydroxylamines (aminooxy compounds) and aldehydes or ketons.

- *Huisgen*s 1,3-dipolar cycloaddition between azides and alkynes (click-chemistry).

- The coupling reaction between N-terminal cystein bearing peptides and fragments carrying thioesters, known as native chemical ligation (NCL).

To allow the introduction of appropriate chemical functionalities into the side chains of poly(2-oxazoline)s the novel monomers **1**[1], **2** and **3** and the bifunctional linker **5** were prepared (Figure 5.1).

[1]prepared by Taubmann in a Diploma Thesis

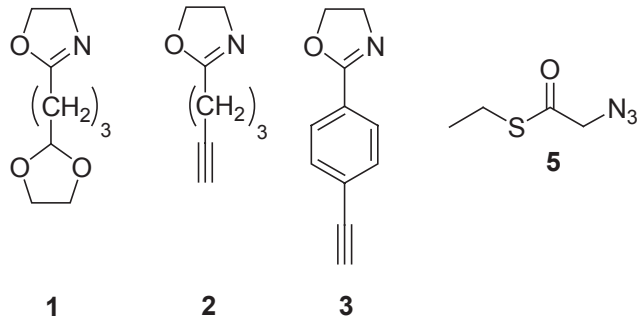

Figure 5.1: Prepared monomers **1**, **2** and **3** and the bifunctional azide **5** for NCL.

Polymer preparation and analytics Copolymerization of **1** and **2** with 2-methyl-2-oxazoline (MeOx) and 2-ethyl-2-oxazoline (EtOx) by cationic ring-opening polymerization (CROP) gave water-soluble polymers with pending functional groups. The polymers were analyzed with ^{1}H-NMR and ATR-IR spectroscopy as well as GPC and MALDI-TOF MS. These polymers had narrow polydispersities (PDI < 1.2) and by the living character of the polymerization a control over the degree of polymerization was possible via the initial monomer to initiator ratio $[M]_0/[I]_0$. Monomer **3** did not give a copolymer with MeOx, which is attributed to the reduced reactivity of **3** due to phenyl ring adjacent to the oxazoline.
Figure 6.2 shows exemplary the MALDI-TOF mass spectrum of **P24**. Analysis of this spectrum showed that the content of the functional monomer **2** within a copolymer can be controlled in narrow limits, which is important for the projected application in the biomedical field. Furthermore, kinetic studies on the copolymerization of **1** or **2**

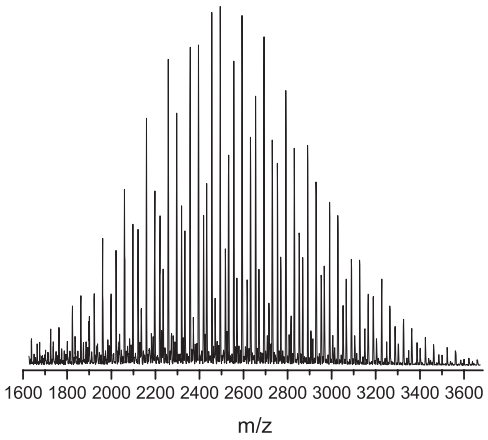

Figure 5.2: MALDI-TOF mass spectrum of P($EtOx_{20}PynOx_5$)Pip, **P24**.

with MeOx and EtOx showed that random and gradient copolymers are accessible by living CROP. Such control over the microstructure of functional polymers might also be important for future applications.
Structural variation of the polymer carrier from linear to star-like polymers was carried out to allow the future evaluation of the influence of the polymer architecture on the pharmacokinetics. Using multifunctional initiators for the polymerization of 2-oxazolines, a linear dependency between the numbers of initiating groups and the polymerization rate was observed. Thus, it was shown for the first time, that with multifunctional triflate initiators star-like poly(2-oxazoline)s with even length of the different arms can be obtained.

Polymer Modification Polymer analog modifications were applied to obtain poly(2-oxazoline) conjugates for biomedical applications. Polymers **P1**, **P2** and **P5 - P9** were terminated with *N*-Boc-piperazine for characterization and quantification via ^{1}H-NMR spectroscopy. Quantitative removal of the Boc group was facile and fast.
For the coupling of the chelator to the amino terminus of the polymer the isothiocyanate derivative of DOTA, *p*-SCN-Bn-DOTA, was used. It could be shown that up to 100 % of the polymers could be coupled to the chelator, as judged from ^{1}H-NMR spectroscopy. In this way, e.g. homopolymers of MeOx (**P30**) and EtOx (**P31**), and the copolymer of **1** and MeOx (**P34**, Figure 5.3) were successfully coupled with DOTA. After removal of the dioxolane group, **P34** was used to attach aminooxy bear-

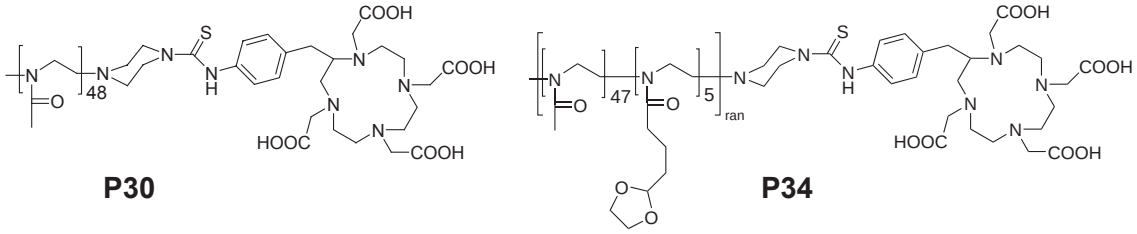

Figure 5.3: Structures of the DOTA containing polymers **P30** and **P34**.

ing peptides. The homopolymers **P30** and **P31** were directly used for biodistribution studies.
In contrast to previous work by *Taubmann*, it was shown that the conversion of the dioxolane group is possible with 5 % HCl_{aq}. The polymer analog side chain modifi-

cation via 'click-chemistry' has been shown to be highly efficient for the attachment of small azides, such as methyl(2-azido)acetate as proven by ^{1}H-NMR and ATR-IR spectroscopy as well as HPLC. The same method was used for the attachment of ethyl(2-azido)thioacetate **5**, introducing a thioester to allow for NCL with poly(2-oxazoline)s for the first time.

With the three novel side chain functionalities, the coupling of three bioactive and tumor-homing peptides c[RGDxK], MTII and CREKA to various poly(2-oxazoline)s was investigated. An azide bearing RGD was coupled to the EtOx copolymer **P33** to give **C1** (Figure 5.4). The precursor polymer **P33** was quantitatively consumed

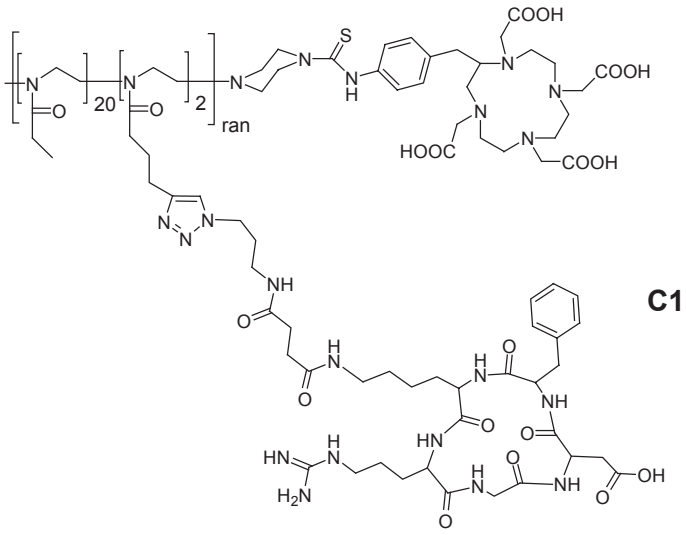

Figure 5.4: Structure of poly(2-oxazoline)-RGD conjugate **C1**

(HPLC) and in the ^{1}H-NMR spectrum the triazole specific signals could be assigned. However, peptide specific signals were not observed ^{1}H-NMR. The reason for this remained unknown but is possibly due to residual paramagnetic copper or aggregation of the conjugate in solution.

In contrast to this, it was shown by HPLC, ^{1}H-NMR, IR and UV-spectroscopy that the oxime ligation between RGD and MTII peptides to aldehyde bearing poly(2-oxazoline)s was successful (Figure 5.5). While HPLC was used to follow the conversion of the polymers, ^{1}H-NMR spectroscopy served for quantification of peptide in the conjugates. The peptide content in these conjugates was found to be in good agreement to the values expected from the content of functionalities in the precursor polymers.

Additionally, the linear pentapeptide CREKA was coupled to the prepared thioester

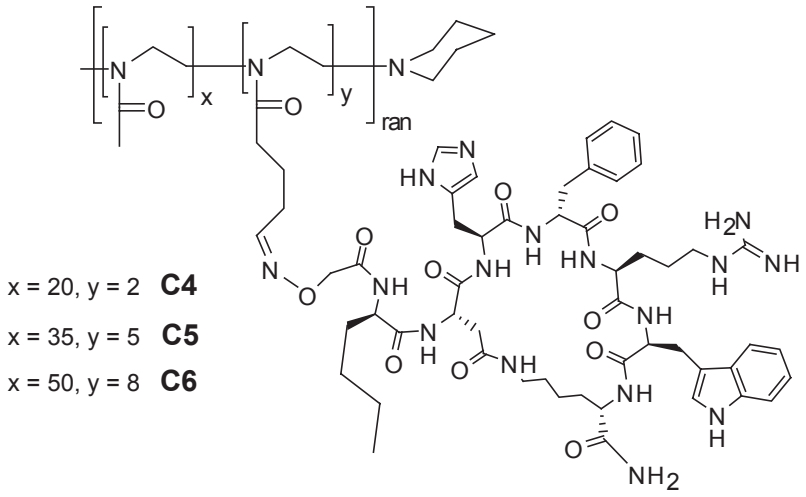

Figure 5.5: Structures of the poly(2-oxazoline)-MTII conjugates **C4**, **C5** and **C6**.

functionalized polymer-DOTA conjugate **P36**. The successful coupling was confirmed by HPLC, ^{1}H-NMR spectroscopy and by olfactory means.
Thus, it was shown for the first time that well-defined water-soluble and injectable polymer-peptide conjugates could be prepared using chemoselective coupling reactions. The amount of polymer bound peptide moieties could be predetermined by the $[M]_0/[I]_0$ ratios for the polymerization. Instead of expensive, ineffective and time-consuming preparative HPLC purification, simple gel filtration can be used to separate residual peptide, salts and solvents from the polymer-peptide conjugates due to the quantitative consumption of polymer precursors.

***In vivo* and *in vitro* studies** Since, until now, only limited data on the biodistribution of poly(2-oxazoline)s can be found in literature, the water-soluble and well-defined homopolymers **P30** and **P31** were radiolabeled with In-111 and their biodistribution studied. It was observed that both poly(2-oxazoline)s showed a very short blood circulation half-life with only 0.2 and 0.4 %ID/g left in the blood 30 min p.i.. Furthermore, no significant uptake in any organ but the kidneys was observed. The moderate kidney uptake can be explained by the rapid renal clearance observed for both polymers (Figure 5.6). In total, only approx. 4 % of the injected amount of **P30** remained in the body after 3 hours. The low organ uptake and rapid renal excretion suggest that these low-molar mass linear poly(2-oxazoline)s are promising candidates for the use

Figure 5.6: γ-Camera image of a mouse injected with [^{111}In]**P30**. The effective renal clearance can be seen in the large amount of radioactivity observed in the bladder 30 min after the administration. Only in the kidneys a significant uptake can be observed, due to the rapid renal clearance.

as polymeric carriers for biomedical applications.

The next step was to investigate the biodistribution of polymer-peptide conjugates. In the present work, the PMeOx-RGD-DOTA conjugate **C2** was radiolabeled with Ga-68 and injected into subcutan M21 tumor bearing mice. It could be shown that the tumor uptake of [^{68}Ga]**C2** was good with 1.81 %ID/g (1 h p.i.). However, uptake in various other organs was also significant, and in a number of cases, higher than in the tumor. The insufficient discrimination between tumor and organs of [^{68}Ga]**C2** can be explained by high levels radioactivity in the blood pool, probably resulting either from free Ga-68 or a prolonged blood retention of [^{68}Ga]**C2**. In the latter case, an enhancement is expected to be observed at later time points (e.g. 24 h p.i.) which will be investigated in future studies.

Finally, affinity studies of the prepared poly(2-oxazoline)-MTII conjugates **C4**, **C5** and **C6** towards various melanocortin receptors were performed by Dr. *Xu* at the University of Arizona. It was observed that conjugation to the polymer diminishes the affinity of MTII, which is compensated by the multimerization of MTII in the case of **C5** (approx. 5 MTII) and **C6** (approx. 8 MTII). The obtained affinity is still lower than that of the parent peptide, but the hydrophilicity of the poly(2-oxazoline)-MTII conjugates and the high molar mass will significantly influence the pharmacokinetics and biodistribution of these conjugates as compared to MTII. This and the possible attachment of DOTA to the polymer carrier makes these conjugates to potential candidates for the use in nuclear medicine.

Preparation of Hydrogels First experiments for the use of the novel side chain functionalities to prepare hydrogels were performed. Hydrogels on the basis of aldehyde, amine and thioester bearing poly(2-oxazoline)s were prepared. With a water uptake of up to 16 times of their own weight, these hydrogels show good swelling properties for such highly cross-linked hydrogels. Furthermore, in the case of the disulfide bridged hydrogel, it could be shown that DTT rapidly breaks down the hydrogels by reduction of the disulfide bridges. A combination of these chemoselectively cross-linked hydrogels with the presented peptide conjugates to give peptide containing hydrogels could allow number of interesting research projects in the near future.

6 Zusammenfassung

Die vorgestellte Arbeit befasste sich mit der Entwicklung eines modularen Systems von hoch-definierten polymeren Trägern auf der Basis von Poly(2-oxazolin)en für die Anwendung in der Radionuklidtherapie. Hierfür wurden funktionelle Polymere niedriger Polydispersität synthetisiert und charakterisiert. Nachfolgend wurden diese mit Krebszell-spezifischen Peptiden und einem Chelator funktionalisiert der das Einbringen von diagnostisch und therapeutisch verwendbaren Radionukliden ermöglicht.

Vorangegangene Arbeiten befassten sich bereits mit der Synthese von Poly(2-oxazolin)-Peptid Konjugaten mittels Standard-Peptidkupplungsmethoden. Dieser Weg erforderte die Verwendung von Schutzgruppen am Peptid sowie eine aufwändige Reinigung der Konjugate mittels präparativer HPLC. Deshalb sollten neue und effektivere Kupplungsmethoden für die Anbringung von bioaktiven Peptiden an wasserlösliche Poly(2-oxazolin)e gefunden werden. Drei Kupplungsreaktionen wurden identifiziert.

- Die Oximligation zwischen Aldehyden oder Ketonen und *O*-Hydroxylaminen (Aminooxy-Verbindungen).

- Die *Huisgen* 1,3-dipolare Zykloaddition zwischen Aziden und Alkinen unter Cu(I) Katalyse (*'Click-Chemie'*).

- Die Verknüpfung von Peptiden mit N-terminalem Cystein, und Thioestern, die sog. *native chemical ligation* (NCL).

Um die notwendigen chemischen Funktionalitäten (Aldehyd, Alkin und Thioester) in die Seitenketten von Poly(2-oxazoline)n einzuführen, wurden drei entsprechende

Monomere **1**[1], **2** and **3**, sowie der Thioester **5** synthetisiert und charakterisiert (Abbildung 6.1).

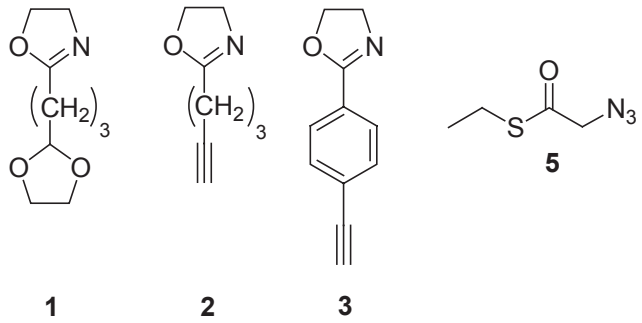

Abbildung 6.1: Synthetisierte Monomere **1**, **2** und **3** sowie der bifunktionelle Thioester **5** für die NCL.

Herstellung und Untersuchung der Polymere Mit den Monomeren **1** und **2** konnten durch lebende kationische ringöffnende Polymerisation wasserlösliche Copolymere mit 2-Ethyl- sowie 2-Methyl-2-oxazoline (EtOx bzw. MeOx) hergestellt werden, während aus **3** und MeOx wegen der geringen Reaktivität von **3** kein Copolymer erhalten wurde. Diese Polymere wurde mit Hilfe von ^{1}H-NMR-Spektroskopie, GPC, HPLC und, in ausgewählten Fällen, MALDI-TOF Massenspektrometrie analysiert. Es konnte gezeigt werden, dass die erhaltenen funktionellen Polymere aufgrund des lebenden Charakters der Polymerisation eine sehr geringe Polydispersität (PDI $<$ 1,2) aufweisen. Anhand der detaillierten Analyse des MALDI-TOF Massenspektrums von Polymer **P24** (Abbildung 6.2) konnte gezeigt werden, dass nicht nur die Molmassenverteilung sehr eng war (PDI_{MALDI} = 1,02), sondern auch der Gehalt an funktionellen Monomereinheiten sehr gut kontrolliert werden kann. Dies ist wichtig im Hinblick auf die spätere Anbindung von bioaktiven Peptiden an diese funktionellen Gruppen.
Kinetische Betrachtungen der Copolymerisation von **1** und **2** mit MeOx und EtOx zeigten, dass sowohl Gradientencopolymere als auch statistische Copolymere erhalten werden. Im Hinblick auf eine potentielle Anwendung im biomedizinischen Bereich ist dieser Aspekt ebenfalls von großer Bedeutung.

[1]Dieses Monomer wurde im Rahmen der Diplomarbeit von C. Taubmann synthetisiert.

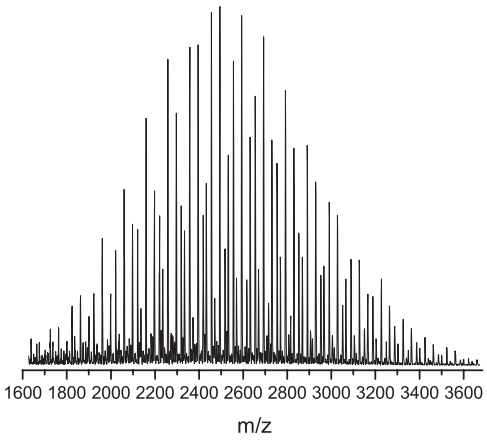

Abbildung 6.2: MALDI-TOF Massenspektrum von Polymer **P24**.

Durch die Verwendung multifunktioneller Triflate als Initiatoren für die Polymerisation von 2-Oxazolinen konnte ein linearer Zusammenhang zwischen der Anzahl an Initiatorgruppen und der Polymerisationsgeschwindigkeit gefunden werden. Dadurch konnte zum ersten Mal anhand kinetischer Betrachtungen gezeigt werden, dass Sternpolymere von 2-Oxazolinen mit homogener Armlänge zugänglich sind.

Polymeranaloge Reaktionen In einigen Fällen wurde zur Termination der lebenden Polymerisation *N*-Boc-Piperazin an Stelle von Piperazin eingesetzt. Dies diente vor allem dazu, eine Gruppe einzuführen, welche durch ^{1}H-NMR-Spektroskopie gut quantifizierbar ist. Es konnte gezeigt werden, dass die Entfernung dieser Schutzgruppe einfach und quantitativ erfolgen kann.
Das Anbringen des Chelators DOTA (1,4,7,10-Tetraazacyclododecan-1,4,7,10-tetraessigsäure) am Aminoterminus des Polymers ist ein wichtiger erster Schritt zur Realisierung von Polymer-Konjugaten für die Anwendung in der nuklearmedizinischen Diagnose und Therapie. Verschiedene Polymere wurden mit DOTA gekuppelt, darunter Homopolymere von MeOx (**P30**) und EtOx (**P31**), sowie das Copolymer aus MeOx und **1** (**P34**, Abbildung 6.3). Polymere wie **P34** konnten nach Freisetzung des Aldehyds dazu benutzt werden, verschiedene aminooxy-haltige Peptide anzukuppeln, um so wasserlösliche und radiomarkierbare Peptidoligomere zu erhalten. **P30** und **P31** wurden direkt zu Biodistributionsstudien eingesetzt.
Die Entfernung der Dioxolan-Schutzgruppe, resultierend aus der Polymerisation von

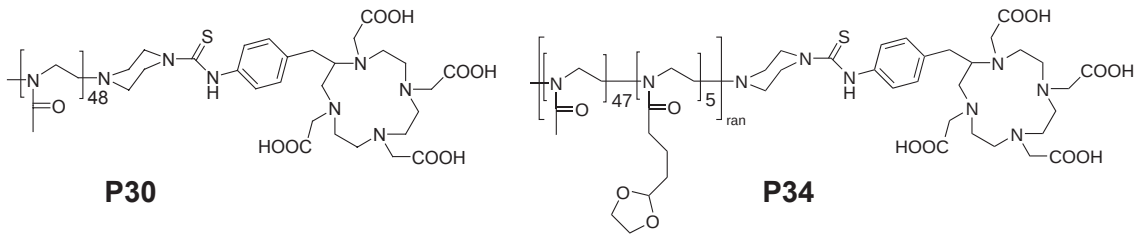

Abbildung 6.3: Polymere-DOTA Konjugate **P30** and **P34**.

1 konnte optimiert werden, in dem gezeigt wurde, dass anstatt 5 % TFA auch 5 % HCl verwendet werden kann.
Die Seitenkettenmodifikation mittels *Click-Chemie* konnte erfolgreich mit Testsubstanzen wie 2-Azidomethylacetat durchgeführt werden, was mittels ^{1}H-NMR- und ATR-IR-Spektroskopie sowie HPLC nachgewiesen werden konnte. Im Rahmen der Messgenauigkeit wurde eine quantitative Umsetzung der Polymere gefunden. Um die NCL zu ermöglichen, wurde der Thioester **5** über *Click-Chemie* quantitativ in Polymerseitenketten eingebracht. Nun standen drei Möglichkeiten zur hochselektiven und effektiven Kupplung von entsprechend funktionalisierten Peptiden zur Verfügung.

Schließlich wurde die chemoselektive Kupplung der drei bioaktiven Peptide c[RGDxK], MTII und CREKA an verschiedene Poly(2-oxazolin)e untersucht. Mittels *Click-Chemie* wurde ein Azid-funktionalisiertes zyklisches RGD an das EtOx Copolymer **P33** unter Kupfer(I) Katalyse zu **C1** verknüpft (Abbildung 6.4). Laut HPLC Analyse wurde **P33** quantitativ umgesetzt und im ^{1}H-NMR Spektrum konnte das spezifische Signal des resultierenden Triazol Ringes nachgewiesen werden. Jedoch fehlen die peptidspezifischen Signale. Dies ist möglicherweise auf verbleibendes paramagnetisches Cu(II) oder auf Aggregationseffekte zurückzuführen.
Im Gegensatz dazu konnte die erfolgreiche Oximligation zwischen aminooxy-funktionalisierten RGD und MTII Peptiden und Poly(2-oxazolin)en mit Aldehydseitenketten (Abbildung 6.5) durch HPLC, ^{1}H-NMR-, ATR-IR- und UV-Spektroskopie bestätigt werden. Außerdem war die Anbringung des Pentapeptids CREKA an das zuvor durch Click-Chemie synthetisierte, Thioester funktionalisierte Polymer **P36** möglich.
Im Rahmen dieser Arbeit konnte damit bestätigt werden, dass die modulare, chemoselektive und hocheffektive Anbringung von bioaktiven Peptiden an definierte, auf Poly(2-oxazolin)en basierten Trägern möglich ist. Die quantitative Umsetzung der polymeren Vorläufer ist hierbei von besonderer Bedeutung. Dadurch wird die Aufreini-

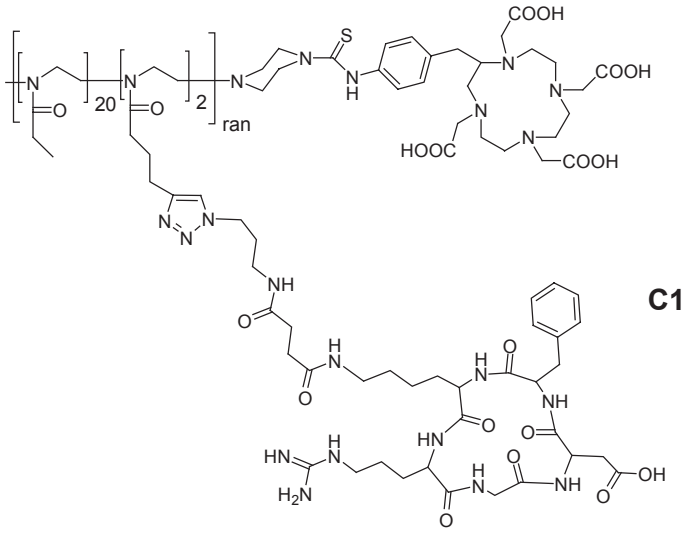

Abbildung 6.4: Struktur des poly(2-oxazolin)-RGD Konjugates **C1**.

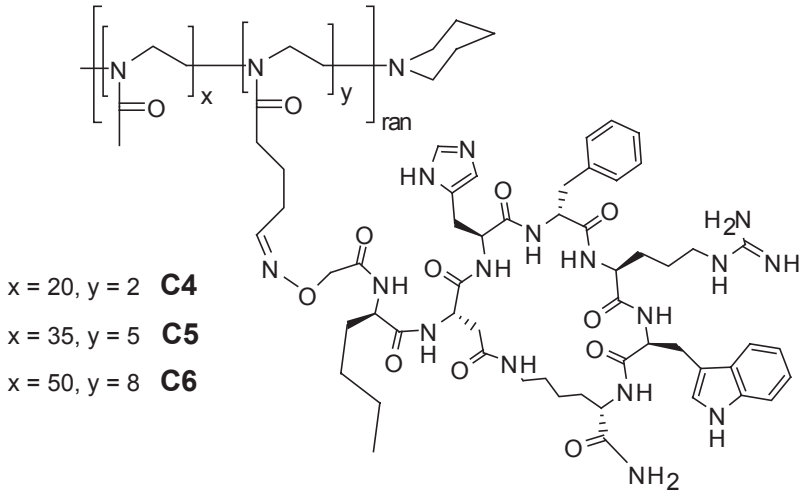

Abbildung 6.5: Strukturen der Poly(2-oxazoline)-MTII Konjugate **C4**, **C5** und **C6**.

gung mittels präparativer HPLC obsolet. Stattdessen kann eine einfache und schnelle Abtrennung der Polymer-Peptid Konjugate von niedermolekularen Verunreinigungen (Salze, Lösemittel, Peptid) durch Gelfiltration erfolgen.

Untersuchungen *in vivo* und *in vitro* Um den ungenügenden Kenntnisstand über die Biodistribution von linearen und definierten wasserlöslichen Poly(2-oxazolin)en zu erweitern, wurden die Homopolymere **P30** und **P31** mit In-111 markiert und deren Verteilung in Mäusen nach intravenöser Verabreichung untersucht. Es konnte gezeigt werden, dass beide Polymere eine sehr kurze Verweilzeit im Blut (0,2 und 0,4 %ID/g, 30 min p.i. für **P30** bzw. **P31**) aufweisen und sich in keinem Organ, außer der Niere, signifikant anreichern. Die moderate Nierenaufnahme erklärt sich durch die ausgeprägte renale Ausscheidung. Insgesamt verblieben bereits nach 3 h p.i. nur rund 4 % des verabreichten [^{111}In]**P30** im Organismus. Diese geringe Anreicherung in Organen (Abbildung 6.6) und schnelle renale Exkretion macht die Poly(2-oxazolin)e zu vielversprechenden Trägern für biomedizinische Anwendungen. Der nächste Schritt war die

Abbildung 6.6: γ-Kamera Aufnahme einer Maus welcher [^{111}In]**P30** injeziert wurde. Die schnelle und ausgeprägte renale Ausscheidung von [^{111}In]**P30** kann auch anhand der hohen Aktivität in der Blase erkannt werden (im Bild 30 min p.i.).

Untersuchung der Biodistribution des Poly(MeOx)-RGD-DOTA Konjugats (**C2**) in tumortragenden Mäusen (M21 Zelllinie, subkutan). Eine Stunde nach intravenöser Gabe von Ga-68 markiertem **C2** wurden die Tiere geopfert und die Verteilung des Konjugats untersucht. Hierbei konnte gezeigt werden, dass die Tumoraufnahme von [^{68}Ga]**C2** mit 1.81 %ID/g gut war, jedoch keine ausreichende Selektivität gegenüber gesundem Gewebe beobachtet werden konnte. Letzteres ist jedoch für Polymer-Peptid Konjugate für frühe Zeitpunkte bekannt und kann z.T. auf die hohe verbleibende Menge von Radioaktivität im Blut zurückgeführt werden. Weitere Untersuchungen zu späteren Zeitpunkten (z.B. 24 h p.i.) sind jedoch notwendig um dies zu bestätigen.

Schließlich wurde das Bindungsverhalten der MTII-Polymer-Konjugate **C4**, **C5** und **C6** an verschiedene Melanocortinrezeptoren (hMC1R, hMC3R, hMC4R und hMC5R) von Dr. *Xu* an der Universität von Arizona untersucht. Dabei wurde festgestellt dass die Verknüpfung des Peptides an das Polymer die Affinität des ansonsten hochaffinen MTII Peptids stark beeinträchtigt. Jedoch wird dies durch die größere Anzahl von Peptiden in **C5** (ca. 5) und **C6** (ca. 8) größtenteils kompensiert. Zwar ist die erreichte Affinität immer noch geringer als die des Ausgangspeptids (außer gegenüber hMC5R), die Erhöhung der Hydrophilie und der Molmasse, und der damit zu erwartenden Veränderung der Pharmakokinetik, machen diese Konjugate dennoch zu potenziellen Trägern von Nukliden für die Diagnose oder Therapie von hMC1R exprimierenden Tumoren.

Synthese von Hydrogelen Biokompatible Hydrogele können als Gerüststrukturen im Rahmen des *tissue engineering* dienen. Die Herstellung von Hydrogelen kann durch Vernetzung von hydrophilen Polymeren erfolgen. Daher wurden erste Versuche zur Herstellung und Charakterisierung von Hydrogelen auf der Basis von Aldehyd-, Amin- und Thioester-funktionalisierten Poly(2-oxazolin)en durchgeführt. Es konnte gezeigt werden, dass in allen Fällen Hydrogele erhalten werden. Mit einer Wasseraufnahme des bis zu 16-fachen des Eigengewichts wurden gute Quellwerte für hochverknüpften Hydrogele erreicht. Im Falle der Disulfid-verknüpften Hydrogele konnte zusätzlich gezeigt werden, dass durch Zugabe von DTT ein reduktiver Abbau möglich ist. Eine Kombination dieser ersten Versuche von chemoselektiv verknüpften Hydrogelen und den vorgestellten Peptidkonjugaten zu peptidhaltigen Hydrogelen könnte zu interessanten Materialien im Bereich des *tissue-engineering* führen.

7 Experimental

7.1 General

7.1.1 Equipment and utilities

NMR spectra were recorded on a
A: Bruker ARX 300 (^{1}H: 300.13 MHz; ^{13}C: 75.47 MHz) or
B: Bruker AC 250 (^{1}H: 250.13 MHz; ^{13}C: 62.90 MHz) or
C: Bruker DMX 500 (^{1}H: 500.13 MHz; ^{13}C: 125.83 MHz)
at 300 K. The spectra were calibrated to the signals of residual protonated solvent signals ($CHCl_3$ 7.26, HDO 4.67, CD_2HOD 3.31, CHD_2SOCD_3 2.49 ppm). Multiplicities of signals are depicted as following: s, singlett; d, dublett; t, triplett; q, quartett, quin, quintett; dt, dublett of tripletts; m, multiplett; b, broad, ps, pseudo.
IR spectroscopy were obtained on a Bruker IFS 55s spectrometer with an ATR sampling accessory from Harrick (single bounce, diamond crystal) and a MCT detector. Data were processed using Opus software. w = weak, m = medium, s = strong, vs = very strong, b = broad.
UV-Vis spectroscopy was performed on Varian Cary 3 (200 - 800 nm) system (Cary WinUV Software).
MALDI-TOF were performed on a *Bruker* Biflex III or a *Bruker-Daltonic*, Ultraflex TOF/TOF using a ditranol matrix. The samples were prepared by mixing $CHCl_3$ solutions of polymer and matrix (10 mg/mL) in a typical ratio of 1:1 (v/v). High performance liquid chromatography (HPLC) was performed on an *Amersham Pharmacia* Äkta Basic 10 F, pump system P-900, detection UV-900, autosampler A 900. Column: Omnicrom-YMC-ODS-A 120 5-C18 (120 Å, 5 μm, 250 mm × 4.6 mm). Mobile

phase: water (0.1% TFA, solvent A) and ACN (0.1% TFA, solvent B) at a flow rate of 1 mL/min.
Gel permeation chromatography was carried out on a Waters system (pump mod. 510, 410 differential RI detector) using a PLgel precolumn and $2 \times$ PL RESIPORE ($3\,\mu$m 300 .$\times$7.5 mm) for measurements in *N*,*N*-dimethylacetamide (DMAc) (containing 75 mmol/L LiBr). The columns were heated to 80 °C, the flow rate was 1 mL/min. Samples were filtered prior to each measurement through $0.2\,\mu$m regenerated cellulose filters (Opti-Flow, WiCom). Calibration was performed with poly(styrene) standards (Polymer Standard Service (PSS), molar masses: $0.192 - 5.67 \times 10^5$ g/mol). Data were processed using Millenium software.
Gas chromatography was performed on a Varian CP 3380 equipped with a CombiPal robot arm and with a Nordion NB-54 column (25 m, 0.20 mm, $0.25\,\mu$m) and FID detector (carrier gas helium). The injection temperature was typically 270 °C.
Elemental analysis was performed at the Microanalytical Laboratory of the Inorganic Chemistry Institute of the TU München.
Statistical analysis of the biodistribution data was performed with BioStat2007 software (shareware version; AnalystSoft, BioStat - statistical analysis program. Version 2007. See http://www.analystsoft.com) using an one-way ANOVA. Statistical significance was assumend when $p < 0.05$.
Prepared low molar mass compounds are numbered with bold numbers (**X**), initiators as **IX**, while polymers are numbered **PX**. Hydrogels are counted as **HX**.

7.1.2 Reagent and solvents

All chemicals were purchased from Sigma-Aldrich or Acros and used as recieved unless otherwise stated. *N*,*N*-Diisopropylethylamine (DIPEA, Hünig base) was refluxed and KOH was added to saturation twice. After decanting, DIPEA was distilled under nitrogen from ninhydrin. Thereafter, CaH_2 was added and DIPEA distilled under nitrogen. Acetonitrile (ACN) and other dry solvents were refluxed over CaH_2 and distilled under nitrogen prior to use. Tetrahydrofuran (THF) (absolute) was refluxed over Na(s) and benzophenone until the blue color of the ketyl radical anion

was observed and distilled subsequently. 2-(4-Isothiocyanatobenzyl)-1,4,7,10-tetraazacyclododecane-1,4,7,10-tetraacetic acid × 2.5HCl × 2.5H_2O (*p*-SCN-Bn-DOTA) was purchased from Macrocyclics (Dallas, TX, USA) and used as recieved.
The RGD peptides c[RGDfK(4-(3-azido-propylamino)-4-oxobutanoate)] (c[RGDfK-(N_3)]), c[R(Pbf)GD(tBu)fK(*N*-Boc(2-aminooxy)acetic acid)] (c[ṘGḊfK(Boc-AOAc)]) and c[RGDyK((2-aminooxy)acetic acid)] (c[RGDyK(AOAc)]) were synthesized by Dr. *Lopéz-García* at the Institut für Organische Chemie und Biochemie, Lehrstuhl für Organische Chemie II of the TU München as previously described[426]. 2-(Aminooxy) acetic acid-Nle-c[Asp-His-DPhe-Arg-Trp-Lys]-NH_2 ($AOAc^0$-MTII) was synthesized by *F. Opperer* in the same group according to a previously described procedure[162].
2-[3-(1,3)-Dioxolan-2-ylpropyl]-2-oxazoline (**1**) was prepared by *C. Taubmann* as described recently[259,400]. The polymers P($MeOx_{20}OBOx_2$)Pid, P($MeOx_{35}DPOx_5$)Pid, P($MeOx_{50}OBOx_8$)Pid, MeOxP($MeOx_{51}AEOx_4$)Pip and P($MeOx_{20}AEOx_5$)Pid were obtained from *T. Anselment*[316]. Ethyl-4-(oxazol-2-yl)butanate (EOB) was obtained from Dr. *Zarka*[255]. Methyl (2-azido)acetate[427] and (trimethylsilyl)methyl azide[428] were prepared according to the literature procedure.
Dialysis was performed with ZelluTrans V Serie dialysis tubes with a nominal molecular weight cut off (MWCO) of 1000 g/mol. Gel filtration was performed with Sephadex G25 (MWCO ∼ 1000 g/mol).

7.2 Methods

7.2.1 Polymerizations, general synthetic procedure 1, GSP1

Unless otherwise stated, all polymerization were carried out according to the following procedure.
Initiator and monomer(s) were dissolved in dry ACN at RT. After stirring at 85 °C for 18 h to 96 h, 20 equivalents of piperazin or 3 equivalents of monofunctional terminating reagent (piperidine or *N*-Boc-piperazine) with respect to the initiator were added as a solution in $CHCl_3$ (ACN for *N*-Boc-piperazine) at RT and the mixture stirred for additional 4 h or over night. An excess of K_2CO_3 (minimum 0.5 eq in respect of the

initiator) was added and the mixture was stirred over night. From the typically turbid solution the solvent was removed and the residual was collected in 5 - 20 mL of a 1/1 (v/v) mixture of $CHCl_3$/MeOH, the solution was centrifuged and decanted. The polymer was precipitated by adding the solution to the ten-fold amount of cold diethylether (if necessary after filtration). The mixture was centrifuged, the precipitate separated, dried by flushing with nitrogen (if necessary in rough vacuum) and lyophylized from water (alternatively benzene) to give the products as colorless powders.

7.2.2 Removal of Boc protection group, general synthetic procedure 2, GSP2

The polymer (50 - 500 mg) was dissolved in a minimum amount (500 μL - 3 mL) of a 95%/2.5%/2.5% mixture of trifluoroacetic acid (TFA)/H_2O/triisobutylsilane (TIBS) (v/v/v) (DeMix). After stirring for 40 min at roomtemperature (or 10 min under sonication) the solvents were removed at reduced pressure and the residual was collected in 1 - 5 mL of a 2:1 mixture of MeOH and $CHCl_3$. After precipitation form the ten fold amount of cold diethylether and decantation (if necessary after centrifugation) the product was lyophylized.

7.2.3 Isothiocyanate coupling, general synthetic procedure 3, GSP3

The piperazine terminated polymer (1 - 20 μmol, 1 eq amine) was dissolved in dry MeOH (250 μL - 1 mL) and 1.2 to 2 equiv of *p*-SCN-Bn-DOTA was added. The mixture was stirred for 3 - 5 days at RT. The solvent was exchanged with 1 mL of water and the product purified over a Sephadex G25 column ($\sim$3 g). The product was obtained as a powder after lyophylization.

7.2.4 Gas chromatographic on-line kinetic measurement

For the kinetic measurements the polymerization mixture was prepared and sealed in a glove-box under inert and dry atmosphere. The agitator was preheated to the indicated temperature. The CombiPal was programmed for 2 syringe wash cycles (ACN) prior and after sampling. The sealed reaction container was introduced to the agitator directly (~ 1 s) prior to the first sampling, in order to obtain a zero-time value. Per injection 2μL of the reaction mixture were taken. The monomerconsumption was followed by the change of the ratio of the monomer to the internal standard (chlorobenzene).

7.3 Initiator synthesis

7.3.1 Propane-1,3-bistriflate, I1

Under nitrogen, 0.47 g 1,3-propanediol (6 mmol, 1 equiv) was added via a syringe to a solution of 3.40 g triflic acid anhydride (12 mmol, 2 equiv) in 15 mL of dry dichloromethane (DCM) at 0 °C. Subsequently, a solution of 0.95 g of pyridine (12 mmol, 2 equiv) in 3 mL dichloromethane was added within approx. 5 minutes. The precipitated solid was filtered and the solvent was removed under reduced pressure. The product was obtained as a brownish oil.

Yield: 1.41 g (69 %)
Empirical formula, molar mass: $C_5H_6F_6O_6S_2$, M = 340.22 g/mol

ATR-IR: $\widetilde{\nu}$ = 2991 (C-H str)(w), 1410 (S=O str) (s), 1193 (S=O str)(vs), 1138 (vs), 1013 (w), 918 (vs), 854 (m) and 814 cm^{-1}(m).

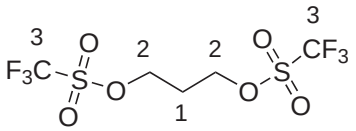

^{1}H-NMR ($CDCl_3$, 300 MHz): $\delta = 4.60$ (t, $^{1}J = 5.8$ Hz, 4H, H^2) and 2.32 ppm (quin, J = 5.8 Hz 2H, H^1).

$^{13}C\{^{1}H\}$-NMR ($CDCl_3$, 75 MHz): $\delta = 112.6$ (q, $^{1}J = 320.2$ Hz, 3H), 71.8 (C^2) and 29.7 ppm (C^1).

7.3.2 1,1,1-Tris(triflatemethyl)ethane, I2

To a solution of 0.389 g 1,1,1-tris(hydroxymethyl)ethane (3.2 mmol, 1 equiv) in 1.65 mL of pyridine (20.5 mmol, 6.3 equiv) and 3 mL ACN was cooled to 0 °C. Slowly, 3.3 g of triflic acid anhydrate (11.7 mmol, 3.7 equiv) were added over 40 min. Besides a pronounced development of fume the reaction mixture turned red. After 2 h the cooling was removed and the mixture was allowed to stir for 2 h. Subsequently, the mixture was neutralized by addition of 14 mL 1M HCl and was cooled with an NaCl-ice mixture. The product, an orange viscous oil, was washed with ACN.

Yield: 0.684 g (41 %)
Empirical formula, molar mass: $C_8H_9F_9O_9S_3$, M = 516.33 g/mol

ATR-IR: $\widetilde{\nu}$ = 2970 (C-H str)(w), 1737 (w), 1407 (S=O str)(m), 1242 ()(m), 1203 (S=O str)(s), 1138 (s), 948 (s) and 824 cm^{-1} (m).

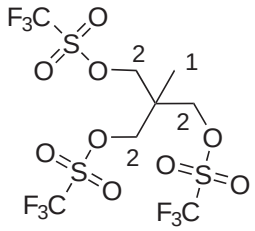

^{1}H-NMR ($CDCl_3$): $\delta = 4.38$ (s, 6H, H^3) and 1.2 ppm (s, 3H, H^1).

^{13}C-NMR ($CDCl_3$): $\delta = 112.5$ (q, $^{1}J_{C-F} = 326.1$ Hz, C^4), 74.6 (C^3), 40.9 (C^2) and 16.0 ppm (C^1).

7.3.3 Pentaerythritoltetrakistriflate, I3

I3 was prepared according to a previously reported procedure[429]. To an ice-cooled suspension of 0.5 g pentaerythritol (3.7 mmol, 1 equiv), 2.5 mL pyridine and 4 mL ACN, 5 g of triflic anhydride (17.7 mmol, 4.8 equiv) was added dropwise over 5 min. After work-up and recrystallization as reported in the literature, the title compound was obtained as a colorless crystalline solid.

Yield: 1.554 g (63 %)
Empirical formula, molar mass: $C_9H_8F_{12}O_{12}S_4$, M = 664.39 g/mol

ATR-IR: $\widetilde{\nu}$ = 3002 (C-H str)(w), 1712 (vs), 1425 (s), 1361 (s), 1245 (m), 1209 (vs), 1145 (vs), 1094 (w), 952 (vs), 831 (m), 765 (w) and 617 cm^{-1}(m).

Elemental analysis:

	C	H	S	F
theor.	16.27	1.21	19.30	34.31
exp.	16.16	1.19	19.46	33.35

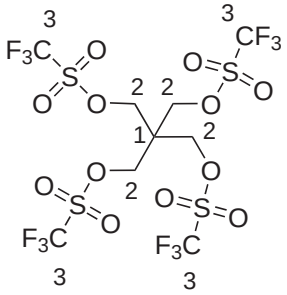

^{1}H-NMR (acetone-d6, 300 MHz): δ = 5.15 ppm (s, H^2).

$^{13}C\{^1H\}$-NMR (acetone-d6, 75 MHz): δ = 119,45 (q, ^1J = 324.5 Hz, C^3), 72.4 (C^2) and 45.6 ppm (C^1).

7.4 Monomer synthesis

7.4.1 2-(Pent-4-ynyl)-2-oxazoline, 2

The alkyne bearing monomer 2-(Pent-4-ynyl)-2-oxazoline (PynOx) was synthesized as recently described[401].

Hex-5-ynoyl chloride

In a flame-dried Schlenkflask and under a dry nitrogen atmosphere 25.485 g (0.227 mol, 1 equiv) of hex-5-ynoic acid and 32.514 g (0.273 mol, 1.2 equiv) of thionylchloride were refluxed at 90 °C for ∼1 h. The end of the reaction was indicated as the gas evolution from the reaction mixture ceased. The dark red mixture was distilled under nitrogen and the product was obtained as a colorless liquid of pungent smell (bp. 104 - 110 °C).

Yield: 25.91 g (92 %)
Empirical formula, molar mass: C_6H_7ClO, M = 130.57 g/mol

ATR-IR: $\widetilde{\nu}$ = 3301 (≡C-H str) (m), 2954 (C-H str) (w), 1791 (C=O str) (s), 626 cm^{-1} (≡C-H wag) (s).

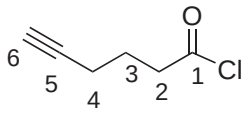

^{1}H-NMR ($CDCl_3$, 300 MHz): δ = 2.97 (t, ^3J = 7.3 Hz, 2H, H^2), 2.21 (dt, ^3J_t = 6.6 Hz, ^3J_d = 2.7 Hz, 2H, H^4), 1.93 (t, ^3J = 2.7 Hz, 1H, H^6) and 1.82 ppm (ps-quin, ^3J = 7.1 Hz, 2H, H^3).

^{13}C{^{1}H}-NMR ($CDCl_3$, 300 MHz): δ = 173.4 (C^1), 82.1 (C^5), 70.0 (C^6), 45.5 (C^2), 23.6 (C^4) and 17.2 ppm (C^3).

Hex-5-ynoic acid (2-chloroethyl)amide

Hex-5-ynoyl chloride (24.973 g, 191 mmol, 1 equiv) was dissolved in 220 mL of dry DCM. 2-Chloroethylamine hydrochloride (22.35 g, 192.7 mmol, 1 equiv) (99 %) was added, and the mixture was ice-cooled. Over a period of 1 h, 65 mL (0.47 mol) of triethylamine (TEA) was added dropwise. After additional stirring for 30 min at 0 °C, the mixture was allowed to equilibrate to RT and was stirred overnight. The yellow reaction mixture and a colorless precipitate was observed. Water ($\sim$ 50 mL) was added until the precipitate dissolved. The organic layer was removed and extracted twice with 30 mL of water and once with 30 mL of brine. The organic layer was separated and dried over Na_2SO_4, and finally, the solvent was removed. The product remained as an orange, highly viscous oil and was used without further purification.

Yield: 24.35 g (73 %)
Empirical formula, molar mass: $C_8H_{12}ClNO$, M = 173.64 g/mol

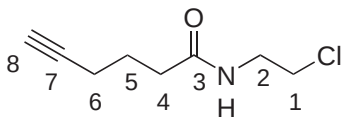

^{1}H-NMR ($CDCl_3$, 300 MHz): δ = 6.32 (br, 1H, H^{amide}), 3.55 (m, 4H, $H^{1,2}$), 2.29 (t, ^3J = 7.4 Hz, 2H, H^4), 2.21 (td, ^3J_t = 7.1 Hz, ^3J_d = 2.7 Hz, 2H, H^6), 1.93 (t, ^3J = 2.7 Hz, 1H, H^8) and 1.82 ppm (ps-quin, ^3J = 7.1 Hz, 2H, H^5).

^{13}C{^{1}H}-NMR ($CDCl_3$, 300 MHz): δ = 172.5 (H^3), 83.3 (H^7), 69.2 (H^8), 43.8 (H^1), 41.1 (H^2), 34.8 (H^4), 24.0 (H^6) and 17.7 ppm (H^5).

2-(Pent-4-ynyl)oxazoline, 2

Hex-5-ynoic acid (2-chloroethyl)amide (20 g, 115 mmol, 1 equiv) was dissolved in 70 mL of MeOH and 6 g of freshly ground NaOH (150 mol, 1.3 equiv) were added. The product was distilled as a colorless liquid at $\sim$ 5 mbar and 85 °C after stirring at that temperatur

for 3 h to yield a colorless liquid.

Yield: 4.29 g (27%)
Empirical formula, molar mass: $C_8H_{11}NO$, M = 137.18 g/mol

ATR-IR: $\widetilde{\nu}$ = 3301 (≡C-H str)(m), 2954 (C-H str)(w), 1666 (C=N str)(s), 1432 ($\delta(CH_2$-CO)(m), 630 cm $^{-1}$ (≡C-H wag).

Elemental analysis:

	C	H	N
theor.	70.02	8.08	10.21
exp.	69.91	8.29	10.30

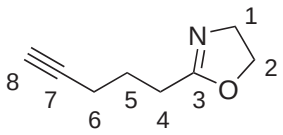

^{1}H-NMR ($CDCl_3$, 300 MHz): δ = 4.23 (t, ^3J = 9.3 Hz, 2H, H^2), 3.82 (t, ^3J = 9.3 Hz, 2H, H^1), 2.41 (t, ^3J = 7.5 Hz, H^4), 2.29 (td, ^3J_t = 7.0 Hz, ^3J_d = 2.7 Hz, 2H, H^6), 1.97 (t, ^3J = 2.7 Hz, 2H, H^8) and 1.87 ppm (ps-quin, ^3J = 7.2 Hz, 2H, H^5).

$^{13}C\{^1H\}$-NMR ($CDCl_3$, 75 MHz): δ = 167.8 (C^3), 83.3 (H^7), 68.9 (H^8), 67.1 (H^2), 54.2 (H^1), 26.6 (H^4), 24.6 (H^6) and 17.7 ppm (H^5).

7.4.2 2-(4-Ethynlyphenyl)-2-oxazoline 3

Ethyl 4-(2-trimethylsilyl)ethynylbenzoate

Under nitrogenm 4.39 g ethyl 4-iodobenzoate (15.9 mmol, 1 equiv) were dissolved in 55 mL TEA. $(Ph_3P)_2PdCl_2$ (53 mg, 0.075 mmol, 0.005 equiv) and 77 mg CuI (0.4 mmol, 0.025 equiv) were added and the mixture was stirred for 10 min at RT. Subsequently, 2.5 g of trimethylsilyl acetylene (25.45 mmol, 1.6 equiv) were added and the mixture

was stirred over night at RT. After filtration, the filtrate was concentrated under reduced pressure and the residual was purified by chromatography (silica, eluent: pentane/ethyl acetate = 4/1 (v/v)). After removal of the solvent, the product remains as brown oil.

Yield: 3.38 g (86%)
Empirical formula, molar mass: $C_{14}H_{18}O_2Si$, M = 246.38 g/mol

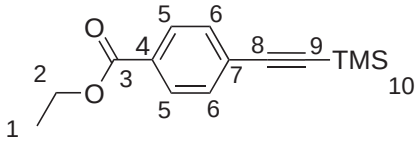

^{1}H-NMR ($CDCl_3$, 300 MHz): $\delta = 7.76$ (d, $^3J = 8.58$ Hz, 2H, H^5), 7.31 (d, 2H, $^3J = 8.58$ Hz, H^6), 4.16 (q, ^3J 7.05 Hz, 2H, H^2), 1.19 (t, $^3J = 7.05$ Hz, 2H, H^1) and 0.07 ppm (s, 9H, H^{10}).

^{13}C{^{1}H}-NMR ($CDCl_3$, 75 MHz): $\delta = 165.9$ (C^3), 131.7 (C^6), 130.0 (C^4), 129.3 (C^5), 127.6 (C^7), 104.1 (C^8), 97.5 (C^9), 61.1 (C^2), 14.3 (C^1) and 0.2 ppm (C^{10}).

4-Ethynylbenzoic acid

Ethyl 4-(2-trimethylsilyl)ethynylbenzoate (3.38 g, 13.7 mmol, 1 equiv) was dissolved in 12 mL ethanol. At 0 °C, 18 mL of 1 M NaOH (18 mmol, 1.3 equiv) were added and the solution stirred for 2 h. The mixture was allowed to warm to RT under stirring over night. The solution was washed twice with 30 mL Et_2O each, the aqueous phase was acidified with 1 M HCl and the red precipitate extracted with 100 mL Et_2O. After washing twice with 15 mL H_2O and drying over $MgSO_4$ the solvent was removed under reduced pressure. The product remained as red solid.

Yield: 1.59 g (80%)
Empirical formula, molar mass: $C_9H_6O_2$, M = 146.14 g/mol

Elemental analysis:

	C	H	O
theor.	73.97	4.14	21.90
exp.	73.33	4.14	n.d.

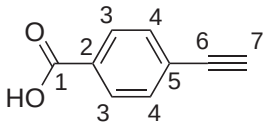

^{1}H-NMR ($CDCl_3$, 300 MHz): $\delta = 7.98$ (d, $^3J = 7.73$ Hz, 2H, H^3), 7.67 (d, $^3J = 7.84$ Hz, 2H, H^4), 4.49 (s, 1H, H^7).

2-(4-Ethynlyphenyl)oxazoline, 3

4-Ethynylbenzoic acid (1.59 g, 10.88 mmol, 1 equiv) was dissolved in 50 mL dry DCM and 2.29 g EDCI × HCl (11.97 mmol, 1.15 equiv), 2.26 g TEA (22.33 mmol, 2 equiv) and 2.56 g 2-bromoethylamine hydrobromide (12.5 mmol, 1.1 equiv) were added and the mixture was stirred under reflux over night. The organic phase was extracted twice with 10 mL H_2O each and the solvent was removed under reduced pressure. The remaining yellow solid was purified with silica chromatography (eluent: methanol/ethyl acetate/n-hexane = 2/2/1, (v/v/v)) and the product was obtained as a colorless solid.

Yield: 0.944 g (46%)
Empirical formula, molar mass: $C_{11}H_9NO$, M = 171.20 g/mol

ATR-IR: $\widetilde{\nu}$ = 3300 (≡C-H str) (m), 2100, 1700 (C=N str)(s), 1600, 1500 cm^{-1}.

Elemental analysis:

	C	H	N
theor.	77.17	5.30	8.18
exp.	76.70	5.31	8.19

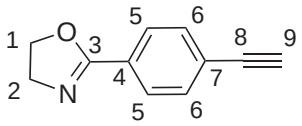

^{1}H-NMR ($CDCl_3$, 300 MHz): $\delta = 7.86$ (d, $^{3}J = 8.2$ Hz, 2H, H^5), 7.47 (d, $^{3}J = 8.4$ Hz, 2H, H^6), 4.38 (t, $^{3}J = 9.5$ Hz, 2H, H^1), 4.00 (t, $^{3}J = 9.5$ Hz, 2H, H^2) and 3.12 ppm (s, 1H, H^9).

^{13}C{^{1}H}-NMR ($CDCl_3$, 75 MHz): $\delta = 164.1$ (C^3), 131.3 (C^4), 129.2 (C^6), 127.9 (C^5), 125.1 (C^7), 81.0 (C^8), 67.8 (C^9), 54.8 (C^1) and 53.1 ppm (C^2).

7.5 Linker for native chemical ligation

7.5.1 Methyl 2-azidoacetate

Methyl 2-bromoacetate (62.32 g, 0.407 mol, 1 equiv) was dissolved in 65 mL MeOH and 31.7 g (0.488 mol, 1.2 equiv) of sodium azide in 28 mL in water were added upon which the solution heated up. The reaction was refluxed for 4 h and the solvent was removed at reduced pressure. After addition of 55 mL of water the precipitated solid dissolved and two phases were observed. Extraction with 4×45 mL Et_2O, drying of the combined organic phases over $MgSO_4$ and removal of the solvent yielded the product a slightly yellowish fluid.

Yield: 40.66 g (87%)
Empirical formula, molar mass: $C_3H_5N_3O_2$, M = 115.09 g/mol

ATR-IR: $\widetilde{\nu}$ = 2958 (C-H str)(w), 2104 (N_3)(vs), 1743 (C=O str)(vs), 1434 (m), 1357 (m), 1282 (s), 1207 (vs), 1182 (vs), 1002 (m), 921 (w), 846 (w), 734 (m) and 652 cm^{-1}(w).

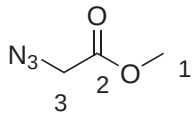

^{1}H-NMR (DMSO, 250 MHz): $\delta = 4.12$ (s, 2H, H^3) and 3.71 ppm (s, 3H, H^1).

$^{13}C\{^{1}H\}$-NMR (DMSO, 62.9 MHz): $\delta = 169.1$ (C^2), 52.1 (C^3) and 49.3 ppm (C^1).

7.5.2 Ethyl (2-azido)thioacetate

Ethyl(2-azido)thioacetate was prepared according to a reported procedure[430].
Under nitrogen and in a dried round-bottomed flask 5.458 g anhydrous aluminium chloride (40.9 mmol, 1.1 eq) were dissolved in 100 mL dry THF (caution, evolution of significant heat!). At RT, 10.45 g (70.0 mmol, 1.7 eq) (ethylthio)trimethylsilane (technical grade, 90 %) and 4.311 g methyl 2-azidoacetate were added and the mixture was refluxed for 1.5 h. The cooled mixture was poured into ice-chilled phosphate buffer (150 mL, pH 7). The product was extracted with Et_2O. After re-extraction of the organic phase with brine and drying over sodium sulfate the solvent was removed at reduced pressure. The product was purified over silica (eluent: pentane/ethyl acetate = 2/1) and was obtained as a yellowish fluid.

Yield: 3.537 g (72%)
Empirical formula, molar mass: $C_4H_7N_3OS$, M = 145.18 g/mol

ATR-IR: $\widetilde{\nu}$ = 2934 (C-H str)(w), 2099 (N_3), 1680 (C=O str)(vs), 1455 (m), 1415 (m), 1263 (s), 1083 (m), 1054 (m), 1005 (m), 970 (m), 897 (s), 786 (w), 675 (m) and 649 cm^{-1}(m).

Elemental analysis:

	C	H	N	S
theor.	33.09	4.86	28.94	22.09
exp.	32.93	4.93	29.22	21.04

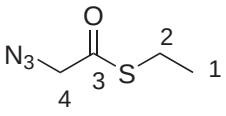

^{1}H-NMR ($CDCl_3$, 250 MHz): $\delta = 3.98$ (s, 2H, H^4), 2.93 (q, $^{3}J = 7$ Hz, 2H, H^2) and 1.27 ppm (t, $^{3}J = 7$ Hz, 3H, H^1).

^{13}C{^{1}H}-NMR ($CDCl_3$, 64 MHz): $\delta = 195.25$ (C^3), 58.00 (C^4), 23.32 (C^2) and 14.38 ppm (C^1).

7.5.3 Ethyl (2-bromo)thioacetate

Under stirring, 45 mL THF were added to an ice-chilled flask containing 2.446 g $AlCl_3$ (18.34 mmol, 1.1 equiv). In order to solubilize all $AlCl_3$, the mixture was heated shortly to 70 °C. After cooling to RT 2.568 g methyl bromoacetate (16.8 mmol, 1 equiv) and 2.416 g (ethylthio)trimethylsilane (24.6 mmol, 1.47 equiv) were added and the mixture was refluxed at 80 °C for 6 h. The turbid, colorless mixture was cooled to RT and poured into 180 mL of phosphate buffer (pH 7, CertiPur©). The product was extracted 3 times with 50 mL Et_2O. The combined organic fractions were dried over $MgSO_4$. After silica gel chromatography (eluent: cyclohexane/ethylacetate = 10/1 (v/v)) the product was obtained as a yellow liquid.

Yield: 2.018 g (66%)
Empirical formula, molar mass: C_4H_7BrOS, M = 183.07 g/mol

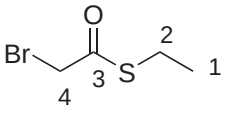

^{1}H-NMR($CDCl_3$, 250 MHz): δ = 4.02 (s, 2H, H^1), 2.95 (q, $^{3}J_{3,4}$=7.4 Hz, 2H, H^3), 1.29 ppm (t, $^{3}J_{4,3}$=7.4 Hz, 3H, H^4).

7.5.4 *tert*-Butyl hydroxycarbamate

To 23.86 g hydroxylamine hydrochloride (0.34 mol, 1.5 equiv) in 150 mL Et_2O 23.9 g Na_2CO_3 (0.23 mol, 1 equiv) in 5 mL H_2O were added. The solution was stirred for one hour at RT and subsequently cooled to 0 °C. During 1 h, 49.27 g di-*tert.*-butyl dicarbonate (0.23 mol, 1 equiv) in 50 mL Et_2O were added. The mixture was stirred for 10 h at RT. The resulting precipitate was filtered and the retentate washed with Et_2O. The filtrate was dried over Na_2SO_4 and the solvent was removed under reduced pressure. After recrystallization from hexane the title compound was obtained as colorless crystalline solid.

Yield: 25.79 g (84%)
Empirical formula, molar mass: $C_5H_{11}NO_3$, M = 133.15 g/mol

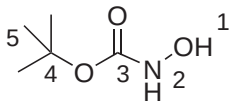

^{1}H-NMR($CDCl_3$, 250 MHz): $\delta = 7.01$ (br, 1H, H^2), 6.59 (br, 1H, H^1) and 1.48 ppm (s, 9H, H^5).

$^{13}C\{^1H\}$-NMR($CDCl_3$, 63 Hz):$\delta = 158.9$ (C^3), 82.0 (C^4) and 28.1 ppm (C^5).

7.5.5 Methyl (2-(N-*tert*-butyloxycarbonyl)aminooxy)acetate

To a solution of 5.0 g *tert*-Butyl hydroxycarbamate (38 mmol, 1 equiv) in 20 mL DCM 5.0 g K_2CO_3 (80 mmol, 2.1 equiv) and 3.5 mL methyl 2-bromoacetate (38 mmol, 1 equiv) were added. The mixture was stirred for 24 h. After washing thrice with 50 mL

1 M HCl and 30 mL brine until the mixture was brownish. The combined organic phases were dried over Na_2SO_4 and the solvent was removed under reduced pressure. Purification by chromatography (silica) gave the product as a colorless crystalline solid.

Yield: 3.29 g (42%)
Empirical formula, molar mass: $C_8H_{15}NO_5$, M = 205.21 g/mol

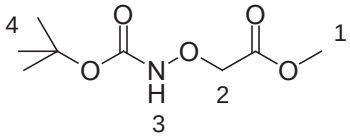

^{1}H-NMR($CDCl_3$, 250 MHz): δ = 7.76 (br, 1H, H^3), 4.44 (s, 2H, H^2), 3.78 (s, 3H, H^1) and 1.47 ppm (s, 9H, H^4).

7.6 Polymerizations

7.6.1 Linear homo- and copolymers

PMeOx$_{48}$BocPip, P1

Initiator:	MeOTf	63 mg (0.38 mmol, 1 equiv)
Monomer:	MeOx	1.56 g (18.3 mmol, 48.2 equiv)
Terminating reagent:	N-Boc-piperazine	188 mg (1 mmol, 2.63 equiv)

Synthesis according to **GSP1** (7.2.1).

Yield: 1.37 g (84 %)
Empirical formula, molar mass: $C_{202}H_{356}N_{50}O_{50}$, M = 4285.29 g/mol

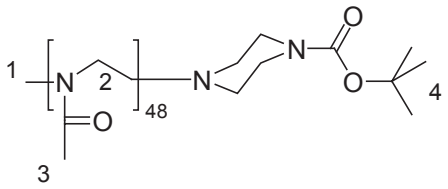

^{1}H-NMR (D_2O, 300 MHz): δ = 3.45 (br, 240H, H^2), 2.98/2.84 (br, 3H, H^1), 2.00 (br, 180H, H^3) and 1.37 ppm (s, 9H, H^4).

GPC(DMAc): M_n = 5545 g/mol, PDI = 1.17 (1), M_n = 6580 g/mol, PDI = 1.16 (2).

HPLC: 10%B $\longrightarrow$ 100%B(30 min), t_r = 10.2 min

PEtOx$_{43}$BocPip, P2

Initiator:	MeOTf	39 mg (0.24 mmol, 1 equiv)
Monomer:	EtOx	1.003 g (10.1 mmol, 43 equiv)
Terminating reagent:	N-Boc-piperazine	125 mg (0.67 mmol, 2.8 equiv)

Synthesis according to **GSP1** (7.2.1).

Yield: 0.94 g (88 %)
Empirical formula, molar mass: $C_{225}H_{407}N_{45}O_{45}$, M = 4462.91 g/mol

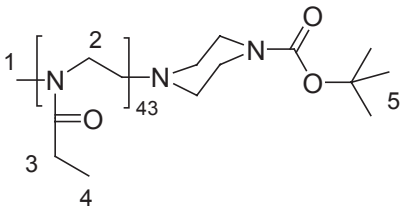

^{1}H-NMR ($CDCl_3$, 300 MHz): δ = 3.39 (br, 222H, H^2), 2.96/2.90 (br, 3H, H^1), 2.34 (br, 124H, H^3), 1.39 (s, 9H, H^5) and 1.06 ppm (br, 170H, H^4).

GPC(DMAc): M_n = 6230 g/mol, PDI = 1.15

HPLC: 10%B $\longrightarrow$ 100%B(30 min), t_r = 16.1 min

P(MeOx$_{51}$EOB$_4$)Pip, P3

Initiator:	MeOTf	23 mg (0.14 mmol, 1.0 equiv)
Monomer:	MeOx	605 mg (7.1 mmol, 50.7 equiv)
	EOB	102 mg (0.55 mmol, 3.9 equiv)
Terminating reagent:	piperazine	238 mg (2.8 mmol, 20 equiv)

Synthesis according to **GSP1** (7.2.1).

Yield: 677 mg (95 %)
Empirical formula, molar mass: $C_{245}H_{429}N_{57}O_{63}$, M = 5181.37 g/mol

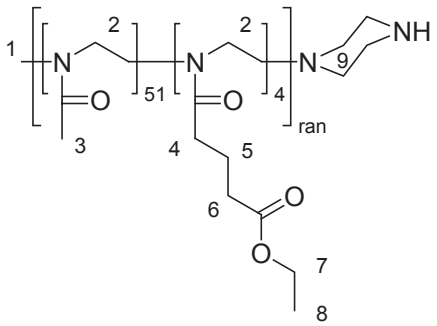

^{1}H-NMR (D_2O, 250 MHz): δ = 4.08 (q, ^3J = 7.17 Hz, 8H, H^6), 3.45 (br, 228H, H^2), 2.6 (br, 3H, H^9), 2.34 (br, 17H, $H^{4,6}$), 2.00 (br, 170H, H^3), 1.76 (br, 10H, H^5) and 1.17 ppm (t, ^3J = 7.13 Hz, 10H, H^8).

GPC (DMAc): M_n = 6777 g/mol, PDI = 1.16

HPLC:10%B $\longrightarrow$ 100%B(30 min), t_r = 10.5 min

P(EtOx$_{43}$EOB$_4$)Pip, P4

Initiator:	MeOTf	22 mg (0.13 mmol, 1.0 equiv)
Monomer:	EtOx	573 mg (5.78 mmol, 43 equiv)
	EOB	106 mg (0.57 mmol, 4.2 equiv)
Terminating reagent:	piperazine	228 mg (2.7 mmol, 20 equiv)

Synthesis according to **GSP1** (7.2.1).

Yield: 413 mg (60 %)
Empirical formula, molar mass: $C_{256}H_{459}N_{49}O_{55}$, M = 5103.68 g/mol

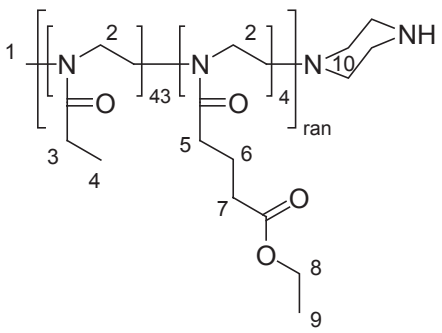

^{1}H-NMR: δ = 4.07 (q, ^3J = 7.25 Hz, 4H, H^8), 3.44 (br, 220H, H^2), 2.66 (br, 7H, H^{10}), 2.31 (br, 127H, H^{3,5,7}), 1.74 (br, 10H, H^6), 1.17 (t, ^3J = 7.13 Hz, 3H,H^9) and 0.97 ppm (br, 162H, H^4).

GPC (DMAc): M_n = 6500 g/mol, PDI = 1.23

HPLC:10%B $\longrightarrow$ 100%B(30 min), t_r = 15.7 min

2-(Hex-5-ynoic acid methylamide)ethyl-poly(2-methyl-2-oxazoline), PynOxPMeOx$_{20}$BocPip, P5

Initiator:	PynOxOTf	23 mg (76.3 μmol, 1.0 equiv)
Monomer:	MeOx	134 mg (1.57 mmol, 20 equiv)
Terminating reagent:	N-Boc-piperazine	58 mg (0.32 mmol, 4 equiv)

Synthesis according to **GSP1** (7.2.1).

Yield: 155 mg (99 %)
Empirical formula, molar mass: $C_{98}H_{171}N_{23}O_{23}$, M = 2040 g/mol

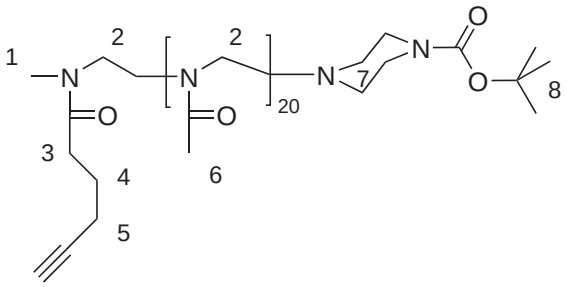

^{1}H-NMR (D_2O, 250 MHz): δ = 3.45 (br, 127H, H^2), 3.01/2.86 (m, 3H, H^1), 2.45 (br, 8H, $H^{3,5,7}$) 2.00 (br, 88H, H^6), 1.65 (br, 2H, H^4) and 1.37 ppm (s, 11H, H^8).

GPC (DMAc): M_n = 3190, PDI = 1.06

MALDI-TOF: M_n = 2055.5, PDI = 1.04

P(MeOx$_{45}$PynOx$_5$)BocPip, P6

Initiator:	MeOTf	50 mg (0.3 mmol, 1.0 equiv)
Monomers:	MeOx	1.170 g (13.7 mmol, 45 equiv)
	PynOx	208 mg (1.52 mmol, 5 equiv)
Terminating reagent:	N-Boc-piperazine	175 mg (0.94 mmol, 3.2 equiv)

The initiator and monomers were added to 7.5 mL ACN in a microwave test tube under nitrogen. Heating to 135 °C for 20 min was performed by mircowave heating (150 W). After cooling to RT the terminating reagent was added. Further handling was according to GSP1 (7.2.1).

Yield: 1.345 g (94%)
Empirical formula, molar mass: $C_{230}H_{390}N_{52}O_{52}$, M = 4716 g/mol

ATR-IR: $\widetilde{\nu}$ = 3282 (≡C-H str)(w), 2938 (C-H str)(m), 1618 (C=O str, amide I)(vs), 1421 ($\delta(CH_2\text{-}CO)$(vs) and 638 cm^{-1} (≡C-H wag)(w).

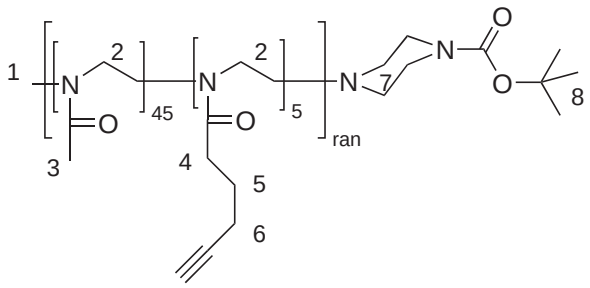

^{1}H-NMR (D_2O, 250 MHz): δ = 3.46 (br, 273H, H^2), 3.02/2.86 (m, 1H, H^1), 2.46 (br, 15H, H^4,7), 2.19 (br, 12H, H^6), 2.00 (br, 190H, H^3), 1.69 (br, 11H, H^5) and 1.37 ppm (s, 9H, H^8).

GPC (DMAc): M_n = 7893 g/mol, 1.06

HPLC:10%B ⟶ 100%B(30 min), t_r = 16.2 min
MALDI-TOF: M_n = 4956.3 g/mol, PDI = 1.03

P(MeOx$_{35}$PynOx$_{12}$)BocPip, P7

Initiator:	MeOTf	13 mg (79 μmol, 1.0 equiv)
Monomers:	MeOx	234 mg (2.7 mmol, 35 equiv)
	PynOx	135 mg (0.98 mmol, 12 equiv)
Terminating reagent:	N-Boc-piperazine	58 mg (1.8 mmol, 4 equiv)

Synthesis according to **GSP1** (7.2.1).

Yield: 315 mg (81%)
Empirical formula, molar mass: $C_{246}H_{397}N_{49}O_{49}$, M = 4825.08 g/mol

ATR-IR: $\widetilde{\nu} = 3261$ (≡C-H str)(w), 2935 (C-H str)(w), 1626 (C=O str, amide I)(vs), 1419 ($\delta(CH_2\text{-}CO)$(s) and 638 cm^{-1} (≡C-H wag)(w).

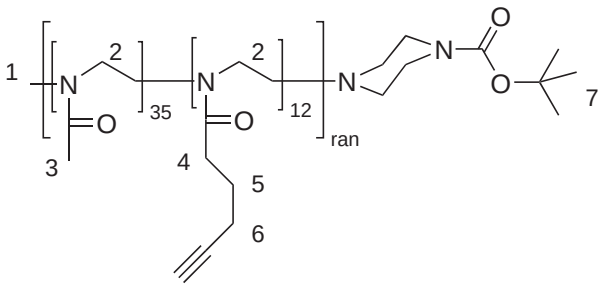

^{1}H-NMR (D_2O, 250 MHz): $\delta = 3.46$ (br, 240H, H^2), 3.02/2.86 (m, 3H, H^1), 2.41 (br, 35H, H^4), 2.20 (br, 35H, H^6), 2.01 (br, 135H, H^3), 1.70 (br, 33H, H^5) and 1.37 ppm (s, 9H, H^7).

GPC (DMAc): M_n = 6962 g/mol, 1.17

P(EtOx$_{20}$PynOx$_2$)BocPip, P8

Initiator:	MeOTf	0.1 g (0.6 mmol, 1 equiv)
Monomers:	MeOx	1.19 g (12.0 mmol, 20 equiv)
	PynOx	182 mg (1.33 mmol, 2.2 equiv)
Terminating reagent:	N-Boc-piperazine	188 mg (1 mmol, 2.63 equiv)
Solvent	ACN	15 mL
GC-standard	Chlorobenzene	300 μL

Before polymerization, an aliqout of 5 mL (4.053 g, 30 % of reaction mixture) was taken for parallel GC-online kinetic measurement. Polymerization of the remaining mixture

was according to **GSP1** (7.2.1) at 80 °C.

Yield: 953 mg (92 %)
Empirical formula, molar mass: $C_{126}H_{222}N_{24}O_{24}$, M = 2457 g/mol

ATR-IR: $\widetilde{\nu}$ = 3247 (≡C-H str)(w), 2929 (C-H str)(m), 1630 (C=O str, amide I)(vs), 1418 ($\delta(CH_2$-CO)(vs) and 638 cm^{-1} (≡C-H wag)(w).

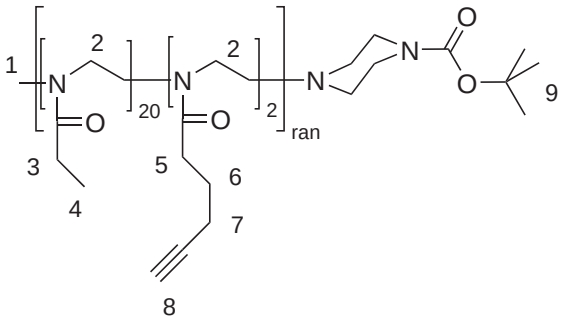

^{1}H-NMR ($CDCl_3$, 250 MHz): δ = 3.41 (br, 88H, H^2), 2.98/2.92 (m, 3H, H^1), 2.37 (br, 58H, $H^{3,5,7}$, H^{Pip}), 1.99 (br, 3H, H^8), 1.80 (br, 4H, H^6), 1.40 (s, 9H, H^9), 1.07 ppm (br, 57H, H^4).
GPC (DMAc): M_n = 4004 g/mol, PDI = 1.04

PPynOx$_{23}$BocPip, P9

Initiator:	MeOTf	27 mg (0.17 mmol, 1.0 equiv)
Monomer:	PynOx	523 mg (3.81 mmol, 23 equiv)
Terminating reagent:	N-Boc-piperazine	90 mg (0.48 mmol, 3 equiv)

Synthesis according to **GSP1** (7.2.1).

Yield: 400 mg (72 %)
Empirical formula, molar mass: $C_{194}H_{273}N_{25}O_{25}$, M = 3355 g/mol

ATR-IR: $\widetilde{\nu} = 3282$ (≡C-H str)(w) and 2913 (C-H str)(w), 1627 (C=O str, amide I)(vs), 1423 (δ(CH_2-CO)(s), 633 cm^{-1} (≡C-H wag)(s).

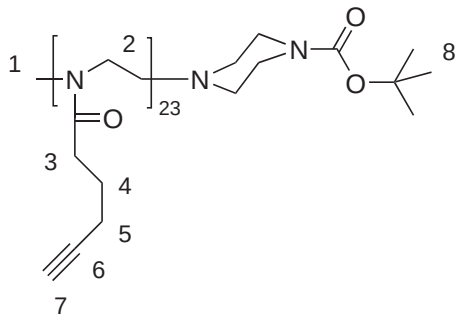

^{1}H-NMR (CD_3OD, 250 Hz): $\delta = 3.48$ (br, 100H, H^2), 3.04/2.90 (br, 3H, H^1), 2.46 (br, 53H, H^3), 2.21 (br, 55H, H^5), 1.76 (br, 54H, H^4) and 1.39 ppm (s, 5H, H^8).

GPC (DMAc): M_n = 6161, PDI = 1.09

P(MeOx$_{47}$DPOx$_5$)Pip, P10

Initiator:	MeOTf	26 mg (0.16 mmol, 1.0 equiv)
Monomers:	MeOx	640 mg (7.52 mmol, 47 equiv)
	DPOx	145 mg (0.783 mmol, 4.9 equiv)
Terminating reagent:	piperazine	275 mg (3.2 mmol, 20 equiv)

Polymerization was performed according GSP1 (7.2.1).

Yield: 0.8 g (99 %)
Empirical formula, molar mass: $C_{238}H_{416}N_{54}O_{62}$, M = 5026 g/mol

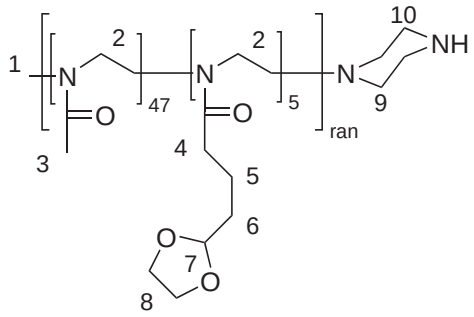

^{1}H-NMR (D_2O, 250 MHz): $\delta = 4.89$ (br, 6.5H, H^1), 3.92 (br, 27H, H^8), 3.45 (br, 248H, H^2), 3.02/2.96 (br, 3H, H^1), 2.87 (br, 3H, H^9), 2.55 (br, 4H, H^{10}), 2.35 (br, 13H, H^4), 2.04 (br, 182H, H^3) and 1.64 ppm (br, 30H, $H^{5,6}$).

GPC (DMAc): M_n = 9428 g/mol, PDI = 1.09

P(EtOx$_{19}$DPOx$_3$)Pip, P11

Initiator:	MeOTf	105 mg (0.640 mmol, 1.0 equiv)
Monomers:	EtOx	1.194 g (12.04 mmol, 18.8 equiv)
	DPOx	324 mg (1.75 mmol, 2.7 equiv)
Terminating reagent:	piperazine	1.15 g (13.4 mmol, 20.9 equiv)
Solvent	ACN	10.4 g
GC-standard	Chlorobenzene	100 μL

Before polymerization, an aliqout of 2.605 g (21.7 % of reaction mixture) was taken, the internal standard was added and the mixture was used for parallel GC-online kinetic measurement. Polymerization of the remaining mixture was according to **GSP1**(7.2.1) at 80 °C.

Yield: 1.113 g (90 %)
Empirical formula, molar mass: $C_{127}H_{228}N_{24}O_{28}$, M = 2539 g/mol

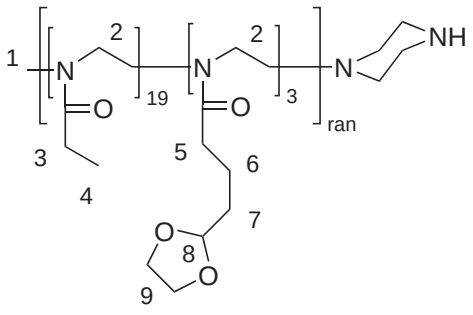

^{1}H-NMR (D_2O): $\delta = 4.85$(br, 2h, H^8), 3.89 (br, 10H, H^9), 3.44 (br, 86H, H^2), 2.97/2.85 (m, 3H, H^1), 2.29 (br, 46H, $H^{3,5}$), 1.60 (br, 9H, $H^{6,7}$) and 0.98 ppm (br, 63H, H^4).

GPC (DMAc): 3560 g/mol, PDI = 1.06

HPLC: 10%B $\longrightarrow$ 100%B(30 min), t_r = 15.5 min

Polymerizations for Kinetik Investigations

Some polymerization reactions were performed only for kinetic measurements. These were P($EtOx_{19}PynOx_2$) **P12**, P($MeOx_{19}PynOx_2$) **P13** and P($MeOx_{20}PynOx_5$) **P14**. The reagents and solvents are combined in a 10 mL crimp vial and the crimp vials were sealed in the glove box under dry and inert atmosphere.

Polymer	m (EtOx/MeOx) [mg]	m (**2**) [mg]	m (MeOTf) [mg]	V (ACN) [mL]	V (PhCl) [mL]
P12	187	26.7	16	5	0.3
P13	161	26.6	17	5	0.3
P14	813	305	80	8	0.6

7.6.2 Star-like homo- and copolymers

P[(EtOx$_{20}$DPOx$_2$)-bl-(EtOx$_{30}$PynOx$_3$)]^4, P20

Initiator:	**I3**	149 mg (0.224 mmol, 1.0 equiv)
Monomers:		
1stBlock	EtOx	1.79 g (18.08 mmol, 80 equiv)
	1	324 mg (1.75 mmol, 7.8 equiv)
2ndBlock	EtOx	2.29 g (23.09 mmol, 120 equiv)
	2	317 mg (2.31 mmol, 12 equiv)
Termination reagent:	piperazine	1.086 g(12.6 mmol, 80 equiv)
Solvent:	ACN	15.53 g (19.75 mL)
GC standard:	PhCl	370 μL

The initiator and the monomers for the first block were dissolved in ACN. An aliquot of 2.615 g (14.7 % of the batch) was removed for a GC kinetic study and sealed in a crimp vial with 100 μL PhCl. Both portions were polymerized at 80 °C for 6 d. After cooling to 0 °C and removal of 66 mg of the main reaction mixture (for GPC analysis) the monomers of the second block and 300 mg PhCl were added. Again an aliquot of 2.653 g (14.7 % of the batch) were removed and sealed in a crimp vial for GC kinetic measurement. The second block was polymerized at 85 °C. After two days the typical termination and work-up procedures were performed and the product is obtained as a colorless solid.

Yield: 3.655 g (99 %)
Empirical formula, molar mass: $C_{1135}H_{2027}N_{228}O_{224}$, M = 22453 g/mol

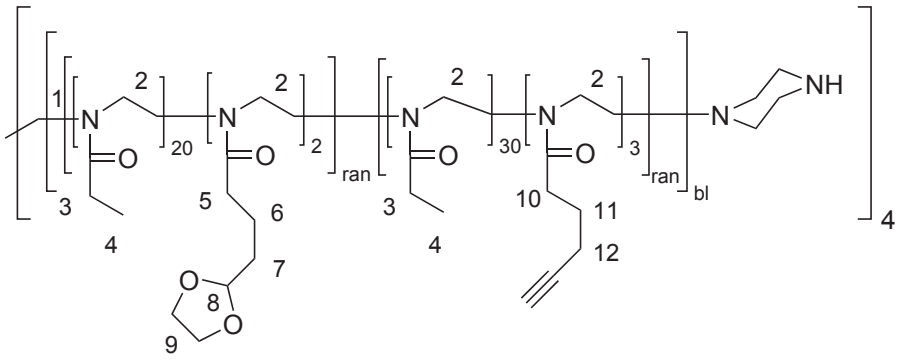

^{1}H-NMR (D_2, 250 MHz): $\delta = 4.83$ (br, 8H, H^8), 3.88 (br, 37H, H^9), 3.43 (br, 894H, H^2), 2.76 (br, 6H, H^1), 2.28 (br, 509H, $H^{3,5,10,12}$), 1.66/1.58 (br, 65H, $H^{6,7,11}$) and 0.96 ppm (br, 655H, H^4).

First Block: GPC (DMAc): $M_n = 3712$, PDI = 1.32 (bimodal)
GPC (DMAc): $M_n = 9395$, PDI = 1.22 (bimodal)
GPC ($CHCl_3$, RI): $M_n = 5145$, PDI = 1.30 (bimodal)
GPC ($CHCl_3$, UV): $M_n = 4555$, PDI = 1.45

HPLC: 10%B $\longrightarrow$ 100%B(30 min), t_r = 18.7 min

Polymerizations for kinetic investigations

According to the procedure described above (see 7.6.1), samples for the kinetic measurements with multifunctional initiators were prepared. The polymerizations were performed at 85 °C.

Polymer	m (MeOx) [g]	Initiator	m (I) [mg]	V (ACN) [mL]	V (PhCl)
P15	1.12	MeOTf	27	16.8	1
P16	0.51	**I3**	50	7.66	0.55
P17	1.123	**I3**	111	16.92	1
P18	1.085	**I1**	55	16.4	1
P19	1.076	**I2**	81	17.1	0.95

7.7 Polymer analog modifications

7.7.1 Boc-deprotection

PMeOx$_{48}$Pip, P21

Deprotection of 169 mg **P1** in 1.8 mL DeMix was performed according to **GSP2** (7.2.2).

Yield: 109 mg (66 %)
Empirical formula, molar mass: $C_{197}H_{348}N_{50}O_{48}$, M = 4185.18 g/mol

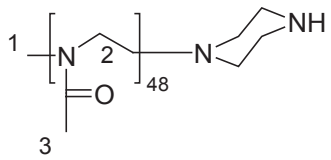

^{1}H-NMR ($CDCl_3$, 300 MHz): δ = 3.40 (br, 240H, H^2), 2.98 (br, 3H, H^1) and 2.08 ppm (br, 183H, H^3).

GPC(DMAc): M_n = 6360 g/mol, PDI = 1.22

HPLC: 10%B $\longrightarrow$ 100%B(30 min), t_r = 9.1 min

PEtOx$_{43}$Pip, P22

Deprotection of 0.21 g **P2** in 1.8 mL DeMix was performed according to **GSP2** (7.2.2).

Yield: 0.18 mg (88 %)
Empirical formula, molar mass: $C_{220}H_{299}N_{45}O_{43}$, M = 4362.8 g/mol

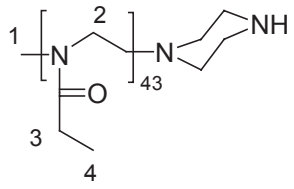

^{1}H-NMR ($CDCl_3$, 300 MHz): δ = 3.38 (br, 222H, H^2), 2.95/2.89 (br, 3H, H^1), 2.33 (br, 121H, H^3) and 1.04 ppm (br, 168H, H^4).

GPC(DMAc): M_n = 6670 g/mol, PDI = 1.18

HPLC: 10%B $\longrightarrow$ 100%B(30 min), t_r = 14.8 min

P(MeOx$_{45}$PynOx$_5$)Pip, P23

Deprotection of 0.3 g **P6** in 3 mL DeMix was performed according to **GSP2** under sonication (7.2.2).

Yield: 0.27 g (92 %)
Empirical formula, molar mass:$C_{225}H_{382}N_{52}O_{50}$, M = 4615.76 g/mol

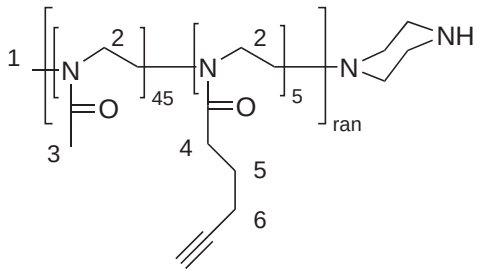

^{1}H-NMR (CD_3OD, 300 MHz): δ = 3.50 (br, 318H, H^2), 3.05/2.9 (m, 3H, H^1), 2.44 (br, 11H, H^6) 2.23 (br, 8H, H^4), 2.05 (br, 217H, H^3) and 1.73 ppm (br, 17H, H^5).

GPC (DMAc): M_n = 7127 g/mol, PDI = 1.04

HPLC: 10%B $\longrightarrow$ 100%B(30 min), t_r = 14.4 min

P(EtOx$_{20}$PynOx$_2$)Pip, P24

Deprotection of P(EtOx$_{20}$PynOx$_2$)BocPip (533 mg, 0.22 mmol) was performed in 3 mL DeMix according to **GSP2** (7.2.2).

Yield: 477 mg (93 %)
Empirical formula, molar mass: $C_{121}H_{214}N_{24}O_{22}$, M = 2357 g/mol

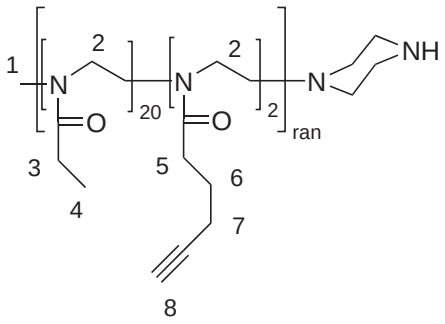

^{1}H-NMR ($CDCl_3$, 250 MHz): δ = 3.44 (br, 80H, H^2), 3.02/3.94 (m, 3H, H^1), 2.38 (b, 46H, H^{3,5,7}), 2.01 (br, 2H, H^8), 1.81 (br, 5H, H^6) 1.09 ppm (br, 57H, H^4).

GPC (DMAc): M_n = 3990 g/mol, PDI = 1.06

HPLC: 10%B $\longrightarrow$ 100%B(30 min), t_r = 18.2 min; 10%B $\longrightarrow$ 80%B(30 min), t_r = 17.1 min; 0%B $\longrightarrow$ 60%B(30 min), t_r = 25.9 min

MALDI-TOF-TOF: M_n = 2549 g/mol, PDI = 1.02

7.7.2 Click-chemistry

P(MeOx$_{45}$^{Triaz}Ac$_5$)BocPip, P25

P6 (303 mg, 64 μmol, 1 equiv) was dissolved in 5 mL H_2O and 42 mg azidoacetic acid (42 mg, 0.37 mmol, 5.7 equiv) were added. After addition of 6.7 mg sodium ascorbate (33.8 μmol, 0.53 equiv) and 4.8 mg copper(II) sulfate pentahydrate (19 μmol, 0.3 equiv), the solution was stirred at RT for 2 days and dialysed. After lyophylisation the product (290 mg, 85 %) was still slightly colored. Of this colored product, 257 mg were dissolved in 4 mL $CHCl_3$/MeOH (1/1, v/v) and after filtration over celite, precipitation from diethylether and subsequent lyophylisation, the product was obtained as a colorless solid.

Yield: 218 mg (73 %)
Empirical formula, molar mass: $C_{245}H_{415}N_{67}O_{62}$, M = 5291.33 g/mol

ATR-IR: $\widetilde{\nu}$ = 2915 (C-H str)(s), 1737 (C=O str, ester)(m), 1630 (C=O str, amide I)(vs), 1423 (δ(CH_2-CO))(vs), 720 cm^{-1} (r(CH_2)).

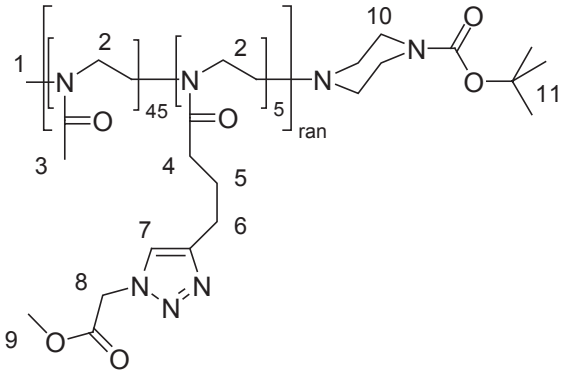

^{1}H-NMR (D_2O, 300 MHz): δ = 7.78 (br, 13H, H^7), 5.27 (br, 27H, H^8), 3.71 (br, 41H, H^9), 3.43 (br, 240H, H^2), 2.92/2.82 (m, 3H, H^1), 2.67 (br, 26H, $H^{6,10}$), 2.27 (br, 34H, H^4), 2.01 (br, 161H, H^3) and 1.37 ppm (br, 7H, H^{11}).

GPC (DMAc): M_n = 7740 g/mol, PDI = 1.07

P(MeOx$_{45}$^{Triaz}TMS$_5$)BocPip, P26

P6 (100 mg, 21 μmol, 1 equiv) and 20 mg of (trimethylsilyl)methyl azide (0.15 mmol, 7.3 equiv) were added to 1 mL of a 1/1 (v/v) mixture of *tert*-BuOH and water . Sodium ascorbate (2.2 mg, 11 μmol, 0.5 equiv) and 1.6 mg $CuSO_4 \times 5\,H_2O$ (6.4 μmol, 0.3 equiv) were added and the mixture was stirred over night. Exchange of the solvent with 2 mL of a 1/1 mixture of MeOH/$CHCl_3$ (v/v) and precipitation from 20 mL cold diethylether yielded the product as a colorless solid after lyophylization.

Yield: 54 mg (48 %)
Emperical formula, molar mass: $C_{250}H_{445}N_{67}O_{53}Si_5$, M = 5362.05 g/mol

ATR-IR: $\widetilde{\nu}$ = 2937 (C-H str)(m), 1616 (C=O str, amide I)(vs), 1423 (δ(CH_2-CO))(s), 730 cm^{-1} (r(CH_2))(w).

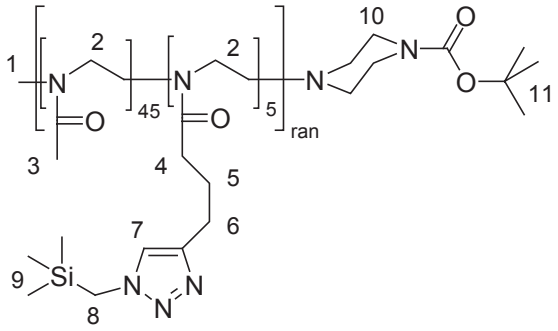

^{1}H-NMR (D_2O, 300 MHz): δ = 7.63 (br, 4H, H^7), 3.96 (br, 12H, H^8), 3.45 (br, 310H, H^2), 2.91/2.82 (m, 3H, H^1), 2.64 - 2.50 (br, 16H, $H^{6,10}$), 2.23 (br, 17H, H^4), 2.00 (br, 240H, H^3), 1.37 (br, 9H, H^{11}) and -0.01 ppm (br, 45H, H^9).

GPC (DMAc): M_n = 8430 g/mol, PDI = 1.06

P(MeOx$_{45}$^{Triaz}ThioAc$_5$)BocPip, P27

P6 (49.7 mg, 10.5 μmol, 1 equiv), 9.7 mg **5** (67 μmol, 6.4 equiv), 1.1 mg $CuSO_4 \times 5\,H_2O$ (4.4 μmol, 0.4 equiv) and 1.7 mg sodium ascorbate (8.6 μmol, 0.8 equiv) were dissolved in 2 mL degassed H_2O and stirred over night at RT. After gel filtration and lyophylisation a slightly yellowish solid was obtained.

Yield: 40 mg (70 %)
Empirical formula, molar mass: $C_{250}H_{425}N_{67}O_{57}S_5$, M = 5441.79 g/mol

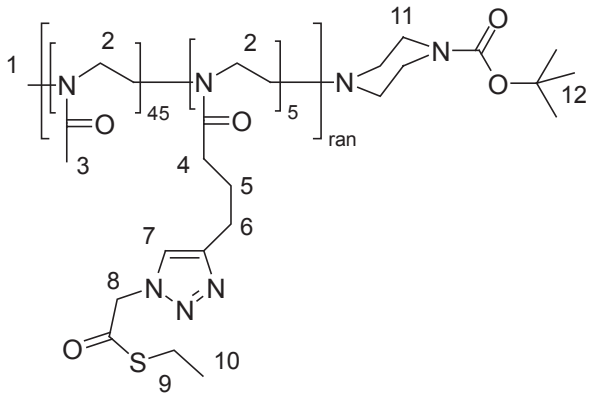

^{1}H-NMR ($CDCl_3$, 250 MHz): δ = 7.55 (br, 5H, H^7), 5.25 (br, 5H, H^8), 3.45 (br, 200H, H^2), 2.93 (br, 9H, H1,9),2.77 (br, 7H, $H^{1,9}$), 2.39 (br, 31H, $H^{4,6,11}$), 2.10 (br, 158H, H^3), 1.44 (br, 9H, H^{12}) and 1.26 ppm (br, 12H, H^{10}).

GPC (DMAc): M_n = 7031 g/mol, PDI = 1.15

P(EtOx$_{20}$^{Triaz}ThioAc$_2$)Pip, P28

P24 (124 mg, 53 μmol, 1 equiv) and 29.3 mg **5** (0.2 mmol, 3.8 equiv) were dissolved in 2.5 mL H_2O/*t*-BuOH (1/1). After addition of 13.2 mg $CuSO_4 \times H_2O$ (53 μmol, 1 equiv) and 16 mg sodium ascorbate (81 μmol, 1.5 equiv), the reaction vessel was

purged shortly with argon and sealed. The solvents were removed and the residue was collected in 1 mL of a 1/1 mixture of $CHCl_3$ and MeOH (v/v). After addition of 46 mg 4,4´-dinonyl-2,2´dipyridyl (113 μmol, 2, equiv), the mixture was stirred for 15 min, filtered and the product precipitated from cold diethyl ether. This procedure was repeated twice (adding 11 mg 4,4´-dinonyl-2,2´dipyridyl the second time) and the product was obtained as a colorless solid after lyophylization.

Yield: 114 mg (84 %)
Empirical formula, molar mass: $C_{129}H_{228}N_{30}O_{24}S_2$, M = 2647.51 g/mol

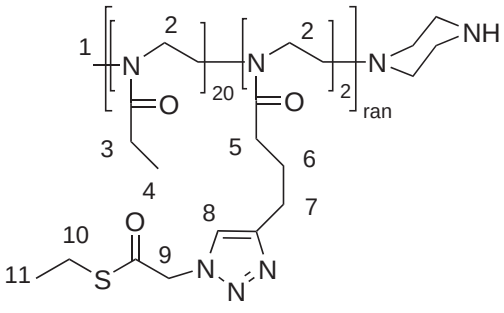

^{1}H-NMR (D_2O, 250 MHz): δ = 7.56 (br, 2H, H^8), 5.25 (br, 3H, H^9), 3.44 (br, 88H, H^2), 3.00/2.94 (br, 9H, $H^{1,10}$), 2.38 (br, 50H, $H^{3,5,7}$), 2.00 (br, 4H, H^6), 1.25 (br, 11H, H^{11}) and 1.10 ppm (br, 65H, H^4).

GPC (DMAc): M_n = 3276 g/mol, PDI = 1.11

HPLC: 10%B $\longrightarrow$ 100%B(30 min), t_r = 15.2 min

7.7.3 Chelator coupling

PMeOx$_{48}$PipBnDOTA, P30

P21	15 mg (3.57 μmol, 1 equiv)
p-SCN-Bn-DOTA	5.1 mg (7.3 μmol, 2 equiv)

K_2CO_3	∼10 mg
MeOH	500 µL

Coupling was performed according to **GSP3** (7.2.3) as described recently[417].

Yield: 10.2 mg (60 %)
Empirical formula, molar mass: $C_{209}H_{360}N_{52}O_{53}S$, M = 4481.48 g/mol

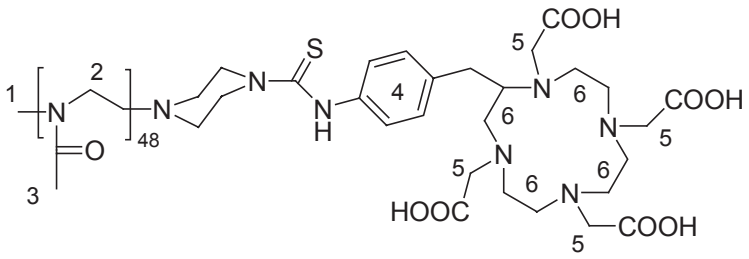

^{1}H-NMR (D_2O, 250 MHz): δ = 7.22/7.14 (br, 3H, H^4), 3.87 (br, 3H, H^5), 3.47 (br, 223H, H^2), 3.16 (br, 10H, H^6), 2.96/2.84 (br, 3H, H^1) 2.62 (br, 5H, H^7) and 2.00 ppm (br, 161, H^3).

GPC (DMAc): M_n = 7282 g/mol, PDI = 1.45

HPLC: 10%B ⟶ 100%B(30 min), t_r = 9.2 min.

PEtOx$_{43}$PipBnDOTA, P31

P22	15.7 mg (3.6 µmol, 1 equiv)
p-SCN-Bn-DOTA	5.7 mg (8.2 µmol, 2.3 equiv)
K_2CO_3	∼10 mg
MeOH	500 µL

Coupling was performed according to **GSP3** (7.2.3) as described recently[417].

Yield: 11 mg (62%)
Empirical formula, molar mass: $C_{244}H_{432}N_{50}O_{51}S$, M = 4914.41 g/mol

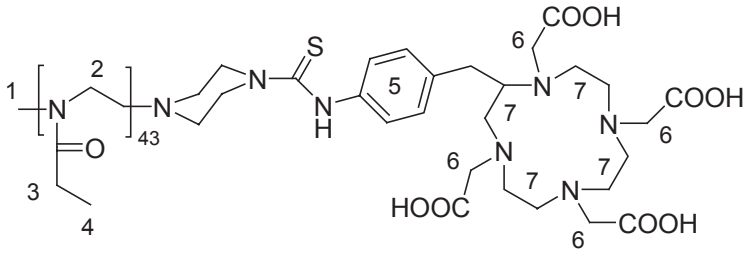

^{1}H-NMR (D_2O, 250 MHz): δ = 7.26/7.16 (br, 4H, H^5), 3.95 (br, 8H, H^6), 3.47 (br, 232H, H^2), 3.2 (br, 18H, H^7), 3.01/2.88 (br, 3H, H^1), 2.67 (br, 8H, H^8), 2.32 (br, 119H, H^3) and 1.02 ppm (180H, H^4).

GPC (DMAc): M_n = 8093 g/mol, PDI = 1.45

HPLC: 10%B $\longrightarrow$ 100%B(30 min), t_r = 14.5 min.

P(MeOx$_{45}$PynOx$_5$)PipBnDOTA, P32

P23	100 mg	(22 μmol, 1 equiv)
p-SCN-Bn-DOTA × 4HCL	18 mg	(26 μmol, 1.2 equiv)
K_2CO_3	∼ 30 mg	
MeOH	2 mL	

Preparation of **P32** was according to **GSP3** (7.2.3). Purification was performed by dialysis against water instead of the sephadex G25 column.

Yield: 59 mg (54 %)
Empirical formula, molar mass: $C_{249}H_{415}N_{57}O_{58}S$, M = 5167 g/mol

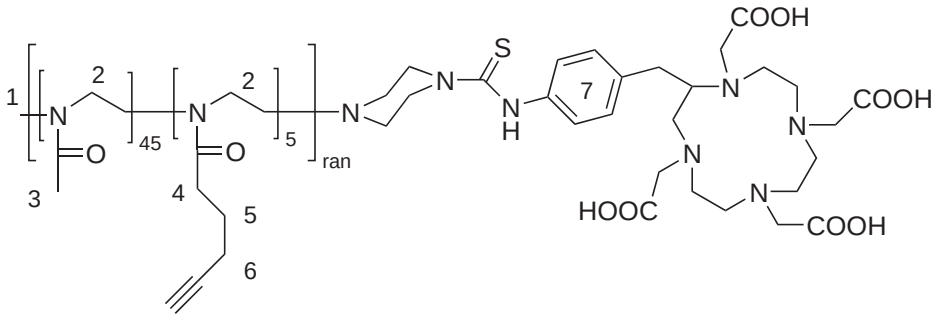

^{1}H-NMR (D_2O, 250 MHz): δ = 7.21 (br, 4H, H^7), 4.0 (br, 4H, H^8), 3.45 (br, 221H, $H^{2,9}$, 3.01/2.87 (br, 3H, H^1), 2.33 (br, 12H, H^6), 2.19 (br, 7H, H^4), 2.00 (br, 135H, H^3) and 1.70 ppm (br, 9H, H^5).

GPC (DMAc): M_n = 22705 g/mol, PDI = 1.03; M_n = 6772 g/mol, PDI = 1.03

HPLC:10%B $\longrightarrow$ 100%B(30 min), t_r = 14.7 min

P($EtOx_{20}PynOx_2$)PipBnDOTA, P33

P24	50 g	(21 μmol, 1 equiv)
p-SCN-Bn-DOTA×4HCl	18 mg	(26 μmol, 1.2 equiv)
K_2CO_3	$\sim$4 mg	
MeOH	250 μL	

P($EtOx_{20}PynOx_2$)PipDOTA was prepared according to **GSP3** (7.2.3).

Yield: 42 mg (68 %)
Empirical formula, molar mass: $C_{145}H_{247}N_{29}O_{30}S$, M = 2909.75 g/mol

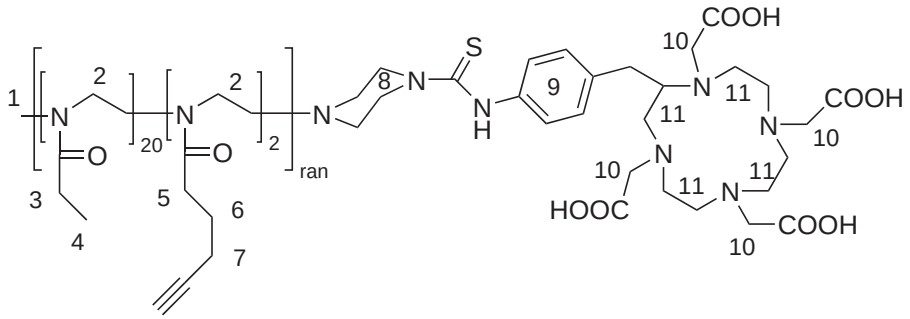

^{1}H-NMR (D_2O, 500 MHz): $\delta = 7.24/7.14$ (br, 3H, H^9), 3,92 (br, 2H, H^{10}), 3.43 (br, 101H, $H^{2,11}$), 2.97/2.83 (m, 3H, H^1), 2.67 (br, 3H, H^8), 2.27 (br, 43H, $H^{3,5,7}$), 1.67 (br, 5H, H^6) and 0.97 ppm (br, 45H, H^4).

GPC (DMAc): M_n = 3895 g/mol, PDI = 1.05

HPLC: 10%B $\longrightarrow$ 100%B(30 min), t_r = 18.3 min; 10%B $\longrightarrow$ 80%B(30 min), t_r = 18.3 min (new column)

P(MeOx$_{47}$DPOx$_5$)PipBnDOTA, P34

P10	16.8 mg	(3.34 μmol, 1 equiv)
p-SCN-Bn-DOTA × 4HCL	2.8 mg	(4 μmol, 1.2 equiv)
K_2CO_3	$\sim$ 2.7 mg	
MeOH	2 mL	

Preparation of **P34** was according to **GSP3** (7.2.3). Purification was performed by dialysis against water instead of the sephadex G25 column.

Yield: 15 mg (81 %)
Empirical formula, molar mass: $C_{262}H_{449}N_{59}O_{70}S$, M = 5577.79 g/mol

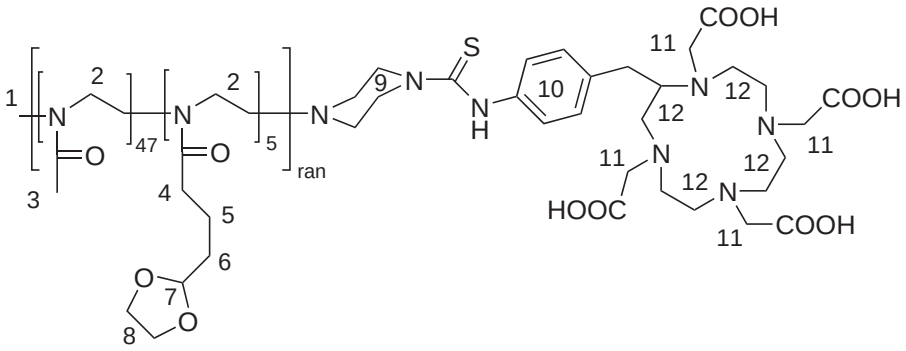

^{1}H-NMR (D_2O, 250 MHz): δ = 7.25 (br, 3H, H^{10}), 4.83 (br, 5H, H^{7}), 3.88 (br, 24H, $H^{8,11}$), 3.45 (br, 283H, $H^{2,12}$), 2.97/2.84 (br, 3H, H^{1}), 2.66 (br, 2H, H^{9}), 2.31 (br, 8H, H^{4}), 1.99 (br, 173H, H^{3}) and 1.59 ppm (br, 26H, $H^{5,6}$).

P(EtOx$_{19}$DPOx$_3$)PipBnDOTA, P35

P11 (58.1 mg, 23.2 μmol, 1 equiv) and 18 mg *p*-SCN-Bn-DOTA (25.8 μmol, 1.1 equiv) were dissolved in 3.7 mL phosphate buffer (pH 8.5) and 1 mL ACN and 10 μL TEA were added. HPLC control showed that no significant coupling occurred and the solvents were removed by freeze drying. The residual was collected with 1 mL MeOH and 3 mL H_2O and stirred for 6 h, but HPLC analysis suggested that still only very limited coupling occurred. Subsequently, additional 17.8 mg *p*-SCN-Bn-DOTA (25.5 μmol) of a fresh batch of chelator were added. After 3 days at RT, gel filtration and lyophylisation, the product was obtained as a colorless solid.

Yield: 41 mg (58 %)
Empirical formula, molar mass: $C_{132}H_{223}N_{29}O_{36}S$, M = 2824.42 g/mol

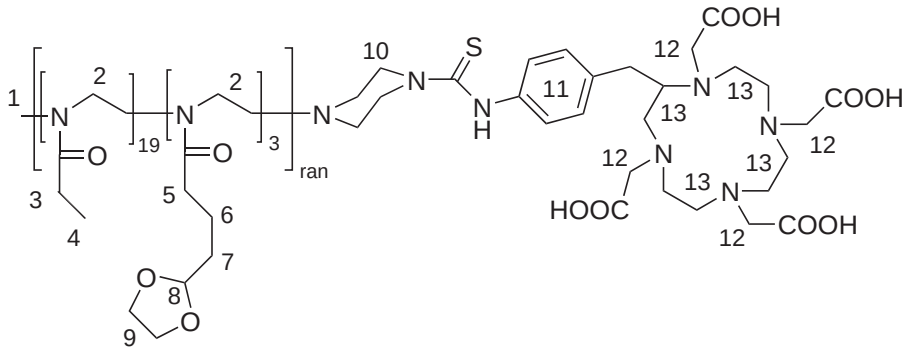

^{1}H-NMR (D_2O, 250 MHz): δ = 7.25 (br, 1.3H, H^{11}), 4.83 (br, 2H, H^{8}), 3.87 (br, 9H, $H^{8,12}$), 3.43 (br, 87, $H^{2,13}$), 2.97/2.83 (m, 3H, H^{1}), 2.6 (br, 1H, H^{10}), 2.27 (br, 41H, $H^{4,5}$), 1.58 (br, 8H, $H^{6,7}$) and 0.96 ppm (br, 55H, H^{3}).

GPC (DMAc):

HPLC: 10%B $\longrightarrow$ 100%B(30 min), t_r = 15.7 min

P(EtOx$_{20}$^{Triaz}ThioAc$_2$)PipBnDOTA, P36

P28	46 g	(17 μmol, 1 equiv)
p-SCN-Bn-DOTA×4HCl	22 mg	(34 μmol, 2 equiv)
K_2CO_3	$\sim$4 mg	
MeOH	250 μL	

P(EtOx$_{20}$^{Triaz}ThioAc$_2$)PipBnDOTA was prepared according to **GSP3** (7.2.3).

Yield: 33 mg (61%)
Empirical formula, molar mass: $C_{153}H_{261}N_{35}O_{32}S_3$, M = 3199.12 g/mol

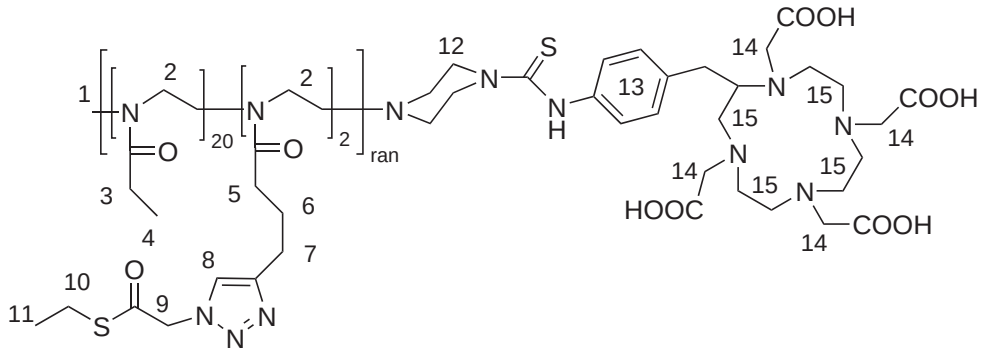

^{1}H-NMR (D_2O, 250 MHz): δ = 7.80 (br, 2H, $H^{8,trans}$), 7.68 (br, 1H, $H^{8,cis}$), 7.21/7.15 (br, 2H, H^{13}), 5.40 (br, 3H, $H^{9,trans}$), 4.90 (br, 2H, $H^{9,cis}$), 4.1 (br, 2H, H^{14}), 3.42 (br, 92H, $H^{2,15}$), 2.96 (br, 2H, H^1), 2.84 (br, 5H, $H^{1,10}$), 2.68 (br, 6H, $H^{7,12}$), 2.27 (br, 42H, $H^{3,5}$), 1.83 (br, 4H H^6), 1.13 (br, 4H, H^{11}) and 0.96 ppm (br, 56H, H^4).

HPLC: 10%B $\longrightarrow$ 100%B(30 min), t_r = 15.5 min

7.7.4 Aldehyde deprotection

P(MeOx$_{47}$OBOx$_5$)PipDOTA, P37

P34 (15 mg, 2.6μmol) was dissolved in 7 mL of 5 % TFA and dialysed against 500 mL 5 % TFA for 2.5 h. The TFA was exchanged with 2 L of water and the solution was dialysed for 16 h and another 2.5 h against 2 L H_2O. The product was obtained as a colorless solid after lyophylisation.

Yield: 11 mg (76 %)
Empirical formula, molar mass: $C_{252}H_{429}N_{59}O_{65}S$, M = 5357.52 g/mol

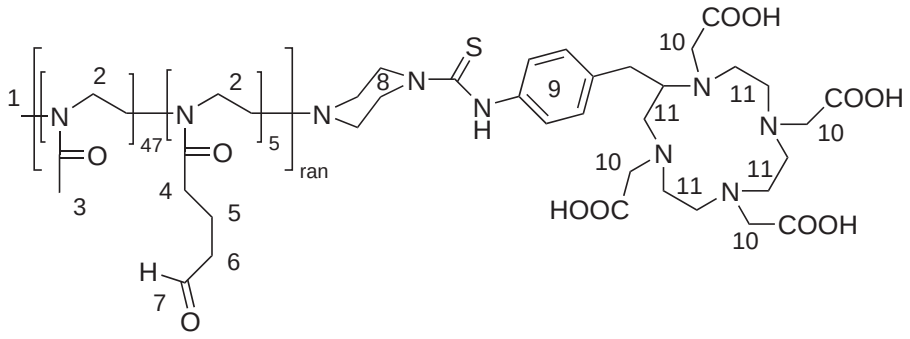

^{1}H-NMR (D_2O, 250 MHz): δ = 9.54 (s, 3H, H^7), 7.11 (br, 3H, H^9), 4.90 (br, 3H, $H^{7,acetal}$, 3.40 (br, 239H, $H^{2,10,11}$), 2.93/2.80 (br, 3H, H^1), 2.48 (br, 4H, $H^{5,8}$), 2.24 (br, 10H, H^4), 1.94 (br, 154H, H^3), 1.72 (br, 8H, H^5) and 1.47 ppm (br, 12H, $H^{5,6,acetal}$).

GPC (DMAc): M_n = 7205 g/mol, PDI = 1.06; M_n = 26492 g/mol, PDI = 1.05; M_n = 97657 g/mol, PDI = 1.06

HPLC: 10%B $\longrightarrow$ 100%B(30 min), t_r = 8.4 min

P(MeOx$_{35}$OBOx$_5$)Pid, P38

A solution of 124 mg P(MeOx$_{35}$DPOx$_5$)Pid (41 μmol) in 2 mL of 5 % HCl_{aq} (w/w) was dialysed against 1.3 L of the same HCl_{aq}. After 2 h, HCl_{aq} was exchanged and the reaction was dialysed against water (1.5 L) twice for 2 h. After lyophylization, the product was obtained as a colourless solid.

Yield: 260 mg (82 %)
Empirical formula, molar mass: $C_{181}H_{313}N_{41}O_{45}$, M = 3783.67 g/mol

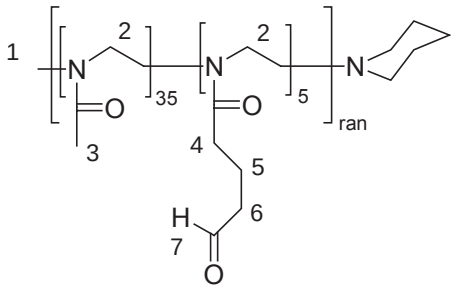

^{1}H-NMR ($CDCl_3$, 250 MHz): δ = 9.73 (br, 7H, H^7), 3.43 (br, 237H, H^2), 3.01/2.91 (br, 3H, H^1), 2.52 (br, 17H, H^6), 2.27 (br, 38H, H^4), 2.11 (br, 159H, H^3) and 1.91 ppm (br, 16H, $H^{5,Pid}$).

GPC (DMAc): M_n = 6946 g/mol, PDI = 1.22

HPLC: 10%B $\longrightarrow$ 100%B(30 min), t_r = 10.1 min

P($MeOx_{50}OBOx_8$)Pid, P39

P39 was prepared analog to **P38** from 124 mg of P($MeOx_{50}DPOx_8$)Pid.

Yield: 96.3 mg (83 %)
Empirical formula, molar mass: $C_{262}H_{451}N_{59}O_{66}$, M = 5483.47 g/mol

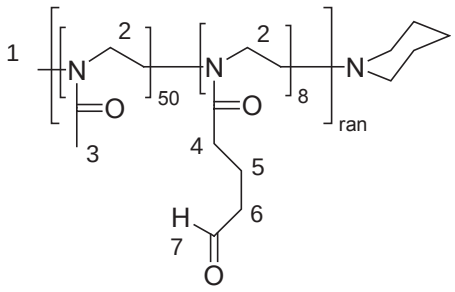

^{1}H-NMR ($CDCl_3$, 250 MHz): δ = 9.72 (br, 7H, H^7), 3.43 (br, 248H, H^2), 3.01/2.92 (br, 3H, H^1), 2.52 (br, 18H, H^6) 2.3 (br, 18H, H^4), 2.11 (br, 184H, H^3) and 1.91 ppm

(br, 28H, $H^{5,Pid}$).

GPC (DMAc): M_n = 11980 g/mol, PDI = 1.25
HPLC: 10%B $\longrightarrow$ 100%B(30 min), t_r = 10.4 min

7.8 Peptide coupling

7.8.1 Click Chemistry

P(EtOx$_{20}{}^{Triaz}$RGD$_2$)PipBnDOTA, C1

P(EtOx$_{20}$PynOx$_2$)PipDOTA	7 mg	(2.4 μmol, 1 equiv)
c[RGDfK(N$_3$)]	6.7 mg	(8.6 μmol, 3.5 equiv)
4,4´-dinonyl-2,2´dipyridyl	18 mg	(44 μmol, 18 equiv)
CuBr	5.6 mg	(39 μmol, 16 equiv)

Under nitrogen, **P33** (7 mg, 2.4 μmol, 1 equiv) and 6.7 mg of c[RGDfK(N$_3$)] (8.6 μmol, 3.5 equiv) were dissolved in 400 μL of 60% aqueous THF (v/v). After addition of 18 mg 4,4´-dinonyl-2,2´-dipyridyl (44 μmol, 18 equiv) and 5.6 mg CuBr (39 μmol, 16 equiv) the mixture was stirred for 3 days at RT. The solvents were removed under reduced pressure, the residual collected in 500 μL 1/1 MeOH/$CHCl_3$ (v/v) and the product was obtained by precipitation in 10 mL cold Et_2O. Repeating this procedure twice (adding approx. 25 mg 4,4´-dinonyl-2,2´-dipyridyl to the polymer solution before precipitation) the product was obtained as a colourless solid after freeze drying from *t*-BuOH/H_2O.

Yield: 7 mg (65%)
Empirical formula, molar mass: $C_{213}H_{349}N_{55}O_{48}S$, M = 4480.45 g/mol

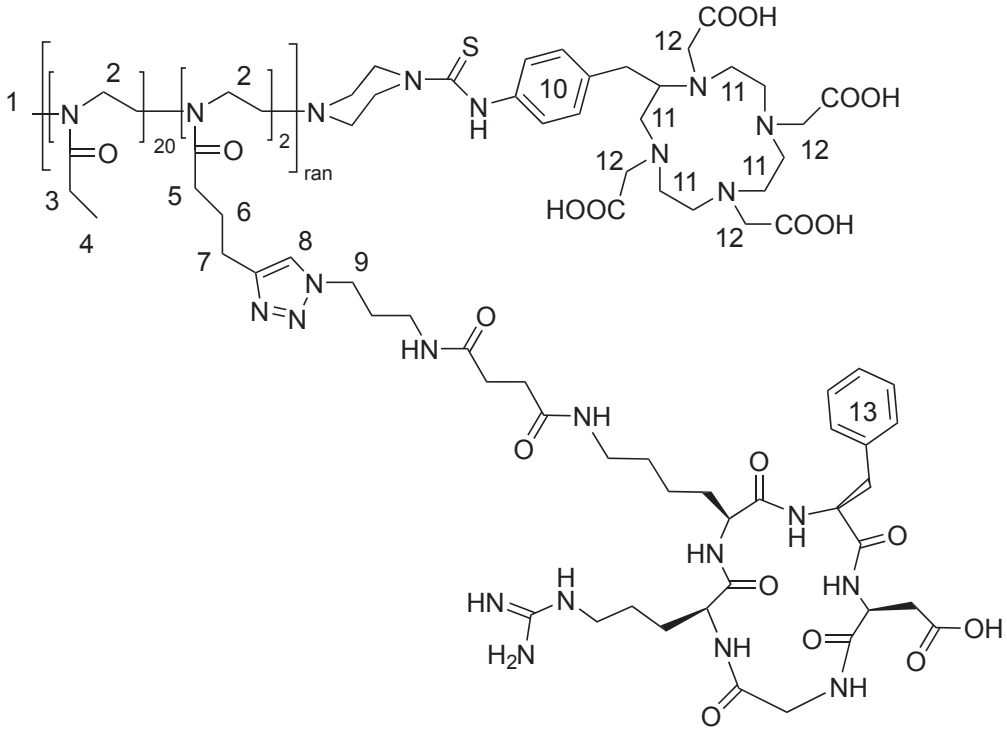

^{1}H-NMR (D_2O, 500 MHz): $\delta = 7.69$ (br, 1H, H^8), 7.23 (br, 3H, $H^{10,13}$), 4.90 (br, 3H, H^9), 3.84 (br, 2H, H^{12}), 3.42-3.2 (br, 87H, $H^{2,11}$), 2.98/2.85 (m, 3H, H^1), 2.68-2.52 (br, 10H, $H^{5,7}$), 2.25 (br, 37H, H^3), 1.82 (br, 4H, H^6), 0.96 ppm (br, 43H, H^4).

HPLC: 10%B $\longrightarrow$ 80%B(30 min), t_r = 17.0 min (new column)

7.8.2 Oxim Ligation

P(MeOx$_{47}{}^{Oxim}$RGD$_5$)PipBnDOTA, C2

The protected peptide c[ṘGḊfK(Boc-AOAc)] (8.4 mg, 7.7 μmol, 6 equiv) was dissolved in a mixture of 190 μL TFA, 14 μL TIBS and 5 μL H_2O and stirred for 3 h at RT. The mixture turned blue after 1 h. **P37** (6.8 mg 1.27 μmol, 1 equiv) was dissolved in 2 mL of buffer (CertiPur®, pH 4) and the solution, together with 1.8 mL of ACN, was added to the peptide solution. The mixture was allowed to react for 3 days and then lyophylized. The residual was collected with 0.8 mL H_2O and 0.3 mL ACN and purified by

gel filtration. After two additional filtration and fractionations steps using sephadex G25 the product was obtained as a colorless solid.

Yield: 6.2 mg (56 %)
Empirical formula, molar mass: $C_{397}H_{639}N_{109}O_{105}S$, 8651.05 g/mol

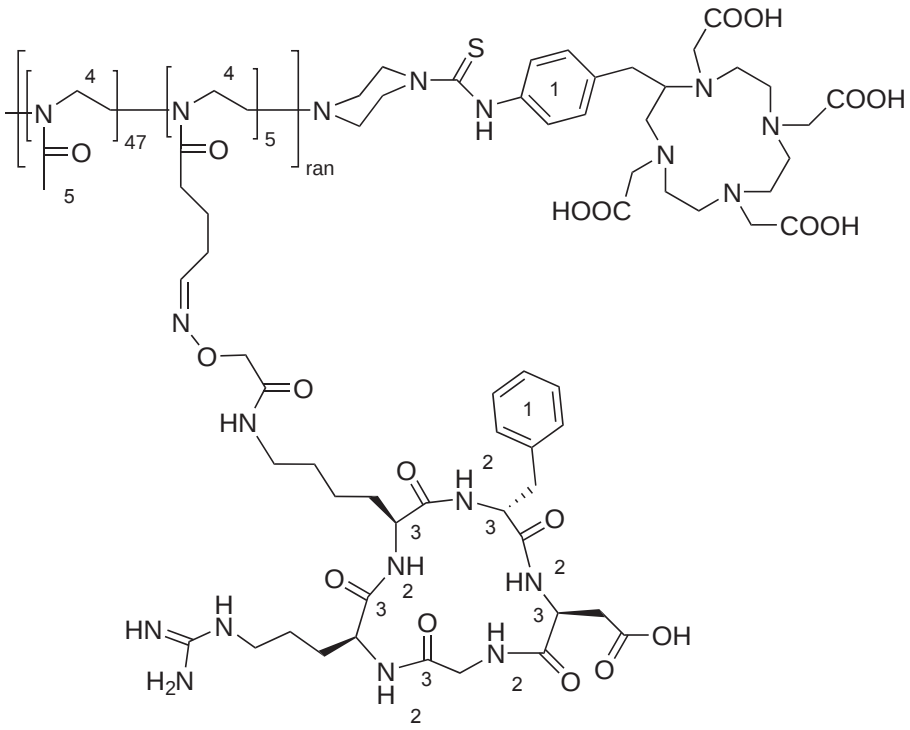

^{1}H-NMR (DMSO-d6, 250 MHz): δ = 8.3 - 7.2 (m/br, 60H, $H^{1,2}$), 4.7 - 4.3 (br, 30H, H^3), 3.36 (br, 310H, H^4) and 2.0 ppm (br, 97H, H^5).

HPLC: 10%B $\longrightarrow$ 100%B(30 min), t_r = 10.5 min

P(MeOx$_{50}$^{Oxim}RGD$_8$)Pid, C3

P39 (0.82 mg, 0.1 μmol, 1 equiv) and 1.0 mg c(RGDyK(AOAc)) were dissolved in 600 μL of phosphate buffer (100 mM, pH 2.5). After 3 h at RT, an aliquot was taken

for HPLC analysis. After additional 2 h at RT, the solution was fractionated by gel filtration (3 g)). The product was obtained as a colorless solid after lyophylization.

Yield: 2 mg (quantitative)
Empirical formula, molar mass: $C_{494}H_{787}N_{139}O_{130}$, 10753.39 g/mol

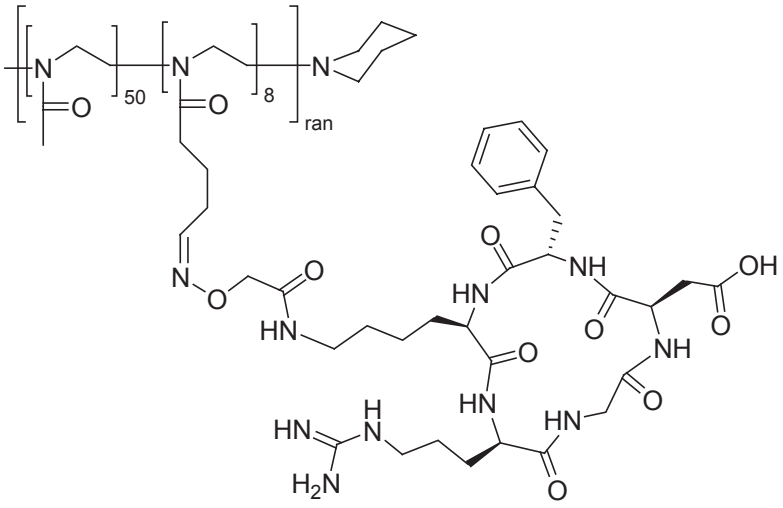

HPLC: 10%B $\longrightarrow$ 100%B(30 min), t_r = 10.8 min.

P(MeOx$_{20}{}^{Oxim}$MTII$_2$)Pid, C4

P(MeOx$_{20}$OBOx$_2$)Pid (4.9 mg, 2.4 μmol, 1 equiv) was dissolved in 1.2 mL buffer (CertiPur®, pH 4) and 6 mg of AOAc^0-MTII (5.7 μmol, 2.4 equiv) were added. The mixture was stirred over night and subsequently fractionated by gel filtration. After lyophylization the product was obtained as a colorless solid.

Yield: 5 mg (50 %)
Empirical formula, molar mass: $C_{200}H_{311}N_{55}O_{42}$, 4157.95 g/mol

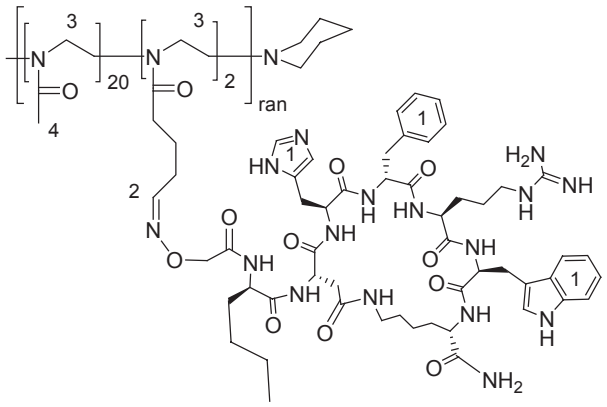

^{1}H-NMR (H_2O, 250 MHz): δ = 7.5 - 6.7 (br, 13H, H^1), 4.9 (br, 4H, H^2), 4.0 - 3.6 (br, 34H, $H^{\alpha-CH}$), 3.45 (br, 103H, H^3), 3.0 (br, 12H), 2.02 (br, H^4), 1.7 - 0.7 ppm (br, 24H).

HPLC: 10%B $\longrightarrow$ 100%B(30 min), t_r = 12.1 min

P(MeOx$_{35}$^{Oxim}MTII$_5$)Pid, C5

P38 (4.6 mg, 1.2 μmol, 1 equiv) and 7.7 mg AOAc^0-MTII (7.3 μmol, 6 equiv) were dissolved in 300 μL of aqueous TFA (pH 3). The mixture was allowed to stir over night. After addition of 0.6 mL H_2O, the solution was filtrated over Sephadex G25 and the product was obtained as a colorless solid after lyophylization.

Yield: 6.6 mg (61 %)
Empirical formula, molar mass: $C_{431}H_{653}N_{121}O_{90}$, 8969.55 g/mol

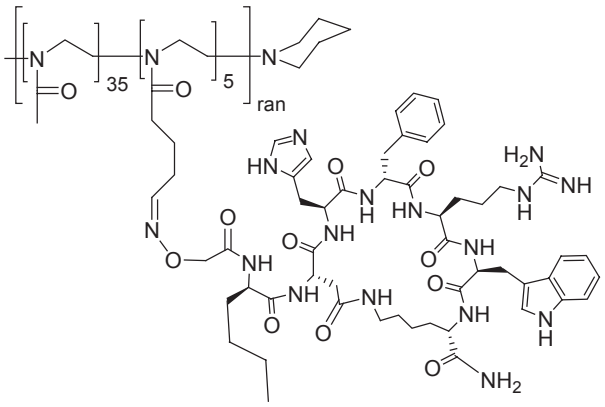

^{1}H-NMR (H_2O, 250 MHz): δ = 7.5 - 6.7 (br, 76H, H^1), 4.9 (br, 5H, H^2), 4.4 - 4.1 (br, 34H, $H^{\alpha-CH}$), 3.43 (br, 162H, H^3), 3.2 - 2.2 (br, 84H), 2.00 (br, 105H, H^4) and 1.7 - 0.7 ppm (br, 125H).

HPLC: 10%B $\longrightarrow$ 100%B(30 min), t_r = 13.5 min

P(MeOx$_{50}{}^{Oxim}$MTII$_8$)Pid, C6

P39 (3.9 mg, 0.71 μmol, 1 equiv) and 7.6 mg AOAc^0-MTII (7.2 μmol, 10 equiv) were dissolved in 350 μL of aqueous TFA (pH 3). The mixture was allowed to stir over night. After addition of 0.6 mL H_2O, the solution was purified by gel filtration and the product was obtained as a colorless solid after lyophylization.

Yield: 7.7 mg (79 %)
Empirical formula, molar mass: $C_{662}H_{995}N_{187}O_{138}$, 13781.15 g/mol

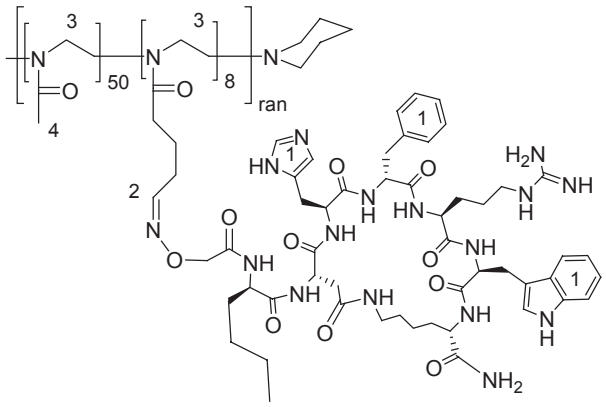

^{1}H-NMR (H_2O, 250 MHz): δ = 7.5 - 6.7 (br, 102H, H^1), 4.9 (br, 22H, H^2), 4.6 - 3.6 (br, 231H, $H^{\alpha-CH}$), 3.43 (br, 276H, H^3), 3.2 - 2.2 (br, 142H), 2.00 (br, 150H, H^4) and 1.7 - 0.7 ppm (br, 182H).

HPLC: 10%B $\longrightarrow$ 100%B(30 min), t_r = 14.4 min

7.8.3 Native Ligation

P(EtOx$_{20}$^{NCL}CREKA$_2$)PipBnDOTA, C7

Under argon**P36** (15 mg, 4.5 μmol, 1 equiv) and 6.2 mg CREKA (10 μmol, 2.2 equiv) were dissolved in 250μL degassed carbonate buffer (pH 7.2), the vial was sealed and the mixture was stirred over night. After gel filtration the product was obtained as a colorless solid.

Yield: 15.4 mg (%)
Empirical formula, molar mass: $C_{195}H_{335}N_{53}O_{48}S_3$, 4286.27 g/mol

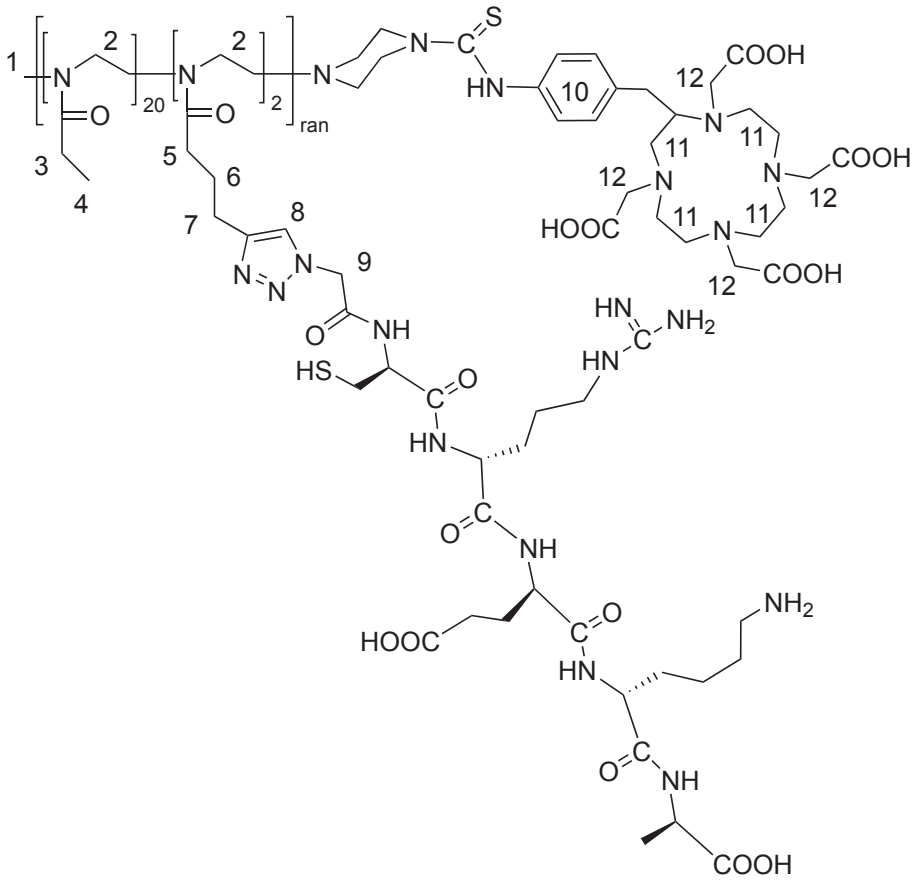

^{1}H-NMR (H_2O, 250 MHz): δ = 7.75 (br, 1.1H, $H^{8,trans}$), 7.65 (br, 0.8H, $H^{8,cis}$), 7.18/7.11 (br, 1H, H^{10}), 5.19 (br, 1.6H, $H^{9,trans}$), 4.88 (br, 2.5H, $H^{9,cis}$), 4.3 - 3.6 (br, 24H, $H^{\alpha-CH,12}$), 3.40 (br, 92H, $H^{2,11}$), 3.07 (br, 9H, H^1), 2.89 (br, 8H, H^1), 2.65 (br, 9H, H^7), 2.24 (br, 47H, H^3), 1.8 - 1.2 (br, 15H, $H^{aliph.-H,6}$) and 0.94 ppm (br, 60H, H^4).

HPLC: 10%B $\longrightarrow$ 100%B(30 min), t_r = 11.5 min

7.9 ^{68}Ga labeling of P(MeOx$_{45}$^{Oxim}RGD$_5$)PipDOTA

The work described in this section was performed at the radiopharmaceutical laboratory of Prof. Dr. H.-J. Wester at the Nuklearmedizinische Klinik und Poliklinik of the Klinikum rechts der Isar, TU München.
For radiometallation with $^{68}GaCl_3$, the $^{68}Ge/^{68}Ga$ generator was eluted with 0.1 N HCl. Typically an activity of 1 Ci/L was obtained. Varying amounts of **C2** were dissolved in water and the buffer (2.5 M HEPES or 2.44 M sodium acetate) and appropriate amounts of 0.1 N HCl were added to obtain the desired pH value. Since the radiometallation of the polymer-peptide conjugates could not be followed by TLC, the degree of radiochelation was followed by HPLC.

#	Conjugate [mg]	Buffer [μL]	$^{68}GaCl_3$ [μCi]	T [°C]	time [min]	RCY [%]
1	60	140 HEPES	245	65	15	0
2	120	140 HEPES	484	65	20	30
3	200	140 HEPES	230	95	25	50
4	60	140 HEPES	440	85	40	70
5	60	40 Acetate	9500	95	20	22[a]
6	60	40 Acetate	1150	95	20	15[a]

[a] after purification

After purification by chromatography over a Sep-Pak C_{18} cartridge, typically a radiochemical purity of $>95\,\%$ was obtained. The radiometallation for the *in vivo* experiments is shown as entry 6.

7.10 Preparation of hydrogels

7.10.1 Azine Hydrogels

Preparation of hydrogels from aldehyde bearing polymers, H1 - H10

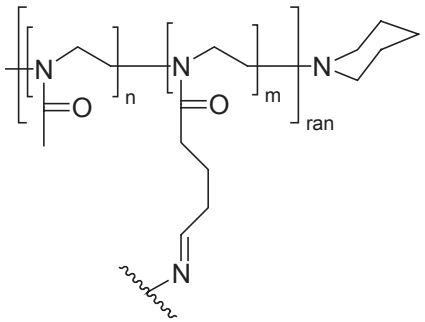

Preliminary tests with 20 % and 30 % (w/w) weight solutions **P38** in water to form hydrogels cross-linked by hydrazine-hydrate (0.5 equiv per aldehyde) were successfull as the mixture rapidly solidified upon hydrazine addition. It was projected to evaluate swelling in deionized water. This was not possible since the hydrogels completely dissolved over night.

Hydrogels from **10 % (w/w)** solutions:

P39 (15.5 mg, 2.8 μmol) were dissolved in 160 mg H_2O and the polymer was cross-linked by addition of 0.5 mg hydrazine hydrate. The formed hydrogel was allowed to swell in pH 4 buffer (twice exchanged). The obtained hydrogel **H1** (187.5 mg) was dried and weighed (13.3 mg, yield: 85.8 %, S_WD = 13.1). The hydrogel was again allowed to swell (pH 4) and 105 mg of hydrogel were recovered.

Hydrogels from **20 % (w/w)** solutions:

Hydrogels from 20 wt % solutions of **P39** were prepared in different buffers as follows:

Table 7.1: Poly(2-oxazoline) azine hydrogels prepared from 20 % (w/w) polymer solutions

Entry	$m_{\mathbf{P39}}$ [mg]	Solvent	Yield[a] [mg]	Yield dry [mg][b]	$S_W D$[c]
H2	23.7	pH 4	108	20.7	4.2
second cycle		H_2O	38	8.2	3.6
third cycle		H_2O	36.1	8.3	3.3
H3	29.5	pH 6	140	26.8	4.2
second cycle		H_2O	61	13.2	3.6
third cycle		H_2O	53	11.8	3.5
H4	20	pH 8	87	23.4	2.7
second cycle		H_2O	138	11	11.5[d]
third cycle		H_2O	45.5	10.2	3.5

[a] amount in obtained swollen gel
[b] after drying of swollen gel
[c] $\frac{\text{m(swollen)-m(dry)}}{\text{m(dry)}}$
[d] this value presumably represents an outlier

Hydrogels from **30 % (w/w)** solutions:
P38 (Entries **H5**, **H10**, 11, Table 7.1) was dissolved in 100 μL of the respective solvent and 1.6 mg hydrazine hydrate in 14.4 mg solvent was added and the mixture was vortexed very shortly (approx. 2 s).
P39 (Entries **H6** - **H9**, Table 7.1) was dissolved in 75 μL H_2O and 32 mg of the respective phosphate buffer were added. After addition of 1.7 μL hydrazine-hydrate in 8.3 μL H_2O the mixtures were vortexed approx. 2 s.
All but the reaction in methanol became immediately solid.

Direct gelation of dioxolane polymers, H11

P($MeOx_{50}DPOx_8$)Pid was dissolved in 150 μL of the respective solvent and 1.4 mg hydrazine hydrate in 3.6 μL of water were mixed in a syringe and injected into the mould. Only with 2 M HCl gelation occurred, however, in this case so rapidly that only approx. 75 % of the reaction mixture could actually be injected into the mould. The gel was removed and allowed to swell in 2 M HCl for 3 h and weighed (Table 7.3).

Table 7.2: Poly(2-oxazoline) azine hydrogels prepared from 30 % (w/w) polymer solutions

Entry	$m_{Polymer}$ [mg]	Solvent	Yield[a] [mg]	Yield dry [mg][b]	S_WD[e]
H5	50	pH 4	159	30.6	4.2
H6	50	pH 5	131.3	39.4	2.3
H7	50	pH 6	86	24.6	2.5
H8	50	pH 7	87.2	27.2	2.2
H9	50	pH 8	76.1	32.4	1.4
H10	50	pH 9	—[c]	—	—
11	50	methanol	—[d]	—	—

[a] amount in obtained swollen gel
[b] after drying of swollen gel
[c] originally formed hydrogel was not stable in buffer, but dissolved overnight
[d] no hydrogel formation was observed
[e] $\frac{\text{m(swollen)-m(dry)}}{\text{m(dry)}}$

Table 7.3: Attempts to prepare hydrogels from P($MeOx_{50}DPOx_8$)Pid and hydrazine hydrate as cross-linker

Entry	$m_{Polymer}$ [mg]	Solvent	Yield[a] [mg]	Yield swollen [mg][b]
1	40.7	buffer pH 4.0	0	n.a.
2	40.3	buffer pH 2.5	0	n.a.
3	40.2	0.1 N HCl	0	n.a.
H11	40.3	2 M HCl	150	187

[a] amount in obtained solid after gelation
[b] in the solvent of preparation

After drying and weighing the procedure was repeated with other solvents (Table 7.4).

Table 7.4: Swelling of **H11** in various aqueous solutions.

Solvent	m (swollen) [mg]	m (dry) [mg]	S_WD^a
2 M HCl	187	29.7	5.3
0.1 N HCl	129	13.2	8.8
pH 4.0 buffer	83.4	18.8	3.4
pH 6.0 buffer	83.7	17.6	3.7
deionized H_2O	93.6	16.2	4.7

a $\frac{\text{m(swollen)-m(dry)}}{\text{m(dry)}}$

7.10.2 Imine Hydrogel, H12/H13

P($MeOx_{35}OBOx_5$)Pid (29 mg, 7.7 μmol, 38 μmol aldehyde groups) was dissolved in 120 mg buffer (pH 4 or pH 9) and combined with a solution of 44 mg MeOxP($EtOx_{51}$-$AEOx_4$)Pip (9 μmol, 40 μmol primary amine groups) in 177 mg H_2O. The mixtures were dried at 50 °C. Subsequently, the respective buffers were added and the hydrogel was allowed to swell.
The pH 4 gel **H12** yielded 166 mg and after drying 24.0 mg were collected (S_WD 5.9). For the pH 9 gel 194 mg were obtained (dry: 23.8 mg, SD 7.2).

7.10.3 Urethane Hydrogel, H14

1,6-Hexanediisocyanate (14 μL/15 mg, 87 μmol, 9 equiv) were dissolved in 400 μL ACN. To this solution, 22 mg P($MeOx_{20}AEOx_5$)Pid (9.3 μmol, 1 equiv) were added and the mixture was vortexed upon which a white polymer pellet was formed. After 20 min, 1 mL H_2O were added. After 21 days, the water was removed and the hydrogel (**H14**) weighed (125 mg). After thorough drying at 50 °C and at reduced pressure, 17.2 mg of dry polymer were obtained. Again the polymer was added to water and 105.5 mg hydrogel were obtained. Subsequent drying yielded 18.4 mg (S_WD = 4.7).

7.10.4 Disulfide brigded hydrogel, H15

P27 (20 mg, 3.7 μmol, 1 equiv) was dissolved in pH 7 buffer. After addition of 2.2 mg cystein (18 μmol, 4.8 equiv) to the solution was dried in air at 50 °C. Subsequent addition of 1.5 mL of water led swelling of the product and 83.8 mg of hydrogel **H15** were obtained. The gel was dried and weighed (4.8 mg, yield: 22 %, S_WD 16.5). In another cycle of swelling and drying S_WD = 15.1 was obtained. Deionized water was added (rapid swelling) before 4.6 mg 1,4-dithio-DL-threitol were added. After 3 h no hydrogel could be observed anymore.

Bibliography

[1] Panyutin, I. G.; Neumann, R. D. *Trends Biotechnol.* **2005,** *23,* 492.

[2] World Health Organization, *http://www.who.int/cancer/en/,* [Accessed 16th january 2006].

[3] zur Hausen, H. *Spektrum der Wissenschaft* **2003,** *Spezial 3,* 6.

[4] Gibbs, W. W. *Spektrum der Wissenschaft* **2003,** *Spezial 3,* 12.

[5] *CA Cancer J. Clin.* **2006,** *56,* 63.

[6] Rechkemmer, G. *Spektrum der Wissenschaft* **2003,** *Spezial 3,* 40.

[7] Blettner, M. *Spektrum der Wissenschaft* **2003,** *Spezial 3,* 34.

[8] Sawyers, C. *Nature* **2004,** *432,* 294.

[9] Ringsdorf, H. *J. Polymer Sci. Pol. Sym.* **1975,** *51,* 135.

[10] Wedding, U.; Höffken, K. *Spektrum der Wissenschaft* **2003,** *Spezial 3,* 62.

[11] Juillerat-Jeanneret, L.; Schmitt, F. *Med. Res. Rev.* **2006,** .

[12] Friess, H. *et al. BMC Cancer* **2006,** *6,* 285.

[13] Allen, T. M. *Nat. Rev. Cancer* **2002,** *2,* 750.

[14] Lo, H.-W.; Day, C.-P.; Hung, M.-C. *Adv. Genet.* **2005,** *54,* 235.

[15] Shi, F.; Rakhmilevich, A. L.; Heise, C. P.; Oshikawa, K.; Sondel, P. M.; Yang, N. S.; Mahvi, M. D. *Mol. Cancer Ther.* **2002,** *1,* 949.

[16] Barajas, M.; Mazzolini, G.; Genove, G.; Bilbao, R.; Narvaiza, I.; Schmitz, V.; Sangro, B.; Melero, I.; Qian, C.; Prieto, J. *Hepatology* **2001,** *33,* 52.

[17] Kirn, D.; Niculescu-Duvaz, I.; Hallden, G.; Springer, C. J. *Trends Mol. Med.* **2002,** *8,* S68.

[18] Mullen, C. A. *Pharmacol. Ther.* **1994,** *63,* 199.

[19] Cross, D.; Burmester, J. K. *Clin. Med. Res.* **2006,** *4,* 218.

[20] Devi, G. R. *Cancer Gene Ther.* **2006,** *13,* 819.

[21] El-Aneed, A. *J. Control. Release* **2004,** *94,* 1.

[22] Griffiths, R. A.; Boyne, J. R.; Whitehouse, A. *Curr. Gene Ther.* **2006,** *6,* 1.

[23] Kaneda, Y.; Tabata, Y. *Cancer Sci.* **2006,** *97,* 348.

[24] Florida Gulf Coast University, *http://coe.fgcu.edu/faculty/greenep/kidney/-Glomerulus.html,* [accessed 06 January 2007].

[25] University of Fribourg, Swiss, *http://www.unifr.ch/histologie/elearningfree/-allemand/rein/niere08.html,* [accessed 17th may 2006].

[26] Asanuma, K.; Mundel, P. *Clin. Exp. Nephrol.* **2003,** *7,* 255.

[27] University of Regensburg, *http://www.biologie.uni-regensburg.de/Anatomie/-Witzgall/Research.html,* [accessed 05th june 2006].

[28] Chang, R. L. S.; Deen, W. M.; Robertson, C. R.; Brenner, B. M. *Kidney Int.* **1975,** *8,* 212.

[29] Brenner, B. M.; Hostetter, T. H.; Humes, H. D. *Am. J. Physiol. Renal Physiol.* **1978,** *234,* F455.

[30] Schaeffer, R. C. J.; Gratix, M. L.; Mucha, D. R.; Carbajal, J. M. *Microcirculation* **2002,** *9,* 329.

[31] Mitra, A.; Nan, A.; Ghandehari, H.; McNeill, E.; Mulholland, J.; Line, B. R. *Pharm. Res.* **2004,** *21,* 1153.

[32] Lammers, T.; Kühnlein, R.; Kissel, M.; Subr, V.; Etrych, T.; Pola, R.;

Pechar, M.; Ulbrich, K.; Storm, G.; Huber, P.; Peschke, P. *J. Control. Release* **2005,** *110,* 103.

[33] Asgeirsson, D.; Venturoli, D.; Rippe, B.; Rippe, C. *Am. J. Physiol. Renal Physiol.* **2006,** *291,* F1083.

[34] Behr, T. M.; Goldenberg, D. M.; Becker, W. *Eur. J. Nuc. Med.* **1998,** *25,* 201.

[35] Matsumura, Y.; Maeda, H. *Cancer Research* **1986,** *46,* 6387.

[36] Potchen, E. J.; Kinzie, J.; Curtis, C.; Siegel, B. A.; Studer, R. K. *Cancer* **1972,** *30,* 639.

[37] Jain, R. K.; Weissbrod, J.; Wei, J. *Adv. Cancer Res.* **1980,** *21,* 37.

[38] Jain, R. K. *Biotech. Prog.* **1985,** *1,* 81.

[39] Jain, R. K. *Cancer Metast. Rev.* **1987,** *6,* 559.

[40] Maeda, H.; Greish, K.; Fang, J. *Adv. Polym. Sci.* **2006,** *193,* 103.

[41] Maeda, H.; Wu, J.; Sawa, T.; Matsumura, Y.; Hori, K. *J. Control. Release* **2000,** *65,* 271.

[42] Duncan, R. *Nat. Rev. Drug Discov.* **2003,** *2,* 347.

[43] Haag, R.; Kratz, F. *Angew. Chem. Int. Ed.* **2006,** *45,* 1198.

[44] Khandare, J.; Minko, T. *Prog. Polym. Sci.* **2006,** *31,* 359.

[45] Twaites, B.; de las Heras Alarcón, C.; Alexander, C. *J. Mater. Chem.* **2005,** *15,* 441.

[46] Duncan, R. *Nat. Rev. Cancer* **2006,** *6,* 688.

[47] Duncan, R.; Ringsdorf, H.; Satchi-Fainaro, R. *Adv. Polym. Sci.* **2006,** *193,* 1.

[48] Vicent, M. J.; Duncan, R. *Trends Biotechnol.* **2006,** *24,* 39.

[49] Satchi-Fainaro, R.; Duncan, R.; Barnes, C. M. *Adv. Polym. Sci.* **2006,** *193,* 1.

[50] Senter, P. D.; Springer, C. J. *Adv. Drug Deliver. Rev.* **2000,** *53,* 247.

[51] Shangguan, D.; Li, Y.; Tang, Z.; Cao, Z. C.; Chen, H. W.; Mallikartchy, P.; Sefah, K.; Yang, C. J.; Tan, W. *P. Natl. Acad. Sci. USA* **2006,** *103,* 11838.

[52] Teply, B. A.; Rocha, F. G.; Levy-Nissenbaum, E.; Langer, R.; Farokhzad, O. C. *Am. J. Drug Del.* **2006,** *4,* 123.

[53] Pasqualini, R.; Ruoslahti, E. *Nature* **1996,** *380,* 364.

[54] Hoffman, J. A.; Giraudo, E.; Singh, M.; Zhang, L.; Inoue, M.; Porkka, K.; Hanahan, D.; Ruoslahti, E. *Cancer Cell* **2003,** *4,* 383.

[55] Gazarian, K. *Front. Drug Des. Discov.* **2005,** *1,* 29.

[56] Suntharalingam, G.; Perry, M. R.; Ward, S.; Brett, S. J.; Castello-Cortes, A.; Brunner, M. D.; Panoskaltsis, N. *N. Engl. J. Med.* **2006,** *355,* 1018.

[57] Ruoslahti, E. *Biochem. Soc. T.* **2004,** *32,* 397.

[58] Pierschbacher, M. D.; Ruoslahti, E. *Nature* **1984,** *309,* 30.

[59] Ruoslahti, E. *Matrix Biol.* **2003,** *22,* 459.

[60] Wright, S. D.; Reddy, P. A.; Jong, M. T. C.; Erickson, B. W. *P. Natl. Acad. Sci. USA* **1987,** *87,* 1965.

[61] Lawler, J.; Weinstein, R.; Hynes, R. O. *J. Cell Biol.* **1988,** *107,* 2351.

[62] Grant, D. S.; Tashiro, K.; Segui-Regal, B.; Yamada, Y.; Martin, G. R.; Kleinman, H. K. *Cell* **1989,** *58,* 933.

[63] Hynes, R. O. *Cell* **2002,** *110,* 673.

[64] Gilcrease, M. Z. *Cancer Lett.* **2007,** *247,* 1.

[65] Hynes, R. O. *Cell* **1992,** *69,* 11.

[66] van der Flier, A.; Sonnenberg, A. *Cell Tissue Res.* **2001,** *305,* 285.

[67] Hersel, U. *Monomere und multimere RGD-Peptide für die integrinvermittelte Zelladhäsion auf Biomaterialien und zur Tumordiagnose,* Thesis, TU München, 2003.

[68] Lodish, H.; Baltimore, D.; Berk, A.; Zipursky, S. L.; Matsudaira, P.; Darnell, J. *Molekulare Zellbiologie;* 2. Aufl.; Berlin; New York: de Gruyter: 1996.

[69] Hogg, N.; Laschinger, M.; Giles, K.; McDowall, A. *J. Cell Sci.* **2003,** *116,* 4695.

[70] Del Pozo, M. A. *Cell Cycle* **2004,** *3,* 725.

[71] Decker, L.; Baron, W.; ffrench Constant, C. *Biochem. Soc. T.* **2004,** *32,* 426.

[72] Sotobori, T.; Ueda, T.; Myoui, A.; Yoshioka, K.; Nakasaki, M.; Yoshikawa, H.; Itoh, K. *Exp. Cell Res.* **2006,** *312,* 3927.

[73] Guan, J.-L. *Science* **2004,** *303,* 773.

[74] Puklin-Faucher, E.; Gao, M.; Schulten, K.; Vogel, V. *J. Cell Biol.* **2006,** *175,* 349.

[75] Vogel, V.; Sheetz, M. *Nat. Rev. Mol. Cell Bio.* **2006,** *7,* 265.

[76] Akiyama, S. K.; Hasegawa, E.; Hasegawa, T.; Yamada, K. M. *J. Biol. Chem.* **1985,** *260,* 13256.

[77] Mammen, M.; Choi, S.-K.; Whitesides, G. M. *Angew. Chem. Int. Ed.* **1998,** *37,* 2754.

[78] Zöller, M. *Spektrum der Wissenschaft* **2003,** *Spezial 3,* 24.

[79] Xiong, J.-P.; Stehle, T.; Diefenbach, B.; Zhang, R.; Dunker, R.; Scott, D. L.; Joachimiak, A.; Goodman, S. L.; Arnaout, M. A. *Science* **2001,** *294,* 339.

[80] Xiong, J.-P.; Stehle, T.; Zhang, R.; Joachimiak, A.; Frech, M.; Goodman, S. L.; Arnaout, M. A. *Science* **2002,** *296,* 151.

[81] McQuade, P.; Knight, L. C.; Welch, M. J. *Bioconjugate Chem.* **2004,** *15,* 988.

[82] Tucker, G. C. *Curr. Oncol. Rep.* **2006,** *8,* 96.

[83] Smith, J. W. *Curr. Opin. Investig. Drugs* **2003,** *4,* 741.

[84] Mattern, R.-H.; Read, S. B.; Pierschbacher, M. D.; Sze, C.-I.; Eliceiri, B. P.; Kruse, C. A. *Cancer Ther.* **2005,** *3A,* 325.

[85] Temming, K.; Schiffelers, R. M.; Molema, G.; Kok, R. J. *Drug Resist. Update* **2005,** *8,* 381.

[86] Burkhart, D. J.; Kalet, B. T.; Coleman, M. P.; Post, G. C.; Koch, T. H. *Mol. Cancer Ther.* **2004,** *3,* 1593.

[87] Chen, X.; Plasencia, C.; Hou, Y.; Neamati, N. *J. Med. Chem.* **2005,** *48,* 1098.

[88] Schiffelers, R. M.; Mixson, A. J.; Ansari, A. M.; Fens, M. H. A. M.; Tang, Q.; Zhou, Q.; Xu, J.; Molema, G.; Lu, P. Y.; Scaria, P. V.; Storm, G.; Woodle, M. C. *J. Control. Release* **2005,** *109,* 5.

[89] Thumshirn, G.; Hersel, U.; Goodman, S. L.; Kessler, H. *Chem.-Eur. J.* **2003,** *9,* 2717.

[90] Dijkgraaf, I.; Kruijtzer, J. A. W.; Frieling, C.; Soede, A. C.; Hilbers, H. W.; Oyen, W. J. G.; Corstens, F. H. M.; Liskamp, R. M. J.; Boerman, O. C. *Nucl. Med. Biol.* **2006,** *33,* 953.

[91] Dijkgraaf, I.; Rijnders, A. Y.; Soede, A.; Dechesne, A. C.; van Esse, G. W.; Brouwer, A. J.; Corstens, F. H. M.; Boerman, O. C.; Rijkers, D. T. S.; Liskamp, R. M. J. *Org. Biomol. Chem.* **2007,** *5,* 935.

[92] Dijkgraaf, I.; Liu, S.; Kruijtzer, J. A. W.; Soede, A. C.; Oyen, W. J. G.; Liskamp, R. M. J.; Corstens, F. H. M.; Boerman, O. C. *Nucl. Med. Biol.* **2007,** *34,* 29.

[93] Koning, G. A.; Fretz, M. M.; Woroniecka, U.; Storm, G.; Krijger, G. C. *Appl. Radiat. Isotopes* **2004,** *61,* 963.

[94] Xiong, Z.; Cheng, Z.; Zhang, X.; Patel, M.; Wu, J. C.; Gambhir, S. S.; Chen, X. *J. Nucl. Med.* **2006,** *47,* 130.

[95] Kok, R. J.; Schraa, A. J.; bos, E. J.; Moorlag, H. E.; Ásgeirsdóttir, S. A.; Everts, M.; Meijer, D. K. F.; Molema, G. *Bioconjugate Chem.* **2002,** *13,* 128.

[96] Montet, X.; Montet-Abou, K.; Reynolds, F.; Weissleder, R.; Josephson, L. *Neoplasia* **2006,** *8,* 214.

[97] Graeter, S. V.; Huang, J.; Perschmann, N.; López-García, M.; Kessler, H.; Ding, J.; Spatz, J. P. *Nano Lett.* **2007,** *7,* 1413.

[98] Gomez, N.; Winter, J. O.; Shieh, F.; Saunders, A. E.; Korgel, B. A.; Schmidt, C. E. *Talanta* **2005,** *67,* 462.

[99] Parrish, B.; Breitenkamp, R. B.; Emrick, T. *J. Am. Chem. Soc.* **2005,** *127,* 7404.

[100] Mitra, A.; Nan, A.; Papadimitriou, J. C.; Ghandehari, H.; Line, B. R. *Nucl. Med. Biol.* **2006,** *33,* 43.

[101] Poethko, T.; Schottelius, M.; Thumshirn, G.; Hersel, U.; Herz, M.; Henriksen, G.; Kessler, H.; Schwaiger, M.; Wester, H.-J. *J. Nucl. Med.* **2004,** *45,* 892.

[102] Nasongkla, N.; Shuai, X.; Ai, H.; Weinberg, B. D.; Pink, J.; Boothman, D. A.; Gao, J. *Angew. Chem. Int. Ed.* **2004,** *43,* 6323.

[103] Montet, X.; Funovics, M.; Montet-Abou, K.; Weissleder, R.; Josephson, L. *J. Med. Chem.* **2006,** *49,* 6087.

[104] Aumailley, M.; Gurrath, M.; Müller, G.; Calvete, J.; Timpl, R.; Kessler, H. *FEBS Lett.* **1991,** *291,* 50.

[105] Koivunen, E.; Wang, B.; Ruoslahti, E. *Biotechnology* **1995,** *13,* 265.

[106] Dechantsreiter, M. A.; Planker, E.; Mathä, M.; Lohof, E.; Hölzemann, G.; Jonczyk, A.; Goodman, S. L.; Kessler, H. *J. Med. Chem.* **1999,** *42,* 3033.

[107] Haubner, R.; Gratias, R.; Diefenbach, B.; Goodman, S. L.; Jonczyk, A.; Kessler, H. *J. Am. Chem. Soc.* **1996,** *118,* 7461.

[108] Haubner, R.; Bruchertseifer, F.; Bock, M.; Kessler, H.; Schwaiger, M.; Wester, H. *Nuklearmedizin* **2004,** *43,* 26.

[109] Beer, A. J.; Haubner, R.; Goebel, M.; Luderschmidt, S.; Spilker, M. E.; Wester, H.-J.; Weber, W. A.; Schwaiger, M. *J. Nucl. Med.* **2005,** *46,* 1333.

[110] Haubner, R.; Kunast, B.; Mang, C.; Weber, W. A.; Kessler, H.; Wester, H.-J.; Schwaiger, M. *Bioconjugate Chem.* **2004,** *15,* 61.

[111] Haubner, R.; Weber, W. A.; Beer, A. J.; Vabuliene, E.; Reim, D.; Sarbia, M.; Becker, K.-F.; Goebel, M.; Hein, R.; Wester, H.-J.; Kessler, H.; Schwaiger, M. *PLoS Medicine* **2005,** *2,* e70.

[112] Assa-Munt, N.; Jia, X.; Laakkonen, P.; Ruoslahti, E. *Biochemistry* **2001,** *40,* 2373.

[113] Hersel, U.; Dahmen, C.; Kessler, H. *Biomaterials* **2003,** *24,* 4385.

[114] Lössner, D.; Kessler, H.; Thumshirn, G.; Dahmen, C.; Wiltschi, B.; Tanaka, M.; Knoll, W.; Sinner, E.-K.; Reuning, U. *Anal. Chem.* **2006,** *78,* 4524.

[115] Hofland, L. J.; Capello, A.; Krenning, E. P.; de Jong, M.; van Hagen, M. P. *J. Nucl. Med.* **2005,** *46,* 191S.

[116] Dasgupta, P. *Pharmacol. Therap.* **2004,** *102,* 61.

[117] Epelbaum, J. *Prog. Neurobiol.* **1986,** *27,* 63.

[118] Zhou, M.; Nakatani, E.; Gronenberg, L. S.; Tokimoto, T.; Wirth, M. J.; Hruby, V. J.; Roberts, A.; Lynch, R. M.; Ghosh, I. *Bioconjugate Chem.* **2007,** *18,* 323.

[119] Schottelius, M.; Schwaiger, M.; Wester, H.-J. *Tetrahedron Lett.* **2003,** *44,* 2393.

[120] Amherdt, M.; Patel, Y. C.; Orci, L. *J. Clin. Invest.* **1989,** *84,* 412.

[121] Mentlein, R.; Held-Feindt, J.; Krisch, B. *Cell Tissue Res.* **2001,** *303,* 27.

[122] Stroh, T.; Jackson, A. C.; Dal Farra, C. a. S.; Vincent, J. P.; Beaudet, A. *Synapse* **2000,** *38,* 177.

[123] Smalley, K. S. M.; Koenig, J. A.; Feniuk, W.; Humphrey, P. P. A. *Brit. J. Pharmacol.* **2001,** *132,* 1102.

[124] Hukovic, N.; Panetta, R.; Kumar, U.; Patel, Y. *Endocrinology* **1996,** *137,* 4046.

[125] Hukovic, N.; Rochville, M.; Kumar, U.; Sasi, R.; Khare, S.; Patel, Y. C. *J. Biol. Chem.* **1999,** *274,* 24550.

[126] Patel, R. C.; Kumar, U.; Lamb, D. C.; Eid, J. S.; Rocheville, M.; Grant, M.; Rani, A.; Hazlett, T.; Patel, S. C.; Gratton, E.; Patel, Y. C. *P. Natl. Acad. Sci. USA* **2002,** *99,* 3294.

[127] Grant, M.; Collier, B.; Kumar, U. *J. Biol. Chem.* **2004,** *279,* 36179.

[128] Grant, M.; Patel, R. C.; Kumar, U. *J. Biol. Chem.* **2004,** *279,* 38636.

[129] Eden, P. A.; Taylor, J. E. *Life Sci.* **1993,** *53,* 85.

[130] Taylor, J. E.; Theveniau, M. A.; Bashirzadeh, R.; Reisine, T.; Eden, P. A. *Peptides* **1994,** *15,* 1229.

[131] Jonas, S.; John, M.; Boese-Landgraf, J.; Haring, R.; Prevost, G.; Thomas, F.; Rosewicz, S.; Riecken, E. O.; Wiedenmann, B.; Neuhaus, P. *Langenbecks Arch. Chir.* **1995,** *380,* 90.

[132] Reubi, J. C.; Schaer, J. C.; Laissue, J. A.; Waser, B. *Metabolism* **1996,** *45,* 39.

[133] Schaer, J. C.; Waser, B.; Mengod, G.; Reubi, J. C. *Int. J. Cancer* **1997,** *70,* 530.

[134] Prasad, V.; Birzin, E. T.; McVaugh, C. T.; van Rijn, R. D.; Rohrer, S. P.; Chicchi, G.; Underwood, D. J.; Thornton, E. R.; Smith III, A. B.; Hirschmann, R. *J. Med. Chem.* **2003,** *46,* 1858.

[135] Patel, Y. C.; Greenwood, M. T.; Panetta, R.; Demchyshyn, L.; Niznik, H.; Srikant, C. B. *Life Sci.* **1995,** *57,* 1249.

[136] Jia, W.-D.; Xu, G.-L.; Xu, R.-N.; Sun, H.-C.; Wang, L.; Yu, J.-H.; Wang, J.; Li, J.-S.; Zhai, Z.-M.; Xue, Q. *J. Cancer Res. Clin. Oncol.* **2003,** *129,* 327.

[137] Ginj, M.; Zhang, H.; Waser, B.; Cescato, R.; Wild, D.; Wang, X.; Erchegyi, J.; Rivier, J.; Mäcke, H. R.; Reubi, J. C. *P. Natl. Acad. Sci. USA* **2006,** *103,* 16436.

[138] Reubi, J. C.; Schär, J. C.; Waser, B.; Wenger, S.; Heppeler, A.; Schmitt, J. S.; Mäcke, H. R. *Eur. J. Nucl. Med.* **2000,** *27,* 273.

[139] Schottelius, M. *New Radiolabelled Somatostatin Receptor Ligands for Diagnosis and Therapy,* Thesis, TU München, 2002.

[140] Reubi, J. C.; Maecke, H. R.; Krenning, E. P. *J. Nucl. Med.* **2005,** *46,* 67S.

[141] Vaidyanathan, G.; Friedman, H. S.; Affleck, D. J.; Schottelius, M.; Wester, H.-J.; Zalutsky, M. R. *Clin. Cancer Res.* **2003,** *9,* 1868.

[142] Schottelius, M.; Rau, F.; Reubi, J. C.; Schwaiger, M.; Wester, H.-J. *Bioconjugate Chem.* **2005,** *16,* 429.

[143] Stahl, A.; Meisetschläger, G.; Schottelius, M.; Bruus-Jensen, K.; Wolf, I.; Scheidhauer, K.; Schwaiger, M. *Eur. J. Nucl. Med. Mol. Imaging* **2006,** *33,* 45.

[144] Adams, R. L.; Adams, I. P.; Lindow, S. W.; Zhong, W.; Atkin, S. L. *Brit. J. Cancer* **2005,** *92,* 1493.

[145] Weckbecker, G.; Lewis, I.; Albert, R.; Schmid, H. A.; Hoyer, D.; Bruns, C. *Nat. Rev. Drug Discov.* **2003,** *2,* 999.

[146] Capello, A.; Krenning, E. P.; Bernard, B. F.; Breeman, W. A. P.; Erion, J. L.; de Jong, M. *J. Nucl. Med.* **2006,** *47,* 122.

[147] MacNeil, D. J. *et al. Eur. J. Pharmacol.* **2002,** *440,* 141.

[148] Getting, S. J. *Trends Pharmacol. Sci.* **2002,** *23,* 447.

[149] Yang, Y. K.; Harmon, C. M. *Obes. Rev.* **2003,** *4,* 239.

[150] Starowicz, K.; Przewlocka, B. *Life Sci.* **2003,** *73,* 823.

[151] Catania, A.; Gatti, S.; Colombo, G.; Lipton, J. M. *Pharmacol. Rev* **2004,** *56,* 1.

[152] Sturm, R. A.; Teasdale, R. D.; Box, N. F. *Gene* **2001,** *277,* 49.

[153] Tatro, J. B.; Atkins, M.; Mier, J. W.; Hardarson, S.; Wolfe, H.; Smith, T.; Entwistle, M. L.; Reichlin, S. *J. Clin. Invest.* **1990,** *85,* 1825.

[154] Vagner, J.; Handl, H. L.; Monguchi, Y.; Jana, U.; Begay, L. J.; Mash, E. A.; Hruby, V. J.; Gillies, R. J. *Bioconjugate Chem.* **2006,** *17,* 1545.

[155] Dębniak, T.; Masojc, R. S. B.; Serrano-Fernández, P.; Huzarski, T.; Byrski, T.; Dębniak, B.; Górski, B.; Cybulski, C.; Mędrek, K.; Kurzawski, G.; van de Wetering, T.; Maleszka, R.; Kładny, J.; Lubinski, J. *Int. J. Cancer* **2006,** *119,* 2597.

[156] Roberts, D. W.; Newton, R. A.; Beaumont, K. A.; Leonard, J. H.; Sturm, R. A. *Pigment Cell Res.* **2005,** *19,* 76.

[157] Sánchez-Laorden, B. L.; Sánchez-Más, J.; Martínez-Alonso, E.; Martínez-Menárguez, J. A.; García-Borrón, J. C.; Jiménez-Cervantes, C. *J. Invest. Dermatol.* **2006,** *126,* 172.

[158] Miao, Y.; Hoffman, T. J.; Quinn, T. P. *Nucl. Med. Biol.* **2005,** *32,* 485.

[159] Miao, Y.; Whitener, D.; Feng, W.; Owen, N. K.; Chen, J.; Quinn, T. P. *Bioconjugate Chem.* **2003,** *14,* 1177.

[160] Hruby, V. J.; Wilkes, B. C.; Hadley, M. E.; Al-Obeidi, F.; Sawyer, T. K.; Staples, D. J.; DeVaux, A. E.; Dym, O.; Castrucci, A. M.; Hintz, M. F.; Riehm, J. P.; Rao, K. R. *J. Med. Chem.* **1987,** *30,* 2126.

[161] de Lauro Castrucci, A. M.; Hadley, M. E.; Sawyer, T. K.; Wilkes, B. C.; Al-Obiedi, F.; Staples, D. J.; DeVaux, A. E.; Dym, O.; Hintz, M. F.; Riehm, J. P.; Rao, K. R.; Hruby, V. J. *Gen. Comp. Endocrinol.* **1989,** *73,* 157.

[162] Opperer, F. "Synthese hoch-N-methylierter α-MSH-Analoga", Master's thesis, TU München, 2004.

[163] Sawyer, T. K.; Sanfilippo, P. J.; Hruby, V. J.; Engel, M. H.; Heward, C. B.; Burnett, J. B.; Hadley, M. E. *P. Natl. Acad. Sci. USA* **1980,** *77,* 5754.

[164] Tatro, J. B.; Reichlin, S. *Endocrinology* **1987,** *121,* 1900.

[165] Haskell-Luevano, C.; Sawyer, T. K.; Trumpp-Kallmeyer, S.; Bikker, J. A.; Humblet, C.; Gantz, I.; Hruby, V. J. *Drug Des. Discov.* **1996,** *14,* 197.

[166] Li, S. J.; Varga, K.; Archer, P.; Hruby, V. J.; Sharma, S. D.; Kesterson, R. A.; Cone, R. D.; Kunos, G. *J. Neurosci.* **1996,** *16,* 5182.

[167] Schiöth, H. B.; Muceniece, R.; Mutule, I.; Wikberg, J. E. S. *Basic Clin. Pharmacol.* **2006,** *99,* 287.

[168] Simberg, D.; Duza, T.; Park, J. H.; Essler, M.; Pilch, J.; Zhang, L.; Derfus, A. M.; Yang, M.; Hoffman, R. M.; Bhatia, S.; Sailor, M. J.; Ruoslahti, E. *P. Natl. Acad. Sci. USA* **2007,** *104,* 3.

[169] La Bella, R.; Garcia-Garayoa, E.; Langer, M.; Bläuenstein, P.; Beck-Sickinger, A. G.; Schubinger, P. A. *Nucl. Med. Biol.* **2002,** *29,* 553.

[170] Liu, S.; Robinson, S. P.; Edwards, D. S. *Top. Curr. Chem.* **2005,** *252,* 193.

[171] Sierra, A. *Drug Resist. Update* **2005,** *8,* 247.

[172] Burger, J. A.; Kipps, T. J. *Blood* **2006,** *107,* 1761.

[173] Cremonesi, M.; Ferrari, M.; Bodei, L.; Tosi, G.; Paganelli, G. *J. Nucl. Med.* **2006,** *47,* 1467.

[174] Müller, C.; Dumas, C.; Hoffmann, U.; Schubiger, P. A.; Schibli, R. *J. Organomet. Chem.* **2004,** *689,* 4712.

[175] Stefflova, K.; Li, H.; Chen, J.; Zheng, G. *Bioconjugate Chem.* **2007,** *18,* 379.

[176] Jain, R. K. *Cancer Res.* **1990,** *50,* 81S.

[177] Jain, R. K. *J. Control. Release* **1998,** *53,* 49.

[178] Jain, R. K. *J. Control. Release* **2001,** *74,* 7.

[179] Li, W. P.; Meyer, L. A.; Anderson, C. J. *Top. Curr. Chem.* **2005,** *252,* 179.

[180] De Leon Rodriguez, L. M.; Kovacs, Z.; Dieckmann, G.; Sherry, A. D. *Chem.-Eur. J.* **2004,** *10,* 1149.

[181] Modlinger, A. *Monosaccharide als α_4-Integrinantagonisten und oligomere Somatostatinanaloga für die Nuklearmedizin,* Thesis, TU München, 2004.

[182] Hovinen, J. *Chem. Biodivers.* **2006,** *3,* 296.

[183] Knör, S.; Modlinger, A.; Poethko, T.; Schottelius, M.; Wester, H.-J.; Kessler, H. *Chemistry* **2007,** *ASAP,* DOI: 10.1002/chem.200700231.

[184] Prasuhn, Jr., D. E. P.; Yeh, R. M.; Obenaus, A.; Manchester, M.; Finn, M. G. *Chem. Commun.* **2007,** 1269.

[185] Liu, S.; Edwards, D. S. *Bioconjugate Chem.* **2001,** *12,* 7.

[186] Breeman, W. A. P.; van der Wansem, K.; Bernard, B. F.; van Gameren, A.; Erion, J. L.; Visser, T. J.; Krenning, E. P.; de Jong, M. *Eur. J. Nucl. Med. Mol. I.* **2003,** *30,* 312.

[187] Velikyan, I.; Beyer, G. J.; Langström, B. *Bioconjugate Chem.* **2004,** *15,* 554.

[188] Chen, X.; Hou, Y.; Tohme, M.; Park, R.; Khankaldyyan, V.; Gonzales-Gomez, I.; Bading, J. R.; Laug, W. E.; Conti, P. S. *J. Nucl. Med* **2004,** *45,* 1776.

[189] Norenberg, J. P.; Krenning, B. J.; Konings, I. R.; Kusewitt, D. F.; Nayak, T. K.; Anderson, T. L.; de Jong, M.; Garmestani, K.; Brechbiel, M.; Kvols, L. *Clin. Cancer Res.* **2006,** *12,* 897.

[190] Antunes, P.; Ginj, M.; Zhang, H.; Waser, B.; Baum, R. P.; Reubi, J. C.; Maecke, H. *Eur. J. Nucl. Med. Mol. Imaging* **2007,** *ASAP,* DOI: 10.1007/s00259-006-0317-x.

[191] Teunissen, J. J. M.; Kwekkeboom, D. J.; de Jong, M.; Esser, J.-P.; Valkema, R.; Krenning, E. P. *Best Pract. Res Cl. Ga.* **2005,** *19,* 595.

[192] Antunes, P.; Ginj, M.; Walter, M. A.; Chen, J.; Reubi, J.-C.; Maecke, H. R. *Bioconjugate Chem.* **2007,** *18,* 84.

[193] Capello, A.; Krenning, E. P.; Bernard, W. A. B. B. F.; de Jong, M. *J. Nucl. Med.* **2003,** *44,* 98.

[194] O´Donoghue, J. A.; Bardies, M.; Wheldon, T. E. *J. Nucl. Med* **1995,** *36,* 1902.

[195] de Jong, M.; Breeman, W. A. P.; Valkema, R.; Bernard, B. F.; Krenning, E. P. *J. Nucl. Med.* **2005,** *46,* 13S.

[196] Frilling, A.; Weber, F.; Saner, F.; Bockisch, A.; Hofmann, M.; Mueller-Brand, J.; Broelsch, C. E. *Surgery* **2006,** *140,* 968.

[197] de Jong, M.; Breeman, W. A.; Bernard, B.; Bakker, W. H.; Visser, T. J.; Kooij, P. P. M.; van Gameren, A.; Krenning, E. P. *J. Nucl. Med* **2001,** *42,* 1841.

[198] de Jong, M.; Valkema, F.; Jamar, R.; Kvols, L. K.; Kwekkeboom, D. J.; Breeman, W. A. P.; Bakker, W. H.; Smith, C.; Pauwels, S.; Krenning, E. P. *Semin. Nucl. Med.* **2002,** *32,* 133.

[199] Arnberg, H.; Westlin, J. E.; Husin, S.; Nilsson, S. *Acta Oncol.* **1993,** *32,* 177.

[200] Ginj, M.; Hinni, K.; Tschumi, S.; Schulz, S.; Maecke, H. R. *J. Nucl. Med.* **2005,** *46,* 2097.

[201] DeNardo, S. J. *J. Nucl. Med.* **2006,** *47,* 4.

[202] de Jong, M.; Barone, R.; Krenning, E.; Bernard, B.; Melis, M.; Visser, T.; Gekle, M.; Willnow, T. E.; Walrand, S.; Jamar, F.; Pauwels, S. *J. Nucl. Med* **2005,** *46,* 1696.

[203] Hammond, P. J.; Wade, A. F.; Gwilliam, M. E.; Peters, A. M.; Myers, M. J.; Gilbey, S. G.; Bloom, S. R.; Calam, J. *Br. J. Cancer* **1993,** *67,* 1437.

[204] de Jong, M.; Rolleman, E. J.; Bernard, B. F.; Visser, T. J.; Bakker, W. H.; Breeman, W. A.; Krenning, E. P. *J. Nucl. Med.* **1996,** *37,* 1388.

[205] Bodei, L.; Cremonesi, M.; Zoboli, S.; Grana, C.; Bartolomei, M.; Rocca, P.; Caracciolo, M.; Mäcke, H. R.; Chinol, M.; Paganelli, G. *Eur. J. Nucl. Med. Mol. Imaging* **2003,** *30,* 207.

[206] Béhé, M.; Kluge, G.; Becker, W.; Gotthardt, M.; Behr, T. M. *J. Nucl. Med.* **2005,** *46,* 1012.

[207] Chen, J.; Giblin, M. F.; Wang, N.; Jurisson, S. S.; Quinn, T. P. *Nucl. Med. Biol.* **1999,** *26,* 687.

[208] Cheng, Z.; Chen, J.; Miao, Y.; Owen, N. K.; Quinn, T. P.; Jurisson, S. J. *J. Med. Chem.* **2002,** *45,* 3048.

[209] Miao, Y.; Hylarides, M.; Fisher, D. R.; Shelton, T.; Moore, H.; Wester, D. W.; Fritzberg, A. R.; Winkelmann, C. T.; Hoffman, T.; Quinn, T. P. *Clin. Cancer Res.* **2005,** *11,* 5616.

[210] Miao, Y.; Fisher, D. R.; Quinn, T. P. *Nucl. Med. Biol.* **2006,** *33,* 723.

[211] Froidevaux, S.; Calame-Christe, M.; Schuhmacher, J.; Tanner, H.; Saffrich, R.; Henze, M.; Eberle, A. N. *J. Nucl. Med.* **2004,** *45,* 116.

[212] Froidevaux, S.; Calame-Christe, M.; Tanner, H.; Eberle, A. N. *J. Nucl. Med.* **2005,** *46,* 887.

[213] Gestwicki, J. E.; Strong, L. E.; Kiessling, L. L. *Chem. Biol.* **2000,** *7,* 583.

[214] Mortell, K. H.; Gingras, M.; Kiessling, L. L. *J. Am. Chem. Soc* **1994,** *116,* 12053.

[215] Mortell, K. H.; Weatherman, R. V.; Kiessling, L. L. *J. Am. Chem. Soc.* **1996,** *118,* 2297.

[216] Kiessling, L. L.; Pohl, N. L. *Curr. Biol.* **1996,** *3,* 71.

[217] Kiessling, L. L.; Gestwicki, J. E.; Strong, L. E. *Curr. Opin. Chem. Biol.* **2000,** *4,* 696.

[218] Gestwicki, J. E.; Cairo, C. W.; Strong, L. E.; Oetjen, K. A.; Kiessling, L. L. *J. Am. Chem. Soc.* **2002,** *124,* 14922.

[219] Kiessling, L. L.; Gestwicki, J. E.; Strong, L. E. *Angew. Chem. Int. Ed.* **2006,** *45,* 2348.

[220] Kessler, H.; Schudok, M.; Haupt, A. Dimerization of cyclic hexapeptides: strong increase of biological activity. In *Peptides*; Jung, G.; E., B., Eds.; de Gruyter: Berlin, New York, 1988; p664.

[221] Ye, Y.; Bloch, S.; Xu, B.; Achilefu, S. *J. Med. Chem* **2006,** *49,* 2268.

[222] Boturyn, D.; Coll, J.-L.; Garanger, E.; Favrot, M.-C.; Dumy, P. *J. Am. Chem. Soc.* **2004,** *126,* 5731.

[223] Temming, K.; Meyer, D. L.; Zabinski, R.; Dijkers, E. C. F.; Poelstra, K.; Molema, G.; Kok, R. J. *Bioconjugate Chem.* **2006,** *17,* 1385.

[224] Kim, W. J.; Yockman, J. W.; Jeong, J. H.; Christensen, L. V.; Lee, M.; Kim, Y.-H.; Kim, S. W. *J. Control. Release* **2006,** *114,* 381.

[225] Thumshirn, G. *Multivalente zyklische RGD-Peptide und RGD-Mimetika für den Einsatz in Tumordiagnostik und Tumortherapie,* Thesis, TU München, 2003.

[226] Poethko, T.; Schottelius, M.; Thumshirn, G.; Herz, M.; Haubner, R.; Henriksen, G.; Kessler, H.; Schwaiger, M.; Wester, H.-J. *Radiochim. Acta* **2004,** *92,* 317.

[227] Suh, W.; Han, S.-O.; Yu, L.; Kim, S. W. *Mol. Ther.* **2002,** *6,* 664.

[228] Sharma, S. D.; Granberry, M. E.; Jiang, J.; Leong, S. P. L.; Hadley, M. E.; Hruby, V. J. *Bioconjugate Chem.* **1994,** *5,* 591.

[229] Sharma, S. D.; Jiang, J.; Hadley, M. E.; Bentley, D. L.; Hruby, V. J. *P. Natl. Acad. Sci. USA* **1996,** *93,* 13715.

[230] Brandenburger, Y.; Rose, K.; Bagutti, C.; Eberle, A. N. *J. Recept. Signal Transduction Res.* **1999,** *19,* 467.

[231] Vagner, J.; Handl, H. L.; Gillies, R. J.; Hruby, V. J. *Bioorg. Med. Chem. Lett.* **2004,** *14,* 211.

[232] Wikipedia, *http://en.wikipedia.org/wiki/Poly_vinyl_pyrrolidone,* [accessed May 14, 2006].

[233] Wikipedia, *http://de.wikipedia.org/wiki/Biokompatibilit%C3%A4t,* [accessed May 14, 2006].

[234] Veronese, F. M.; Pasut, G. *Drug Discov. Today* **2005,** *10,* 1451.

[235] Pasut, G.; Veronese, F. M. *Adv. Polym. Sci.* **2006,** *192,* 95.

[236] Malik, N.; Evagorou, E. G.; Duncan, R. *Anticancer Drugs* **1999,** *10,* 767.

[237] Gillies, E. R.; Dy, E.; Fréchet, J. M. J.; Szoka, F. C. *Mol. Pharm.* **2005,** *2,* 129.

[238] Lee, C. C.; MacKay, J. A.; Fréchet, J. M. J.; Szoka, F. C. *Nat. Biotechnol.* **2005,** *23,* 1517.

[239] Lee, C. C.; Gillies, E. R.; Fox, M. E.; Guillaudeu, S. J.; Fréchet, J. M. J.; Dy, E. E.; Szoka, F. C. *P. Natl. Acad. Sci. USA* **2006,** *103,* 16649.

[240] Mitra, A.; Mulholland, J.; Nan, A.; McMeill, E.; Ghandehari, H.; Line, B. R. *J. Control. Release* **2005,** *102,* 191.

[241] Line, B. R.; Mitra, A.; Nan, A.; Ghandehari, H. *J. Nucl. Med.* **2005,** *46,* 1552.

[242] Gabriel, S.; Eschenbach, G. *Chem. Ber.* **1897,** *23,* 2494.

[243] Meyers, A. I.; Mihelich, E. D. *Angew. Chem. Int. Ed.* **1976,** *15,* 270.

[244] Culbertson, B. M. *Prog. Polym. Sci.* **2002,** *27,* 579.

[245] Andreasch, R. *Monatsh. Chem* **1884,** *5,* 33.

[246] Cozzi, P. G.; Gallo, E.; Floriani, C.; Chiesi-Villa, A.; Rizzoli, C. *Organometallics* **1995,** *14,* 4994.

[247] McPherson, L. D.; Drees, M.; Khan, S. I.; Strassner, T.; Abu-Omar, M. M. *Inorg. Chem.* **2004,** *43,* 4036.

[248] Debono, N.; Besson, M.; Pinel, C.; Djakovitch, L. *Tetrahedron Lett.* **2004,** *45,* 2235.

[249] Eisnor, C. R.; Gossage, R. A.; Yadav, P. N. *Tetrahedron* **2006,** *62,* 3395.

[250] Yan, X.-X.; Peng, Q.; Zhang, Y.; Zhang, K.; Hong, W.; Hou, X.-L.; Wu, Y.-D. *Angew. Chem. Int. Ed.* **2006,** *45,* 1979.

[251] Schneider, N.; César, C.; Bellemin-Laponnaz, S.; Gade, L. H. *J. Organomet. Chem.* **2005,** *690,* 5556.

[252] Decken, A.; Eisnor, C. R.; Gossage, R. A.; Jackson, S. M. *Inorg. Chim. Acta* **2006,** *359,* 1743.

[253] McManus, H. A.; Guiry, P. J. *Chem. Rev.* **2004,** *104,* 4151.

[254] Brunner, H.; Obermann, U.; Wimmer, P. *J. Organomet. Chem.* **1986,** *316,* C1.

[255] Zarka, M. T.; Nuyken, O.; Weberskirch, R. *Chem.-Eur. J.* **2003,** *9,* 3228.

[256] Cesana, S.; Auernheimer, J.; Jordan, R.; Kessler, H.; Nuyken, O. *Macromol. Chem. Phys.* **2006,** *207,* 183.

[257] Witte, H.; Seeliger, W. *Liebigs Ann. Chem.* **1974,** *6,* 996.

[258] Persigehl, P.; Jordan, R.; Nuyken, O. *Macromolecules* **2000,** *33,* 6977.

[259] Taubmann, C.; Luxenhofer, R.; Cesana, S.; Jordan, R. *Macromol. Biosci.* **2005,** *5,* 603.

[260] Aoi, K.; Okada, M. *Prog. Polym. Sci.* **1996,** *21,* 151.

[261] Seeliger, W.; Aufderhaar, E.; Diepers, W.; Feinauer, R.; Nehring, R.; Thier, W.; Hellmann, H. *Angew. Chem.* **1966,** *78,* 913.

[262] Seeliger, W., Chemische Werke Hüls AG, DE Patent 1206585, 1965.

[263] Bassiri, T. G.; Levy, A.; Litt, M. *J. Polymer Sci. Pol. Lett.* **1967,** *5,* 871.

[264] Litt, M. H.; Levy, A. J., BE Patent 666829, 1965.

[265] Kagiya, T.; Narisawa, S.; Maeda, T.; Fukui, K. *J. Polym. Sci. Pol. Lett.* **1966,** *4,* 441.

[266] Tomalia, D. A.; Sheetz, D. P. *J. Polym. Sci. Pol. Chem.* **1966,** *4,* 2253.

[267] Litt, M.; Levy, A.; Herz, J. *J. Macromol. Sci., Chem.* **1975,** *A9,* 703.

[268] Kobayashi, S. *Prog. Polym. Sci.* **1990,** *15,* 751.

[269] Kobayashi, S.; Uyama, H. *J. Polym. Sci. Pol. Chem.* **2002,** *40,* 192.

[270] Hoogenboom, R.; Fijten, M. W. M.; Schubert, U. S. *J. Polym. Sci. Pol. Chem.* **2004,** *42,* 1830.

[271] Kobayashi, S.; Iijima, S.; Igarashi, T.; Saegusa, T. *Macromolecules* **1987,** *20,* 1729.

[272] Hoogenboom, R.; Paulus, R. M.; Fijten, M. W. M.; Schubert, U. S. *J. Polym. Sci. Pol. Chem.* **2005,** *43,* 1487.

[273] Park, J.-S.; Kataoka, K. *Macromolecules* **2007,** *40,* 3599.

[274] Meyer, D. E.; Shin, B. C.; Kong, G. A.; Dewhirst, M. W.; Chilkoti, A. *J. Control. Release* **2001,** *74,* 213.

[275] Meyer, D. E.; Kong, G. A.; Dewhirst, M. W.; Zalutsky, M. R.; Chilkoti, A. *Cancer Res.* **2001,** *61,* 1548.

[276] Raucher, D.; Chilkoti, A. *Cancer Res.* **2001,** *61,* 7163.

[277] Soppimath, K. S.; Tan, D. C.-W.; Yang, Y.-Y. *Adv. Mater.* **2005,** *17,* 318.

[278] Bidwell III, G. L.; Raucher, D. *Mol. Cancer Ther.* **2005,** *4,* 1076.

[279] Uyama, H.; Kobayashi, S. *Chem. Lett.* **1992,** *9,* 1643.

[280] Park, J.-S.; Akiyama, Y.; Winnik, F. M.; Kataoka, K. *Macromolecules* **2004,** *37,* 6786.

[281] Meyer, M.; Antonietti, M.; Schlaad, H. *Soft Matter* **2007,** *3,* 430.

[282] Huber, S.; Jordan, R., *in preparation*.

[283] Percec, V.; Guhaniyogi, S. C.; Kennedy, J. P.; Ivan, B. *Polymer Bull.* **1982,** *8,* 25.

[284] Kobayashi, S.; Uyama, H.; Narita, Y.; Ishiyama, J. *Macromolecules* **1992,** *25,* 3232.

[285] Chujo, Y.; Sada, K.; Kawasaki, T.; Saegusa, T. *Polym. J.* **1992,** *24,* 1301.

[286] Kim, K.-M.; Ouchi, Y.; Chujo, Y. *Polymer Bull.* **2003,** *49,* 341.

[287] McAlvin, J. E.; Scott, S. B.; Fraser, C. L. *Macromolecules* **2000,** *33,* 6953.

[288] Jin, R.-H. *Chem. Commun.* **2002,** 198.

[289] Jin, R.-H. *Chem. Phys. Chem.* **2003,** *4,* 1118.

[290] Jin, R.-H. *J. Mater. Chem.* **2003,** *13,* 672.

[291] Jin, R.-H. *Macromol. Chem. Phys.* **2003,** *204,* 403.

[292] Jin, R.-H. *J. Mater. Chem.* **2004,** *14,* 320.

[293] Jordan, R.; Martin, K.; Räder, H. J.; Unger, K. K. *Macromolecules* **2001,** *34,* 8858.

[294] Lüdtke, K.; Jordan, R.; Hommes, P.; Nuyken, O.; Naumann, C. A. *Macromol. Biosci.* **2005,** *5,* 384.

[295] Kabanov, A. V. *Adv. Drug Deliver. Rev.* **2006,** *58,* 1597.

[296] Chujo, Y.; Sada, K.; Saegusa, T. *Macromolecules* **1990,** *23,* 2636.

[297] Park, I.-H.; Han, I.-S.; Kim, D.-K.; Saegusa, T. *Angew. Makromol. Chem.* **1991,** *190,* 165.

[298] Chujo, Y.; Sada, K.; Saegusa, T. *Macromolecules* **1990,** *23,* 2693.

[299] Chujo, Y.; Sada, K.; Saegusa, T. *Macromolecules* **1993,** *26,* 6320.

[300] Chujo, Y.; Sada, K.; Naka, A.; Nomura, R.; Saegusa, T. *Macromolecules* **1993,** *26,* 883.

[301] De Benneville, P. L.; Luskin, L. S., US Patent 2897182, 1959.

[302] Kagiya, T.; Matsuda, T.; Masanori, N.; Ryuichi, H. *J. Macromol. Sci., Chem.* **1972,** *A6,* 1631.

[303] Kagiya, T.; Matsuda, T. *Polym. J.* **1972,** *3,* 307.

[304] Tomalia, D. A.; Thill, B. P.; Fazio, M. J. *Polym. J.* **1980,** *12,* 661.

[305] Kagiya, T.; Matsuda, T.; Zushi, K. *J. Macromol. Sci., Chem.* **1972,** *A6,* 1349.

[306] Miyamoto, M.; Sano, Y.; Kimura, Y.; Saegusa, T. *Macromolecules* **1985,** *18,* 1641.

[307] Levy, A.; Litt, M. *J. Polymer Sci. A1* **1968,** *6,* 1883.

[308] Bortenschlager, M.; Schütz, J.; von Preysing, D.; Nuyken, O.; Herrmann, W. A.; Weberskirch, R. *J. Organomet. Chem.* **2005,** *690,* 6233.

[309] Rossbach, B. M.; Leopold, K.; Weberskirch, R. *Angew. Chem. Int. Ed.* **2006,** *45,* 1309.

[310] Hsieh, B. R.; Litt, M. H. *Macromolecules* **1985,** *18,* 1388.

[311] Hsieh, B. R.; Litt, M. H. *Macromolecules* **1986,** *19,* 516.

[312] Binder, W. H.; Gruber, H. *Macromol. Chem. Phys.* **2000,** *201,* 949.

[313] Kotre, T.; Nuyken, O.; Weberskirch, R. *Macromol. Chem. Phys.* **2004,** *205,* 1187.

[314] Schönfelder, D.; Nuyken, O.; Weberskirch, R. *J. Organomet. Chem.* **2005,** *690,* 4648.

[315] Luxenhofer, R. *Diploma Thesis;* TU München: 2004.

[316] Anselment, T. *Diploma Thesis;* TU München: 2007.

[317] Cesana, S. *Fuctionalization of poly(2-oxazoline)s with cyclic RGD peptides,* Thesis, TU München, 2005.

[318] Ansari, A. M.; Scaria, P. V.; Martin C. Woodle, M. C., Patent Application PCT WO 03/066069, 2003.

[319] Goddard, P.; Hutchinson, L. E.; Brown, J.; Brookman, L. J. *J. Control. Release* **1989,** *10,* 5.

[320] Woodle, M. C.; Engbers, C. M.; Zalipsky, S. *Bioconjugate Chem.* **1994,** *5,* 493.

[321] Zalipsky, S.; Hansen, C. B.; Oaks, J. M.; Allen, T. M. *J. Pharm. Sci.* **1996,** *85,* 133.

[322] Lee, S. C.; Kim, C.; Kwon, I. C.; Chung, H.; Jeong, S. Y. *J. Control. Release* **2003,** *89,* 437.

[323] Webb II, R. R.; Kaneko, T. *Bioconjugate Chem.* **1990,** *1,* 96.

[324] Ryser, J. E.; Jones, R. M. L.; Egeli, R.; Pèlegrin, A.; Rose, K.; Kurt, A. M.; Perin, M.; Broquet, P. E.; Ambrosetti, P.; Fisch, I.; Pochon, S.; Donath, A.; Mach, J. P.; Offord, R. E. *J. Nucl. Med.* **1992,** *33,* 1766.

[325] Kurth, M.; Pèlegrin, A.; Rose, K.; Offord, R. E.; Pochon, S.; Mach, J.-P.; Buchegger, F. *J. Med. Chem.* **1993,** *36,* 1255.

[326] Peula, J. M.; Alvarez, R. H.; Santos, R.; Forcada, J.; de las Nieves, F. J. *J. Mater. Sci.-Mater. M.* **1995,** *6,* 779.

[327] Mikola, H.; Hänninen, E. *Bioconjugate Chem.* **1992,** *3,* 182.

[328] Rose, K. *J. Am. Chem. Soc.* **1994,** *116,* 30.

[329] Rodriguez, E. C.; Marcaurelle, L. A.; Bertozzi, C. R. *J. Org. Chem.* **1998,** *63,* 7134.

[330] Chen, J.; Zeng, W.; Offord, R.; Rose, K. *Bioconjugate Chem.* **2003,** *14,* 614.

[331] Singh, Y.; Defrancq, E.; Dumy, P. *J. Org. Chem.* **2004,** *69,* 8544.

[332] Guo, Z.; Shao, N. *Med. Res. Rev.* **2005,** *25,* 655.

[333] Henriksen, G.; Schottelius, M.; Poethko, T.; Hauser, A.; Wolf, I.; Schwaiger, M.; Wester, H.-J. *Eur. J. Nucl. Med. Mol. Imaging* **2004,** *31,* 1653.

[334] Lemieux, G. A.; Bertozzi, C. R. *Trends Biotechnol.* **1998,** *16,* 506.

[335] Plunkett, K. N.; Chatterjee, A. N.; Aluru, N. R.; Moore, J. S. *Macromolecules* **2003,** *36,* 8846.

[336] Noren, C. J.; Wang, J.; Perler, F. B. *Angew. Chem. Int. Ed.* **2000,** *39,* 450.

[337] Bergeron, R. J.; Wollenweber, M.; Wiegand, J. *J. Med. Chem.* **1994,** *37,* 2889.

[338] Dawson, P. E.; Muir, T. W.; Clark-Lewis, I.; Kent, S. B. *Science* **1994,** *266,* 776.

[339] Dawson, P. E.; Kent, S. B. H. *Annu. Rev. Biochem.* **2000,** *69,* 923.

[340] Tam, J. P.; Xu, J.; Eom, K. D. *Biopolymers* **2001,** *60,* 194.

[341] Clippingdale, A. B.; Barrow, C. J.; Wade, J. D. *J. Peptide Sci.* **2000,** *6,* 225.

[342] Muir, T. W. *Annu. Rev. Biochem.* **2003,** *72,* 249.

[343] David, R.; Richter, M. P. O.; Beck-Sickinger, A. G. *Eur. J. Biochem.* **2004,** *271,* 663.

[344] Muir, T. W. *Prot. Sci.* **2005,** *14,* 3140.

[345] Schwarzer, D.; Cole, P. A. *Curr. Opin. Chem. Biol.* **2005,** *9,* 561.

[346] Muralidharan, V.; Muir, T. W. *Nat. Methods* **2006,** *3,* 429.

[347] Kalia, J.; Raines, R. T. *ChemBioChem* **2006,** *7,* 1375.

[348] Kolb, H. C.; Finn, M.; Sharpless, K. B. *Angew. Chem. Int. Ed.* **2001,** *40,* 2004.

[349] Tornøe, C. W.; Christensen, C.; Meldal, M. *J. Org. Chem.* **2002,** *67,* 3057.

[350] Rostovtsev, V. V.; Green, L. G.; Fokin, V. V.; Sharpless, K. B. *Angew. Chem. Int. Ed.* **2002,** *41,* 2596.

[351] Rodionov, V. O.; Fokin, V. V.; Finn, M. *Angew. Chem. Int. Ed.* **2005,** *44,* 2596.

[352] Bock, V. D.; Hiemstra, H.; van Maarseveen, J. H. *Eur. J. Org. Chem.* **2006,** 51.

[353] Díaz, D. D.; Punna, S.; Holzer, P.; McPherson, A. K.; Sharpless, K. B.; Fokin, V. V.; Finn, M. G. *J. Polym. Sci. Pol. Chem.* **2004,** *42,* 4392.

[354] Sieczkowska, B.; Millaruelo, M.; Messerschmidt, M.; Voit, B. *Macromolecules* **2007,** .

[355] Lewis, W. G.; Green, L. G.; Grynszpan, F.; Radic, Z.; Carlier, P. R.; Taylor, P.; Finn, M. G.; Sharpless, K. B. *Angew. Chem. Int. Ed.* **2002,** *41,* 1053.

[356] Lewis, W. G.; Magallon, F. G.; Fokin, V. V.; Finn, M. G. *J. Am. Chem. Soc.* **2004,** *126,* 9152.

[357] Link, A. J.; Tirrell, D. A. *J. Am. Chem. Soc.* **2003,** *125,* 11164.

[358] Link, A. J.; Vink, M. K. S.; Tirrell, D. A. *J. Am. Chem. Soc.* **2004,** *126,* 10598.

[359] Gupta, S. S.; Kuzelka, J.; Singh, P.; Lewis, W. G.; Manchester, M.; Finn, M. G. *Bioconjugate Chem.* **2005,** *16,* 1572.

[360] Wang, Q.; Chan, T. R.; Hilgraf, R.; Fokin, V. V.; Sharpless, K. B.; Finn, M. G. *J. Am. Chem. Soc.* **2003,** *125,* 3192.

[361] Hsu, T.-L.; Hanson, S. R.; Kishikawa, K.; Wang, S.-K.; Sawa, M.; Wong, C.-H. *P. Natl. Acad. Sci. USA* **2007,** *104,* 2614.

[362] Hahn, U.; Elhabiri, M.; Trabolsi, A.; Herschbach, H.; Leize, E.; Van Dorsselaer, A.; Albrecht-Gary, A.-M.; Nierengarten, J.-F. *Angew. Chem. Int. Ed.* **2005,** *44,* 5338.

[363] Trabolsi, A.; Elhabiri, M.; Urbani, M.; Delgado de la Cruz, J. L.; Ajamaa, F.; Solladié, N.; Albrecht-Gary, A.-M.; Nierengarten, J.-F. *Chem. Comm.* **2005,** 5736.

[364] Hoogenboom, R.; Moore, B. C.; Schubert, U. S. *Chem. Comm* **2006,** 4010.

[365] Scheel, A. J.; Komber, H.; Voit, B. I. *Macromol. Rapid Commun.* **2004,** *25,* 1175.

[366] Wu, P.; Feldman, A. K.; Nugent, A. K.; Hawker, C. J.; Scheel, A.; Voit, B.; Pyun, J.; Fréchet, J. M. J.; Sharpless, K. B.; Fokin, V. V. *Angew. Chem. Int. Ed.* **2004,** *43,* 3928.

[367] Helms, B.; Mynar, J. L.; Hawker, C. J.; Fréchet, J. M. J. *J. Am. Chem. Soc.* **2004,** *126,* 15020.

[368] van Steenis, D. J. V. C.; David, O. R. P.; van Stijdonck, G. P. F.; van Maarseveen, J. H.; Reek, J. N. H. *Chem. Comm.* **2005,** 4333.

[369] Opsteen, J. A.; van Hest, J. C. M. *Chem. Commun.* **2005,** 57.

[370] Lutz, J.-F.; Börner, H. G.; Weichenhan, K. *Macromol. Rapid Commun.* **2005,** *26,* 514.

[371] Joralemon, M. J.; O´Reilly, R. K.; Matson, J. B.; Nugent, A. K.; Hawker, C. J.; Wooley, K. L. *Macromolecules* **2005,** *38,* 5436.

[372] Altintas, O.; Yankul, B.; Hizal, G.; Tunca, U. *J. Polym. Sci. Pol. Chem.* **2006,** *44,* 6458.

[373] Lee, J. W.; Kim, J. H.; Kim, B.-K. *Tetrahedron Lett.* **2006,** *47,* 2683.

[374] Lecomte, P.; Riva, R.; Schmeits, S.; Rieger, J.; van Butsele, K.; Jérôme, C.; Jérôme, R. *Macromol. Symp.* **2006,** *240,* 157.

[375] Kolb, H. C.; Sharpless, K. B. *Drug Discov. Today* **2003,** *8,* 1128.

[376] Binder, W. H.; Sachsenhofer, R. *Macromol. Rapid Commun.* **2007,** *28,* 15.

[377] Lutz, J.-F. *Angew. Chem. Int. Ed.* **2007,** *46,* 1018.

[378] Van Vlierberghe, S.; Cnudde, V.; Dubruel, P.; Masschaele, B.; Cosijns, A.; De Paepe, I.; Jacobs, P. J. S.; Van Hoorebeke, L.; Remon, J. P.; Schacht, E. *Biomacromolecules* **2007,** *8,* 331.

[379] Dubruel, P.; Unger, R.; Van Vlierberghe, S.; Cnudde, V.; Jacobs, P. J. S.; Schacht, E.; Kirkpatrick, C. J. *Biomacromolecules* **2007,** *8,* 338.

[380] Ishihara, M.; Obara, K.; Nakamura, S.; Fujita, M.; Masuoka, K.; Kanatani, Y.; Takase, B.; Hattori, H.; Morimoto, Y.; Ishihara, M.; Maehara, T.; Kikuchi, M. *J. Artif. Organs* **2006,** *9,* 8.

[381] Augst, A. D.; Kong, H. J.; Mooney, D. J. *Macromol. Biosci.* **2006,** *6,* 623.

[382] Tessmar, J. K.; Göpferich, A. M. *Macromol. Biosci.* **2007,** *7,* 23.

[383] Yeh, P.-Y.; Kopečková, P.; Kopeček, J. *J. Polym. Sci. Pol. Chem.* **1994,** *32,* 1627.

[384] Lutz, J.-F.; Weichenhan, K.; Akdemir, .; Hoth, A. *Macromolecules* **2007,** *40,* 2503.

[385] Kang, G. D.; Cheong, S. H.; Song, S.-C. *Int. J. Pharm.* **2006,** *319,* 29.

[386] Chilkoti, A.; Dreher, M. R.; Meyer, D. E. *Adv. Drug Deliver. Rev.* **2002,** *8,* 1093.

[387] Chilkoti, A.; Christensen, T.; MacKay, J. A. *Curr. Opin. Chem. Biol.* **2006,** *10,* 652.

[388] Simnick, A. J.; Lim, D. W.; Chow, D.; Chilkoti, A. *J. Macromol. Sci., R. M. C.* **2007,** *47,* 121.

[389] Lim, D. W.; Nettles, D. L.; Setton, L. A.; Chilkoti, A. *Biomacromolecules* **2007,** *8,* 1463.

[390] Junger, A.; Kaufmann, D.; Scheibel, T.; Weberskirch, R. *Macromol. Biosci.* **2005,** *5,* 494.

[391] Schmaljohann, D. *e-polymers* **2005,** 021.

[392] Li, C.; Finn, M. G. *J. Polym. Sci. Pol. Chem.* **2006,** *44,* 5513.

[393] Brandl, F.; Sommer, F.; Goepferich, A. *Biomaterials* **2007,** *28,* 134.

[394] Kelyman, J. S., Dow Chemical Co., US Patent 4087413, 1978.

[395] Chujo, Y.; Yoshifuji, Y.; Sada, K.; Saegusa, T. *Macromolecules* **1989,** *22,* 1074.

[396] Chujo, Y.; Sada, K.; Matsumoto, K.; Saegusa, T. *Macromolecules* **1990,** *23,* 1234.

[397] Chujo, Y.; Sada, K.; Saegusa, T. *Macromolecules* **1993,** *26,* 6315.

[398] Chujo, Y.; Ihara, E.; Kure, S.; Saegusa, T. *Macromolecules* **1993,** *26,* 5681.

[399] Chujo, Y.; Sada, K.; Nomura, R.; Naka, A.; Saegusa, T. *Macromolecules* **1993,** *26,* 5611.

[400] Taubmann, C. *Aldehyd-funktionalisierte Poly(2-oxazolin)e;* TU München: 2005.

[401] Luxenhofer, R.; Jordan, R. *Macromolecules* **2006,** *39,* 3509.

[402] Nuyken, O.; Maier, G.; Groß, A. *Macromol. Chem. Phys.* **1996,** *197,* 83.

[403] Bonné, T. B.; Lüdtke, K.; Jordan, R.; Stepánek, P.; Papadakis, C. M. *Colloid. Polym. Sci.* **2004,** *282,* 833.

[404] Lüdtke, K. *Fluoreszenzmarkierte Poly(2-oxazolin)e,* Thesis, TU München, 2005.

[405] Bonné, T. B.; Papadakis, C. M.; Lüdtke, K.; Jordan, R. *Colloid. Polym. Sci.* **2007,** *285,* 491.

[406] Bertini, I.; Pierattelli, R. *Pure Appl. Chem.* **2004,** *76,* 321.

[407] Sharp, R. R. *Nucl. Mag. Res.* **2005,** *34,* 553.

[408] A. Modlinger, M. López-García and F. Opperer, personal notes.

[409] Wikipedia, *http://en.wikipedia.org/wiki/Ethanethiol,* [accessed April 21, 2007].

[410] Shaffer, C. B.; Critchfield, F. H. *Am. J. Physiol.* **1947,** *36,* 152.

[411] Shaffer, C. B.; Critchfield, F. H.; Carpenter, C. P. *Am. J. Physiol.* **1948,** *152,* 93.

[412] Berglund, F.; Engberg, A.; Persson, E.; Ulfendahl, H. *Acta physiol. scand.* **1969,** *76,* 458.

[413] Jørgensen, K. E.; Møller, J. V. *Am. J. Physiol. Renal Physiol.* **1979,** *236,* F103.

[414] Furuichi, Y.; Takahashi, T.; Imaizumi, K.; Sugano, M. *Agric. Biol. Chem.* **1984,** *48,* 1777.

[415] Iqbal, T. H.; Cox, M. A.; Lewis, K. O.; Cooper, B. T. *Clin. Sci.* **1995,** *89,* 299.

[416] Gauchel, G.; Huppertz, B.; Feiertag, H.; Keller, R. *J. Chromatogr. B* **2003,** *787,* 271.

[417] Gaertner, F. C.; Luxenhofer, R.; Blechert, B.; Jordan, R.; Essler, M. *J. Control. Release* **2007,** *119,* 291.

[418] Wikipedia, *http://en.wikipedia.org/wiki/Blood#_note-1,* [accessed April 22, 2007].

[419] The Physics Factbook, *http://hypertextbook.com/facts/2004/MichaelShmukler-.shtml,* [accessed April 22, 2007].

[420] Wikipedia, *http://de.wikipedia.org/wiki/Blutplasma,* [accessed April 22, 2007].

[421] Haubner, R. *Eur. J. Nucl. Med. Mol. Imaging* **2006,** *33,* S54.

[422] Lendvai, G.; Velikyan, I.; Bergström, M.; Estrada, S.; Laryea, D.; Välilä, M.; Salomäki, S.; Långström, B.; Roivainen, A. *Eur. J. Pharm. Sci.* **2005,** *26,* 26.

[423] Haskell-Luevano, C.; Nikiforovich, G.; Sharma, S. D.; Yang, Y.-K.; Dickinson, C.; Hruby, V. J.; Gantz, I. *J. Med. Chem.* **1997,** *40,* 1738.

[424] Wikberg, J. E. S.; Muceniece, R.; Mandrika, I.; Prusis, P.; Lindblom, J.; Post, C.; Skottner, A. *Pharm. Res.* **2000,** *42,* 393.

[425] Schiöth, H. B.; Muceniece, R.; Mutulis, F.; Prusis, P.; Lindeberg, G.; Sharma, S. D.; Hruby, V. J.; Wikberg, J. E. S. *Peptides* **1997,** *18,* 1009.

[426] Luxenhofer, R.; López-García, M.; Frank, A.; Kessler, H.; Jordan, R. *PMSE Preprints* **2006,** *95,* 283.

[427] Allen, M. S.; Hamaker, L. K.; La Loggia, A. J.; Cook, J. M. *Synthetic Commun.* **1992,** *22,* 2077.

[428] Anderson, W. K.; Milowsky, A. S. *J. Med. Chem.* **1986,** *29,* 2241.

[429] Menger, F. M.; Migulin, V. A. *J. Org. Chem.* **1999,** *64,* 8916.

[430] Mukaiyama, T.; Takeda, T.; Atsumi, K. *Chem. Lett.* **1974,** *3,* 187.

[431] Wikipedia, *http://en.wikipedia.org/wiki/Auger_electrons,* [accessed January 5, 2007].

[432] Halperin, E. C. *Lancet Oncol.* **2006,** *7,* 676.

[433] Langhorst, M. F.; Reuter, A.; Luxenhofer, G.; Boneberg, E.-M.; Legler, D. F.; Plattner, H.; Stuermer, C. A. O. *FASEB J.* **2006,** *20,* 711.

[434] Wikipedia, *http://en.wikipedia.org/wiki/Neoplasm,* [accessed January 16, 2006].

[435] Rufini, V.; Calcagni, M. L. C.; Baum, R. P. *Semin. Nucl. Med.* **2006,** *36,* 228.

List of Figures

List of Tables

Glossary

Medical terms are generally taken from the 260^{th} edition of the Pschyrembel® (Publisher: de Gruyter, Berlin, New York) or from other encyclopedias such as Römpp and Wikipedia.

agonist a molecule which binds to a receptor and is able to trigger a response/action, thus mimicking the the natural ligand(s) of this receptor

affinity binding strength between two molecules (or particles), in this context typically between a receptor and its ligand where only one mutual binding site is present (in contrast to AVIDITY).

antagonist a molecule that inhibits the function of a receptor, by binding (without triggering response) or blocking the ligand binding site

antigen **anti**body **gen**erating substances; i.e. a substance that can induce an immune response

aptamers are short (40 - 70 bases) single-stranded DNA or RNA sequences which bind specifically to molecular targets through their 3D structure and electrostatic interaction and hydrogen bonds. Their affinity ranges from pico- to nanomolar.

auger-electrons when an electron is removed from a core level of an atom (e.g. by ionisation or electron capture), leaving a vacancy, an electron from a higher energy level may fall into the vacancy, resulting in a release of energy. Although sometimes this energy is released in the form of an emitted photon, the energy can also be transferred to another electron, which is then ejected from the atom[431]

avidity binding strength between particles with multiple binding motifs, in contrast to AFFINITY

basementmembrane structure that separates the endothelium from other tissue.

B-cell are an important part of the humoral immune respone. These lymphocytes are responsible for the production of antibodies against soluble antigens.

bystander effect when cells are killed because they are in close proximity to the actual target, rather than being the actual target[13].

cancer general term for maligne neoplasia. More specific terms for various cancer types typically refer to the origin of the corresponding cells, such as carcinoma (epithelial cells), sarkoma (cells derived from the mesoderm)

cyclotron a device used to produce high-energy particles including electrons, protons, alpha particles, and heavy ions. It consists of two hollow D-shaped sections (known as dees) assembled with a space between them to form a circle. A magnetic field is used to deflect the particles into a circular path inside the circle. The particles are accelerated by alternating the voltage between the two dees. The alternating voltage gives the particles a boost of energy as they pass between the dees.[432]

endocytosis is the uptake of substances (solutes or solids) into the cell by engulfment of the substance with the cell membrane.

endothelium term for the cell layer that coats (thus defines) the inner surface of the circulatory system (both blood and lymphatic vessels), a specialized form of epithelium

epithelium term for the cell layer that coats all outer and inner surfaces of an organism.

extracellular matrix (ECM) term for any part of a tissue that is not part of any cell. The ECM is the defining feature of connective tissue.

fibronectin high-molecular weight glycoprotein and component of the extracellular matrix and various extracellular fluids (e.g. blood, spinal fluid)

gastroenteropancreatic related to the organs of the digestive system (stomach = gastro, intestines = entero and pancreas)

Gleevec trade name in the US (Glivec in europe) for imatinib (4-[(4-methylpiperazin-1-yl)methyl]-*N*-[4-methyl-3- [(4-pyridin-3-ylpyrimidin-2-yl)amino]-phenyl]-benzamide), a potent inhibitor for tyrosine kinase enzyme for the treatment of e.g. chronic myelogenous leukemia

glomerulus a capillary inversion into the bowman capsule in the kidneys. In the glomerular capillaries the blood is filtrated to produce the primary urine.

G-protein guanine nucleotide binding proteins, short G-proteins are a family of proteins which is very important for the regulation of cell processes and signal transduction. Usually G-protein refers to membrane receptor associated proteins which become active upon ligand binding of the respective receptor.

hepatobiliary concerning the liver and bile, e.g. hepatobiliary excretion: excretion via the liver and the bile

Herceptin trade name of trastuzumab, a humanized monoclonal antibody. It acts on a receptor named HER2/neu and is used for the therapy of tumors overexpressing this receptor (e.g. breast cancers).

immune response a part of the immune response involves cytosolic and extracellular peptides which are degraded by the proteasome or in lysosomes respectively. Fragments of 8 - 10 or 15 - 24 amino acids length are bound the MHC class I or MHC class II molecules, respectively, and the complex is presented on the cell surfaces. Recognition of these fragments in combination with the MHC molecules by T-cells triggers the cellular immune response.

linear energy transfer (LET) the linear energy transfer describes the amount of energy that is dissipated by radiation per way ($\Delta E/s\Delta$ [LET] = keV/μm). The LET depends on the type of radiation and its energy. The higher the LET, the higher the biological impact.

lipid raft cholesterol and sphingolipid rich microdomains in cell membranes. Considered to be modulating a number of signaling pathways by protein sorting and assemblance of signaling complexes[433].

Malpighian corpuscle consists of the glomerulus and the surrounding Bowman capsule. In M. c. formation of the primary urine takes place.

Mylotarg trade name of gemtuzumab ozogamicin, a monoclonal anti-CD33 antibody carrying calicheamicin, a cytostatic. Used to treat acute myelogenous leukemia.

neoplasia neoplasia (greek: new growth) is abnormal, disorganized growth in a tissue or organ, usually forming a distinct mass. Such a growth is called a neoplasm, also generally referred to as a tumor. The terms neoplasia and cancer are often incorrectly used interchangeably. Neoplasia refers to both benign and malignant growths, while ´cancer´ refers specifically to malignant[434].

nephrotoxicity toxic for the kidneys

neuroendocrine originating from endocrine cells, which are characterized by the presence of secretory granules as well as the ability to produce biogenic amines and polypeptide hormones.[435]

phage-display is a technique in which a library of phages displaying different proteins are injected into a organism (e.g. mice). Some of these proteins will interact with a target organ (e.g. tumor). The organ is resected and the phages are collected. After several repetitions, this allows the isolation of phages (thus, peptides), that bind highly specific to this organ.

pharmacokinetics the fate of substances and its metabolites brought into an organism, its distribution within the blood stream and the body tissues and its excretion or accumulation within the body.

positron emission tomography (PET) is a imaging method in nuclear medicine. A β^+-emitting isotope is incorporated into a metabolically/pharmacologically active molecule. Upon administration (typically intravenously) the molecule distributes and concentrates in areas/tissues/organs of interest. As the β^+-particle is emitted, it combines very rapidly in the vicinity of its origin, with an electron of the surrounding matter. As a result, two annihilation (γ) photons are emitted at almost 180° from another. Detectors around the patient detect the photon pair and their origin can be calculated from the time difference in the impact. As a result, a three dimensional image of the radionuclide distribution within the body can be obtained. The most common PET-tracer is ^{18}F-fluorodeoxyglucose (FDG) which accumulates e.g. in tumor cells and can be therefore used for diagnosis and staging of cancer and localization of metastasis.

prodrug a drug which becomes only active upon a external stimulus, typically cleavage of a chemical bond to release the active form of the drug

renal concerning the kidneys

reticuloendothelial system (RES) is part of the immune system and consists of phagocytic cells. These are closely related with the lymphatic system. Spleen and liver are major organs which contribute to the RES.

SMANCS conjugate of neocarcinostatin (NCS) and copolymer containing **s**tyrene, **m**aleic **a**cid as well as n-butylester and anhydride thereof (SMA)

single photon emission computed tomography (SPECT) imaging technique in nu-

clear medicine using γ-emitter. SPECT gives three dimensional images in contrast to planar γ-cameras

transcription factors proteins involved in recognition by RNA polymerases of specific regulatory sequences in eukaryotic genes, i.e. protein mediating the binding of RNA polymerase to DNA, thus initiating transcription (reading) of the DNA.

tumor abnormal swelling of tissue which can be due to acute or chronical inflammation, edema, aneurysm or neoplasia.

Zevalin trade name of ibritumomab tiuxetan, an anti-CD20 monoclonal antibody coupled to the chelator *p*-SCN-Bn-DTPA (carrying ^{111}In for imaging and ^{90}Y for therapy).